

LASER INDUCED BREAKDOWN SPECTROSCOPIC STUDIES FOR MATERIAL CHARACTERIZATION

By

ARNAB SARKAR

Homi Bhabha National Institute, Mumbai, INDIA

A thesis submitted to the

Board of Studies in Chemical Sciences

In partial fulfillment of requirements

For the Degree of

DOCTOR OF PHILOSOPHY

of

HOMI BHABHA NATIONAL INSTITUTE

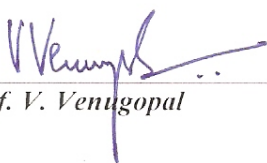


September, 2010

Homi Bhabha National Institute

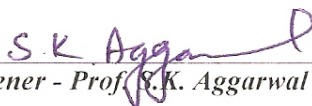
Recommendations of the Viva Voce Board

As members of the Viva Voce Board, we certify that we have read the dissertation prepared by Mr. Arnab Sarkar entitled "*Laser induced breakdown spectroscopic studies for material characterization*" and recommend that it may be accepted as fulfilling the dissertation requirement for the Degree of Doctor of Philosophy.



Chairman - Prof. V. Venugopal

Date: 3/6/11



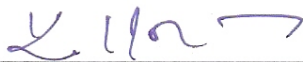
Guide / Convener - Prof. S.K. Aggarwal

Date: 3/6/11



External Examiner – Prof. Awadhesh K. Rai

Date: 3/6/11



Member 1 - Prof. K.L. Ramakumar

Date: 3.6.2011



Member 2 – Dr. S.K. Mukerjee

Date:

Final approval and acceptance of this dissertation is contingent upon the candidate's submission of the final copies of the dissertation to HBNI.

I hereby certify that I have read this dissertation prepared under my direction and recommend that it may be accepted as fulfilling the dissertation requirement.

Date: 3/6/2011

Place: RLG, BARC, Mumbai

STATEMENT BY AUTHOR

This dissertation has been submitted in partial fulfillment of requirements for an advanced degree at Homi Bhabha National Institute (HBNI) and is deposited in the Library to be made available to borrowers under rules of the HBNI.

Brief quotations from this dissertation are allowable without special permission, provided that accurate acknowledgement of source is made. Requests for permission for extended quotation from or reproduction of this manuscript in whole or in part may be granted by the Competent Authority of HBNI when in his or her judgment the proposed use of the material is in the interests of scholarship. In all other instances, however, permission must be obtained from the author.

(Arnab Sarkar)

DECLARATION

I, hereby declare that the investigation presented in the thesis has been carried out by me. The work is original and has not been submitted earlier as a whole or in part for a degree / diploma at this or any other Institution / University.

(Arnab Sarkar)

DEDICATIONS

To

BABA, MA

&

SWARNA

ACKNOWLEDGEMENTS

This thesis owes its existence to the help, support, and inspiration of many people. In the first place, I would like to express my sincere appreciation and gratitude to Prof. S.K. Aggarwal for his patient guidance, encouragement and excellent advice for more than three years of this thesis' work. Deepest gratitudes are also due to the members of the HBNI Doctoral Committee, Prof. V. Venugopal, Prof. K.L. Ramakumar and Dr. S.K. Mukerjee without whose critical comments and suggestions, this study would not have taken the present shape.

Special thanks are to Dr. (Ms) D. Alamelu for introducing me to this field. My big thanks are due to my colleagues Mr. Pranaw Kumar, Mr. P.G. Jaison, Mr. A.R. Parab, Mr. V.M. Telmore, Mr. Sashibhusan, Mr. T.V.V. Vittal Rao, Mr. Y.R. Bamankar for helping me wherever needed. I also extend my appreciation to Mr. R. Shivaraman for his assistance.

My acknowledgements are also to Dr.(Ms) P. Purohit, Mr. S. Panja, Dr. S. Ansari, and Dr. K. Shivanna of B.A.R.C., who helped me in various parts of my work.

I wish to place my special thank to my Post Graduation teachers especially to Dr. Pinaki Benerjee who taught me how to tackle a scientific problem.

I would also like to thank my friends Dr. A. Bhattachariyya, Dr. B.P. Mandal, Mr. D. Benerjee, Mr. S. Ghosh and Dr. D. Dutta for their constant support.

Finally, I owe special gratitude to my father, mother and my wife Swarna for continuous and unconditional support of all my undertakings, scholastic and otherwise.

.....*Arnaab*

CONTENTS

SYNOPSIS	i
LIST OF FIGURES	xv
LIST OF TABLES	xx
CHAPTER I	1
1.1. Introduction	2
1.2. Historical summary	2
1.3. The LIBS concept & related phenomena	6
1.3.1. Laser ablation	6
1.3.2. Formation of laser induced plasma (LIP)	7
1.3.3. Plasma growth & termination	13
1.3.4. Plasma shielding	15
1.3.5. Local thermodynamic equilibrium	16
1.3.6. Plasma opacity	17
1.3.7. Plasma temperature	18
1.3.8. Plasma electron density	20
1.4. Quantitative analysis	22
1.4.1. Calibration curves	23
1.4.2. Limit of detection (LOD) in LIBS	27
1.5. Advantages & limitations of LIBS	28
1.6. Scope of the present work	33
CHAPTER II	35
2.1. LIBS instrumentation	36
2.1.1. Lasers	36

2.1.1.1. Q-switching	41
2.1.1.2. Pockel's cell	42
2.1.1.3. Properties of laser important for LIBS	43
2.1.1.3.1. Wavelength	43
2.1.1.3.2. Pulse energy & irradiance	43
2.1.1.3.3. Spatial quality	44
2.1.1.3.4. Directionality	44
2.1.1.3.5. Monochromaticity	44
2.1.2. Sample chamber	44
2.1.3. Optical system	45
2.1.3.1. Focusing & light collection system	45
2.1.3.2. Lenses	45
2.1.3.3. Fiber optic cables	45
2.1.4. Detection system	48
2.1.4.1. Grating spectrographs	48
2.1.4.2. Detectors	49
2.1.5. Control electronics	57
CHAPTER III	58
3.1. Introduction	59
3.2. Determination of uranium in MOX Fuel	61
3.2.1. Background	61
3.2.2. Sample preparation and analysis	62
3.2.3. Results and discussion	64
3.2.3.1. Selection of emission line	64
3.2.3.2. Effect of laser fluence	65

3.2.3.3 Temporal resolution for acquisition	65
3.2.3.4. Calibration curves and precision	68
3.2.4. Conclusions	73
3.3. Determination of trace constituents in thoria	74
3.3.1. Background	74
3.3.2. Experimental	75
3.3.2.1. Samples	75
3.3.2.2. LIBS analysis	76
3.3.3. Results and discussion	76
3.3.3.1. Time resolution	76
3.3.3.2. ThO ₂ spectra	77
3.3.3.3. Calibration curves	78
3.3.3.4. Precision and detection limit	82
3.3.3.5. Matrix effect in ThO ₂ –MOS	82
3.3.4. Conclusions	89
CHAPTER IV	90
4.1. Introduction	91
4.2. Methodology for liquid analysis	93
4.3. Determination of high atomic number element (U & Th) in solution by LIBS	94
4.3.1. Background	94
4.3.2. Samples preparation & analysis	94
4.3.3. Results & discussions	98
4.3.3.1. Selection of emission line	98
4.3.3.2. Effect of substrate	98
4.3.3.3. Time resolution	99

4.3.3.4. Reproducibility	99
4.3.4. Calibration curves	103
4.3.4.1. Individual elemental calibration & LOD	103
4.3.4.2. Th – U mixture calibration & LOD	107
4.3.5. Conclusions	109
4.4. Determination of middle atomic number elements (platinum group metals) in solution by LIBS	110
4.4.1. Background	110
4.4.2. Preparation of samples	112
4.4.3. Results & discussion	113
4.4.3.1. Selection of emission lines for analysis	113
4.4.3.1.1. Pure solution	113
4.4.3.1.2. Simulated high level liquid waste	113
4.4.3.2. Optimization of experimental conditions	118
4.4.3.3. Calibration curves	121
4.4.4. Analytical results	125
4.4.5. Conclusions	130
4.5. Determination of lower atomic number elements (B & Li) in solution by LIBS	131
4.5.1. Determination of B in ground water samples	131
4.5.1.1. Background	131
4.5.1.2. Sample preparation & analysis	133
4.5.1.3. Results & discussion	133
4.5.1.3.1. Selection of substrate	133
4.5.1.3.2. Selection of emission lines	135
4.5.1.3.3. Optimization procedure	136

4.5.1.3.4. Effect of interfering elements	136
4.5.1.3.5. Calibration curves	139
4.5.1.3.6. B in ground water samples	139
4.5.1.4. Conclusion	142
4.5.2. Determination of Li in organic solution	142
4.5.2.1. Background	142
4.5.2.2. Sample preparation & analysis	144
4.5.2.3. Results & discussion	145
4.5.2.4. Conclusion	150
CHAPTER V	151
5.1. Introduction	152
5.2. Experimental	153
5.2.1. Materials	153
5.2.2. Sample preparation	153
5.2.3. LIBS spectral library for papers	155
5.3. Results & discussion	155
5.4. Conclusion	164
ANNEXURE I	165
REFERENCES	171
List of Publications	191

Synopsis

Laser induced breakdown spectroscopy (LIBS) is a type of atomic emission spectroscopy that was first reported in 1962 and has since evolved into a technique for laboratory chemical analysis [1]. When a pulsed laser beam of high intensity is focused on the surface of material of interest, it generates plasma if the irradiance is sufficient enough. As the plasma cools down, atomic and/or ionic species present in the focal volume emit light at their characteristic wavelengths. These colors, wavelengths or frequencies are a unique signature for each atom or ion. Hence the generated spectrum is a fingerprint of the emitting atomic species (atoms and/or ions). The emission from plasma plume is collected, dispersed, detected and then subsequently analyzed for quantification of elements present in the material of interest. This is the basis of laser based spectrochemical analysis or presently known as LIBS. During the last two decades, LIBS has undergone a dramatic transformation in terms of hardware, software and application areas. It has become a powerful sensor technology for both laboratory and field applications. In order to obtain a reliable quantitative elemental analysis of a sample using LIBS, one needs to control several parameters that strongly affect the measurements. Some of these parameters are the laser wavelength, its irradiance, time resolution of emission light acquisition, the morphology of the sample surface, and the amount of ablated and vaporized sample. If these and the related parameters are properly optimized, the spectral line intensities will be proportional to the elemental concentrations and will generate suitable calibration curves.

LIBS has high dynamic range, good sensitivity, and is capable of rapid elemental analysis in a variety of matrices like solids [2], liquids [3, 4], gases [5], aerosols [6], ceramics [7], radioactive waste [8, 9], environmental system [10] etc. LIBS has been developed for a number of applications due to its many advantages in comparison to other emission spectroscopic techniques. These include (i) minimal or no sample preparation (ii)

simultaneous multi-elemental analysis capability (iii) applicable to both electrically conducting and non-conducting samples (iv) possibility to use in hazardous and industrial environments etc. Its major limitations are its sensitivity to fluctuations in the analysis conditions such as laser fluence etc. and limited sensitivity for some of the elements due to small amount of material consumption. This technique is non-destructive in the sense that very small amount ($\sim\mu\text{g}$) of material is ablated to create plasma.

Elemental determinations at bulk, minor, trace and ultra-trace levels are important for different applications in various areas of research and development and in particular, for the effective utilization of materials in nuclear science and technology. For example, chemical quality assurance of fuels and fuel materials demands data on major elements like Th, U and Pu and also of different trace constituents present in various materials like fuel, clad, coolant tubes etc.

Therefore, in the present thesis, the application of LIBS for material characterization needed in the various fields of research and development in nuclear industry, environmental studies and forensic application was investigated. The work described in this thesis is divided into five chapters.

Chapter I

This chapter gives an introduction to the historical development of LIBS, its fundamental working principles and its application in various matrices. The details of the advantages and disadvantages of the LIBS technique are also described in this Chapter. Finally, the scope of the work is presented.

Chapter II

The details of the instrument employed are described in this Chapter. In the experimental setup, a commercially available LIBS system, Spectrolaser 1000M from Laser Analysis Technologies (now known as XRF scientific), Victoria, Australia was employed.

The instrument is an integrated analysis system comprising a high-power Q-switched Nd:YAG laser that yields 200mJ of pulse energy at the fundamental IR wavelength (1064 nm) with a 7 ns pulse width, at a repetition rate of 10 Hz. The laser is focused onto the sample by a plano-convex lens with a focal length of 5 cm. The sample holder is fixed to a step – up motor so that every laser shot hits on a fresh site. The emitted plasma radiation is then collected at a 45° angle with respect to the laser beam direction. The emission output is focused through four fiber optic cables onto the entrance slit of Czerny–Turner (CT) spectrographs with CCDs as detectors. The system has a wide spectral coverage from 180 nm to 850 nm while maintaining the resolution of 0.6 nm at 300 nm that is required for observation of elemental emissions with minimal interferences. The spectral acquisition can be delayed by a software controlled delay generator to achieve the required delay between plasma ignition and recording of the emission spectrum. The photograph of the instrument is shown in Fig. 1.

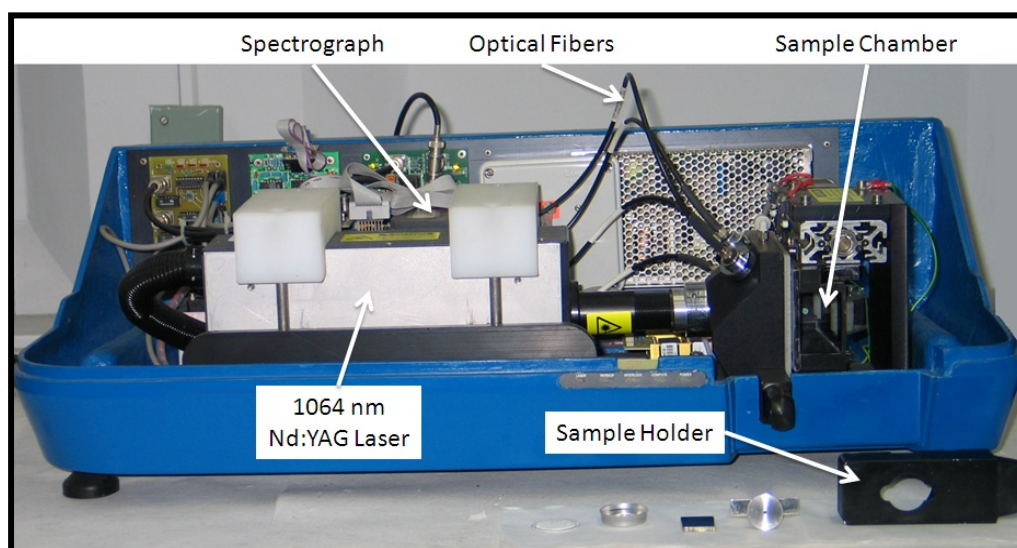


Figure 1. *Photograph of LIBS system used in this study*

Chapter III

This chapter deals with the application of LIBS for material characterization in solid matrix. The application of LIBS in solid matrix has been the front runner in the research and development work, but there have been a few applications in characterizing nuclear materials.

This chapter discusses both the bulk characterization and also trace characterization of nuclear materials.

LIBS methodology was developed for determining the percentage level of bulk uranium in thorium–uranium mixed oxide fuel samples required as a part of the chemical quality assurance of fuel materials. Due to non - availability of commercial certified reference materials (CRMs) for mixed oxide of U and Th, a series of synthetic mixed oxide calibration standards were prepared on weight basis with U amount varying from 0 to 32% by weight. High purity (99.5%) boric acid powder was used as a binder for pelletization. The experimental parameters, laser fluence and acquisition time delay were optimized by studying signal to noise ratio, and were found to be 56 Jcm^{-2} and $3.5 \text{ } \mu\text{s}$. To select an appropriate emission line for U, spectra of pure U, pure Th and a mixed oxide sample were recorded and compared critically and four U emission lines [U(II) 263.553 nm, U(II) 367.007 nm, U(II) 447.233 nm and U(II) 454.363 nm] were identified and selected (Fig. 2). Calibration curves were established by plotting normalized emission line intensity with respect to B(I) 249.774 nm against U amount. The uranium amount determined in two samples using calibration curves agreed well with the expected values. The reproducibility of the determination was $\pm 2\%$ with an accuracy of $\sim 7\%$. The calibration curves showed a linear behavior below 8 wt.% U in the Th–U mixed oxide. Above 8 wt.% U, saturation was observed which was fitted to the following non-linear equation (Fig. 3).

$$y = y_0 + A e^{\left(\frac{-x}{t}\right)} \quad \dots\dots(1)$$

The absolute value of “t” indicates the degree of non-linearity of the calibration curve. Except from the U(II) 263.553 nm, the absolute value of “t” for the other three emission lines is close to 20, and in case of U(II) 263.553 nm, it is 31.9. The methodology was found to be very useful for fast and routine determination of uranium in mixed oxide samples of Th and

U, without the need for dissolution, which is difficult and time consuming due to the refractory nature of ThO_2 .

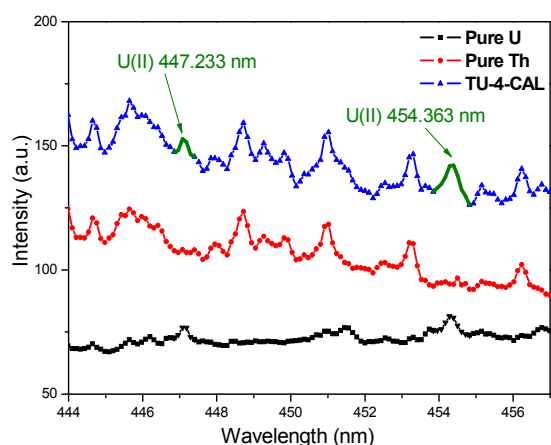


Figure 2. Comparison of the spectra of the individual actinides (U and Th) with the mixed oxide standard under identical conditions of analysis

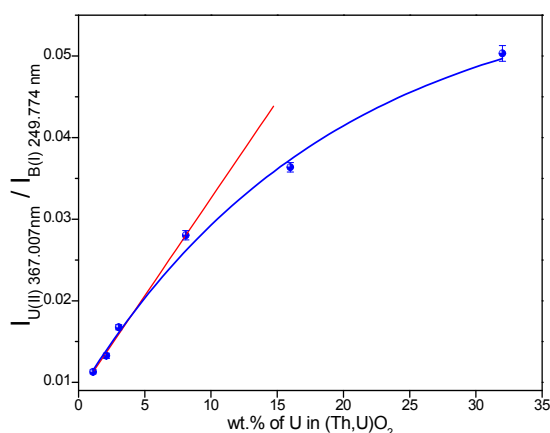


Figure 3. Calibration curves obtained for U(II) 367.007 nm. The red line corresponds to linear behavior of optically thin plasma

Determination of trace constituents in nuclear fuel materials is equally important as bulk characterization. Specification limits have been laid down for various impurities in different nuclear fuels. LIBS analysis conditions were optimized for the determination of trace impurities in ThO_2 samples. Thoria CRMs prepared in the Department of Atomic Energy (DAE), India were employed in this work. For LIBS analysis, samples were pelletized. The choice of time resolution parameter was assessed experimentally with zirconium as a model, as the melting point of Zr (2125 K) is close to that of Th (2115 K). This particular approach was followed because studying the time resolution in ThO_2 spectrum is difficult due to the numerous emission lines. In this work, laser energy of 50 mJ and an acquisition delay of 6 μs were used. After critical evaluation of the ThO_2 spectrum, a total of 14 emission lines of different impurities were selected (Fig. 4). 7 elemental impurities (Mg, Al, Ca, Ni, Fe, Cu and Mo) in the ThO_2 samples were found to give good calibration and the

rest 7 elemental impurities (Mn, Na, V, BE, Ce, B and Cr) were only detected. The calibration curves were constructed by plotting the intensity ratio of impurity with respect to Th(II) 318.019 nm versus the known element concentration. On validating the calibration plot, the precision values varied in the range of 7 to 22%, which is acceptable for quality assurance.

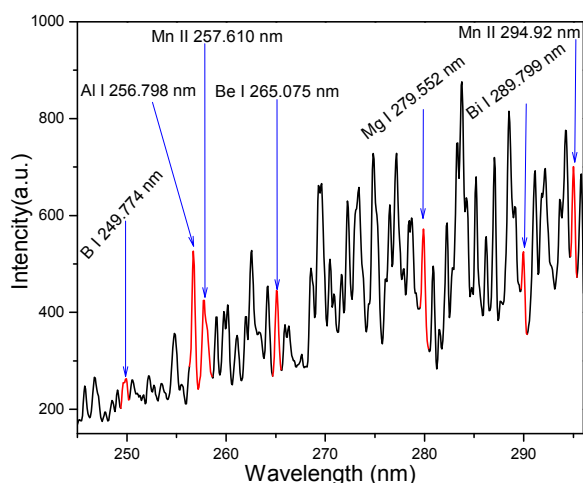


Figure 4. Emission spectrum of $\text{ThO}_2\text{-S}$ in the 245 nm to 295 nm region with the emission lines of impurities.

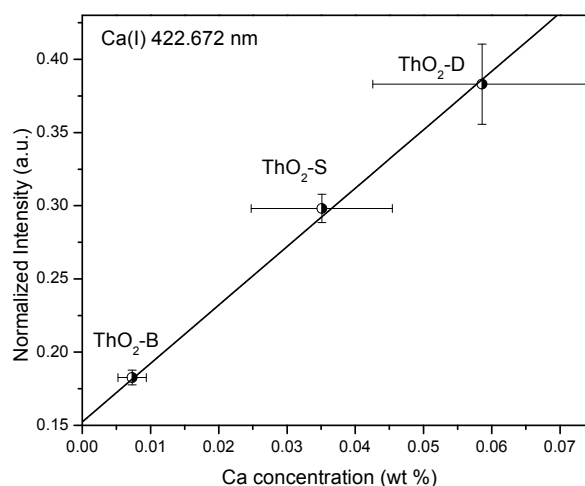


Figure 5. Calibration curves obtained for the normalized Ca(I)422.672 nm in thoria matrix.

Detection limits for 7 impurity elements in ThO_2 were determined using the formula $\text{LOD} = 3\sigma/m$, where m is the slope of the calibration line and σ is the uncertainty in the intensity for the calibration point with the lowest concentration. The LODs were found to be much better than the LOD's for these elements in UO_2 and PuO_2 reported previously. Mixed oxide sample ($\text{ThO}_2 - \text{MOS}$) containing around 2.5% weight of UO_2 was also analyzed by LIBS under the identical conditions of analysis. The LIBS spectrum obtained was quite different from those of ThO_2 samples. The results for impurities were found to be positively biased when compared to the expected concentration values. This observation is characteristic of matrix effect, implying the need to have calibration standards with similar composition.

Chapter IV

This Chapter discusses the development of analytical methodologies using LIBS for the quantification of elements in liquid matrix. This chapter has been sub-divided according to the region of Periodic Table from where the elements are selected – (i) high atomic number (Z) elements (U and Th) (ii) middle Z elements (Ru, Rh and Pd) (iii) low Z elements (B and Li). For liquid analysis, several methodologies have been proposed by many authors such as freezing samples, laminar flows and liquid jets, the double-pulse technique, the liquid-to-solid conversion technique, on droplets etc. In the present work, a different approach without modifying the present equipment setup was tried. The liquid was taken on a solid support and dried; subsequently the material was allowed to cool to room temperature and was then mounted in the sample holder for analysis. The solid surface analysis technique exploits the strengths of LIBS without the problems inherent to liquid analysis while maintaining the main advantages of the LIBS.

An experimental methodology was developed to analyze thorium (Th) and uranium (U) separately and also in the presence of each other in aqueous solutions by LIBS. Standard solutions of Th and U were used in the 0–5000 ppmw range to establish calibration plots. 40 μL of the sample was loaded on a Whatman-42 membrane filter paper and analyzed. The experimental parameters were optimized by studying signal to noise ratio against laser energy and acquisition time delay parameters, and were found to be 100 mJ and 600 ns. The emission lines for Th and U determination were selected from the regions in which minimal spectral interferences were observed and their intensities were ratioed with respect to C (I) 193.029 nm to generate calibration plot. Saturation effects were observed for Th and U above 1000 ppmw and 800 ppmw, respectively. The LODs determined for U(II) 367.007 nm and Th(II) 401.913 nm were 18.5 and 0.72 ppmw, respectively. This is the first report of Th quantification in a solution by LIBS; the LOD for U is much lower than the previously reported LOD of 0.1 g L^{-1} .

The relative precision in both cases was less than 5%. It was observed that the quantification of trace levels of U in a bulk amount of Th was not possible because of strong spectral interference from Th at the most intense lines of U, but traces of Th in bulk of U could be determined. The calibration curve obtained by plotting the intensity ratio of Th(II) 401.913nm with respect to U(II) 367.007nm versus the Th/U amount ratio was found to be linear up to Th/U ratio of 0.035, beyond which non-linearity was observed (Fig. 6). The LOD was determined to be 0.0007 for the Th/U ratio.

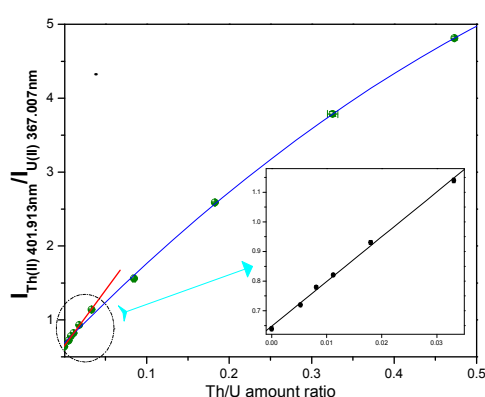


Figure 6. Calibration curve of U-Th mixture in aqueous solution.

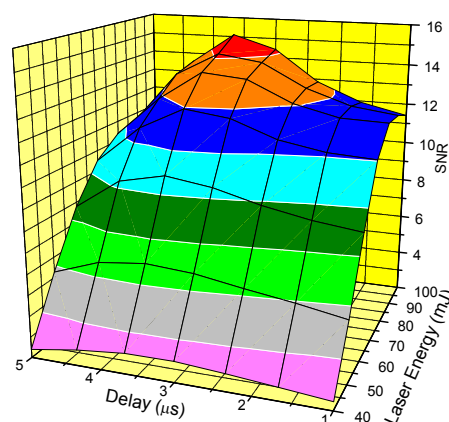


Figure 7. Variation of SNR of Pd(I) 324.270 nm with laser energy and acquisition time delay.

The second part of the chapter includes the details of the development for the quantification of platinum group metals (PGM), namely Pd, Rh and Ru in a simulated high level liquid nuclear-waste (SHLLW). The composition of nuclear HLLW solution is very complex, with as many as 30 elements present in it with varying concentrations. Therefore, the quantification of Pd, Rh and Ru without matrix separation becomes extremely difficult. Initially pure elemental solutions were prepared by dissolving chloride samples of the elements in 3 M HNO₃ and subsequently analyzed for selection of emission lines and analysis conditions optimization. The solid surface analysis technique with spectroscopically pure graphite planchets was used. For pure elemental solution, as many as 5, 6 and 6 emission

ines were selected based on their spectral purity for Pd, Rh and Ru, respectively. The situation is very complicated in SHLLW where only Pd(I) 276.309 nm, Pd(I) 340.457 nm, Rh(II) 233.477 nm, Ru(II) 245.657 nm and Ru(I) 372.802 nm emission lines were observed as spectrally pure. For optimization, SNR was studied with laser energy and acquisition delay time (Fig. 7). The optimized conditions were identical for Pd and Ru and slightly different from those of Rh. Considering the problem of simultaneous quantification of all the PGMs, optimum condition was fixed as that of Pd and Ru, i.e., 100 mJ laser energy and 3.5 μ s of acquisition time delay. Applying these conditions, calibration curves for the individual PGMs were constructed and were validated by analyzing a mixture of the three PGMs selected within 5% accuracy and 10% precision. Two synthetic waste samples SHLLW – 2 and SHLLW – 3, differing only for the amount U present in the sample (no U in the SHLLW – 2 mixture), were also analyzed. While satisfactory agreement was obtained in case of SHLLW – 2 but for SHLLW – 3, very high positively biased results were obtained due to the presence of \sim 6000 ppmw U. It was found that up to 700 ppmw of U concentration, PGM quantification results are not significantly affected. It may be noted that the concentration of U expected in HLLW solution under normal reprocessing conditions is in the range of 500 - 1000 ppmw. Since LIBS is a non-contact method, and has remote analysis capabilities, it is highly attractive in HLLW solutions due to the high radioactivity associated with these samples.

For evaluating applicability of LIBS for analyzing low Z elements, boron in ground water and lithium in complex organic mixture analysis are discussed in this chapter. For the determination of elements of low Z, a few analytical methods are available. Further, for elements like B, Li where adventitious contamination or loss of sample is quite possible during sample pretreatment, there is a need to develop and validate methods which do not involve elaborate sample preparation steps.

To characterize ground water for B concentration, a calibration curve was constructed using synthetically prepared B standards in Milli-Q water. The experimental parameters were optimized by studying signal to noise ratio against laser fluence and acquisition time delay, and were found to be 50 J.cm^{-2} and $1.5 \text{ }\mu\text{s}$. The two emission lines B(I) 208.957 nm and B(I) 249.773 nm showed good linearity up to concentration of $20 \text{ }\mu\text{g.g}^{-1}$ (Fig. 8). The possible spectral interferences expected at B(I) 208.957 nm are due to Al(I) 208.915 nm and Mo(II) 208.952 nm; and at B(I) 249.773 nm line are due to Fe(I) 249.653 nm and Cr(I) 249.630 nm. These were examined and no interference was observed. The LOD was $0.01 \text{ }\mu\text{g.g}^{-1}$ for boron using the B(I) 249.773 nm emission line. Ground water samples collected from the states of Tamilnadu and Gujarat, India were analyzed and the results agreed within 10% with ICP-MS data. The method is considered to be promising for the rapid determination of boron, with an acceptable degree of accuracy and without the need for elaborate sample treatment, preconcentration and purification steps.

During the preparation of Li_2TiO_3 (with enriched ^6Li) by sol - gel process, the microspheres are washed with ^6Li containing organic mixture $\{0.54\text{M NH}_4\text{NO}_3 + 0.24\text{M NH}_4\text{Cl} + 0.075\text{M HMTA} + 0.075\text{M Urea} + \text{LiOH}\}$ so that leaching of ^6Li from the sol-gel particles during washing can be minimized.

A methodology based on LIBS was developed where Li can be determined directly in the organic mixture. The solid surface analysis method with Whatman – 42 membrane based filter paper as a solid support was used to construct a calibration in the concentration range of 33 mM to 2M. 100 mJ energy and $2.5 \text{ }\mu\text{s}$ were found to be the optimum conditions. 5 lithium emission lines were selected, Li(I) 670.79 nm, Li(I) 610.364 nm, Li(I) 812.644 nm, Li(I) 497.174 nm, Li(I) 460.288 nm. Li(I) spectral line 670.79 nm was found to be very sensitive and provided a linear calibration upto 0.54M concentration. The other emission lines, Li(I)

812.644 nm, Li(I) 497.174 nm, Li(I) 460.288 nm were detected only above the concentration of 0.75M of Li. The methodology generated results with ~5% precision.

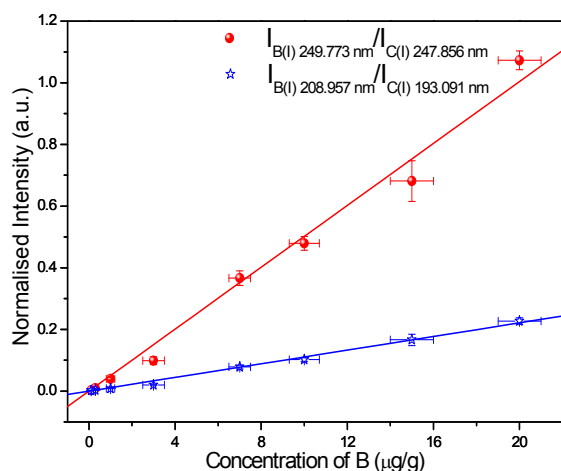


Figure 8. *Normalized boron emission intensity as a function of concentration of boron*

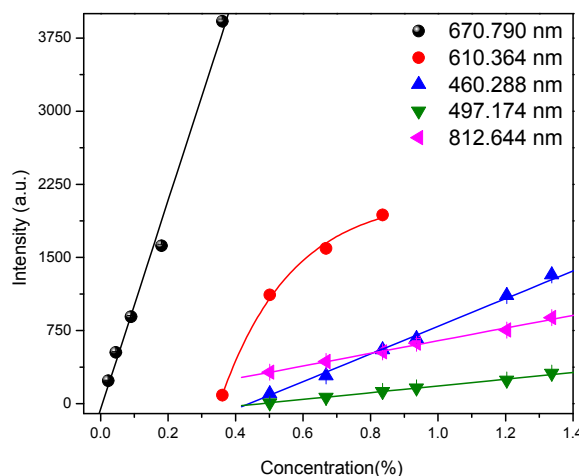


Figure 9. *Calibration curve of the Li emission lines in the complex mixture of organic.*

Chapter V

In this chapter, the development of a qualitative methodology using LIBS for rapid identification of different types of paper of various qualities, forms and sizes (e.g. will paper, badges, passports, credit cards etc.) for forensic applications is discussed. The application of parametric (linear) and non-parametric (rank) correlations for identification of several confidential papers in the Department of Atomic Energy (DAE), India using LIBS is discussed and demonstrated. YCR paper pages were collected for the last 10 years (1999–2008) for analysis. A spectral library of every years paper with known identification was prepared by analyzing with LIBS for the spectral range of 200–460 nm. For each of the unknown paper samples, similar to the library samples, ten LIBS spectra were recorded. Every spectrum consisted of 4096 data points, which were enough to permit statistical analysis like linear correlation and non-parametric rank correlation. Linear and rank correlation were obtained by using the following equations (Eq. No. 1 and 2)

$$r(\text{linear}) = \frac{\sum_i (x_i - \bar{x})(y_i - \bar{y})}{\sqrt{\sum_i (x_i - \bar{x})^2} \sqrt{\sum_i (y_i - \bar{y})^2}} \dots (1)$$

$$r(\text{rank}) = \frac{\sum_i (R_i - \bar{R})(S_i - \bar{S})}{\sqrt{\sum_i (R_i - \bar{R})^2} \sqrt{\sum_i (S_i - \bar{S})^2}} \dots (2)$$

where x_i and y_i are the intensity values of library spectrum and unknown LIBS spectrum respectively at wavelength λ_i . Here i varies from 1 to 4096. \bar{x} is the mean of x_i 's, and \bar{y} is the mean of y_i 's. In Eq. no (2), x_i is replaced by its corresponding ranks R_i . All the 10 LIBS spectra of each of the 10 unknown YCR papers were correlated with 10 library spectra and the average correlation coefficient values are shown in Fig. 10 for linear correlation.

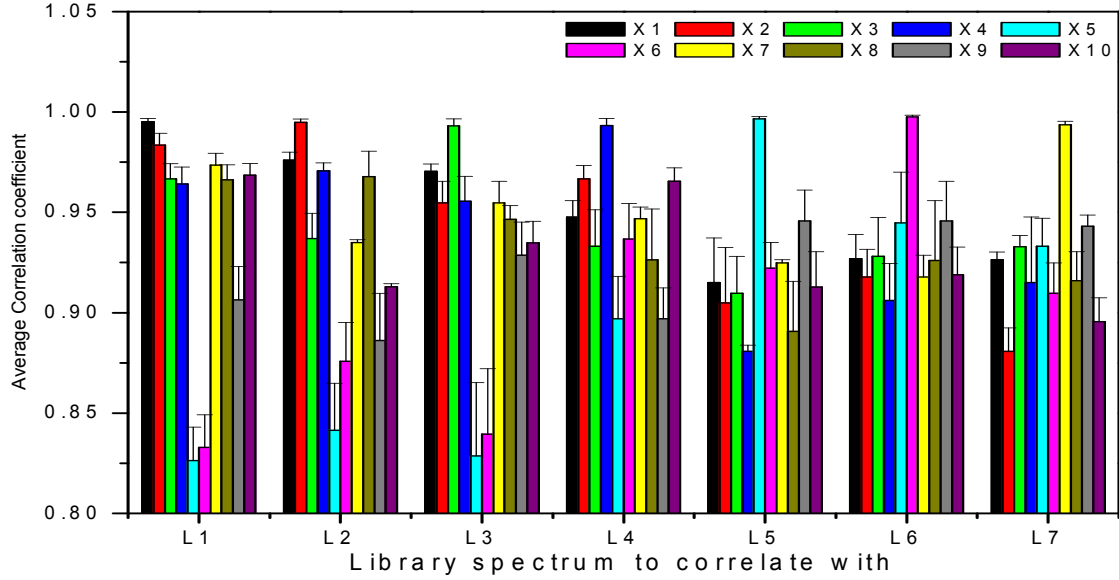


Figure 10. Linear correlation coefficients for the YCR papers.

From Fig. 10, it is clear that the identical pair of samples are (L1–X1), (L2–X2), (L3–X3) etc., which is 100% identification. To have more statistical weightage on the results, F-test and Student's t - test were performed. A statistical confidence of more than 99.6% was obtained by both the linear and rank correlation. The most attractive features of the technique are its simplicity, non-destructiveness, low cost and a good potential for identification of various kinds of paper, provided that the spectral library is available for the same variety of papers.

In summary, the important highlights of the work are as follows:

1. A novel methodology using LIBS was developed for the determination of U in (Th-U) oxide sample. The present method will be useful for fast and routinely verifying and checking the amount of uranium in mixed oxide samples of Th and U, without the need for dissolution, which is difficult and time consuming due to the refractory nature of ThO₂.
2. LIBS methodology was developed for trace characterization of 7 elemental impurities (Mg, Al, Ca, Ni, Fe, Cu and Mo) in thorium without any dissolution or removal of bulk of Th.
3. LIBS was successfully developed to quantify thorium (Th) and uranium (U) in solution individually as well as in a mixture using membrane-based filter paper as a sample support. The methodology gave results agreeing within 5% with the expected values. The LODs for Th and U were found in the range of a few ppmw to a few tens of ppmw.
4. LIBS was developed for the quantification of platinum group metals (PGM), namely Pd, Rh and Ru in simulated high level liquid nuclear-waste (SHLLW). The results agreed well with the expected values when the concentration of uranium was up to 700 ppmw, while positive bias was observed in the presence of larger amounts of uranium (above 700 ppmw). For such samples, satisfactory accuracy of the results was obtained after extraction of uranium with TBP.
5. LIBS was successfully applied to the determination of B in ground water samples of Gujarat and Tamilnadu present in ppmw level.
6. LIBS methodology was optimized for instant identification of confidential documents for forensic application by comparison with a spectral library data using linear and rank correlations. Both correlation methods yielded probabilities of correct identification close to unity for all the studied samples.

In conclusion, the work reported in this thesis has led to the development of several new methodologies using LIBS for characterization of material in different matrices that are important for nuclear science and technology.

The studies carried out during the present work and the methodologies developed have led to publications in peer reviewed International Journals (7) and the results were also presented in various International (4) and National Conferences (3).

List of Figures

Figure No.	Figure Caption	Page No.
Figure 1.1	Schematics of the interactions of laser with different pulsed widths on solid surfaces.	10
Figure 1.2	Sequence of events following the striking of a focused short laser pulse on the surface of a solid sample. e^- , I, m, m^* , represents free electrons, ionic species, molecular species, excited species, respectively.	11
Figure 1.3	Representation of basic principle of LIBS.	12
Figure 1.4	Generalized calibration curve with three regions of different sensitivity clearly evident.	26
Figure 1.5	Diagram illustrating the origin of self-absorption.	26
Figure 2.1	A schematic diagram of the experimental LIBS setup.	37
Figure 2.2	Photograph of LIBS system used in this study.	39
Figure 2.3	Energy level structure of the trivalent neodymium ion.	40
Figure 2.4	Fiber Optic Cable (FOC) connected with sample chamber (right) and spectrometer (left).	47
Figure 2.5	Design of fiber optics.	47
Figure 2.6	FOC's internal reflection mechanism.	50
Figure 2.7	Schematic diagram of a Czerny Turner Spectrograph.	50
Figure 2.8	Cross sectional view of a pixel of CCD (Red circles represent: holes; Green circles represent: electrons).	54
Figure 2.9	Arrangement of pixels in CCD.	54
Figure 2.10	Charge generation in CCD.	55
Figure 2.11	Transfer of charges.	55

Figure 2.12	Schematic overview of the temporal history of LIBS plasma. The delay and gate window are shown	56
Figure 3.1	Comparison of the spectra of Th and U with their mixed oxide standard under identical conditions of analyses.	66
Figure 3.2	Effect of laser fluence on the U(II) 367.007 nm emission line (TU - 4 – CAL).	67
Figure 3.3	Effect of acquisition delay on the U(II) 367.007 nm (TU – 4 – CAL).	70
Figure 3.4a	Calibration curve obtained for the lines U(II) 263.553 nm. The red line corresponds to the linear behavior of optically thin plasma	71
Figure 3.4b	Calibration curve obtained for the lines U(II) 367.007 nm. The red line corresponds to the linear behavior of optically thin plasma	70
Figure 3.4c	Calibration curves obtained for the lines U(II) 447.233 nm.	71
Figure 3.4d	Calibration curve obtained for the lines U(II) 454.363 nm. The red line corresponds to the linear behavior of optically thin plasma	71
Figure 3.5	Emission spectrum of ThO ₂ -S in the (a) 245 nm to 295 nm region and (b) 340 nm to 425 nm region with the emission lines of impurities (red line).	81
Figure 3.6a	Calibration curves obtained for different impurities in thoria by LIBS.	84
Figure 3.6b	Calibration curves obtained for different impurities in thoria by LIBS.	85

Figure 3.7	A comparison of LIBS results of six replicate determinations of Al concentration in thoria with certified concentration of (50±13) ppmw (Table 3.7).	86
Figure 3.8	Calibration curves obtained for different impurities in thoria by LIBS including out of line signal from ThO ₂ – MOS sample.	88
Figure 4.1	Sample loading procedure for solid surface analysis technique.	96
Figure 4.2	Carbon emission lines from Whatman – 42 membrane based filter paper	97
Figure 4.3	Emission spectra of U and Th obtained by LIBS under identical conditions of analysis.	101
Figure 4.4	Reproducibility of (a) Th(II) 401.913 nm (b) U(II) 367.007 nm line emission from ten measurements carried out using independent filter papers under the identical experimental conditions. The horizontal straight line represents mean value and the inset shows peak region used for integration.	102
Figure 4.5	Calibration curves of (a) U and (b) Th in aqueous solution fitted with polynomial equation. Error bars show standard deviation from multiple measurements at each concentration value.	105
Figure 4.6	Calibration curve of U-Th mixture in aqueous solution. Error bars show standard deviation from multiple measurements at each value.	108
Figure 4.7	Comparison of the spectra of the individual PGMs with the SHLLW - 2 under identical conditions of analysis in the emission range (a) 230 – 277 nm (b) 335 – 380 nm.	116

Figure 4.8	Variation of SNR of Pd(I) 324.270 nm with laser energy and acquisition time delay	119
Figure 4.9	Variation of SNR of (a) Rh(I) 369.235 nm and (b) Ru(I) 372.802 nm with laser energy and acquisition time delay	120
Figure 4.10	Normalized elemental emissions from LIBS as a function of concentration of Pd	122
Figure 4.11	Normalized elemental emissions from LIBS as a function of concentration of Rh.	123
Figure 4.12	Normalized elemental emissions from LIBS as a function of concentrations of Ru.	124
Figure 4.14	Effect of varying U concentration of the absolute and normalized intensities of Pd(I)276.309 nm and Ru(I) 372.802 nm emission lines.	129
Figure 4.15	LIBS spectrum of boric acid solution on a graphite planchet (laser fluence 50 J.cm ⁻² and acquisition delay 1.5 μs).	134
Figure 4.16	LIBS spectrum of graphite disk at a laser fluence of 50 J.cm ⁻² and acquisition delay of 1.5 μs.	134
Figure 4.17	The dependence of the SNR of the B(I) 249.773 nm emission line on laser fluence and acquisition delay.	138
Figure 4.18	Normalized boron emission intensity as a function of concentration of boron.	138
Figure 4.19	The dependence of the SNR of the Li(I) 670.79 nm emission line on laser fluence and acquisition delay.	147

Figure 4.20	Calibration curve of Li in organic mixture solution. Error bars show standard deviation from multiple measurements at each value.	148
Figure 4.21	Comparison of the Li concentrations determined for two sets of wash solution by different calibration lines.	149
Figure 5.1	Part of the LIBS spectra of four YCR papers used to develop library.	157
Figure 5.2	Linear and rank correlation plots for the sample L1 (library) vs. unknown X1.	159
Figure 5.3	Linear (a) and rank (b) correlation coefficients for the YCR papers. Arrows indicate samples showing the best correlation coefficients. If identification is correct, the indicated sample is the same as the library sample given on the x-axis.	161

List of Tables

Table No.	Table Caption	Page No.
Table 1.1	Historical development of laser induced breakdown spectroscopy	5
Table 1.2	Factors affecting quantitative analysis using LIBS	25
Table 1.3	Advantages and disadvantages of LIBS for direct spectrochemical analysis	30
Table 2.1	Typical Components of an LIBS System and their Functions	38
Table 2.2	Specifications of Tempest-10Hz Nd:YAG laser	40
Table 2.3	Characteristic of the detectors used in LIBS	53
Table 2.4	Details of all the components used in the present LIBS system	56
Table 3.1	Composition of the calibration standards and two synthetically prepared samples	63
Table 3.2	Characteristics of spectral lines employed for determination of U by LIBS.	63
Table 3.3	Parameters of Eq. (1) obtained by fitting calibrations curves and the correlation coefficients	72
Table 3.4	Comparison of analytical results for U determination in Th – U mixed oxide samples with expected values	72
Table 3.5	Concentrations of impurities (ppmw) in different thoria samples used for calibration in LIBS. The mean values and %RSD are taken from ILCE evaluation report	79
Table 3.6	Chosen emission lines and their spectroscopic data for various elements	81
Table 3.7	Elemental concentrations (in ppmw) in mixture of ThO ₂ – S and ThO ₂ -D mixed in a 3:1 amount ratio	86

Table 3.8	Comparison of LODs in ThO ₂ matrix with those reported in literature for UO ₂ and PuO ₂ matrix	87
Table 3.9	Excitation temperature created on different thoria samples placed in the simulated remote sensing analysis condition	87
Table 4.1	Concentrations of pure U and Th solutions prepared for analysis	96
Table 4.2	Concentrations of the pure U and Th solutions used to prepare mixtures for analysis	97
Table 4.3	Characteristics of Spectral lines employed for LIBS analysis of U and Th	100
Table 4.4	Trace elements in the Whatman – 42 membrane filter paper	100
Table 4.5	Fitted parameters obtained from calibration curves for U and Th using polynomial equation $y = a + bx + cx^2$	104
Table 4.6	Limits of detection for U and Th	106
Table 4.7	Comparison of analytical results of LIBS with expected values.	106
Table 4.8	Composition of SHLLW-1 used in present study (acidity 3M HNO ₃)	115
Table 4.9	Concentrations of added elements in other SHLLW used in the present study	115
Table 4.10	Composition of PGM mixtures with varying U concentrations	115
Table 4.11	Calibration parameters for spectral lines employed for LIBS analysis of Pd, Rh and Ru	117
Table 4.12	Comparison of analytical results for PGMs determination in a mixture of only three PGMs (PGM – 1) sample with expected values	126

Table 4.13	Comparison of analytical results for PGMs determination in two different SHLLW samples with expected values	126
Table 4.14	Comparison of analytical results for PGMs determination in SHLLW – 3, after TBP washing of sample, with expected values	127
Table 4.15	Characteristics of spectral lines employed for B determination by LIBS	137
Table 4.16	Concentrations of elements in ground water samples (giving spectral interference at boron emission lines in LIBS) determined by ICP-AES	137
Table 4.17	Fitted parameters obtained from calibration curves for B	140
Table 4.18	Comparison of boron concentration values determined by LIBS, in ground water samples with ICP-AES	140
Table 4.19	Limits of detection (LODs) of LIBS and those reported by other methods	141
Table 4.20	Comparison of detection limits for boron determination by LIBS	141
Table 4.21	Characteristics of Spectral lines employed for LIBS analysis of Li along with their fitted parameters obtained from calibration curves.	147
Table 5.1	Printed information on YCR papers used for generating of LIBS library	154
Table 5.2	Printed information on YCR papers used as unknown	154
Table 5.3	Linear correlation coefficient values when L4 was linearly correlated with spectra of X1 to X10 samples	160

Table 5.4a	Calculated probabilities that differences in YCR papers were detected using 50 shot-averaged library spectra using linear correlation	162
Table 5.4b	Calculated probabilities that differences in YCR papers were detected using 50 shot-averaged library spectra using rank correlation.	163
Table 6.1	F-test results between the set of r-values of L4 vs. X4 against the other r-values of different columns	169
Table 6.2	Student t-test results between the set of r-values of L4 vs. X4 against the other r-values of different columns	170

Introduction



Chapter I

1.1. INTRODUCTION

Analytical techniques are needed for the detection and quantification of major as well as trace elements in various matrices. As a result of increasing demands of electricity production by nuclear energy and the growing concern to protect the environment, there is growing need to develop and modify different analytical techniques and procedures to reduce the amount of waste generated. Techniques based on direct sample analysis, i.e., no or minimal sample preparation promote this goal of waste minimization and can be used in situ to provide a rapid determination of the elements. Atomic emission spectroscopy of laser induced plasmas is one such method, which not only analyses samples directly without any sample preparation, but can be used for several types of matrices such as solid, liquid, gas, aerosol, conducting, non-conducting, ceramics etc. The thesis presents the various developments carried out with experimental facility of LIBS (**L**aser **I**nduced **B**reakdown **S**pectroscopy) for in-situ characterization / monitoring of chemical composition of materials in solid or liquid phase applicable in nuclear industry, for environmental studies and in forensic sciences.

1.2. HISTORICAL SUMMARY

The acronym LIBS has a history almost parallel to the more popular acronym LASER (**L**ight **A**mplification by **S**timulated **E**mission of **R**adiation) with the difference that the former is about twenty years younger. The devastating power of the laser was demonstrated soon after its invention when a focused laser beam produced a bright flash in air similar to the spark produced by the lightening discharge between two clouds [1]. The production of sparks in air by a focused beam from a pulsed ruby laser was observed in 1963. The use of spark emission for elemental analysis became a reality only around 1983, due to the pioneering spectroscopic investigations of L. J. Radziemski and D. A. Cremer at Los Alamos National

Laboratory in U.S.A. They also coined the name Laser-Induced Breakdown Spectroscopy (LIBS) for this technique [2].

Prior to 1960, the ability to produce dielectric breakdown in gases had been known for at least 100 years. These discharges were produced in low-pressure gas tubes with or without electrodes, at frequencies in the range of hundreds of kilohertz (kHz) to a few tens of megahertz (MHz). Examination of the spectra from these sources reveals the atomic line emissions characteristic of the gas composition. In subsequent years, the breakdown of gases induced by frequencies of the order of gigahertz (GHz) was demonstrated at reduced pressures using microwave range electromagnetic fields. At atmospheric pressures, the electric field required for breakdown is of the order of tens of kilovolts per centimeter. At optical frequencies, the situation requires much stronger fields of the order of 10 MV/cm. Such strong fields are not attainable using conventional optical sources, thereby requiring a new light source. This new light source is LASER.

Einstein predicted the possibility of stimulated emission in 1917 [3], yet it took more than four decades to build the first laser (ruby laser) by Maiman [4] in 1960. Subsequently Brech and Cross [5] in 1962, for the first time, recorded the spectrum of luminous plasma using the ruby laser. Following this, in 1963, the development of a “giant pulse” or Q-switched laser was announced. This laser had the capability of producing high focused power density from single pulse of short duration sufficient to initiate laser induced breakdown and to produce analytically useful laser induced plasma (LIP). This was the “birth” of the LIBS technique and in subsequent years, significant milestones were reached in its development of the method. A list of some of the major milestones is given in Table 1.1 [6].

The first direct spectral analysis using LIBS technique can be attributed to Runge *et al.* in 1964 [7] and the first model for the laser induced breakdown of a gas was proposed

only one year later by Zeldovich *et al.* [8]. In 1963, Debras-Guédon *et al.* published the first analytical use for spectrochemical analysis of surfaces [9]. In the period from 1964 to 1967, the instruments based primarily on laser ablation with cross-excitation were developed by Zeiss (Germany), Jarrell-Ash (USA) and JEOL Ltd. (Japan). These instruments employed the energy of the laser pulse only to ablate the sample while excitation was made by an electric arc. The instruments could not typically compete in accuracy and precision with conventional spark spectroscopy, although they could handle nonconducting samples. Some instruments continued to be used through the 1990s. The advent of more stable, fast and robust lasers with better beam quality, high resolution/wide spectral range dispersion optics (such as the echelle based spectrographs), and sensitive gated image detectors based on arrays of intensified charge coupled devices (ICCD) provided strong motivation towards improving and applying LIBS since the beginning of the 80's [10, 11]. In 1984, the spectrochemical analysis of liquid sample was demonstrated by Cremers *et al.* [12]. As the field progressed into the 1990s, applications and fundamental studies developed rapidly. There were several useful reviews during this decade [13-16]. Later in the 1990s, the applications turned towards practical problems, such as monitoring environmental contamination, control of materials processing, sorting of materials to put them in proper scrap bins, and slurry monitoring. The last 30 years have witnessed the result of the efforts made by a number of companies and research laboratories towards the development of commercial instruments, of new applications and of theoretical models providing a profound insight into the fundamentals of LIBS and associated phenomena. In the last decade, the number of research papers related to fundamentals studies and applications of LIBS reached about 700 [17].

Table 1.1: *Historical development of laser induced breakdown spectroscopy [6]*

1960	First laser demonstrated.
1962	Brech and Cross demonstrate the first useful laser-induced plasma on a surface.
1963	The first analytical use involving surfaces, hence the birth of LIBS.
1963	First report of laser plasma in a gas.
1963	Laser micro-spectral analysis demonstrated, primarily with cross-excitation.
1964	Time-resolved laser plasma spectroscopy performed.
1966	Characteristics of laser-induced air sparks studied.
1966	Molten metal directly analyzed with the laser spark.
1970	Continuous optical discharge reported.
1970	Q-switched and non-Q-switched lasers used and results compared.
1972	Steel analysis carried out with Q-switched laser.
1980	LIBS developed for analysis of hazardous aerosols.
1980	LIBS used for diagnostics in the nuclear power industry.
1984	Analysis of liquid samples demonstrated.
1989	Metals detected in soils using the laser plasma method.
1992	Portable LIBS unit for monitoring surface contaminants developed.
1992	Stand-off LIBS for space applications demonstrated.
1993	Underwater solid analysis via dual-pulse LIBS.
1995	Demonstration of LIBS using fiber optic delivery of laser pulses.
1997	Use of LIBS for pigment identification in painted artworks.
1998	Subsurface soil analysis by LIBS-based cone penetrometers.
2000	Demonstration of LIBS on a NASA Mars rover.
2000	1st International conference on LIBS, Pisa, Italy.
2002	2nd International conference on LIBS, Orlando, FL.
2004	3rd International conference on LIBS, Malaga, Spain.
2004	LIBS approved for 2009 Mars mission.
2006	4th International conference on LIBS, Montreal, Canada.
2007	NASLIBS conference, New Orleans, LA.
2008	5th International conference on LIBS, Berlin, Germany.
2009	NASLIBS conference, New Orleans, LA, USA.

1.3. THE LIBS CONCEPT & RELATED PHENOMENA

1.3.1. Laser ablation

Ablation is the sampling process of the LIBS analytical technique when applied to solid or liquid samples [18]. It limits the amount of constituents (analytes) that will be detached from the sample by the laser pulse and introduced induced plasma. In fact, if a plasma is formed in a surrounding medium of gaseous species with high ionization potential (helium, for instance), the only way it can be sustained is by means of the presence of the ablated material. The ablation process is stoichiometric in nature, thus the ablated portion of the sample is true representative of the original sample.

Ablation has been the subject of many studies, whose prime objectives were to understand the relationship between the various instrumental parameters (pulse duration, laser wavelength, pulse irradiance and fluence), sample characteristics (thermal conductivity, thermal diffusivity, surface reflectivity, optical absorption coefficient, melting point and boiling point), environmental atmospheric composition and the amount of ablated material [19, 20]. Remarkable differences were observed when the pulse duration is reduced from nano- to pico- to femto-seconds [19]. Ultrafast (femto-second) lasers offer very high photon intensities ($>10^{15} \text{ W cm}^{-2}$) with a pulse duration shorter than many fundamental time scales (phonon vibrations). Laser ablation on the femto-second time scale is predominantly non-thermal, offering the potential to eliminate fractionation and matrix dependence. Femto-second ablation also provides no laser–plasma interaction [21] and gives higher efficiency. Since pico-second is the time scale of phonon vibration, hence the efficiency is much higher than ns – pulsed laser ablation, but sufficiently less than fs - pulsed width laser pulse ablation. Figure 1.1 gives the schematics of the interactions of laser with different laser pulse widths on solid surfaces. The μs and ns interactions proceed through heating, melting and

vaporization. Pulses shorter than the plasma initiation time lead to direct vaporization and the ability, for example, to drill holes with very high precision.

1.3.2. Formation of laser induced plasma (LIP)

The acronym LIPS and LIBS both can be found in literature for the same technique. Recently, it has been accepted that the acronym LIBS should be used [17]. The name of the technique does not include a “plasma” term. The main reason for this omission is the fact that LIBS is not always characterized by plasma formation. A Debye Number with value equal or higher than unity is not always observed in a LIBS experiment, which is essential criterion that need be fulfilled to be characterized as plasma. Therefore the acronym LIPS where the “P” states for “plasma” is not recommended,

The LIBS concept, which distinguishes the technique from others based on induced spectral emission, is that of using a laser pulse to ablate a minute quantity of the material to a condition that may then be excited by the energy supplied by the same pulse or by a subsequent pulse. The basic phenomena which need be considered to understand and control LIBS experiment for its development into a useful analytical tool are:

- (a) Phenomenon related with the laser interaction directly with the sample.
- (b) The laser interaction with the ablated material and coupling of its remaining laser pulse energy.

Figure 1.2 shows schematically what happens at and near the point where a short duration laser pulse (e.g. a few ns range) of sufficient energy strikes the surface of a solid sample. This initial interaction of the laser beam with a material depends on many characteristics of both the laser and the material e.g., on the duration, wavelength and irradiance of the laser pulse, the thermal properties of the target. The intense local heating

experienced by the target causes a rapid rise in the surface temperature of the material of about 10^{10} K s^{-1} [22]. Heat is conducted into the interior of the target and a thin molten layer forms below the surface [23]. As the thermal energy deposited at the surface increases, a point is reached where the deposited energy exceeds the latent heat of vaporization. When this happens, heat cannot be conducted away from the point of irradiation fast enough to prevent the surface reaching its boiling temperature and evaporation occurs from the surface. The surface temperature is then governed by the evaporation process and the main effect of heat conduction is to preserve a thin layer of molten material behind the evaporation front.

The energy density deposited at the surface of the target by an irradiance I is $I.t$, where t is the duration of the laser pulse. Hence the average energy per unit mass acquired by the thin layer of molten metal is $[I.t/\rho(\alpha t)^{1/2}]$, where ρ is the mass density of the target, α is the thermal diffusivity. For evaporation to occur, the energy deposited in this layer must exceed the latent heat of vaporization (L_v) of the target. Thus, the following threshold condition is obtained for the minimum absorbed irradiance (I_{\min}), below which no evaporation will occur, where “ a ” is thermal diffusivity (m^2s^{-1}) [24].

$$I_{\min} = \rho L_v \left(\frac{a}{t} \right)^{\frac{1}{2}} \quad \dots\dots(1.1)$$

For irradiances just above threshold, 10 to 100 GW m^{-2} (1GigaWatt = 1×10^9 Watt), evaporation from the liquid boundary layer proceeds at the normal boiling temperature of the material [23, 25]. Such low density vapors are virtually transparent to the incident laser beam, consequently little heating of the vapor occurs. Such low temperature vapors are of little use in spectrochemical analysis. At irradiances well above threshold, greater than about 1 PW m^{-2} (1PetaWatt = 1×10^{15} Watt), on the other hand, extremely dense, high temperature plasmas are formed which are primarily of interest in studies of laser induced fusion. Only plasmas

produced by irradiances between these two extremes (100 GW m^{-2} to 1 PW m^{-2}) are generally useful in LIBS.

For irradiances within the range specified above, the density is sufficient enough that the effects of laser absorption must be considered. This absorption is assumed to occur in a thin, dense, partially ionized layer which exists between the solid and vapor phases [24]. The electron density (n_e) within this layer approaches (up to a few ps) the critical electron density (n_c) which will prevent laser light reaching the target. The emitted light at this time would be primarily black body radiation from the hot dense gas. As the density falls below n_c , the vapor becomes highly absorbing and enters the so-called ‘self-regulating’ regime [23, 26]. In this regime, light is absorbed in the vapor by inverse bremsstrahlung resulting in heating and expansion, which in turn, reduces the vapor density. Laser light can now reach the target and evaporate more material, thereby increasing the vapor density once more. The process repeats itself till the existence of pulsed width and then it starts to cool and decay.

The mechanism of plasma initiation differs for different media. If the target material is a gas, seed electrons will be generated by multiphoton absorption or cascade ionization. Cascade ionization will start if, at least, one free electron is present in the path of the laser beam. This electron can be produced by the effect of cosmic ray ionization or by means of a breakdown induced in a gas impurity. This electron will gain energy by means of inverse bremsstrahlung [27]. The energetic electrons will induce, by collision, the ionization of other atoms whose electrons will continue to absorb energy from the laser, causing an exponential increase in the number of free electrons. Multiphoton absorption causes ionization if the sum of the energy of the absorbed photons is greater than the ionization potential of an atom. Only short wavelength photons can supply such energy since the ionization potential for most of the gases is greater than 10 eV.

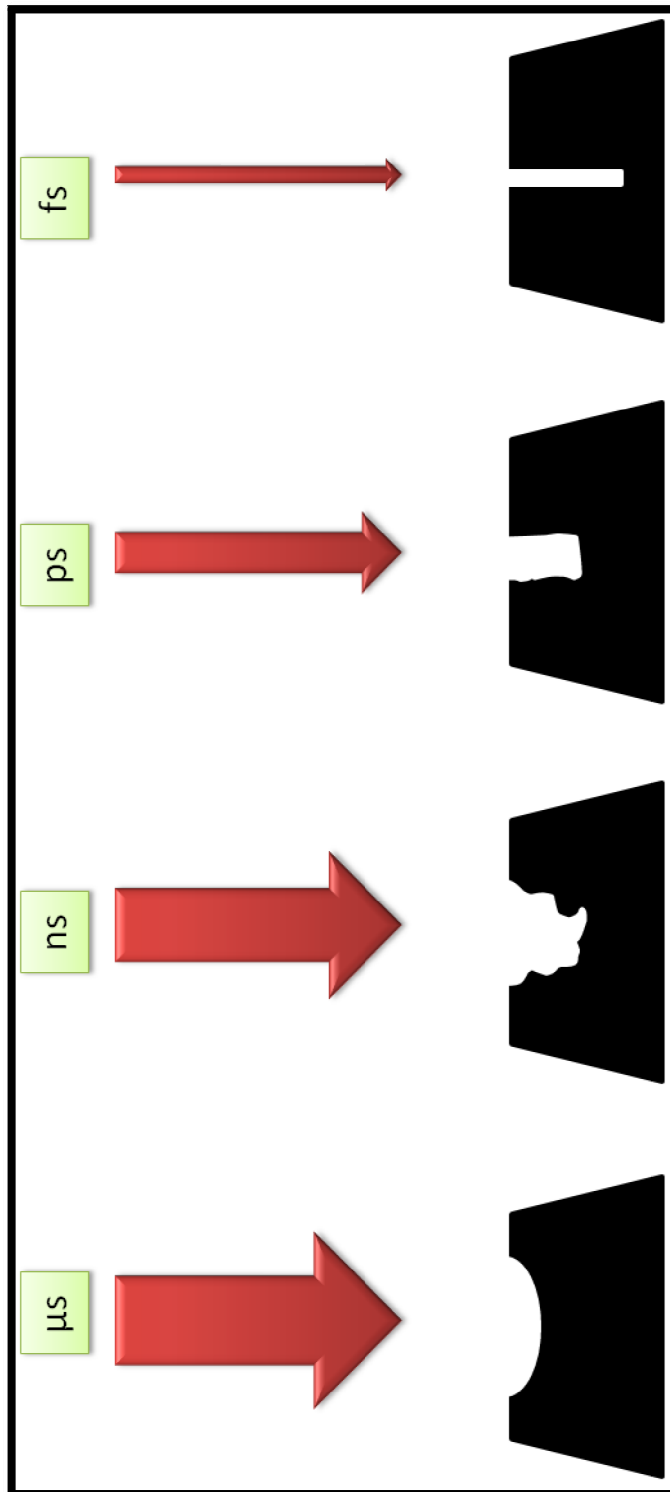


Figure 1.1: Schematics of the interactions of laser with different pulsed widths on solid surfaces.

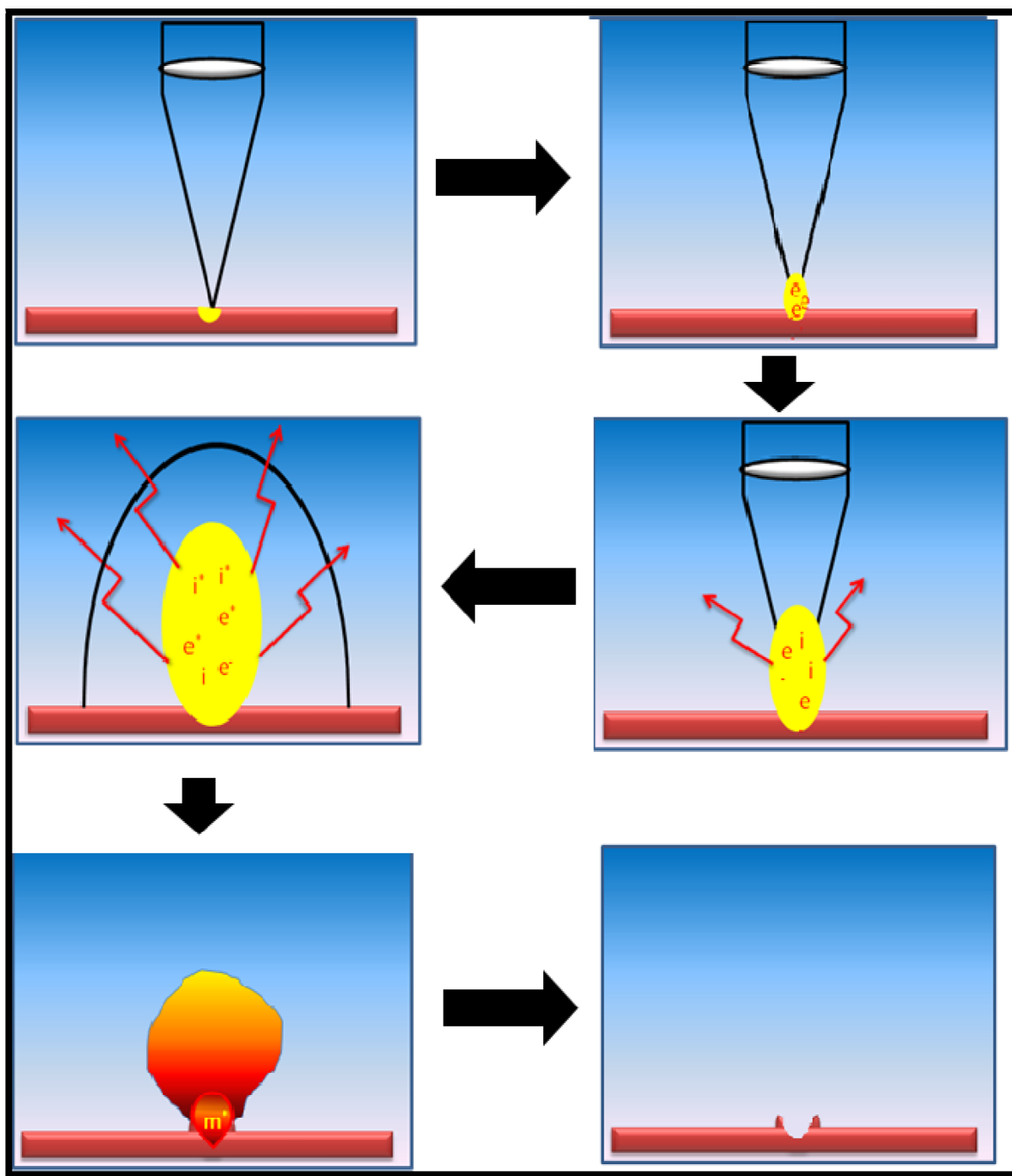


Figure 1.2: Sequence of events following the striking of a focused short laser pulse on the surface of a solid sample. e^- , I , m , m^* , represents free electrons, ionic species, molecular species, excited species, respectively.

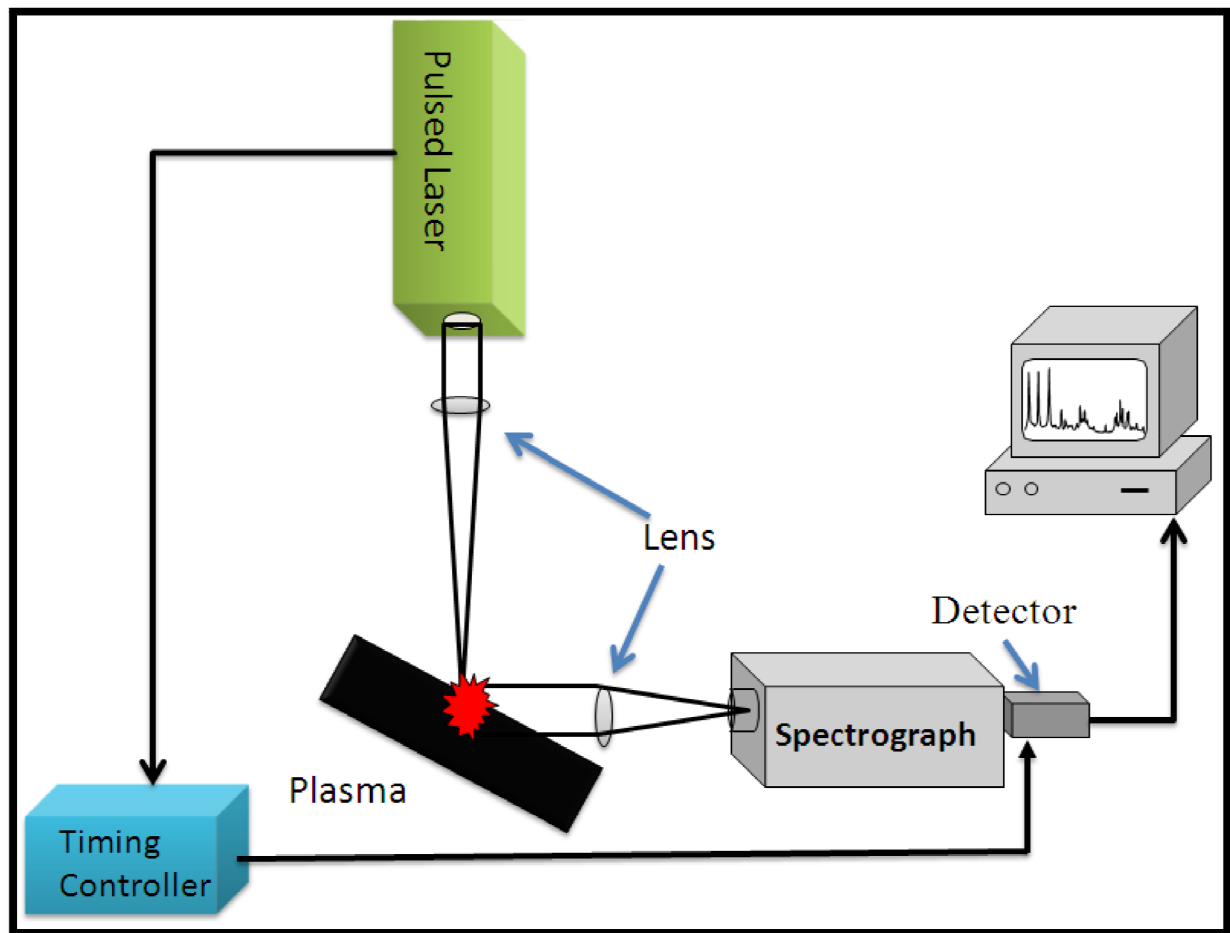


Figure 1.3: *Representation of basic principle of LIBS.*

In the case of liquid samples, the mechanism of breakdown is not as well known as in the case of gases. The liquid is treated as an amorphous solid and its electron movement is quite complex [28]. However, the formation of an initial number of free electrons is described by the same type of interactions, based on cascade ionization or multiphoton absorption.

For solid samples, their conductive (metallic) or nonconductive (isolator) nature is relevant to define the mechanism of initiation of the laser-induced plasma. For metallic samples, electrons of the conduction band absorb laser photons and the energy of excited electrons is dissipated by their collisions with the lattice of the material. This is a thermal conductivity phenomenon. In semiconductor and isolator solids, the creation of electron-hole pairs by multiphoton absorption, instead of the electron heating that occurs in metals and their recombination, among other electron-lattice interactions, is considered to be one of the main mechanisms of energy dissipation acting during the initialization of the plasma in this type of material [29].

1.3.3. Plasma growth & termination

LIBS is based on the analysis of spectral lines emitted from laser induced plasmas and thus is equivalent to atomic emission spectroscopy. The atoms spontaneously emit radiations as they revert back to lower energy state, with emission intensity being proportional to the concentration of the atoms present in the test samples [16, 30]. The basic principle of LIBS is illustrated in Figure 1.3. A pulsed laser is focused onto the surface of material of interest to produce a micro-plasma, which is a rich source of emission.

Although the creation of the initial breakdown plasma depends on the nature of the target samples, yet its further evolution does not depend on the target. The ablated material expands with supersonic velocities producing a shock wave, which propagates from the target

surface into the surrounding atmosphere. The plasma plume continues to absorb energy from the latter part of the laser pulse and different atomic species in the plasma emit electromagnetic radiation, which makes it luminous. As the expanding plasma cools down, recombination between electrons and ions generates neutral species and clusters after plasma extinction. A typical time interval between the initiation of the plasma and its extinction may vary from a few tenths of microseconds to a few milliseconds.

After the initial LIBS plasma formation, the plasma is commonly maintained by absorption of optical energy and electrons cascade breakdown. Electrons in laser field will gain energy through electron – neutral inverse bremsstrahlung collisions and will lose energy by elastic and inelastic collisions with the neutral particles through excitation of rotational and vibration degree of freedom of molecules and excitation of electronic states. While a few electrons will be lost by attachment, new electrons will be produced by ionization collisions. Once the LIBS plasma is formed, the growth is governed by the rate Eq. No. 1.2 [2].

$$\frac{dN_e}{dt} = \nu_i N_e + W_m I^m N - \nu_a N_e - \nu_R N_e + \nabla (D \nabla N_e) \dots (1.2)$$

where, D = electron diffusion coefficient; m = number of photons; N = number of atoms per unit volume; N_e = number of electrons per unit volume; ν_i = impact ionization rate; ν_a = attachment rate; ν_R = recombination rate; W_m = multiphoton ionization rate; I = laser irradiance.

The left term is the rate of change of the number of electrons with time. On the right side of the equation, the first term is the electron generation due to impact ionization. The second term is multiphoton ionization rate. The 3rd, 4th and 5th terms represent electron attachment, recombination and diffusion, respectively. The combination of the two source

terms (impact ionization, multiphoton ionization) and three sink term (electron attachment, recombination and diffusion) control the development of plasma.

In the initial stage of the plasma formation, the light coming from it is dominated by a “white light” continuum. This emission is caused by bremsstrahlung and recombination radiation from the plasma as free electrons and ions recombine. If the plasma emission is integrated over the entire life time of the plasma, this continuum light can seriously interfere with the weak characteristic spectral lines of minor and trace elements present in the target material. For this reason, LIBS spectra are recorded using time-resolved detection.

The laser induced plasma can be divided into three parts for a nanosecond laser pulse:

- a) The breakdown occurs during first part.
- b) The second part is the interaction of the latter part of the laser pulse with the plasma where its energy is used to maintain and heat the plasma. This step involves the motion of plasma front maintained by the laser irradiance, heating the plasma to a very high temperature, and absorption and reflection of laser beam by the plasma.
- c) The third part is the decay of the luminous plasma.

Thus, between its initiation and decay, the plasma evolves through several transient phases, which are well described by Root [31]. There are three models which describe the propagation and expansion of the plasma; laser-supported combustion (LSC), laser-supported detonation (LSD), and laser-supported radiation (LSR). At laser irradiances used in LIBS technique, the models that most closely match with experimental results are LSC and LSD.

1.3.4. Plasma shielding

The amount of residual pulse energy which reaches the sample surface plays an important role in plasma expansion. It is dependent on the reduction of laser energy by the

ablated matter and is called plasma shielding. If the plasma shielding occurs too early, the mass ablated may not be enough to produce a measurable analytical signal. The main process leading to plasma shielding is the absorption of laser energy by the electrons (inverse bremsstrahlung) and multiphoton ionization (mainly for shorter laser wavelengths). The presence of an easily ionizable gas increases the electron density in the plasma. For example, if the sample is placed in Ar (a gas with a low ionization potential) atmosphere, the plasma shielding is stronger than when it is in He (high ionization potential) atmosphere. The intensity of spectral lines of Cu in the LIBS spectra of pure metallic sample was enhanced by about 16 times when He is replaced by argon in the surrounding atmosphere [32].

The collective behavior of the optically dense plasma obtained at high power density defines a plasma resonant frequency, ν_p , given by Eq. (1.3)

$$\nu_p = \left(4\pi n_e e^2 / m_e\right)^{1/2} = 8.9 \times 10^3 (n_e)^{1/2} \dots (1.3)$$

where, n_e is the electron density (cm^{-3}) in the plasma, e is the electron charge, and m_e is the electron mass. There could be a critical electron density for which the plasma frequency equals the laser frequency ν_l , (i.e. $\nu_p = \nu_l$) causing the laser radiation to be strongly absorbed by the plasma. On the other hand when $\nu_l < \nu_p$, the laser radiation is reflected by the plasma. In both the conditions, the ablated mass from the sample is reduced.

1.3.5. Local thermodynamic equilibrium

The complex inter relationship between the spectral emission from a plasma and its constituents depends on the plasma being in thermal equilibrium with its surroundings. Because of the transitory nature of laser produced plasmas, atomic and ionic populations are rapidly varying functions of position and time, and the temperature of the plasma will show

this variation. Thus thermodynamic equilibrium can only be assumed to prevail for a given point and time in the plasma development. In fact, thermodynamic equilibrium is rarely complete, so a useful approximation, local thermodynamic equilibrium (LTE), has been adopted. This demands that the equilibrium occurs in the small region of space, although it may be different from region to region. For LTE to exist, collisions must dominate the other energy transfer processes (viz. radiative decay and recombination) establishing a Boltzmann distribution among the bound energy levels, since the radiative lifetimes of these levels tend to be short and their collisional cross-sections are small [33]. In a partially ionized vapor, electron collisions will be the dominant mechanism of energy transfer because of their high velocities and long-range coulomb interaction. However, the populations of the resonance levels of the major constituents of a plasma are nearly always established by radiative processes. Also, self-absorption and self-reversal can frequently occur for the resonance lines.

For LTE to exist, a criterion was proposed by McWhirter [34] based on critical electron density, which required collisional rates to be at least ten times of the radiative rates. For an energy gap difference of ΔE (eV) between the two neighboring states with an allowed transition, the criterion for LTE is:

$$N_e \geq 1.6 \times 10^{12} T^{1/2} (\Delta E)^3 \text{ cm}^{-3} \dots\dots\dots(1.4)$$

1.3.6. Plasma opacity

Fundamentally, plasma is optically thin when the emitted radiation traverses and escapes from the plasma without significant absorption or scattering. In other words, after the initial plasma decay and during all the observation interval, the LTE conditions are assumed to hold. The intensity of radiation emitted from a plasma is given by [6, 35]:

$$I(\lambda) = [\varepsilon(\lambda)/\alpha(\lambda)] \{1 - \exp(-\alpha(\lambda)L)\} \dots (1.5)$$

Where $\varepsilon(\lambda)$ is the emissivity, $\alpha(\lambda)$ is the absorption coefficient (cm), and L is the plasma length along the line of sight to the observer. When α is small, Eq. (1.5) can be written as

$$I(\lambda) = [\varepsilon(\lambda)/\alpha(\lambda)] [\alpha(\lambda)L] \approx \varepsilon(\lambda)L \dots (1.6)$$

which is the condition for plasma to be optically thin.

Some easy ways of checking for the optical thickness of a plasma is strong spectral lines of elements where it has well known relative intensities, determined either from atomic physics coupling theory or experimentally. When re-absorption becomes noticeable, the observed intensities will deviate from the expected values, the stronger lines effectively are saturated. In more extreme cases, a single line will appear to have a dip at the central frequency. In such a case, the line is said to be self-reversed [6, 36].

Due to the difficulty in determining the optical thickness without assuming strong approximations (plasma homogeneity, LTE etc.), when it is possible, transitions involving high energy levels should be selected for the spectral analysis in order to minimize the self-absorption problem and considering the LIP as a thin medium [6, 35, 36].

1.3.7. Plasma temperature

Under the LTE conditions in a plasma, the population of the energy levels for a particular species at a given position within the plasma is given by the Boltzmann equation [37]. The number of species N_i in the i^{th} excited state is given by

$$N_i^z = N^z \frac{g_i^z}{U^z(T_e)} \exp\left(-\frac{E_i^z}{k_B T_e}\right) \quad \dots\dots\dots (1.7)$$

Here ionization of the species is referred to by the superscript z. Neutral and singly ionized atomic species are represented by z=0 and z=1, respectively. N_i^z , N^z , E_i^z and g_i^z are the population density at ith level (m^{-3}), total population density (or number density) (m^{-3}), energy (Joule) of upper energy level and degeneracy or statistical weight factor (dimensionless) of the upper level of the species with ionization z, respectively. k_B is the Boltzmann's constant (J K^{-1}), T_e is the electron temperature (K) and $U^z(T_e)$ is the partition function of the species z at temperature T_e .

$$U^z(T_e) = \sum_i g_i^z e^{-E_i^z/k_B T_e} \quad \dots\dots\dots (1.8)$$

When an optical transition occurs between two levels of an atom or ion in a homogeneous optically thin plasma of unit dimension, then observed intensity (I_{ij}^z) of wavelength λ_{ij} of the species z, per unit solid angle, integrated over the line profile, and measured along the line of sight, in plasma can be written as

$$I_{ij}^z = N_i^z A_{ij}^z \frac{hc}{4\pi\lambda_{ij}} \quad \dots\dots\dots (1.9)$$

where h is the Planck's constant (J s^{-1}), c is the speed of light (m s^{-1}) in vacuum, A_{ij}^z is the Einstein's coefficient of transition probability for spontaneous transition from upper level i into lower level j of the species z. Substituting Eq. (1.7) and Eq. (1.8) in Eq. (1.9) gives

$$I_{ij}^z = N^z A_{ij}^z \frac{hc}{4\pi\lambda_{ij}} \frac{g_i^z}{U^z(T_e)} \exp\left(-\frac{E_i^z}{k_B T_e}\right) \quad \dots\dots\dots (1.10)$$

Taking the natural logarithm, Eq. (1.10) is transformed into:

$$\ln\left(\frac{I_{ij}^z \lambda_{ij}}{A_{ij}^z g_i^z}\right) = \ln\left(\frac{hc N^z}{4\pi U^z(T_e)}\right) - \frac{E_i^z}{k_B T_e} \quad \dots\dots\dots (1.11)$$

On plotting the left side of Eq. (1.11) against the upper level energy E_i^Z (Boltzmann plot), a straight line is expected, whose slope yields the temperature. For high accuracy, the range of upper level energies of the so-called Boltzmann plot should be as large as possible [37]. The accuracy of the measurement, however, largely depends on values of tabulated A_{ij}^Z coefficients; their error may be quite large and usually is in the range of 5% to 50%. The intensity values are the only factors affected by the experimental error. Temperatures achieved in LIBS plasmas are, of course, dependent on the energy deposition, hence the fluence and irradiance. For irradiance values of $\sim 10^{10}$ W/cm², the temperature is typically 15,000-20,000 K at early plasma lifetime.

1.3.8. Plasma electron density

Generally, the electron density (the number of free electrons per unit volume) grows linearly with time. In the collision-induced ionization process, free electrons in the focal volume are accelerated by the electric field of the laser and gain energy by colliding with neutral atoms. After the electrons have gained sufficient energy, they can ionize atoms by collision and this causes the electron density to grow exponentially with time. This process is dominant at high pressure of gases and long wavelength laser pulse ($\lambda > 1$ mm) [38 - 40].

Two spectroscopic methods are commonly used to measure the plasma electron density, n_e . The first requires measuring the Stark broadening of plasma lines; the second requires measuring the population ratio of two successive ionization states of the same element [39].

The electric field generated by fast moving electrons in the plasma perturbs the energy levels of the individual ions, thereby broadening the emission lines from these excited

levels. The Stark broadening of a well-isolated line is thus a useful tool for estimating the electron density, provided that the Stark broadening coefficient is known (by measurement or by calculation). For non-hydrogen neutral atoms and singly ionized atoms, the FWHM (full width at half maximum) due to Stark broadening of a line, expressions are given as follows [41]. For lines of neutral atoms:

$$\Delta\lambda_{1/2} = 2W\left(\frac{N_e}{10^{16}}\right) + 3.5A\left(\frac{N_e}{10^{16}}\right)^{1/4} \left[1 - \frac{3}{4}N_D^{-1/3}\right] W\left(\frac{N_e}{10^{16}}\right) A \dots\dots(1.12)$$

For lines of singly ionized atoms:

$$\Delta\lambda_{1/2} = 2W\left(\frac{N_e}{10^{16}}\right) + 3.5A\left(\frac{N_e}{10^{16}}\right)^{1/4} \left[1 - \frac{6}{5}N_D^{-1/3}\right] W\left(\frac{N_e}{10^{16}}\right) A \dots\dots(1.13)$$

W is the electron impact parameter (or half-width), A is the ion broadening parameter and N_D is the number of particles in the Debye sphere

$$N_D = 1.72 \times 10^9 \frac{[T_e(eV)]^{3/2}}{[N_e(cm^{-3})]^{1/2}} \dots\dots(1.14)$$

On the right of the Eq. (1.12) the first part is electron contribution to the Stark broadening and the second is the ion correction. Since Stark broadening of well isolated lines from neutral atoms is predominantly caused by electron impact, the expression can be simplified as:

$$\Delta\lambda_{1/2} \cong 2W\left(\frac{N_e}{10^{16}}\right) \dots\dots(1.15)$$

When the plasma is sufficiently close to LTE conditions, the electron density can be derived from the intensity ratio of two lines corresponding to different ionization stages of the same element (Saha-Boltzmann method) [6,39]. Saha equation relates the densities of subsequent ionization species for a temperature T_e [33]:

$$N_e = \frac{N^z}{N^{z+1}} \frac{2U^{z+1}(T_e)}{U^z(T_e)} \left(\frac{2\pi m k_B T_e}{h^2} \right)^{3/2} \exp\left(-\frac{E_\infty^z - \Delta E_\infty^z}{k_B T_e} \right) \dots\dots\dots (1.16)$$

Here, N_e is the electron number density, E_∞^z is the ionization energy of species z for an isolated system, ΔE_∞^z is the correction to this quantity for interactions in the plasma, and m is mass of electron (kg). The correction factor in the ionization energy is given by

$$\Delta E_\infty^z = 3z \frac{e^2}{4\pi\epsilon_0} \left(\frac{4\pi n_e}{3} \right)^{1/3} \dots\dots\dots (1.17)$$

From Eq. (1.10), the emitted intensity ratio of two emission lines from two species of two different states of ionization can be written as:

$$\frac{I_{ij}^{z+1}}{I_{ij}^z} = \frac{N^{z+1}}{N^z} \frac{A_{ij}^{z+1} g_i^{z+1}}{A_{ij}^z g_i^z} \frac{\lambda_{ij}^z U^z(T_e)}{\lambda_{ij}^{z+1} U^{z+1}(T_e)} \exp\left(\frac{E_i^z - E_i^{z+1}}{k_B T_e} \right) \dots\dots\dots (1.18)$$

Eq. (1.18) can be rearranged as:

$$\frac{N^z}{N^{z+1}} = \frac{I_{ij}^z}{I_{ij}^{z+1}} \frac{A_{ij}^{z+1} g_i^{z+1}}{A_{ij}^z g_i^z} \frac{\lambda_{ij}^z U^z(T_e)}{\lambda_{ij}^{z+1} U^{z+1}(T_e)} \exp\left(\frac{E_i^z - E_i^{z+1}}{k_B T_e} \right) \dots\dots\dots (1.19)$$

Incorporating Eq. (1.19) in Eq. (1.16), the expression of electron density can be written as:

$$N_e = \frac{2I_{ij}^z}{I_{ij}^{z+1}} \frac{A_{ij}^{z+1} g_i^{z+1}}{A_{ij}^z g_i^z} \frac{\lambda_{ij}^z}{\lambda_{ij}^{z+1}} \left(\frac{2\pi m k_B T_e}{h^2} \right)^{3/2} \exp\left(\frac{E_i^{z+} - E_i^{z+1} - E_\infty^z - \Delta E_\infty^z}{k_B T_e} \right) \dots\dots\dots (1.20)$$

All the right hand side parameters in the Eq. (1.20) can either be measured or obtained from compilation of atomic properties.

1.4. QUANTITATIVE ANALYSIS

The ultimate goal of any analytical technique is to provide quantitative data with high precision and accuracy. Several ways have been proposed to obtain quantitative information from LIBS measurements. One possible approach is to determine the concentration of each element independently by working with elemental emission lines of

accurately known transition probabilities and making absolute measurements of the integrated intensities [6, 42].

The most common approach is to measure the LIBS intensities in relation to known calibration standards. This approach is generally the most practical for extracting quantitative information on sample composition, despite the fact that the laser material interaction is highly matrix dependent and, therefore, variations in the matrix between the unknown sample and the standard must be minimal [6, 42].

In LIBS analysis, there are many parameters that affect the precision and accuracy of a measurement. Some of these can be controlled, such as the stability of the laser pulse energy, and others are dependent on the sample and sampling procedure over which there may not be a high degree of control. The advantage of LIBS, viz. materials can be sampled directly with little or no sample preparation, is also a challenge to the method because the physical and chemical properties of the sample can have a strong effect on the ability to obtain quantitative data. A list of important parameters that affect LIBS analysis is presented in Table 1.2.

1.4.1. Calibration curves

Calibration has been an important issue since Cremers *et al.* first demonstrated the ability of LIBS for detection of atomic species from aerosol samples [12]. For quantitative analysis, a calibration curve of instrument response (e.g. element signal) versus absolute mass (gram, nanogram, etc.) or concentration (% , part per-million or ppm) of the element to be detected is usually prepared. Ideally, there will be a linear relationship between the element response and the mass or concentration over the entire range investigated and a linear fit to the data would pass through the origin. This approximation can be

considered satisfactory only if all parameters affecting the plasma characteristics (including the sample morphology and composition) are constant during calibration and measurement. In this case, the distribution of the elements among the different excitation can be assumed and ionization states remains the same. Also, in the best case, the signal will double in magnitude if the concentration doubles. Actual calibration curves deviate from these ideal qualities. Nonlinear behavior is sometimes observed at the lower and higher concentrations [6, 43].

The slope of the calibration curve at a certain concentration is termed the sensitivity and it is the change in signal for a given incremental change in the concentration (or mass). The calibration curve shown in Figure 1.4 presents a typical calibration curve with a loss of sensitivity at high and low concentrations, on either side of the central linear region. The loss of sensitivity or flattening of the curve, at low concentrations can be due to [6, 39]:

- (a) A spectral interference of the analytical line with the concentration of the interfering species remaining constant as the analyte concentration decreases.
- (b) A constant background concentration of the analyte being determined that is not included in the stated concentration of the analyte.
- (c) Incorrect determination of the analyte signal so that a portion of the background signal is included in what is assumed to be only the analyte signal.

The loss of sensitivity at high concentrations is most often due to 'self-absorption'. Self absorption typically is observed in those emission lines in which the lower level of the transition is the ground state or close to the ground state. Because transitions are element specific and quantized or of a specific wavelength, a given species has the highest probability of re-absorbing a photon emitted by a member of the same species.

Table 1.2: *Factors affecting quantitative analysis using LIBS*

	Source	Factor	Comments
1.	Laser	Laser pulse energy, laser pulse power, repetition rate	Typically stable to within a few percent for constant temperature operation
2.	Detector	Detector gain	Keep constant or calibrate response, if gain is changed
		Linearity of response	Operate in region of linear response or change gain to maintain linearity
3.	Sampling parameters	Lens-to-sample distance	May be maintained through an automated focusing system; less problem with longer focal lengths; use of a collimated beam to form the plasma can minimize effects
		Changes in optical path transmission to/from sample	Absorption/scattering of laser pulse over optical path to sample by gases and aerosols
		Change of atmosphere above sample	Gas pressure and composition affect ablation and plasma properties
4.	Sample	Uniformity of composition	Sufficient averaging to obtain representative sample
		Uniformity of surface	Sufficient averaging to obtain representative sample

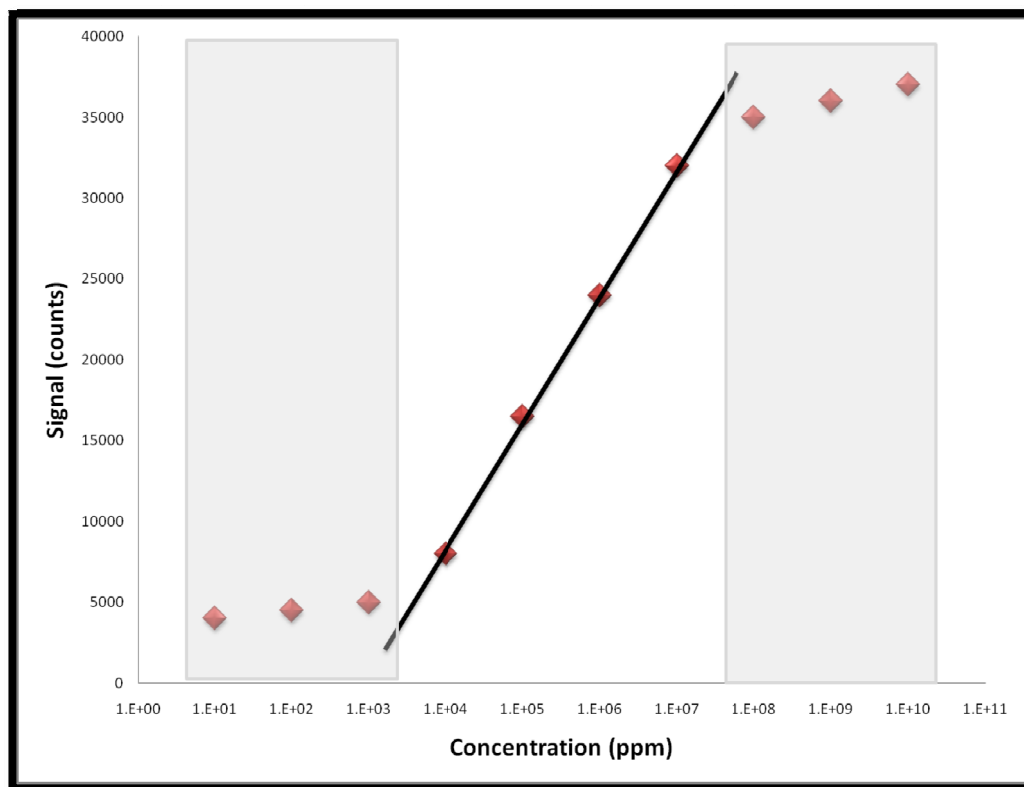


Figure 1.4: Generalized calibration curve with three regions of different sensitivity clearly evident [6].

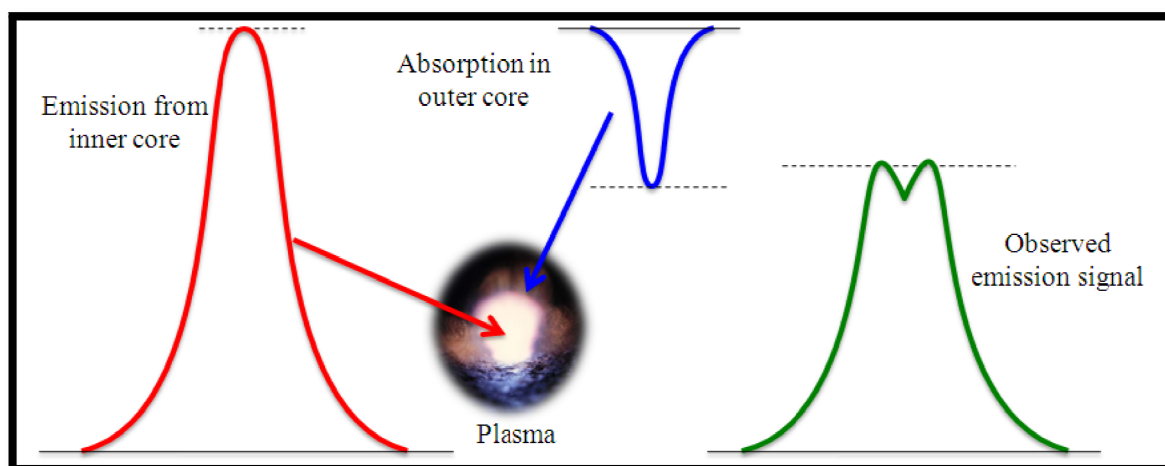


Figure 1.5: Diagram illustrating the origin of self-absorption.

Because of the high density of atoms in the microplasma and its characteristically high temperature and electron density gradients, the outer layer of the plasma will be populated by 'cool' atoms, residing mostly in the ground state. The central core of the plasma will contain a higher density of excited atoms. As these atoms decay to the ground state, the emitted photons corresponding to the resonance transitions will have a high probability of being absorbed by the 'cooler' atoms in the outer layers, thereby reducing the observed intensity of the emission line. As the concentration of the atoms in the target sample increases, the number of 'cooler' atoms in the outer layer increases and self-absorption becomes evident [6]. Figure 1.5 illustrates the origin of self-absorption pictorially.

A loss of sensitivity in the calibration curve can also be due to saturation of the detector response, that is, the intensity of light upon the detector is so large that there is no longer a linear response of the detector signal to the change in light intensity. In the linear operating regime of the detector, a change in the incident light intensity by x% should change the output signal by x%. This is most often evaluated using a neutral density filter to reduce the light intensity by a known amount and monitoring the resulting signal.

1.4.2. Limit of detection (LOD) in LIBS

According to IUPAC, 1997 definition the limit of detection is defined as [44]:

“The limit of detection, expressed as the concentration, c_L , or the quantity, q_L , is derived from the smallest measure, x_L , that can be detected with reasonable certainty for a given analytical procedure. The value of x_L is given by the equation”

$$x_L = \bar{x}_{bi} + ks_{bi} \dots\dots(1.21)$$

where \bar{x}_{bi} is the mean of the blank measures, s_{bi} is the standard deviation of the blank measures, and k is a numerical factor chosen according to the confidence level desired.”

Because the relationship between the measure (or signal) and the concentration (or mass) is given by the slope of the calibration curve $m = \Delta c_L / \Delta x_L$, we have $c_L = c_{bi} + k s_{bi} m$ but c_{bi} typically zero (no analyte concentration in the blank sample) so that $c_L = k s_{bi} m$. This is the formula that is often used to compute the LOD with $k = 3$. Ideally, $k = 3$ value would correspond to a confidence level of 95% but because s_{bi} is determined from a small number of measurements, a 90% confidence level is more reasonable. The detection limit should be considered as the minimum amount of the analyte that can be present and be determined to be present, rather than the minimum amount of the sample that can be actually measured. LOD can be affected by many measurement parameters such as laser pulse energy and the values of time delay and gate width used for detection as well as sample characteristics [45].

1.5. ADVANTAGES & LIMITATIONS OF LIBS

The principal advantages of LIBS over conventional analytical techniques, such as Inductively Couple Plasma Atomic Emission Spectrometry (ICP-AES), Inductively Couple Plasma Mass Spectrometry (ICP-MS) and Graphite Furnace Atomic Absorption Spectroscopy (GFAAS) are its simplicity, the sampling speed, and requirement of least sample preparation [38].

In particular, the required sample size, analysis time, and sample manipulation are minimal. The most appealing quality of LIBS is the suitability for remote and in situ applications. First, LIBS instrumentation is readily adaptable to field portable configurations due to simplicity of operation and compact size. Although most units used for LIBS research are user-assembled, several commercial instruments are presently available [38].

A few field portable instruments have also been developed over the years in various research laboratories. Since LIBS is a laser based technique, only optical access to a sample

is required for analysis. LIBS offers the ability to transfer the laser energy through an optical fiber to ablate a remote sample, then transport the resulting emission back through the fiber to a remote spectrometer while keeping the sample free from contamination and the analyst isolated from potentially harmful environments. In applications to radioactive environments, in situ analysis is preferred since the samples present a hazard to the analyst and are subject to stringent regulations regarding transport, storage, and disposal [39, 42, 46]. Although LIBS offers many features that have driven development over the years, distinct problems with LIBS analysis have been documented including material specific laser-sample interactions, nonlinear calibrations, low sensitivity, and concerns associated with sample heterogeneity on the micro-scale [46].

Sensitivity in remote analysis may also be limited by damage thresholds of the optical fiber. In addition, a tremendous portion of the emitted radiation is masked by the bright continuum background requiring time gating for reasonable signal to noise ratios. Furthermore, plasma generation in liquids presents several problems. For example, the strong splashing and sloshing of the liquid produced by the shock waves generated by powerful laser pulses [39]. For high repetition lasers, this behavior induces a relevant change in the position of the surface with respect to the laser focus, which in turn produces adverse effects in the statistical treatment of the data. In addition, the luminous phase of the plasma is rather short and the spectral lines originating from transitions between high-energy states are severely reduced. Specific advantages and disadvantages of LIBS for direct elemental analysis over conventional atomic spectroscopic techniques are summarized in Table 1.3.

Table 1.3: *Advantages and disadvantages of LIBS for direct spectrochemical analysis*

LIBS: Advantages	
1)	As only a minute amount of sample (~0.1µg to 1mg) is consumed during the LIB process without destroying the whole material, the technique is essentially non-destructive or minimally-destructive, and with an average power density of less than one watt radiated onto the specimen, there is almost no specimen heating surrounding the ablation site.
2)	The need for little or no sample preparation results in increased throughput, fewer opportunities for contamination to occur and a reduction of tedious and time-consuming procedures (however, this can lead to inaccuracy through contamination).
3)	Versatile types of matrices such as solid, liquid, gas, aerosol etc. all can be analyzed, including both electrically conducting and non-conducting materials.
4)	Permits analysis of extremely hard materials that are difficult to digest or dissolve, e.g. ceramics, glasses and superconductors.
5)	Local analysis in micro-regions offers a spatial resolving power of 1-100 µm.
6)	Simultaneous multi-elemental analysis can be carried out.
7)	The direct determination of aerosols or ambient air is possible.
8)	The analysis is simple and high-speed (ablation and excitation processes are carried out in a single step). LIBS gives results within seconds, making it particularly useful for high volume analyses or on-line industrial monitoring.
9)	LIBS is an entirely optical technique. Therefore, it requires only optical access to the

specimen. This is of major significance as fiber optics can be employed for remote analyses. Being an optical technique, it is non-invasive, non-contact and can even be used as a stand-off analytical technique when coupled to appropriate telescopic apparatus.
10) The remote sensing capability is significance for use in areas from hazardous environments to space exploration.
11) LIBS systems can easily be coupled to an optical microscope for micro-sampling adding a new dimension of analytical flexibility.
12) Underwater analysis is possible.
13) Development of field instruments is possible.
14) Remote capabilities.
15) Cleaning shot capability of LIBS.
16) Large dynamic range for trace analysis.
17) One of the major advantages of the LIBS technique is its ability to depth profile a specimen by repeatedly discharging the laser in the same position, effectively going deeper into the specimen with each shot.
18) LIBS does not use ionizing radiation to excite the sample, which is both penetrating and potentially carcinogenic.
19) The direct determination of aerosols or ambient air is possible.
20) The analysis is simple and high-speed (ablation and excitation processes are carried

out in a single step). LIBS gives results within seconds, making it particularly useful for high volume analyses or on-line industrial monitoring
21) LIBS is an entirely optical technique. Therefore, it requires only optical access to the specimen as fiber optics that can be employed for remote analyses. Being an optical technique, it is non-invasive, non-contact and can even be used as a stand-off analytical technique when coupled to appropriate telescopic apparatus.
LIBS: Disadvantages
1) Current systems are expensive and complex.
2) Obtaining suitable matrix-matched standards is difficult, which makes the technique qualitative or at best semiquantitative.
3) Interference effects can be large (including matrix interference and, in the case of LIBS in aerosols, the potential interference of particle size).
4) Detection limits are generally 1–100 times poorer than conventional techniques. The detection limits for LIBS vary from element to element depending on the specimen type and the experimental apparatus used. Detection limits of 1 to 30 ppm by mass are common, but can range from >100 ppm to <1 ppm.
5) Poor precision, typically 5-10%, depending on the sample homogeneity, sample matrix and excitation properties of the laser.
6) Safety measures are required to avoid ocular damage by the high-energy laser pulses.

1.6. SCOPE OF THE PRESENT WORK

The main emphasis of the present thesis is the development of laboratory based LIBS methodology for the material characterization needed in the various fields of research and development in nuclear industry, environmental studies and forensic applications. The thesis is divided into five Chapters with optimization of experimental parameters for the precise and accurate qualitative and quantitative measurements of both bulk and trace constituent present in matrices from different part of nuclear fuel cycle. Besides the successful demonstration of this technique for characterization of different elements in both solid and liquid matrices, the investigation of high concentration high atomic mass elements for quantification of other elements was studied in the present thesis. A qualitative approach to identify origin of paper used as confidential report papers in the Department of Atomic Energy (DAE), India by statistical methods is also an important part of this thesis. The organization of the present thesis is as follows:

Chapter I: A brief description of LIBS and its historical development, basic concept, fundamentals and a review of LIBS' unique advantages and disadvantages are documented in Chapter I.

Chapter II: This Chapter consists of the details of the instrument employed and their working principles.

Chapter III: Determination of trace as well as bulk constituents in nuclear fuel materials is very important part of chemical quality assurance.. Specification limits have been laid down for various impurities in different nuclear fuels.

This chapter deals with the application of LIBS for material characterization in solid matrix. This chapter discusses both the (i) bulk characterization and (ii) trace characterization of nuclear materials.

Chapter IV: This Chapter discusses the development of analytical methodologies using LIBS for the quantification of elements in liquid matrix. In the present work, a different approach without modifying the present equipment setup was tried and will be discussed.

This Chapter has been sub-divided according to the region of Periodic Table from where the elements are selected – (i) high atomic number (Z) elements (U and Th) (ii) middle Z elements (Ru, Rh and Pd) (iii) low Z elements (B and Li).

Chapter V: In this Chapter, the development of a qualitative methodology using LIBS for rapid identification of different types of paper of various qualities, forms and sizes (e.g. will paper, badges, passports, credit cards etc.) for forensic applications is discussed. The application of parametric (linear) and non-parametric (rank) correlations for identification of several confidential papers in the Department of Atomic Energy (DAE), India using LIBS is discussed and demonstrated.

Instrumentation



Chapter II

2.1. LIBS INSTRUMENTATION

LIBS is a plasma based method of emission spectroscopy. A schematic diagram of the experimental setup is shown in Figure 2.1. Typical components of an LIBS system and their functions are explained in Table 2.1.

For the present work, Spectrolaser 1000M, from Laser Analysis Technologies (now known as XRF scientific), Victoria, Australia was used. Figure 2.2 shows a photograph of the Instrument used. The LIBS instrument is an integrated analysis system comprising an excitation laser, optical fibers, optical spectrograph, and charge-coupled-device (CCD) array camera and is fully software controlled through a PC. The details of each and every part of the integrated system are discussed in below.

2.1.1. Lasers

A high power pulsed laser of short duration is used to produce luminous plasma in laser induced breakdown spectroscopy. The high power can be achieved by means of pulsed and Q-switched lasers. A number of lasers have been employed for LIBS. These include (i) Nd-YAG laser both fundamental (1064 nm) and its harmonics (532 nm, 355 nm & 266 nm) (ii) Excimer lasers such as XeCl (308 nm), KrF (248 nm) and ArF (194 nm) (iii) CO₂ laser (10.6 μ m) etc. Due to certain advantages of separating the plasma heating from sample evaporation, multi pulse lasers are being developed. The pulse widths of the lasers typically employed for LIBS are in the range of 5 to 20 ns. Lasers having their pulse width in the region of pico-second as well as femto-second have also been employed for LIBS measurements. In the present instrumental set-up, a Nd-YAG laser of fundamental frequency (1064 nm) with 7 ns pulse width from *New Wave Research, Inc.*, USA, Model No. *Tempest-10Hz* was used. Table 2.2 summarizes the specifications of the laser.

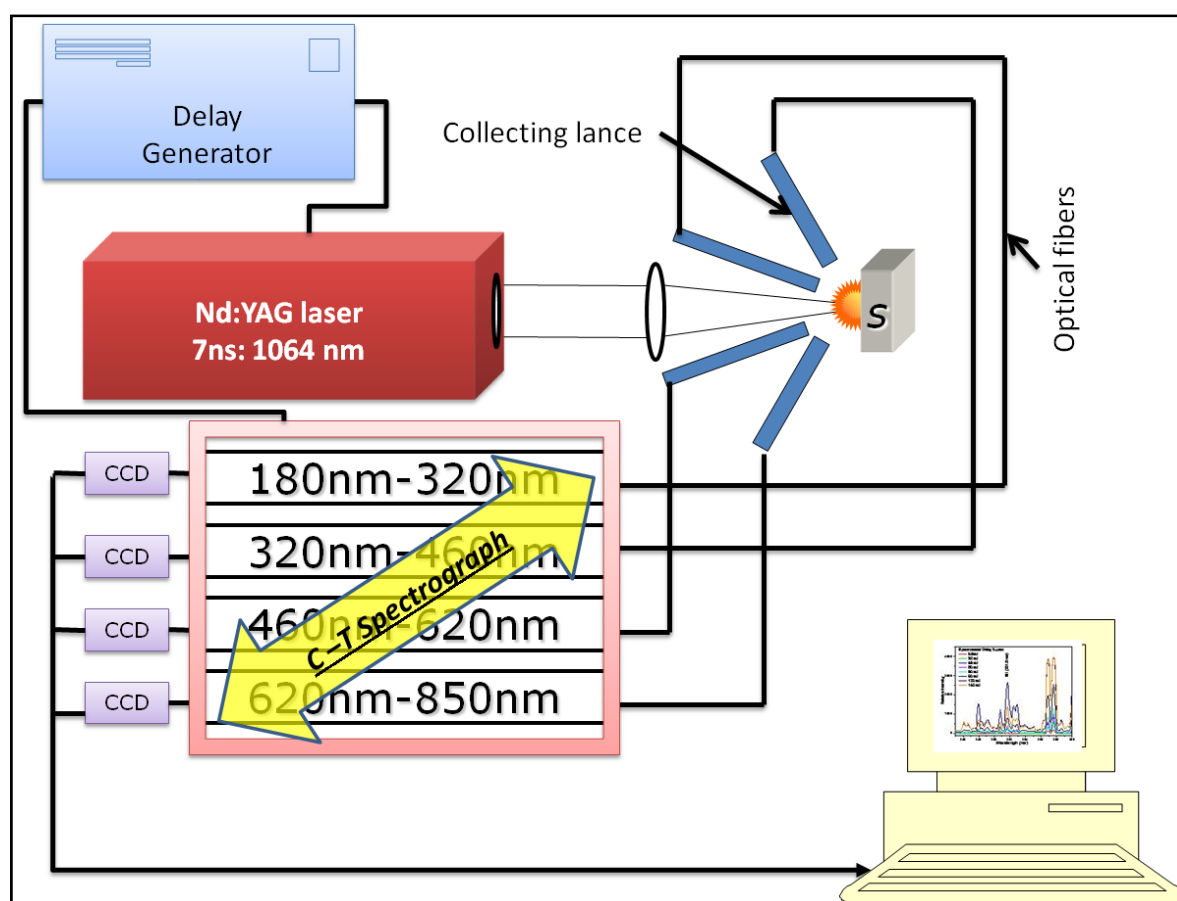


Figure 2.1: A schematic diagram of the experimental LIBS setup

Table 2.1: *Typical Components of an LIBS System and their Functions*

Component	Function
Pulsed laser	Generates the powerful pulse to create a micro-plasma on the surface of the sample.
Sample chamber	For placing the sample at a particular geometry reproducibly with suitable movement for bringing fresh sample surface for individual laser shots; air tight arrangement for use under vacuum or under different gaseous atmosphere.
Focusing system	The focusing system consisting of lens to focus the laser pulse on the target sample and provide sufficient fluence for the formation of micro plasma.
Collection system	The spectral emission from the plasma is collected and transported through fiber optic to the detection system.
Detection system	The detection system consisting of grating to spectrally filter or disperse the light.
Detector	Such as charge coupled devices (CCDs) for recording the spectra.
Control electronics	For suitably controlling the gating of the detection system, storage of the spectrum for further analysis etc.
Software	For spectrum analysis and calculations.

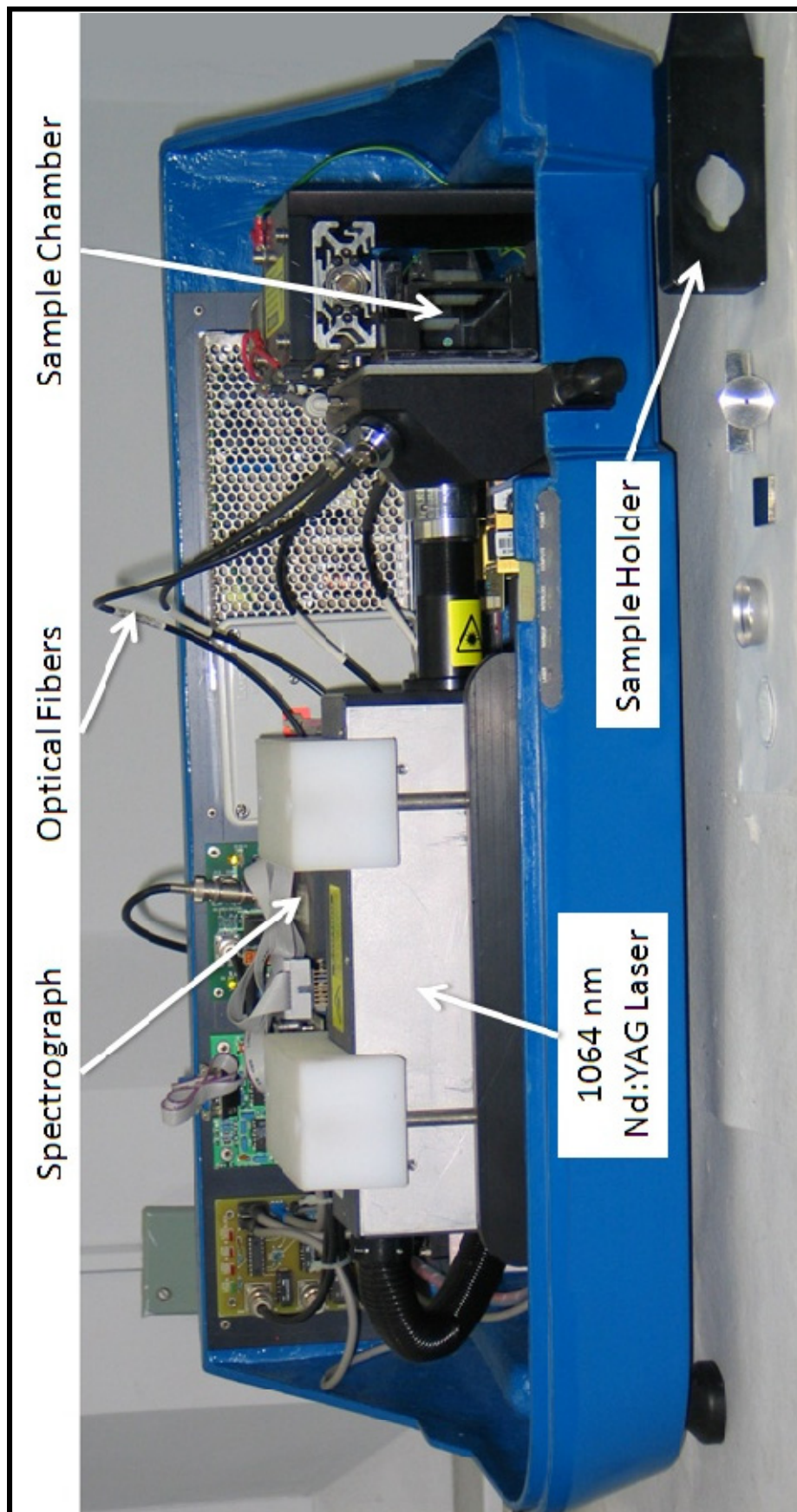
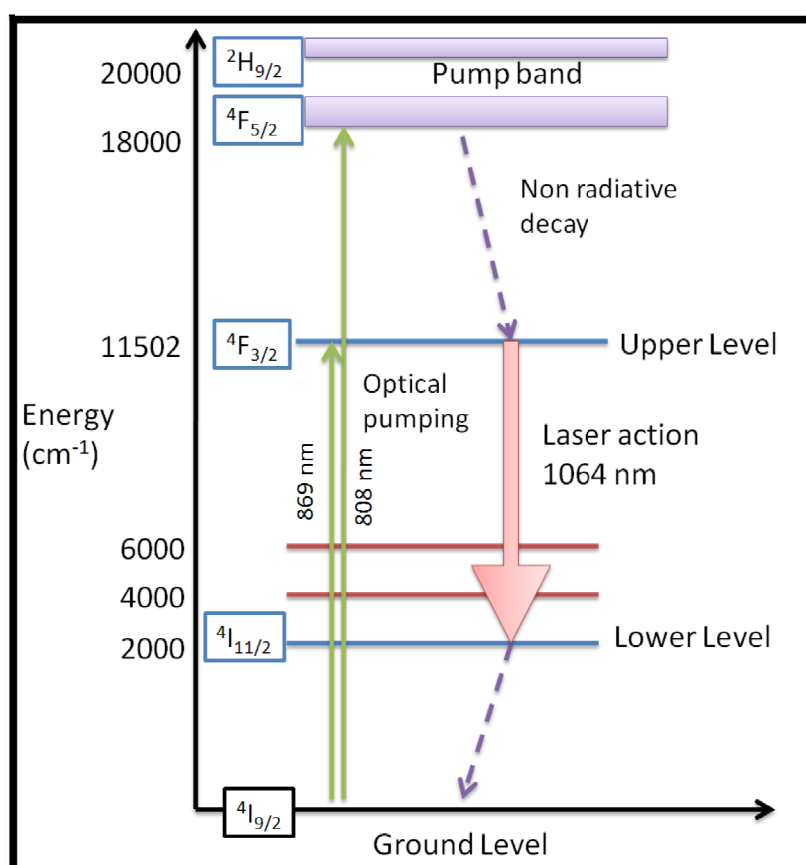


Figure 2.2: Photograph of LIBS system used in this study.

Table 2.2: *Specifications of Tempest-10Hz Nd:YAG laser*

Description	Tempest-10Hz
Emission Line	1064 nm
Maximum Energy	200 mJ
Energy Stability	$\pm 2\%$
Pulse width	7 nano second
Beam Divergence	< 1 mrad
Beam Pointing stability	< 200 μ rad
Beam diameter	5 mm
Repetition rate	Variable; maximum upto 10 Hz

**Figure 2.3:** *Energy level structure of the trivalent neodymium ion.*

Nd:YAG is basically Yttrium Aluminum Garnet ($\text{Y}_3\text{Al}_5\text{O}_{12}$), where the rare earth dopant ion (Nd^{3+}) substitutes for Yttrium (Y^{3+}) in the crystal lattice. For laser gain applications, YAG is typically doped with Nd^{3+} at the 0.2 to 1.4% (atomic) level. Nd:YAG is an efficient 4-level laser material and may be used in both pulsed and CW operation. The principal Nd:YAG emission is at 1064.14 nm. The energy levels of Nd^{3+} ion involved in the Nd:YAG laser are shown in Figure 2.3. The ions are excited to higher energy states ($^4\text{F}_{5/2}$, $^2\text{H}_{9/2}$ and $^4\text{F}_{3/2}$) by optical absorption in the wavelength bands centered around 808 nm or 869 nm and quickly decay non-radiatively to the metastable $^4\text{F}_{3/2}$ level located 11502 cm^{-1} above the ground level $^4\text{I}_{9/2}$. Thus a large population is thus created in $^4\text{F}_{3/2}$ level following the optical pumping. The stimulated emission radiatively transfers Nd^{3+} ions from the $^4\text{F}_{3/2}$ state to $^4\text{I}_{11/2}$ (which is 2000 cm^{-1} above the ground state) resulting in laser emission at $1.064\text{ }\mu\text{m}$. Since, the lifetime (10^{-8} s) of lower laser level $^4\text{I}_{11/2}$ is much smaller than the lifetime ($250\text{ }\mu\text{s}$) of upper laser level $^4\text{F}_{3/2}$, there is normally negligible population in lower level, so that Nd-YAG gain media exhibits a four-level laser behavior [47, 48]. The generated heat in the YAG crystal is cooled by means of circulating water [19]. The optical pumping is achieved through light from xenon flash lamp which covers the wavelength range from near UV to near IR. A Q-switch is used to reduce the pulse duration and raise its peak power.

2.1.1.1. Q-switching

Q-switching is used for high peak power of the laser pulse and is achieved by placing some type of variable attenuator inside the laser's optical resonator. When the attenuator is functioning, light which leaves the gain medium does not return, and lasing cannot begin. This attenuation inside the cavity corresponds to a decrease in the Q factor or quality factor of the optical resonator. A high Q factor corresponds to low resonator losses per roundtrip and vice versa. The variable attenuator is commonly called a "Q-switch", when used for this purpose.

Initially, the laser medium is pumped while the Q-switch is set to prevent feedback of light into the gain medium (producing an optical resonator with low Q). This produces a population inversion, but laser operation cannot yet occur since there is no feedback from the resonator. Since the rate of stimulated emission is dependent on the amount of light entering the medium, the amount of energy stored in the gain medium increases as the medium is pumped. Due to losses from spontaneous emission and other processes, after a certain time the stored energy will reach some maximum level; the medium is said to be gain saturated. At this point, the Q-switch device is quickly changed from low to high Q, allowing feedback and the process of optical amplification by stimulated emission begins. The intensity of light in the laser resonator builds up very quickly because the large amount of energy is already stored in the gain medium; this also causes the energy stored in the medium to be depleted almost as quickly. The net result is a short pulse of light output from the laser, known as a giant pulse, which has very high peak intensity.

In the Nd: YAG laser used in the present work, active Q-switching is obtained by applying an electro-optic device called Pockel's cell. The reduction of losses (increase of Q) is triggered by applying an electrical signal on the faces of Pockel's cell and hence the pulse repetition rate is externally controlled.

2.1.1.2. Pockel's cell

The Pockel's cell consists of a crystal which becomes birefringent under the influence of an electrical field and at a certain voltage, this crystal act as a quarter wave plate. Depending on the applied voltage on the cell, either it prevents the feedback of light into gain medium (producing the optical resonator at high loss) or it permits the light feedback through gain medium (producing an optical resonator cavity at low loss). Thus, Pockel cell is used to quickly change the cavity losses from high to low and vice-versa. A glass plate cut at Brewster angle is used as polarizing element inside the cavity and it couples the light through

the cavity when it passes through the Pockel Cell just after one round trip. When a high voltage, normally 3.1 kV, is applied to the Pockels cell, it acts like a quarter-wave plate and the state of polarization of light which passes through it after one round trip, is rotated through 90° and hence polarizing element prevents the light passing through it. Thus, laser oscillation does not sustain but the population inversion becomes quite large due to the optical pumping during this period. When the voltage applied to the Pockel cell is cut off after a suitable time gating (very short time), then the light passes through the polarizing element and hence laser oscillations are build-up very quickly which results in high power pulse of short duration.

2.1.1.3. Properties of laser important for LIBS

Several properties of the laser are important for LIBS analysis. The following section briefly describes their effects.

2.1.1.3.1. Wavelength

The wavelength of the laser is to be selected is based on the material under study. Some laser wavelengths couple readily with the sample when compared to other wavelengths. For example, CO₂ wavelength (10600 nm) is highly reflected by many metals (e.g. Cu) while this couples well with glasses and aqueous solutions which have high absorption in the IR region. During present work, Nd:YAG fundamental wavelength of 1064 nm was used.

2.1.1.3.2. Pulse energy & irradiance

Lasers are unique light sources that can yield very high intensities or irradiance in the region of GW.cm^{-2} required for the breakdown to occur in a material. The pulse energy must be also sufficiently high for LIBS measurements. If the pulse energy is low, even if the pulse power density is in the order of GW, sufficient material would not be ablated and vaporized

to provide a useful, strong emission signal for analysis. In the present instrument, the laser can generate up to 200 mJ of laser energy.

2.1.1.3.3. Spatial quality

This determines the minimum spot size to which a laser beam can be focused. It may not be possible to focus a beam with poor beam quality to a sufficiently small spot for achieving the required power densities for creation of a plasma. In the present set-up, the beam can be focused to $7.85 \times 10^{-5} \text{ cm}^2$ area.

2.1.1.3.4. Directionality

The ability of the laser beam to propagate over long distances as a collimated beam is highly useful in standoff and remote LIBS applications. A high quality laser operating at the lowest Gaussian mode (TEM00) produces a laser beam that replicates closely a uniform, plane wave having a constant phase distribution across the wave front and this was used in the present study.

2.1.1.3.5. Monochromaticity

Laser light has an inherent ability for generating the majority of its light output in a narrow spectral range due to its origin from a well defined transition in the lasing medium. In terms of the excitation properties of the laser plasma, monochromaticity is typically not important and analytically useful laser plasma can be generated with IR, visible or UV wavelengths. Monochromaticity may be of importance in LIBS instruments designed to use optical components that selectively reflect the narrow band of the excitation wavelength and pass the broad spectrum of the laser plasma for collection and analysis.

2.1.2. Sample chamber

The laser light interacts with the sample placed in the sample chamber and produces the plasma which is then collected and analyzed suitably for obtaining the elemental distribution on the surface. The sample chamber, in the present instrument, is located on a

fast XY-translational stage, which moves the sample between two successive laser pulses, exposing a new and fresh region of the sample for each laser pulse.

2.1.3. Optical System

2.1.3.1. Focusing & light collection system

In LIBS, laser pulses are focused on the sample using lenses and mirrors. For systems in which the lens to sample distance is changeable, such as in the case of industrial systems, a multi-lens system is necessary. In the present system, single lens is used to focus the laser to a sufficiently small spot for achieving analytically useful plasma.

2.1.3.2. Lenses

Dependent on the apparatus, a lens or a mirror is usually employed for collecting the plasma light which is then directed to the spectrograph for further analysis. The lens or a mirror system should be suitably selected to eliminate aberrations (such as chromatic aberration, astigmatism etc.) which distort the output image at the inlet of the spectrograph. Suitably coated optical components are generally employed in LIBS. Multiple lenses are usually employed for collection to provide the input for multiple spectrograph systems covering a wide wavelength range, as in the present case (four plano-convex lenses).

2.1.3.3. Fiber optic cables

Fiber optic cables (FOC) are used in LIBS as they simplify the collection of plasma light. These are extremely useful in applications like hostile environments, when the detection system cannot be positioned near the target. While using a fiber optic cable, the plasma light may either be focused on to the fiber end to increase the light collection or the fiber can simply be pointed at the plasma. Focusing of the light increases the sensitivity of light collection but with increased sensitivity to the alignment of the optical system. On the other hand, pointing the fiber to the plasma reduces this alignment sensitivity. In addition to collecting the plasma light, the fibers can also be used to deliver the laser light to remotely

locate targets which are extremely useful for remote LIBS applications. As shown in Figure 2.4, every FOC's one end is connected to the spectrometer, while the other end is connected to a collimating lens (0-45° field of view) placed at an angle of 45° to the direction of the plasma expansion. The transmission of light through FOC is based on the principle of total internal reflection. The basic function of a fiber is to guide light without much attenuation over long distances. A typical fused silica FOC design is shown in Figure 2.5. The fiber transmits the light using total internal reflection and those light rays entering the fiber within acceptance cone angle will be reflected down the fiber with high efficiency (Figure 2.6).

Figure 2.5 shows the view of fiber in which light propagation occurs in a region of increased refractive index around the fiber axis, called the fiber core. The core is surrounded by a material of lower refractive index called cladding which is usually protected with a polymer coating. A light beam approaching the core-cladding interface from the core region is totally internally reflected, provided that the incidence angle is greater than the critical angle.

The maximum angle at which a particular fiber can accept the light that will be transmitted through it is defined by the semi-vertical angle (θ) of the cone. Numerical Aperture (NA) which defines the maximum angle (2θ , the cone of acceptance) at which the light can be coupled into the fiber can be expressed by the equation

$$NA = (n_f^2 - n_c^2)^{1/2} \dots (2.1)$$

where n_f is the refractive index of the core and n_c is the refractive index of the cladding. Higher is the optical fiber's NA, larger the cone of light that can be coupled into its core. In the present system, four FOCs (core diameter 200 μ m) were used. Two FOCs with core made of fused silica were used for visible range (320 nm – 620 nm). For UV range (180 nm – 320 nm), high OH containing fused silica core FOC and for IR region (620 nm – 850 nm) low OH containing fused silica core FOC were used.

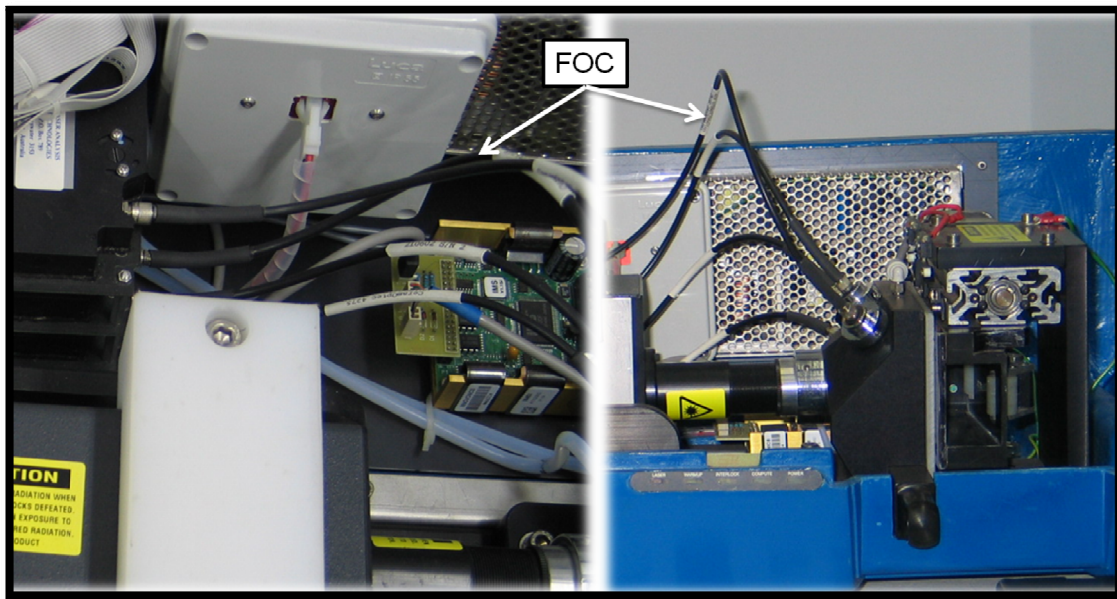


Figure 2.4: *Fiber Optic Cable (FOC) connected with sample chamber (right) and spectrometer (left).*

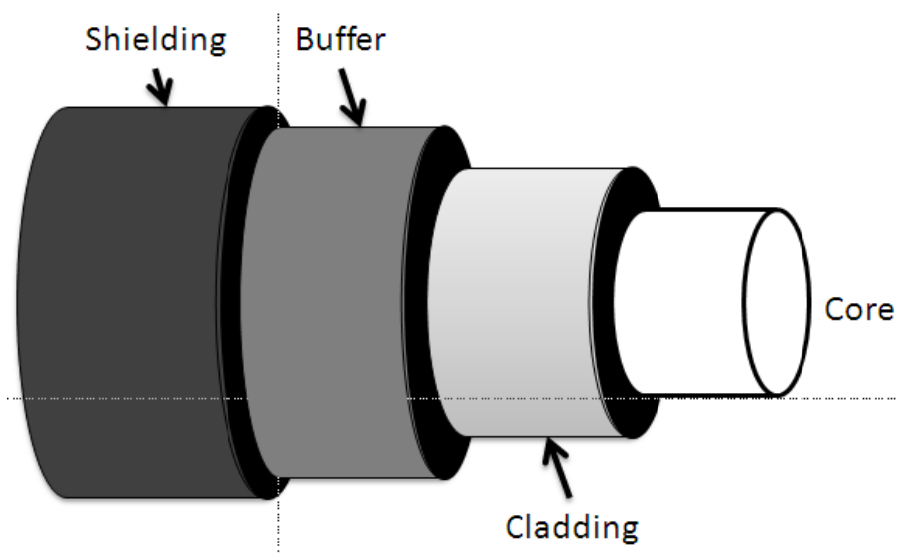


Figure 2.5: *Design of fiber optics.*

2.1.4. Detection system

This system consists of a spectrograph and a CCD plate as a dispersive and detecting device, respectively. A computer linked with spectrometer is used to store and analyze the spectrum.

Light from the laser plasma contains information about the elements present in the material via the set of characteristic emission lines of the elements in the plasma. In laser plasmas, where the density of the atomic species is quite high, many processes will act to increase the width of the spectral line. These include pressure broadening (due to the collisions between the different species in the plasma) and stark broadening (due to the high electron density of the plasma). Spectral broadening of the lines by these processes is quite common and requires devices for obtaining the necessary spectral details from the plasma.

The method of resolution depends on the application and can vary from a simple spectral line filter to a sophisticated echelle spectrograph for monitoring a large spectral range with high resolution. Of the different techniques, the Grating spectrograph which was employed for spectral analysis in the present work would be described in detail in this Chapter. These detection systems can fully use the multielemental analysis capabilities of LIBS covering the entire spectral range from 180 nm to 850 nm simultaneously.

2.1.4.1. Grating spectrographs

There are many designs or mountings of the grating in spectrographs namely (i) Littrow (ii) Ebert-Fastie (iii) Czerny Turner (iv) Paschen Runge and (v) crossed Czerny Turner. The basic design differences relate to whether one or two mirrors are used for collimating and focusing the light and the position of the slits relative to the grating. The present system employed the Czerny –Turner Spectrograph and is shown in Figure 2.7.

Light from the plasma is imaged on to the entrance slit. The light passing through the slit then reaches the first mirror which collimates the light directing it onto the grating. Light is reflected off the grating at different angles according to the wavelength. This light then falls on to the second mirror which focuses the light onto the focal plane in the form of a spectrum having a horizontal distribution, which then passes through the exit slit to the detector. The $f\#$ of a spectrograph is determined by diameter of the mirror (d) and the distance from entrance slit to the first mirror (f) according to the following equation

$$f\# = f/d \dots\dots\dots (2.2)$$

To achieve maximum light throughput, it is important that the $f\#$ of the spectrograph matches the $f\#$ of the optical system directing the light onto the entrance slit. If the $f\#$ for the optics is smaller than that of the spectrograph, the scattering will be more. In the other case, the emission spectra are not collected sufficiently resulting in loss of sensitivity.

2.1.4.2. Detectors

The type of detector used in LIBS is dependent on many factors including the number of elements that are to be monitored and the type of spectral acquisition method used. A comparison of the detectors used in LIBS is given in Table 2.3. The detectors based on PDA and CCD can fully exploit the capabilities of LIBS. The present system uses a CCD detector, which is described in the following section.

A charge-coupled device (CCD) is an array of metal-oxide-semiconductor (MOS) capacitors which can accumulate and store charge due to their capacitance. A cross-section of a CCD is shown in Figure 2.8. Usually a CCD consists of a number of MOS capacitors combined for spectral acquisition.

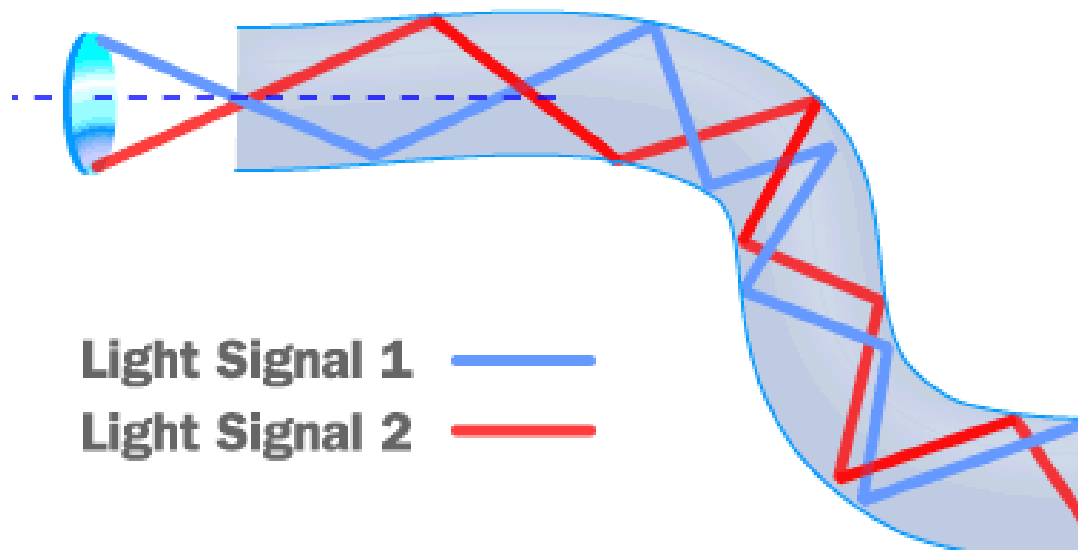


Figure 2.6: *FOC's internal reflection mechanism.*

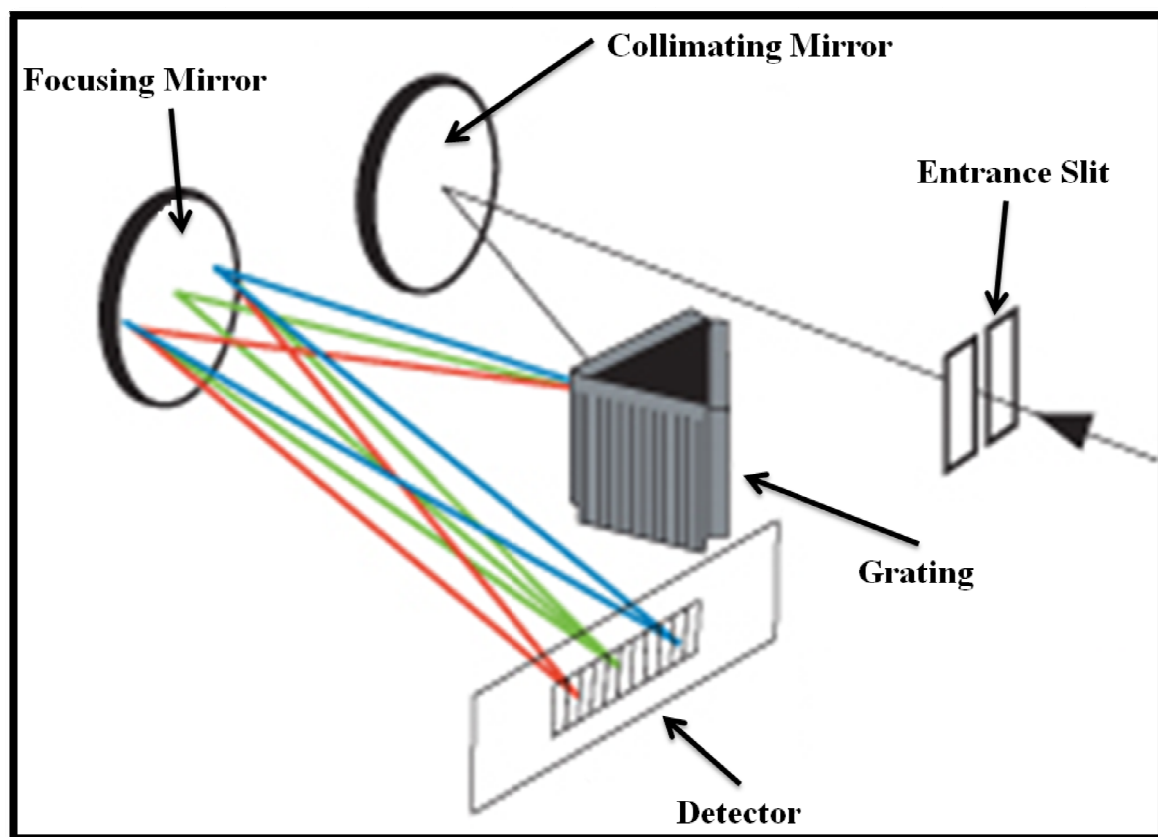


Figure 2.7: *Schematic diagram of a Czerny Turner Spectrograph.*

It is divided into a large number of light-sensitive microscopic areas (known as pixels) which form an image of the pattern of light falling on the CCD plate. A photon of light which falls within the area defined by one of the pixels is converted into one (or more) electrons and the number of electrons collected will be directly proportional to the intensity of the light at each pixel. When the CCD is clocked out, the number of electrons in each pixel is measured and the optical image can be reconstructed [50].

Figure 2.8 shows a simplified cross sectional view of a pixel of the CCD. It can be seen that the silicon itself is not arranged to form individual pixel but the pixels are defined by the positions of electrodes. If a positive voltage is applied to the electrode, then all the electrons close to the area under the electrode will be attracted while the positively charged 'holes' will be repelled from the area around the electrode. Consequently, a "potential well" is formed in which all the electrons produced by incoming photons are stored. As more and more light falls onto the CCD, the potential well surrounding this electrode will attract more electrons (the amount of electrons that can be stored under a pixel is known as the full well capacity). While filling up the potential well, it is essential to ensure that the full well capacity is not exceeded. Therefore, the light must be prevented from falling onto the CCD after a defined length of time which is usually controlled by a shutter. Thus, an image can be formed by opening the shutter, "integrating" for a length of time to fill up the most of the electrons in the potential well, and then closing the shutter to ensure that the full well capacity is not exceeded [51]. A CCD consists of a large number of pixels (*i.e.*, potential wells), arranged horizontally in rows and vertically in columns (Figure 2.9).

(a) Charge generation

Photons entering the CCD create electron-hole pairs as shown in Figure 2.10. The electrons are then attracted towards the most positive potential in the device where they create 'charge packets'. Each packet corresponds to one pixel.

(b) Charge collection and transfer

Figure 2.11 shows a cross-section through a row of a CCD. Each pixel actually consists of three electrodes $I\emptyset_1$, $I\emptyset_2$, and $I\emptyset_3$. Only one of these electrodes is required to create the potential well, while other electrodes are required to transfer the charge out of the CCD. The upper section of the Figure 2.11 (section 1) shows charge being collected under one of the electrodes say $I\emptyset_2$. To transfer the charge out of the CCD, a new potential well can be created by holding $I\emptyset_3$ high, the charge is now shared between $I\emptyset_2$ and $I\emptyset_3$ (section 2). If $I\emptyset_2$ is now taken low, the charge will be fully transferred under electrode $I\emptyset_3$ (section 3). To continue clocking out the CCD, taking $I\emptyset_1$ high and then taking $I\emptyset_3$ low will ensure that the charge cloud now drifts across under the $I\emptyset_1$ electrodes. As this process is continued, the charge cloud will progress either down the column, or across the row depending upon the orientation of the electrodes.

In most of the CCD's, the electrodes in each pixel are arranged so that the charge is transferred downwards along the columns. Thus, during the CCD clocking operation, rows are transferred downwards to the final row (the readout register) which is used to transfer the charge in each pixel out of the CCD so that it can be measured [52].

(c) How the charge is measured

The final process on the CCD is the reading of each pixel so that the size of the associated charge cloud can be measured. At the end of the read-out register, there is an amplifier which measures the value of each charge cloud and converts it into a voltage. A typical conversion factor is around 5-10 μ V per electron with "typical" full well values of about 100,000 electrons [52].

Table 2.3: *Characteristic of the detectors used in LIBS*

Detector	Characteristics
Photomultiplier Tube (PMT)	Inexpensive, single wavelength detection, temporal response < 1 ns.
Avalanche Photodiode (APD)	High gain, fast response, high signal to noise ratio, high quantum efficiency, fabrication as array possible.
Photo Diode Array (PDA)	Provides one dimensional spatial information on light intensity, simultaneous detection over a certain spectral range.
Intensified PDA	PDA + time resolved detection (upto a few ns), expensive.
Charge Coupled Devices (CCDs)	Provides two dimensional spatial information about light intensity, useful for simultaneous detection over a certain spectral range.
Intensified CCDs (ICCD)	CCD + time resolved characteristics down to a few ns, expensive.

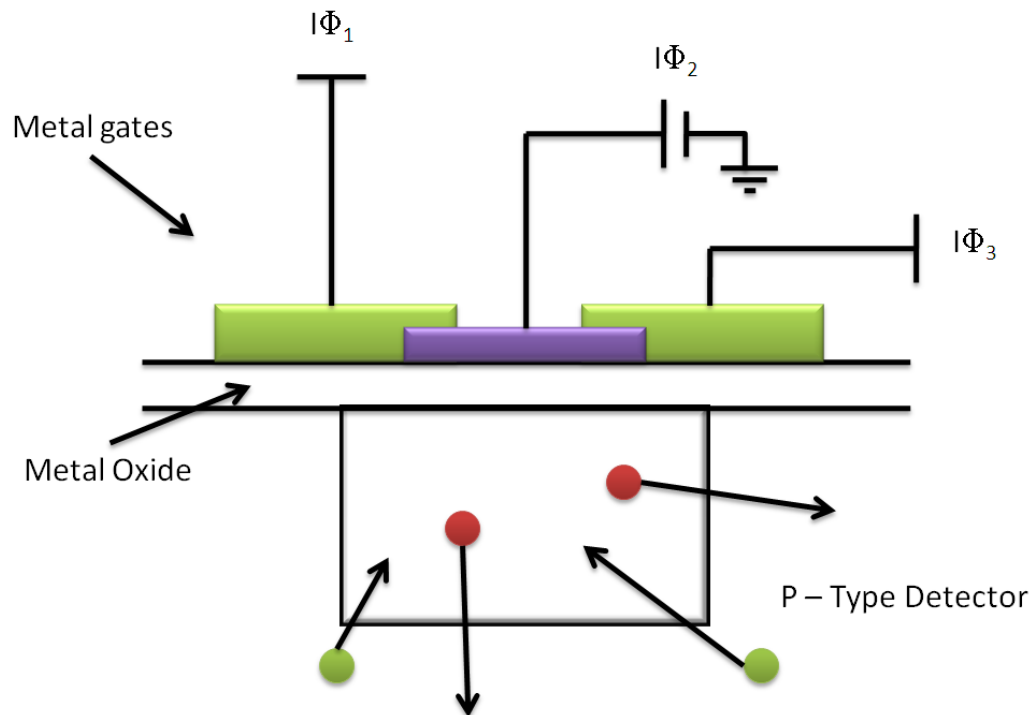


Figure 2.8: Cross sectional view of a pixel of CCD (Red circles represent: holes; Green circles represent: electrons).

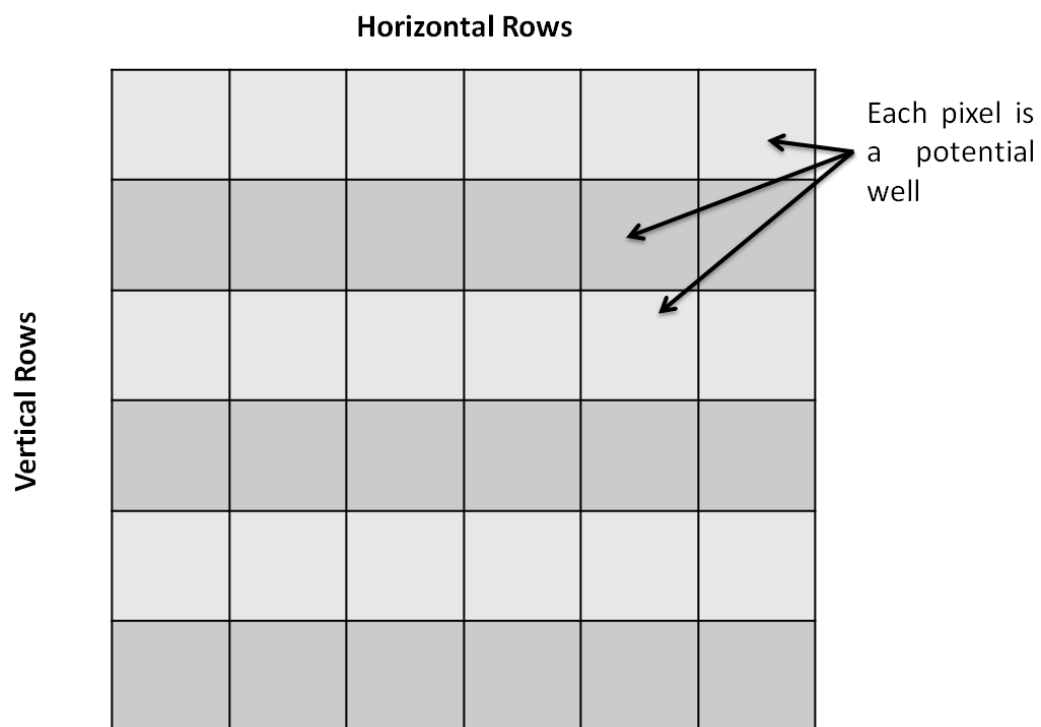


Figure 2.9: Arrangement of pixels in CCD.

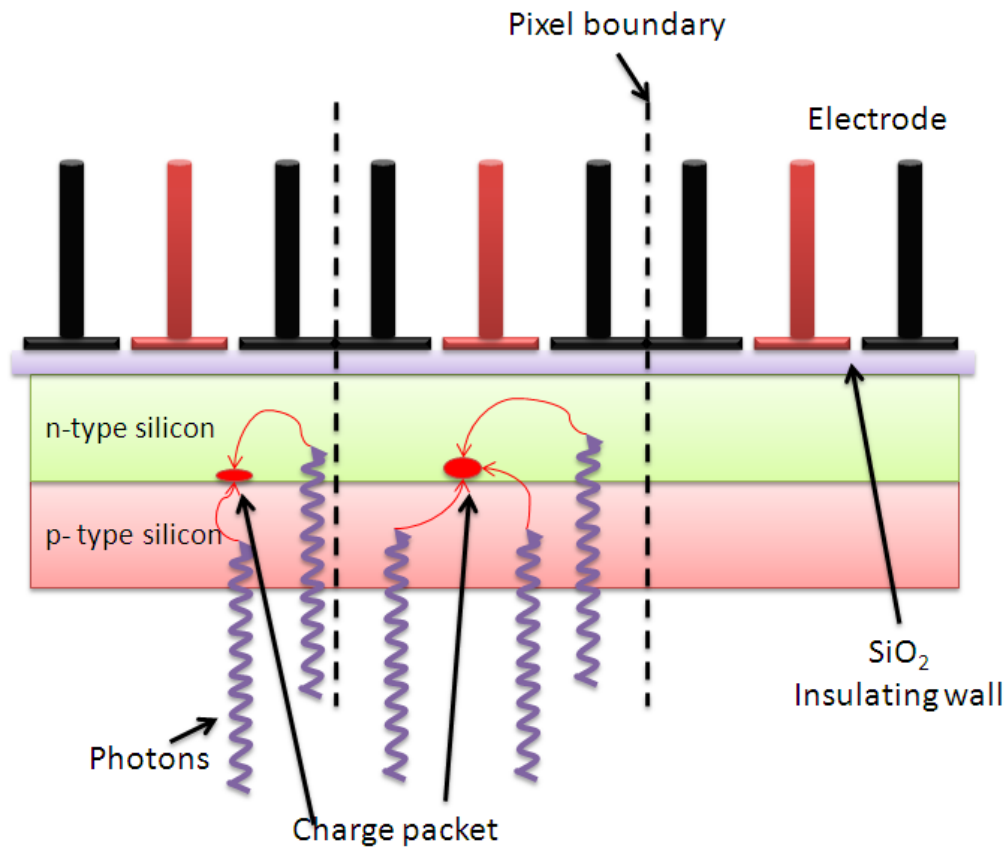


Figure 2.10: Charge generation in CCD.

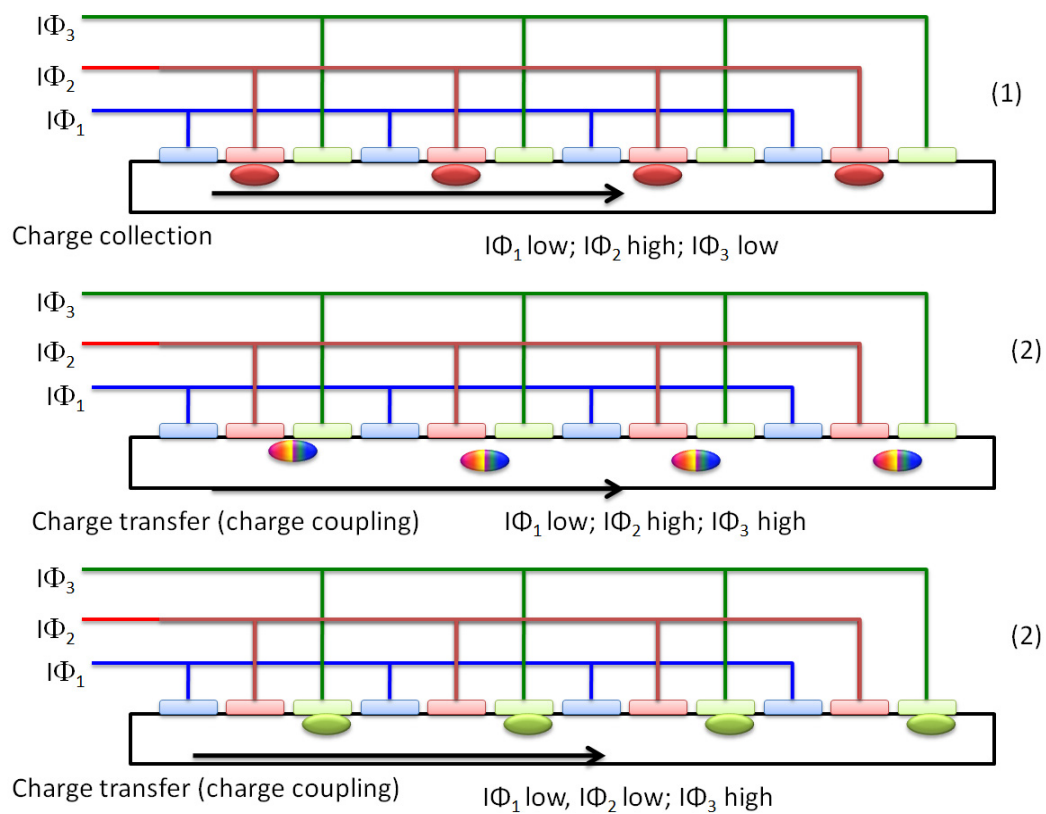


Figure 2.11: Transfer of charges.

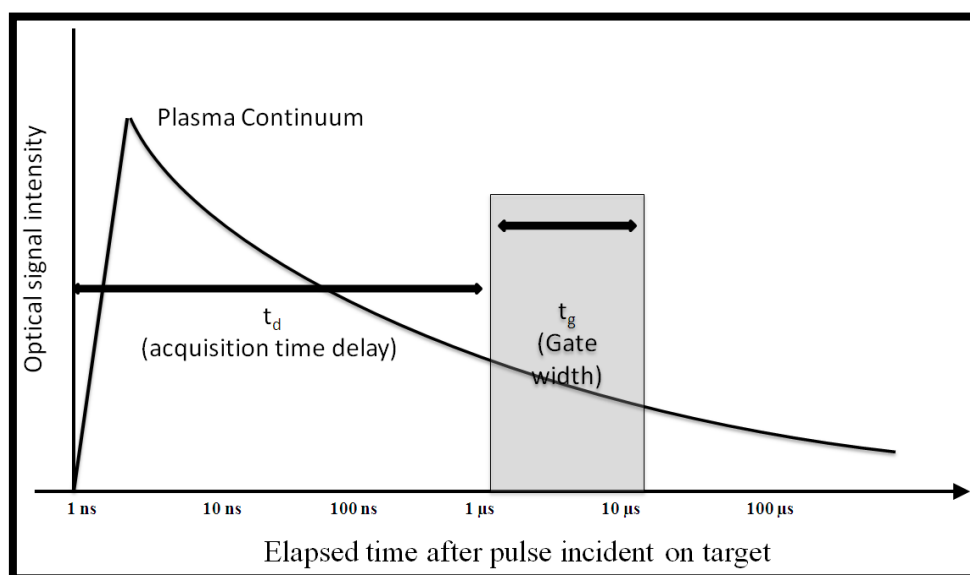


Figure 2.12: Schematic overview of the temporal history of LIBS plasma. The delay and gate window are shown.

Table 2.4: Details of all the components used in the present LIBS system

Components	Used in the present system
Laser	Nd-YAG at 1064 nm
Focusing system	Plano-convex lenses
Collecting system	Fiber optic cables
Spectrograph	Czerny –Turner Spectrograph
Detector	Charge Coupled Devices (CCDs)
Software	Spectrolaser 6.625

2.1.5. Control electronics

The intense continuous background, due to the major bremsstrahlung emission mechanism, predominates at the first instants of the plasma life (Figure 2.12). Emission lines are broad mainly due the stark effect caused by the high density of free electrons. However, after a few hundreds of nanoseconds, characteristic atomic lines can be very clearly distinguished as the free electrons start to be captured by ions and neutral atoms and the highly excited species decay to lower energy levels. At the same time, line narrowing is observed as the major effects causing line broadening (collision and stark) become weaker. As the plasma expands and cools, the relative intensities of the emission lines can change due to energy distribution among the plasma species. Finally after a while, the emission signal is representative only of the most persistent lines of the elements present in higher concentrations in the sample.

Therefore, a careful timing is necessary between the laser pulse and the gate pulse for acquisition by the detector. This is frequently achieved by control electronics in the LIBS systems. The laser flash lamp and Q-switch are triggered by a pulse generator synchronized to the data acquisition system controlled by a computer. The pulse generator produces an external trigger that clocks the detector readout with the laser pulse. Table 2.4 tabulated the important sub-system or components used in the present LIBS system

Elemental Characterization in Solid Matrix by LIBS



Chapter III

3.1. INTRODUCTION

The applications of LIBS are dominated by examples in solid matrices. Very few techniques can be used directly for the determination of trace/ bulk constituents in solid samples, without involving dissolution of the samples. These include Energy Dispersive X-ray Spectroscopy (EDXRF), Wavelength Dispersive X-ray Spectroscopy (WDXRF), Glow Discharge Mass Spectrometry / Atomic Emission Spectrometry (GD-MS/AES), Spark Source Mass Spectrometry (SSMS) etc. Among all these techniques, LIBS has several advantages as discussed in Chapter I, which makes this technique highly attractive. Several types of solid matrices have been analyzed by LIBS, e.g., asbestos [53], paper [54], glass [55], herbal products [56], cinematographic films [57], polymers [58, 59], organic solid [60], steel [61], soil [62, 63], explosive [64, 65], ceramics [66], marble [67], alloys [68], human skin [69] etc. However, LIBS has not been extensively used for characterization of nuclear materials, where the technique offers several advantages over the conventional by used emission spectrometric technique.

Davies *et al.* [70] showed remote analytical system based on LIBS for the study of steel components in an operating nuclear reactor at the Berkeley Nuclear Research Laboratory without the requirement of reactor shut-down. Fichet *et al.* [71] showed the applicability of LIBS for impurities quantification in both UO_2 and in PuO_2 targets at atmospheric pressure. Eighteen impurities at concentrations of about 500 ppm and twelve at concentrations of about 100 ppm, respectively, were observed in the rich emission of matrices UO_2 and PuO_2 . The standard addition method was applied by Fichet *et al.* X. K. Shen *et al.* showed the applicability of uranium detection up to 462 ppm in glass samples using LIBS in combination with laser-induced fluorescence at an excitation wavelength of 385.96 nm for resonant excitation of U II and a fluorescence line wavelength of 409.0 nm

from U II [72]. They also showed that although atomic and ionic lines can be selected to detect their fluorescence, ionic lines are more suitable for LIBS-LIF measurements, since the strong uranium atomic lines have interference from other elements present in the glass matrix. With the help of very high resolution spectrometer, the isotopic ratios of U and Pu were also determined by LIBS [73 - 75]. Whitehouse *et al.* [76] reported application of a fiber-optic LIBS system for remotely determining the copper content of 316H austenitic stainless steel super-heater bifurcation tubing within the pressure vessels of Advanced Gas Cooled Reactor nuclear power stations. The system was deployed during the routine reactor outage programs for Hunterston 'B' and Hinkley Point 'B' stations during the summer of 1999 and used successfully to determine the copper content of the bifurcations over the range $0.04\% < \text{Cu} < 0.60\%$ (by mass). Measurement times per bifurcation were typically less than 3 min and measurement accuracy was $< 25\%$. Tripathi *et al.* [77] showed application of LIBS to determine elemental concentration of plutonium oxide surrogate (cerium oxide) residue for monitoring the fabrication of plutonium lanthanide borosilicate glass. Multivariate calibration was applied to LIBS data to predict the concentrations of Ce, Cr, Fe, Mo, and Ni. A total of 18 different samples were prepared to compare calibration from univariate data analysis and from multivariate data analysis. Application note [78] of Applied Photonics Ltd showed industrial application of LIBS in both remote analyses of several parts inside a reactor and for spent fuels.

In this Chapter, applications of LIBS for bulk and trace elemental characterization in two different nuclear fuel materials which are important in the present scenario of Indian nuclear program, are presented.

3.2. DETERMINATION OF URANIUM IN MOX FUEL

3.2.1. Background

Thorium (Th) and uranium (U) are the major resource elements for any nuclear power program. Monazite, containing thorium as a major constituent, is amongst the abundant minerals available at certain locations in India. In view of the fast growing energy demands, it is essential to achieve efficient conversion of abundant fertile nuclear materials, such as ThO_2 into fissile materials such as ^{233}U and use the latter for producing energy.

The Indian nuclear power program has been conceived bearing in mind the optimum utilization of domestic uranium and thorium reserves with the objective of providing long-term energy security to the country. Keeping in mind that India has to fall back on its vast thorium resources, which account for about one third of the world's thorium reserves (~ 300,000 tons) [79, 80], third stage of the Indian nuclear power program is based on Th- ^{233}U fuel cycle and advanced heavy water reactors (AHWRs). Two different compositions of Th-U mixed oxide have been proposed for AHWR fuel containing 3 wt. % and 3.75 wt. % of ^{233}U [81]. The Th – U mixed oxide pellets are generally prepared by the conventional powder metallurgy route which has been tested and used for U and Pu based fuels. The qualitative as well as quantitative characterization of the fuel materials for major as well as minor constituents is required as a part of chemical quality assurance of nuclear fuels. At present, chemical and mass-spectrometric methods are being employed to determine the composition of major / minor elements in Th – U mixed oxide with the desired accuracy and precision.

Instrumental techniques such as LIBS have huge potential for the determination of uranium in mixed oxides of Th and U. Thoria being a refractory material, the dissolution of sintered thoria pellets or a U-Th mixed oxide pellets is difficult and time consuming which can be avoided in LIBS. However, this is a pre-requisite for chemical as well as mass-spectrometric methods.

The present work reports the application of LIBS for the rapid determination of U in Th – U mixed oxide samples in the range up to 20% of uranium. The emission spectra of both Th and U being very complex, proper choice of emission lines is very important. Calibration curves were obtained for four emission lines of U in Th – U mixed oxide. This chapter presents details of the work carried out to optimize the experimental parameters like laser fluence and acquisition delay time and gives the results obtained for U determination in two synthetic samples of Th – U mixed oxide.

3.2.2. Sample preparation & analysis

Since certified reference materials (CRMs) for mixed oxide of U and Th are not available commercially, a series of synthetic mixed oxide calibration standards were prepared. Known amounts of highly pure ThO₂ and U₃O₈ powders were weighed and then blended and ground thoroughly for about 30 minutes. Initially, six Th–U mixed oxide calibration standards with U amount varying from 0–32% by weight were prepared. Subsequently, two more synthetic samples with U amounts of 4% and 20% were prepared and were treated as unknown to validate the calibration. The powders were mixed with high purity (99.5%) boric acid powder, procured from S. D. Fine Chem. Ltd, Mumbai, India in equal-amount ratio for 15 minutes by blending and grinding thoroughly to obtain homogeneous mixture. Mixed powder samples were then pelletized to 3 cm diameter pellets by applying a pressure of 2×10^9 Pa for 5 minutes. Table 3.1 gives the compositional data of the calibration standards prepared in this work. The emission lines for U determination were selected from the regions where minimal Th spectral interferences were observed and their intensities were normalized with respect to the B(I) 249.774 nm. Boron was chosen as an internal standard since boric acid was used as the binder and its concentration in the pellet was maintained constant irrespective of the composition of the mixed oxide.

Table 3.1: *Composition of the calibration standards and two synthetically prepared samples*

Standards	U concentration (%)	Th concentration (%)
TU-1-CAL	1.1	98.9
TU-2-CAL	2.1	97.9
TU-3-CAL	3.0	97.0
TU-4-CAL	8.1	91.9
TU-5-CAL	16.0	84.0
TU-6-CAL	32.0	68.0
TU-7-Unknown	4.0	96.0
TU-8- Unknown	20.3	79.7

Table 3.2: *Characteristics of spectral lines employed for determination of U by LIBS [82]*

Element	λ_{ij} (nm)	A_{ij} ($10^8 s^{-1}$)	E_j (cm^{-1})	E_i (cm^{-1})
U(II)	263.553	-	-	-
U(II)	367.007	0.26	914.765	28154.450
U(II)	447.233	0.018	289.036	22642.473
U(II)	454.363	-	914.765	22917.451
λ_{ij} is the transition wavelength; A_{ij} is the transition probability; E_i and E_j are the energies of the upper and lower level, respectively.				

Identical conditions of laser fluence, repetition frequency and acquisition delay were used for all analyses. In the present experiment, 1 Hz repetition rate of laser pulse was used. For the LIBS analysis, spectra of 100 shots were averaged. On each pellet including the calibration standards as well as the unknowns, triplicate analyses, i.e., three 100 shot measurements were performed. The stepping motor was fixed with a velocity of 0.2 mm/sec so that each laser pulse focused on a fresh surface. The emission line intensity can vary due to a variety of reasons that include fluctuations in laser power due to dust in the beam path, time jitter, as well as due to the changes in the focusing and collection optics. In order to reduce these effects and eliminate their effects on the results obtained by LIBS, the software was programmed to discard the raw data from analysis where the raw net line intensity was more than $\pm 10\%$ of the average intensity and then again re-averaging was done to get intensity.

3.2.3. Results & discussion

3.2.3.1. Selection of emission line

The four spectrographs allow simultaneous acquisition of a wide range of spectra, 180 nm to 850 nm for each laser shot, which contains almost all the intense emission lines of the two actinide elements under study. Emission spectra of actinides are generally very complex and the situation gets aggravated when two actinides are present in major amount, as in the present case. Presence of a large number of emission lines makes the spectra of mixed oxide as a band of emission lines at the present instrumental resolution (0.6 nm at 300 nm). To select an appropriate emission line for U, spectra of pure U, pure Th and a mixed oxide sample were recorded and compared carefully. The pure U pellets were prepared in such a way that the amount of U in the pure U pellets and in the mixed oxide pellets was same. The pure Th pellet was also prepared in the same manner. Figure 3.1 shows a comparison of the three spectra under identical conditions of analysis (laser energy of 100 mJ and acquisition delay of 3.5 μ s). By comparison of the emission spectra, four spectral regions where spectral

interferences from Th spectrum were minimal in the region of U emission lines were identified and the suitable emission lines were selected for U. The emission lines along with their spectroscopic data are listed in Table 3.2. Among these four emission lines, U(II) 263.553 nm and U(II) 367.007 nm are among the reported prominent lines in ICP-AES [83].

3.2.3.2. Effect of laser fluence

To optimize the laser fluence, the calibration standard TU – 4 - CAL was analyzed at different laser fluence. Figure 3.2 shows a comparison of the spectra observed at different laser fluences. It is seen that with increasing laser fluence, the U(II) 367.007 nm emission line becomes more and more prominent. At fluence above 56 J/cm^2 , the pellet was not intact and gets fragmented during analysis and, therefore, laser fluence was not increased further.

3.2.3.3. Temporal resolution for acquisition

The importance of optimization of the temporal resolution has been discussed in literature [84, 85] and in previous Chapter. A series of measurements were made to determine the optimal time delay between the laser pulse and the start of data acquisition of the LIBS spectra. Figure 3.3 shows a comparison of emission spectra recorded using TU – 4 – CAL at different acquisition delays at a laser fluence of 56 J/cm^2 . For the U(II) 367.007 nm emission line, the best spectral purity with sufficient signal intensity was obtained at an acquisition delay of $3.5 \mu\text{s}$ which was selected as optimum acquisition delay for subsequent analyses.

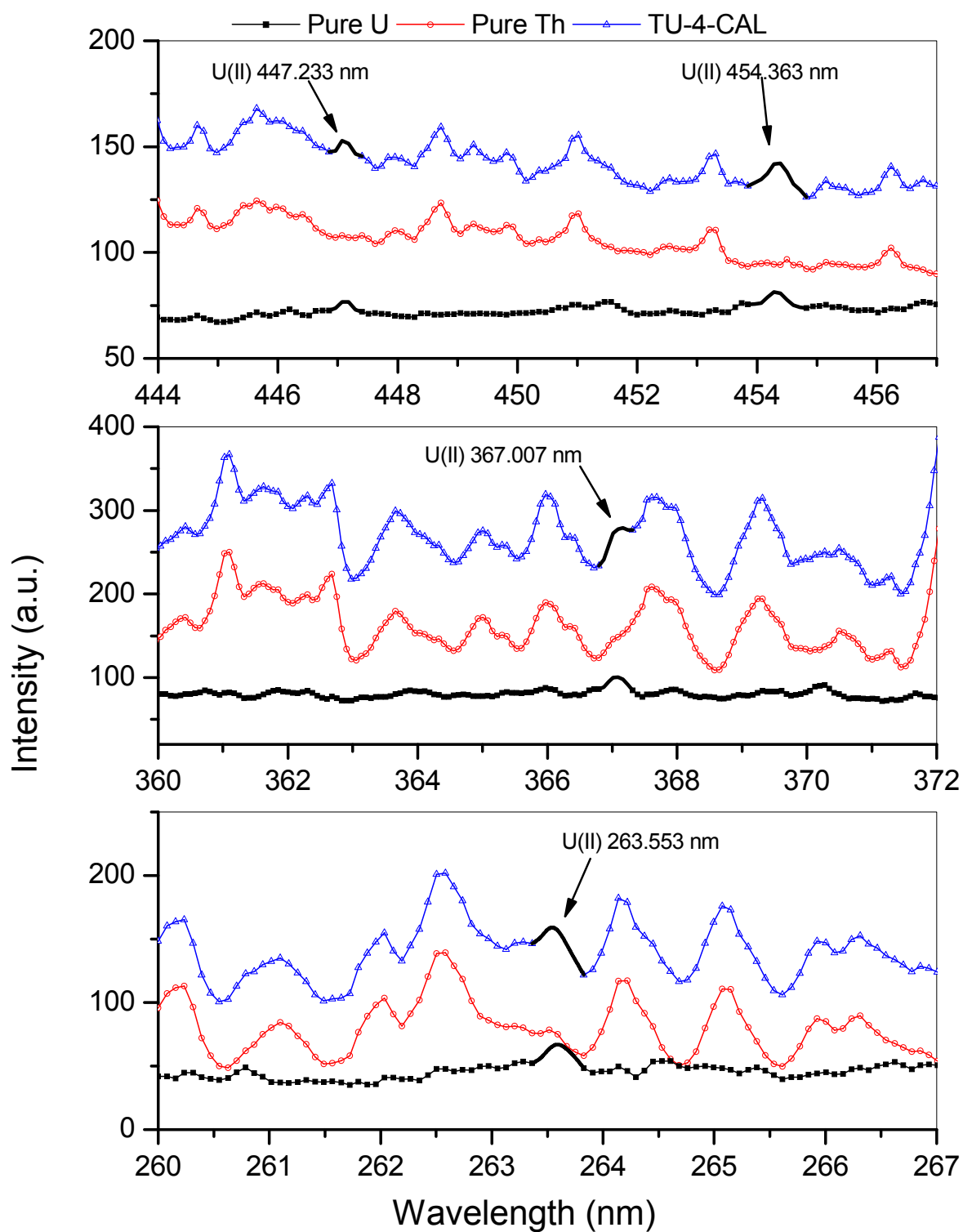


Figure 3.1: Comparison of the spectra of Th and U with their mixed oxide standard under identical conditions of analyses.

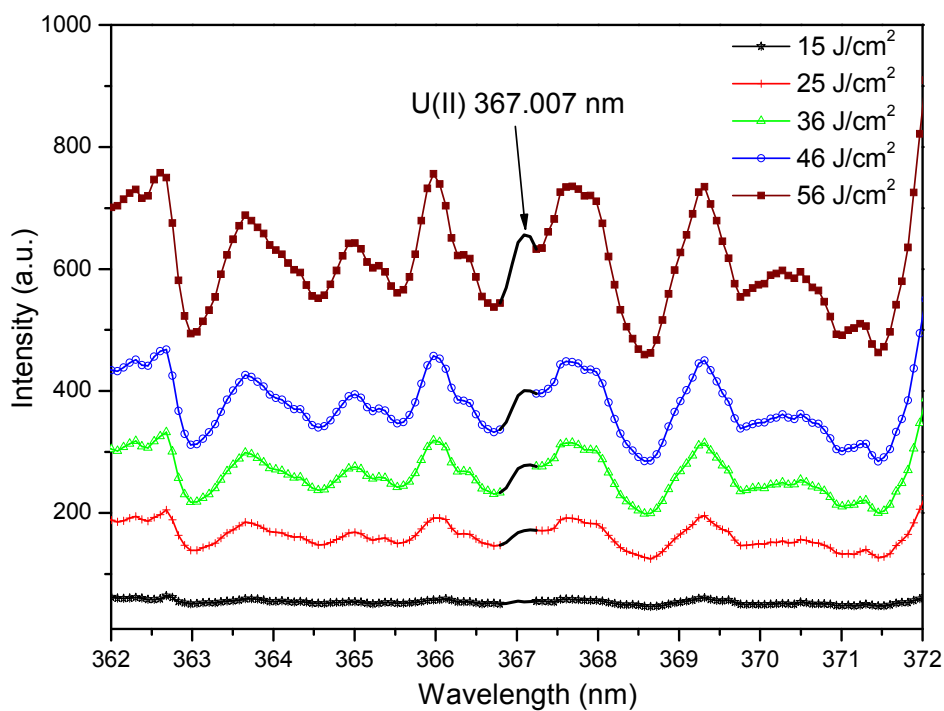


Figure 3.2: *Effect of laser fluence on the U(II) 367.007 nm emission line (TU - 4 – CAL).*

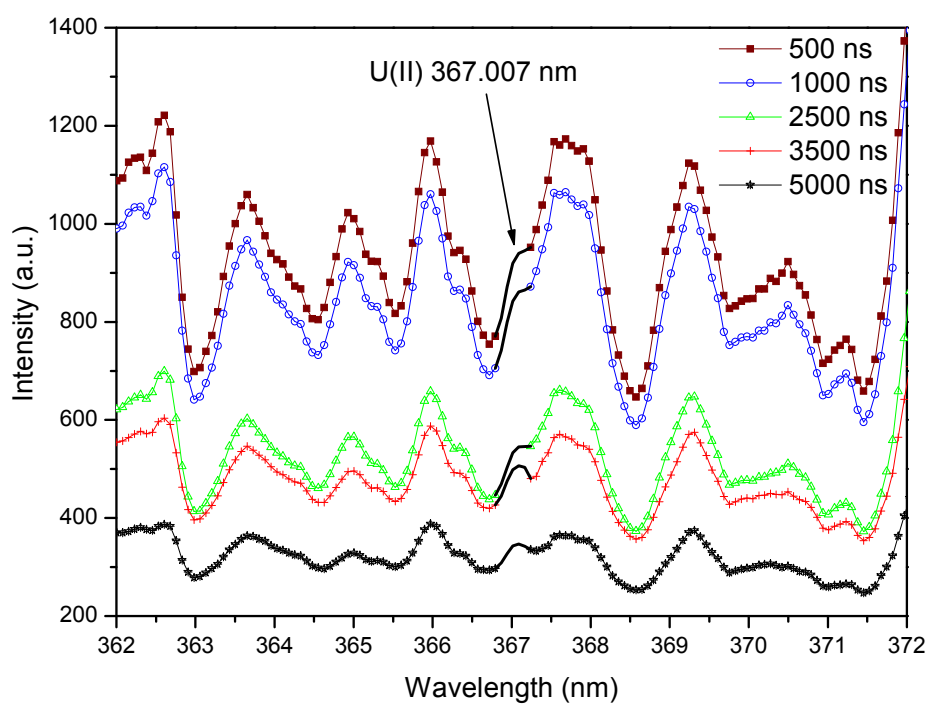


Figure 3.3: *Effect of acquisition delay on the U(II) 367.007 nm (TU – 4 – CAL)*

3.2.3.4. Calibration curves & precision

Standards of mixed oxide of the Th and U were used to prepare calibration curves of all the four normalized line intensities of U emission lines with respect to B(I) 249.774 nm versus the corresponding concentration of U, as shown in Figure 3.4 (a to d). Each calibration point corresponds to an average of three measurements at different locations of the corresponding pellet. The practice of discarding spectra with raw line intensity more than $\pm 10\%$ than the average value was also followed here as discussed in the Section 3.2.2. The number of spectra discarded under this criterion would be useful to determine the statistical significance of the results obtained in this study. Since there is no provision in the present software employed for the spectral analysis to obtain this information, so this detail could not be shown in Figure 3.4. The error bars on calibration points are the standard deviations ($\pm 1\sigma$), calculated by measuring the normalized peak intensity of the emission line. Normalization of emission line intensity was done after discarding outlier spectra as stated above. The calibration data were analyzed using the instrument software and applying least squares regression analysis.

The calibration curves show a linear behavior below 8 wt. % U in the Th-U mixed oxide. Above 8 wt. % U, saturation is observed due to self-absorption of the lines in the plasma, a feature commonly observed in laser-induced plasmas at atmospheric pressure [35, 86, 87]. For this region, a non - linear equation was used to fit the experimental data, similar to the expression proposed by Aragon et al. [88],

$$y = y_0 + A e^{\left(\frac{-x}{t}\right)} \dots\dots(3.1)$$

where x denotes weight % of U and y stands for normalized emission line intensity. In equation (1), the absolute value of “t” indicates the concentration where the calibration slope decreases by a factor of 1/e from its value of (A/t) at x = 0. Hence this value (i.e., x = t) can

be regarded as the critical amount above which laser induced self-absorption becomes appreciable and, therefore, the analysis of such elements in the sample should be restricted up to this value for using the particular calibration curve. Table 3.3 gives the data of different parameters in equation 1 for the four U emission lines. Except from the U(II) 263.553 nm, the values of “t” for the other three emission lines is close to 20. This indicates that the amount of U species in plasma for the Th-U mixed oxide composition with 20 wt. % U is sufficiently high. The value of “t” in case of U(II) 263.553 nm is 31.9. Extent of self-absorption is usually high for resonant emission lines or lines having lower energy level close to the ground level. E_{lower} for both the U(II) 367.007 nm and U(II) 454.363 nm emission lines is 914.765 cm^{-1} , and for U(II) 447.233 nm it is 289.036 which is very near to the ground level, indicating the possibility of higher degree of self-absorption. The higher value of “t” in case of U(II) 263.553 nm is not understood at present, but a proper energy diagram for the above transition might be able to explain the observed effect. The E_{lower} of U(II) 263.553 nm seems to be situated at a much higher energy from its ground state.

Table 3.4 show the results obtained for uranium in the two synthetic samples treated as unknown. The wt. % U determined is in good agreement with the expected value and there is no systematic bias. The calibration curve of U(II) 447.223 nm was not used for unknown synthetic sample with U amount of 4 wt. %, as the calibration curve obtained using this emission line was not sensitive in lower concentration range (Figure 3.4c).

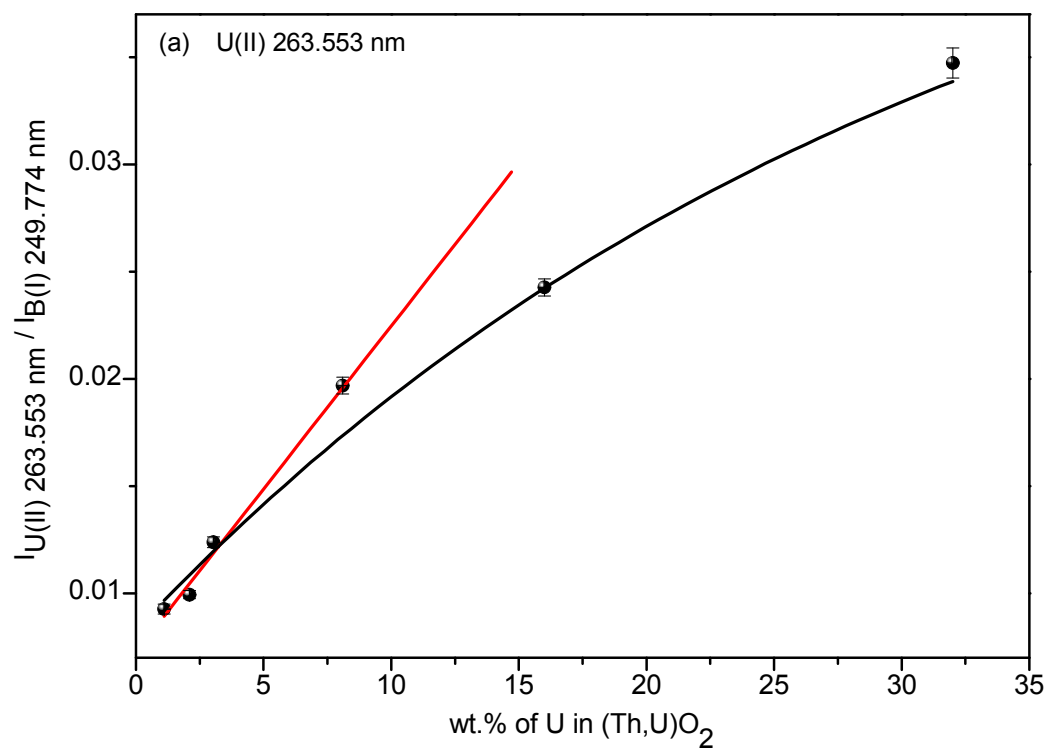


Figure 3.4a: Calibration curve obtained for the lines U(II) 263.553 nm. The red line corresponds to the linear behavior of optically thin plasma.

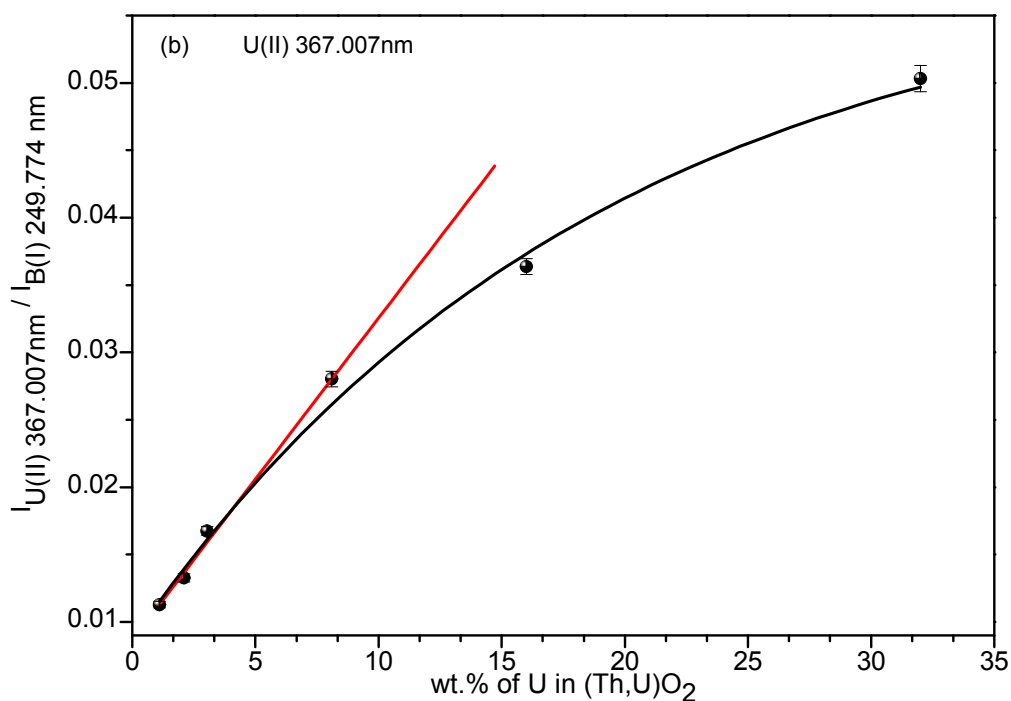


Figure 3.4b: Calibration curve obtained for the lines U(II) 367.007 nm. The red line corresponds to the linear behavior of optically thin plasma.

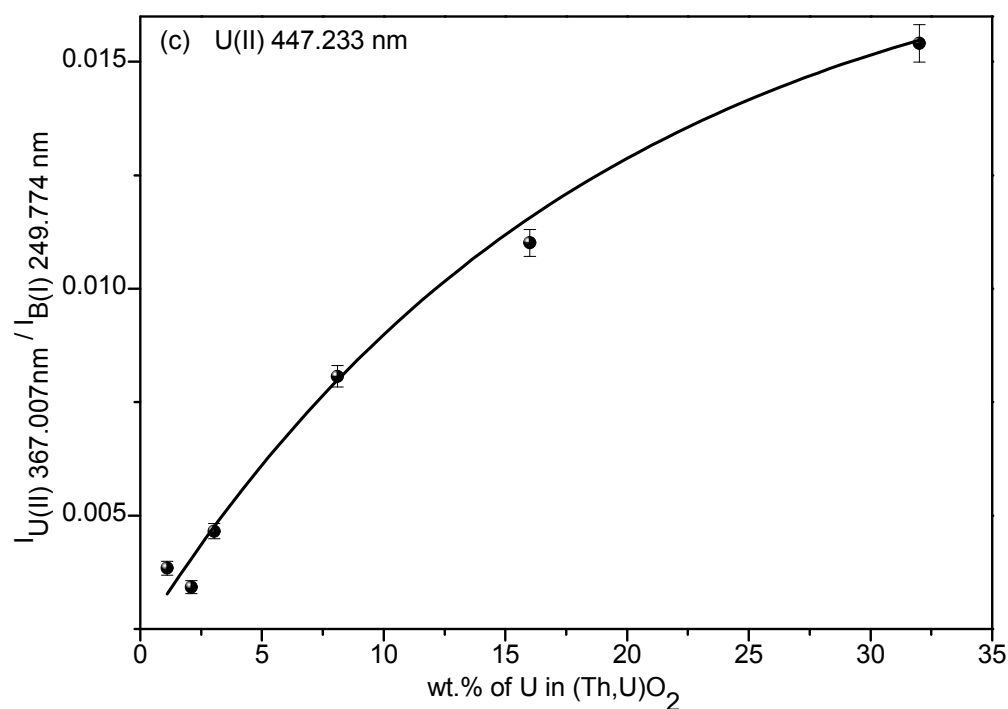


Figure 3.4c: Calibration curves obtained for the lines U(II) 447.233 nm.

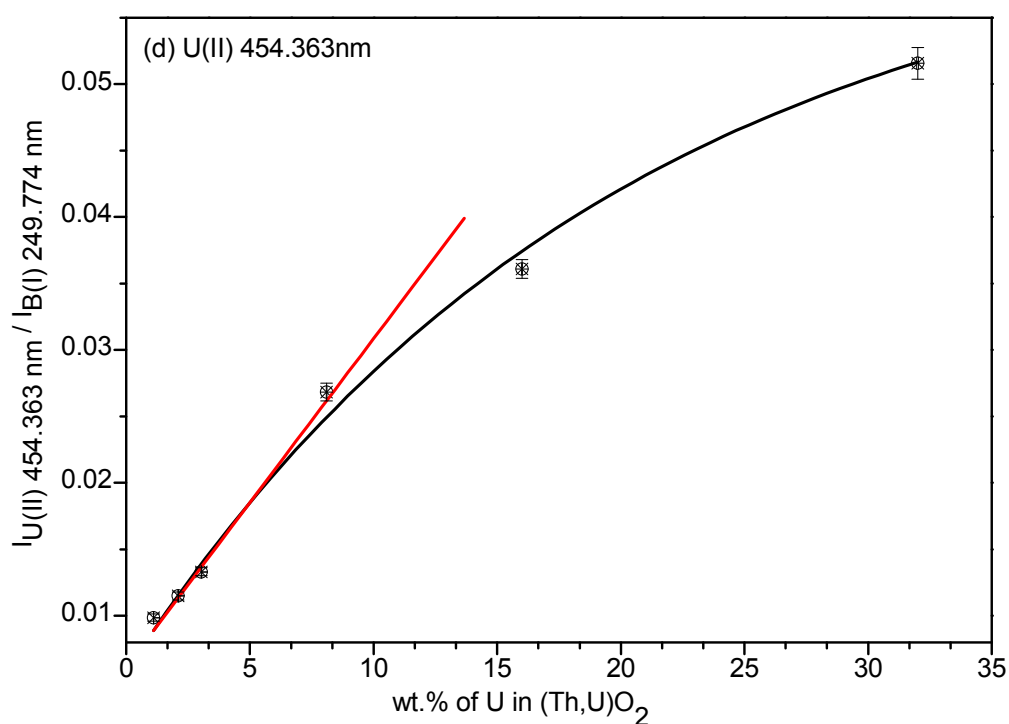


Figure 3.4d: Calibration curve obtained for the lines U(II) 454.363 nm. The red line corresponds to the linear behavior of optically thin plasma.

Table 3.3: Parameters of Eq. (1) obtained by fitting calibrations curves and the correlation coefficients

Wavelength (nm)	y_0	A	t	R^2
U(II) 263.553	0.049	-0.04	31.92	0.979
U(II) 367.007	0.059	-0.05	19.08	0.996
U(II) 447.233	0.018	-0.02	18.73	0.994
U(II) 454.363	0.063	-0.06	20.04	0.995

Table 3.4: Comparison of analytical results for U determination in Th – U mixed oxide samples with expected values

Sample	Emission wavelength (nm)	Wt. % U		(A/B)
		LIBS (A)	Expected (B)	
TU – 7 - Unknown	263.553	3.72 ± 0.43	4	0.93
	367.007	3.82 ± 0.29		0.96
	447.233	-----		-----
	454.363	3.41 ± 0.52		0.85
TU – 8 - Unknown	263.553	19.4 ± 1.13	20.3	0.96
	367.007	19.4 ± 0.14		0.96
	447.233	20.67 ± 2.01		1.02
	454.363	21.14 ± 2.44		1.04

3.2.4. Conclusions

LIBS methodology has been developed for the determination of U in mixed oxides of thorium and uranium. The approach will be useful for the rapid determination of U in similar samples, avoiding rigorous dissolution required by other solution based analytical techniques. The reproducibility of the determination is $\pm 2\%$ (1σ). Though the addition of boron in nuclear material is undesirable, the result shows the potential of the LIBS method in nuclear industry. The effect of alternative carbon based binder such as starch, nitrocellulose, can also be explored for these studies.

Considering the poor resolving power of the instrument and also the relatively rough optimization procedure employed, the agreement between the expected and experimental results is quite good, which indicates the enormous potential of LIBS and the possibility of using a high-resolution LIBS for routine work for U-Th mixed oxide characterization. LIBS also provides an independent approach based on different physico-chemical principle for the determination of U in Th - U matrix. This would be useful for the development of certified reference materials for these matrices in thorium based fuel cycle.

3.3. DETERMINATION OF TRACE CONSTITUENTS IN THORIA

3.3.1. Background

Determination of impurities in nuclear materials is of great importance as their presence affects the mechanical property of the material during irradiation as well as the neutron economy inside a reactor. Specification limits have been laid down for various impurities in different nuclear fuels. Quantitative determination of impurities constitutes an important step for quality assurance at different stages of fuel fabrication. Since many of the nuclear materials pose radiation hazards, it is desirable to develop methods which involve minimum sample handling procedures with an objective to minimize the radiation exposure to the workers.

At present, in the Indian nuclear industry, thoria bundles are used for neutron flux flattening in Pressurized Heavy Water Reactors (PHWR) and also as blanket in the Fast Breeder Test Reactor (FBTR). But, thoria being a refractory material, the dissolution of sintered thoria pellets is time consuming and difficult. The conventional emission spectrometric techniques such as ICP-AES require quantitative dissolution of the samples. Also the complex emission spectrum of thorium necessitates chemical separation of impurities from bulk of thorium. These limitations can be circumvented by employing techniques having capability for direct solids analysis. Some of these include DC-arc-carrier distillation method, Laser Ablation Inductively Coupled Mass Spectrometry (LA-ICP-MS), Glow Discharge Mass Spectrometry (GD-MS), Glow Discharge Optical Emission Spectrometry (GD-OES) and LIBS.

This Chapter discusses the optimization of the LIBS analysis conditions for the determination of trace impurities in ThO₂ samples. Since impurity standards in thoria matrix are not available commercially, certified reference materials (CRM) prepared by M/s. Nuclear Fuel Complex, Hyderabad, India in association with Radio Chemistry Division

(RCD), BARC, Mumbai, were employed in this work. The emission spectrum of ThO_2 being very complex, impurities which were present in significant amounts (above tens of ppmw) were analyzed. Linear calibration curves were obtained for 7 impurities using these standards. Details of the work carried out to optimize the experimental parameters like laser energy and acquisition delay time in LIBS, along with the calibration curves obtained for different impurities in thorium matrix are discussed below.

3.3.2. Experimental

3.3.2.1. Samples

The material used in the present work to establish calibration curves was produced during an Inter Laboratory Comparison Experiment (ILCE) conducted by the Department of Atomic Energy (DAE), India. During this ILCE, 13 laboratories of DAE had participated.

The impurities in these ThO_2 samples were determined using five different analytical techniques based on different physico-chemical principles. Thorium powder was prepared based on the method used by Allred et. al. [89] through the oxalate precipitation route. The techniques employed were (1) Inductively Coupled Plasma-Atomic Emission Spectrometry (ICP-AES), (2) Inductively Coupled Plasma-Mass Spectrometry (ICP-MS), (3) Atomic Absorption Spectrometry (AAS), (4) Total Reflection X-ray Fluorescence (TXRF) and (5) DC-arc-Carrier Distillation. Four samples of homogeneous ThO_2 powder were prepared containing 20 impurities in varying amounts. The following samples were prepared in view of the application of ThO_2 as a fuel for AHWR reactors. (a) ThO_2 –B containing impurities at base level, (b) ThO_2 –S containing impurities at specified level, (c) ThO_2 –D containing impurities at double the specified limit and (d) ThO_2 –MOS mixed oxide of Th and U in the composition that has been proposed for the fuel of AHWR.

Table 3.5 gives data on different impurities present in the samples. For certification of impurities, F-test was conducted on the data obtained by different techniques employed.

Though the RSD values are quite large for some of the elements in Table 3.5, they are within expected limits for material to be used in nuclear industry and follow the statistical evaluation criteria of International Atomic Energy Agency (IAEA) for inter-comparison experiments [90].

3.3.2.2. LIBS analysis

For LIBS analysis, 4 gm of each of the samples (particle size 10 – 40 μm) was taken in an aluminum cup having an inner diameter of 3 cm and 8 mm height. A pressure of 2×10^9 Pa was applied for 5 minutes to prepare a pellet. The spectra of 30 shots were averaged and used for analysis in the present work. During these analyses, the spectra with variation of intensity ratio more than $\pm 10\%$ of the average intensity ratio were neglected. The LIBS spectral data were analyzed using the instrument software and applying nonlinear least squares regression analysis.

3.3.3. Results & discussion

3.3.3.1. Time resolution

The sensitivity of LIBS analysis increases when the plasma light detection is time resolved and the technique is then referred to as time resolved laser induced breakdown spectroscopy (TRLIBS) [91, 92]. The high temperature plasma formed immediately after the laser bombardment contains highly ionized species and emits a broad continuum due to “Inverse Bremsstrahlung” along with the emission lines of different species. The emission lines are also broadened by Stark effect due to high electron density that exists in the initial life-time of the emission. The signal to noise ratio (SNR) can, therefore, be improved by electronically gating off the early part of signal. The choice of time parameter was assessed experimentally with zirconium as a model. Zr was chosen as its melting point (M. P.) (2125 K) is closer to that of Th (2115 K). M. P. has been found to be an important parameter in the variation of ablation threshold fluence [93]. This particular route was taken because studying

the time resolution in ThO₂ spectrum is difficult due to the numerous emission lines. In this work, laser energy of 50 mJ and an acquisition delay of 6 μ s was used; with fixed gate width of 10 μ s available in the instrument.

3.3.3.2. ThO₂ spectra

Figures 3.5 (a) and (b) show the typical spectrum obtained for one of the samples used for obtaining the calibration curves for different impurities. A relatively smaller number of shots (30) were chosen considering our ultimate aim to develop an on-line remote analysis technique, and to reduce the spreading of thorium dust in the sample chamber. As can be seen, the emission spectrum is quite complex and identification of suitable emission lines for different impurities are a major challenge. For every element, the region of interest was selected on the basis of the well known criteria:

- (a) The emission lines used in ICP-AES experiment during ILCE work performed were selected for LIBS analysis. It must be noted that for analysis by ICP-AES, the matrix thorium was separated by solvent extraction initially using 40% solution of tri-n-butylphosphate (TBP) in CCl₄ and later with 0.2 M tri-n-octylphosphinic oxide (TOPO) in CCl₄. If ICP-AES experimental line was not detectable, then emission line reported by other researchers from LIBS experiments in literature was used.
- (a) The emission line should be spectrally pure.
- (b) The emission line with $E_{\text{lower}} = 0$ or as low as possible was preferred.
- (c) The emission line having a high transition coefficient (A) is desirable.
- (d) High SNR at the particular condition.

Table 3.6 gives the data on the spectral lines used for determination of 7 impurities present (Mg, Al, Ca, Ni, Fe, Cu and Mo) in the ThO₂ samples along with 7 other elements (Mn, Na, V, Be, Ce, B and Cr) which could only be detected. The Mg(II) 279.552 nm line was the same as that used in ICP-AES work. Ca(I) 422.672 nm, Cu(I) 327.395 nm, Fe(I)

277.210 nm lines were based on the reported LIBS work [94]. Emission lines of other three elements (Al, Ni and Mo) were selected from the spectrum obtained under the present experimental conditions. These seven elements were chosen for quantitative analysis, since they were present in significant concentrations in the calibration standards as well as the range of the concentration variation in the standards was more than 10%.

3.3.3.3. Calibration curves

The calibration curves for different impurities in thoria matrix were obtained by using three ThO₂ calibration standards as shown in Figure 3.6a & b. The calibration curves were constructed by plotting the intensity ratio of impurity with respect to Th(II) 318.019 nm versus the known element concentrations (weight %). Each point displayed in the calibration graphs is the mean value obtained from triplicate measurements and the error bars correspond to one standard deviation ($\pm 1\sigma$). The calibration curves were found to be linear for all the impurities in the concentration range present in the samples. The Root Mean Square Error in Prediction (RMSEP) for the calibration curve is given by

$$\sqrt{\frac{\sum \{y_i - y_m(I_i)\}^2}{n}} \dots (3.2)$$

where n is the number of points in the calibration, y_i is the concentration of the i^{th} calibration point and $y_m(I_i)$ is the concentration predicted by the calibration curve for the i^{th} intensity. This measure indicates the likely difference between the actual concentration of an impurity in the sample and the value predicted by the calibration curve. The plots have RMSEP of 10^{-3} range, which is reasonable, considering the limited number of calibration points.

Table 3.5: Concentrations of impurities (ppmw) in different thoria samples used for calibration in LIBS. The mean values and %RSD are taken from ILCE evaluation report

Element	ThO ₂ -B		ThO ₂ -S		ThO ₂ -D		ThO ₂ -MOS	
	Mean	% RSD	Mean	% RSD	Mean	% RSD	Mean	% RSD
Al	6.9	42.2	39	28.2	65	24.2	38	27.7
B	0.77	66.8	1.2	50	0.8	50	0.79	49.2
Be	<0.1	-	0.34	23.4	<0.1	-	<0.1	-
Ca	73	28.5	351	29.5	586	27.8	479	23.7
Cd	<0.1	-	1.1	46.1	2.0	37.3	1.3	43.6
Ce	1.3	62.5	5.6	41.1	11	22.4	7.6	43.7
Cr	8.5	17.6	7.3	28.2	13	30.2	19	20.4
Cu	3.1	27.4	63	29.5	110	29.1	71	18.7
Dy	<0.1	-	0.28	41.1	0.55	42.7	0.3	45.5
Er	<0.1	-	0.28	43.7	0.54	31.6	0.34	48
Eu	<0.1	-	0.12	41.1	0.22	38.3	0.12	37.1
Fe	56	29.7	78	29	134	29.1	137	30
Gd	-	-	0.42	49.8	0.7	42.9	0.48	47
Mg	4.8	37.2	168	29	74	29.7	36	24.1
Mn	3.0	34.8	4.3	37.5	7.3	36.4	5.5	28
Mo	1.2	52.2	22	27.5	45	25.7	22.4	33.2
Ni	11	20.9	32	25.7	57	29.1	38	21.9
Sb	<0.5	-	2.4	40.5	5.0	36.4	1.9	33.6
Sm	-	-	0.63	45.8	1.2	40.9	0.81	46.5
V	0.21	50.9	3.0	42.1	5.9	37.5	3.3	33.9

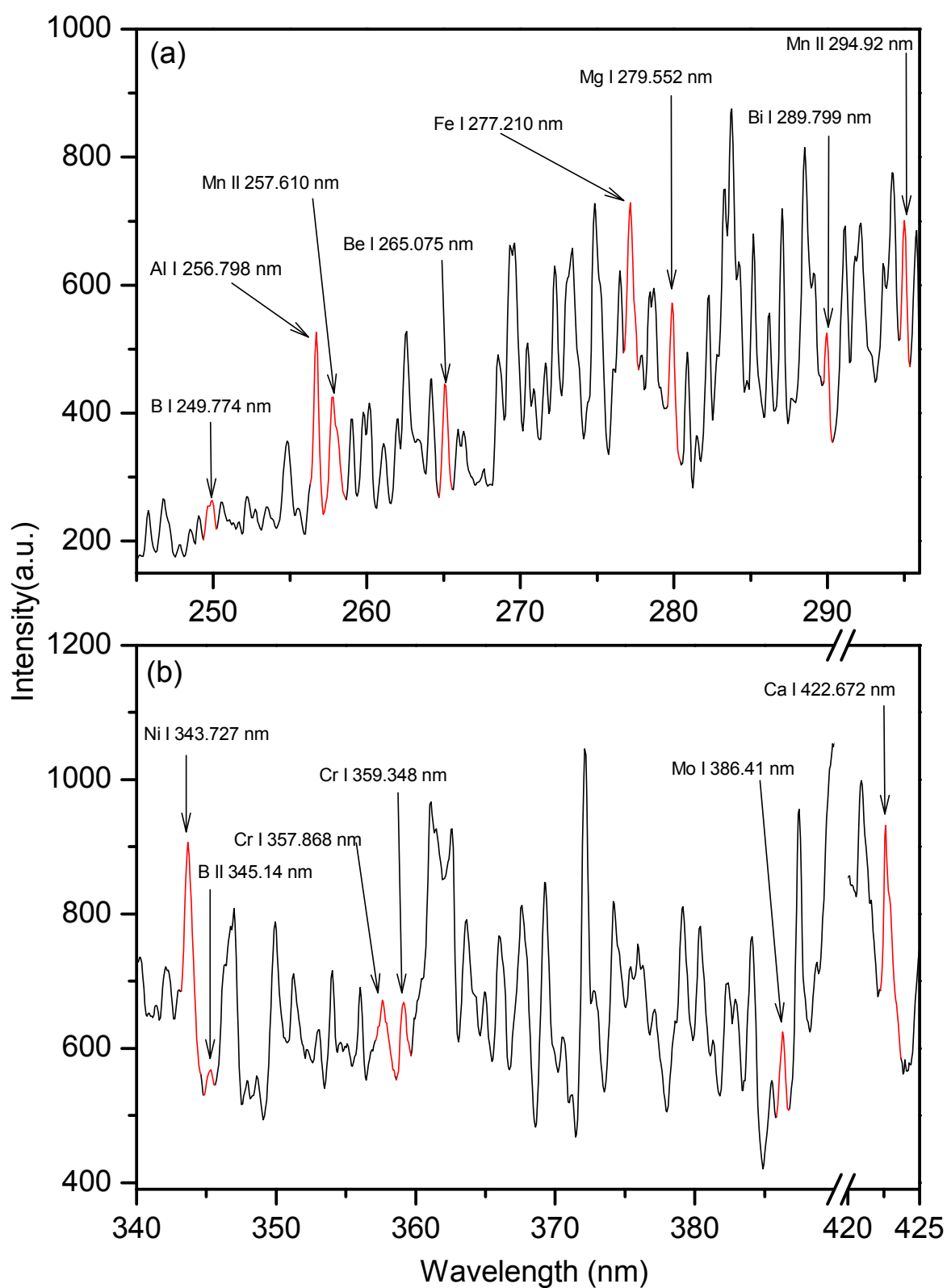


Figure 3.5: Emission spectrum of $\text{ThO}_2\text{-S}$ in the (a) 245 nm to 295 nm region and (b) 340 nm to 425 nm region with the emission lines of impurities (red line).

Table 3.6: Chosen emission lines and their spectroscopic data [82] for various elements

Element	Species*	Wavelength (nm)	E _{lower} (cm ⁻¹)	Transition coefficient (A) (10 ⁸ s ⁻¹)	Remarks
Mg [†]	II	279.552	0	2.600	Quantification possible
Al [†]	I	256.798	0	0.230	
Ca [†]	I	422.672	0	2.200	
Ni [†]	I	301.914	0	0.06	
Fe [†]	I	277.210	704	0.4199	
Cu [†]	I	327.395	0	1.400	
Mo [†]	I	386.410	0	0.624	
Mn ^γ	II	257.610	0	2.8	Only detection was possible
	II	294.920	9472.97	1.94	
Na ^γ	I	588.994	0	0.616	
	I	589.592	0	0.614	
V ^γ	I	478.353	2311.36	0.089	
Be ^γ	I	265.075	21981.27	4.24	
Ce ^γ	I	487.704	0	12	
B ^γ	I	249.774	15.287	1.67	
	II	345.14	73396.51	0.54	
Cr ^γ	I	357.868	0	1.48	
	I	359.348	0	1.50	

* I and II denote atomic and ionic lines, respectively

† Calibration curves of these elements were constructed.

γ Elements were only detected.

3.3.3.4. Precision & detection limit

To check the calibration curves obtained in the present work, a sample was prepared by mixing ThO₂ - S with ThO₂ - D in 3:1 amount ratio by weight. Table 3.7 gives the results obtained from six replicate analyses of this mixture under the identical LIBS conditions as those used for calibration samples. It can be seen that the mean values of concentrations of different impurities are in good agreement with the expected values and the precisions lies in the range of 7 to 22%. Figure 3.7 shows the distribution of the six replicate analysis values for Al. The distribution clearly indicates the random nature of the analytical values against the certified values.

Detection limits for 7 impurity elements in ThO₂ were determined using the formula $LOD = 3\sigma/m$, where m is the slope of the calibration line and σ is the uncertainty in the intensity for the calibration point with the lowest concentration. The LOD's of the elements in ThO₂ matrix are given in Table 3.8. As is seen, these LODs are better than the LOD's for these elements in UO₂ and PuO₂ reported about a decade ago [71], which were based on two point extrapolation method.

3.3.3.5. Matrix effect in ThO₂ –MOS

In the calibration curves, the points representative of ThO₂-B, ThO₂-S and ThO₂-D lie along common calibration curves (Figure 3.6a & b) indicating that no matrix effects are observable among these samples. On the contrary, the line intensities for the ThO₂-MOS sample are not in line with those obtained from other samples (the concentration of traces in ThO₂-MOS are normalized by a factor 0.975 to compensate the matrix effect) as shown in Figure 3.8 .

To investigate this, we determined the plasma temperature by the usual method of the Boltzmann plot slope as recommended in [37, 95] using the set of neutral Fe lines available in the 350–400 nm spectral region. For each sample, this method was applied to one mean

spectrum calculated from the 30 spectra recorded on different sample spots. Table 3.9 gives the resulting excitation temperatures for the different thorium samples. No evident correlation is observed between the variations of plasma excitation temperatures. In particular, we do not observe a lower/higher temperature for ThO₂-MOS in spite of their “not in line” analytical response. As the uncertainties on the knowledge of statistical weights and transition probabilities are between 10% and 25% [96] and the precision of measurement depends on the detected signal level, we conclude that there is no major difference between the plasma temperatures obtained on the different samples as shown.

Consequently, the signal variations observed between the different matrices would principally result from different numbers of vaporized atoms rather than various plasma excitation temperatures. By elimination of the temperature effect, the number of vaporized atoms must be the driving parameter which varies between ThO₂-MOS and the other thorium samples. The difference in the number of vaporized atoms in case of ThO₂-MOS may be due to the hygroscopic nature of the UO₂ present in the ThO₂-MOS causing moisture uptake in the sample and thereby altering the numbers of vaporized atoms in the plasma. To eliminate this effect, ThO₂-MOS sample was dried in a furnace at 100° C for more than 2 days and then cooled overnight in desiccator prior to LIBS analysis. This procedure helped the MOS signal to come closer to the calibration line but not up to satisfactory level. Among the seven impurities, Fe(I) 277.210 nm, Mg(II) 279.552 nm and Mo(I) 386.410 nm could not be identified due to high spectral background. The results for other impurities were found to be positively biased (out of calibration range) when compared to the expected concentration values. This observation is characteristic of matrix effect, i.e., the influence of UO₂, which also has a complex emission spectrum causing enhancement and/or retardation of the line intensity, implying the need to have calibration standards with similar composition.

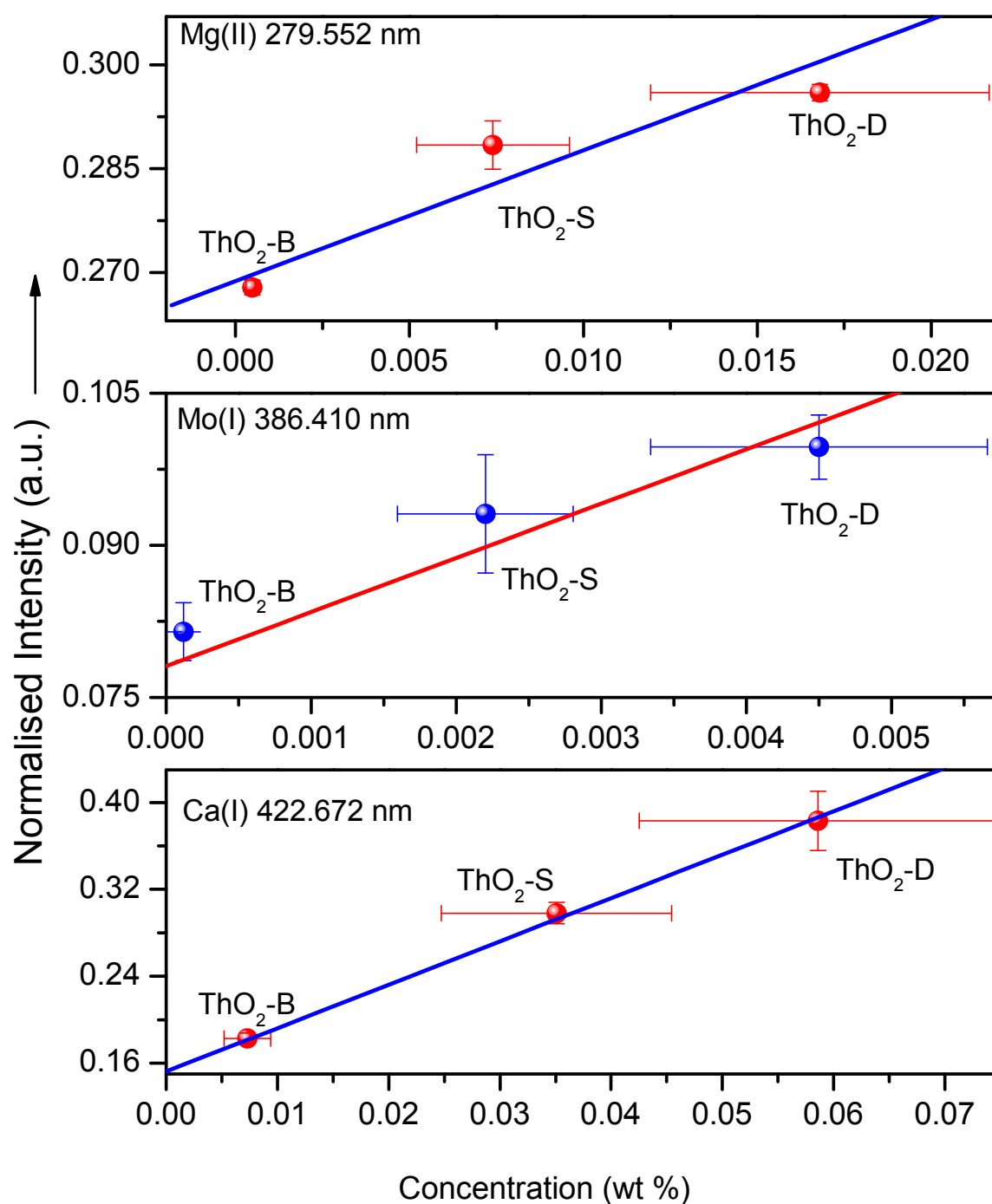


Figure 3.6a: Calibration curves obtained for different impurities in thoria by LIBS.

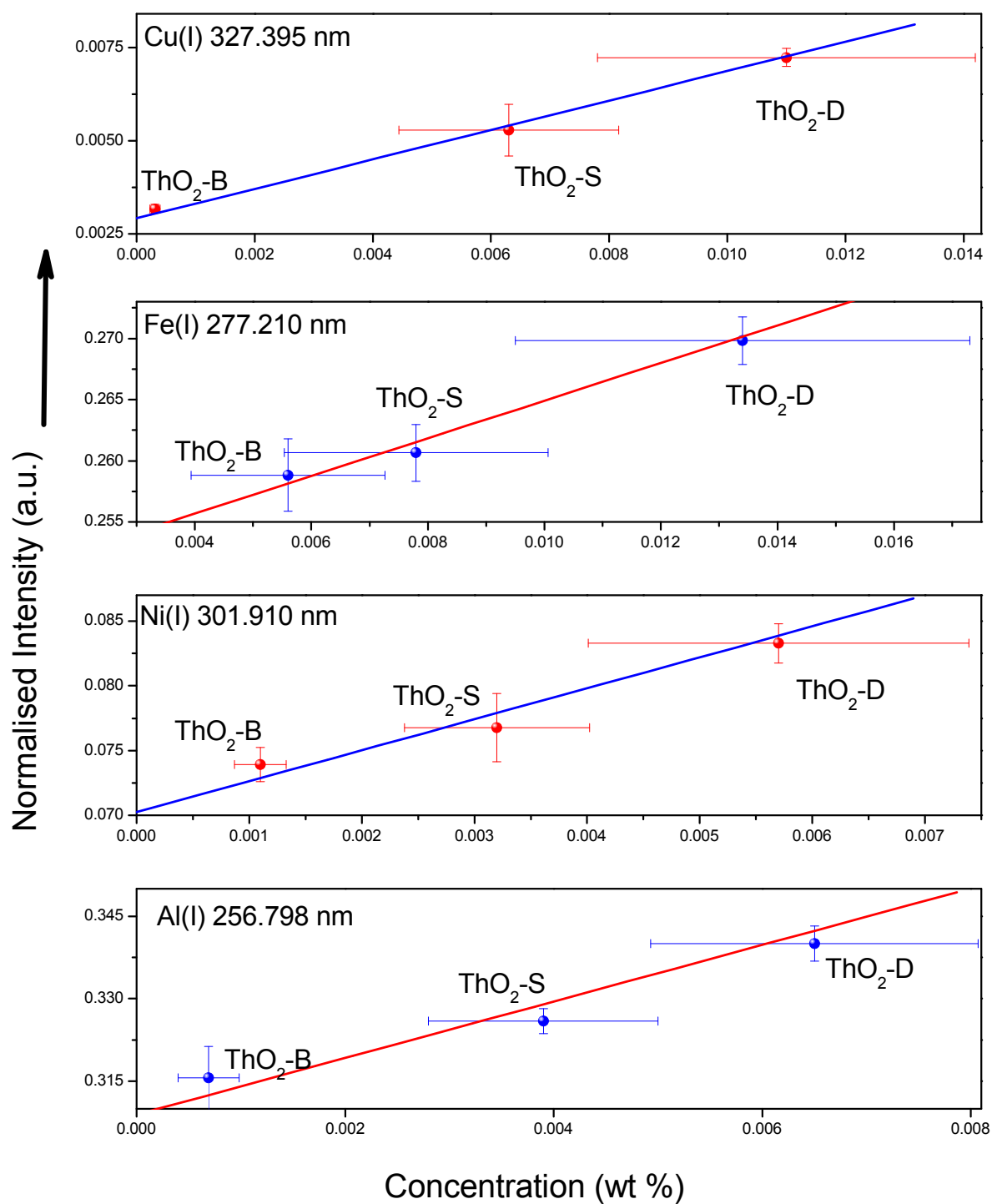


Figure 3.6b: Calibration curves obtained for different impurities in thoria by LIBS.

Table 3.7: *Elemental concentrations (in ppmw) in mixture of ThO₂ – S and ThO₂-D mixed in a 3:1 amount ratio*

Element	Emission line used (nm)	Expected concentration		LIBS	
		Mean (ppmw)	% RSD	Mean (ppmw)	% RSD
Al (I)	256.798	50	27.3	53.7	21.8
Ca(I)	422.672	449	31.1	524	7.3
Cu(I)	327.395	82	33.6	90	10
Fe(I)	277.210	113	30.4	134	11.4
Mg(II)	279.552	56	33.8	68	21
Mo(I)	386.410	33	30	55	21
Ni(I)	301.914	45	31.8	55	18

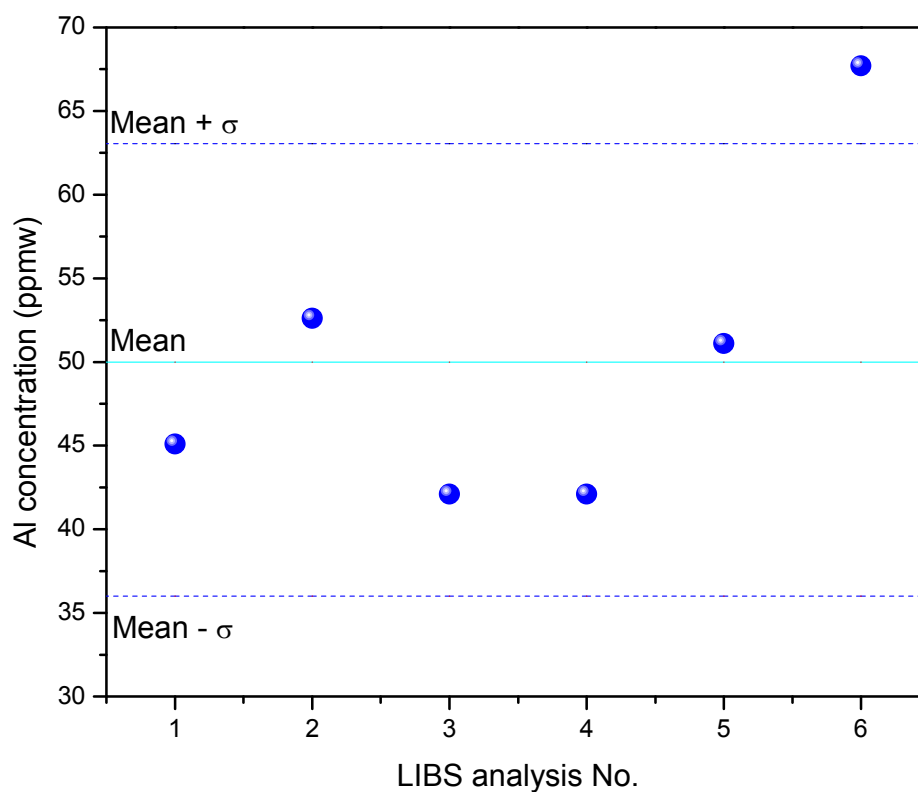


Figure 3.7: *A comparison of LIBS results of six replicate determinations of Al concentration in thoria with certified concentration of (50±13) ppmw (Table 3.7).*

Table 3.8: Comparison of LODs in ThO_2 matrix with those reported in literature for UO_2 and PuO_2 matrix

Element	Literature			Present Work	
	Wavelength (nm)	Matrix	Detection limit (ppmw)	Wavelength (nm)	Detection limit (ppmw)
Al	396.153	UO_2	200[71]	256.798	18
Ca	---	--	--	422.672	26
Cu	324.754	UO_2	150[71]	327.395	46
		PuO_2	90[71]	---	--
Fe	---	--	--	277.210	32
Mg	285.213	UO_2	70[71]	279.552	38
Mo	---	--	--	386.410	19
Ni	---	--	--	301.914	24

Table 3.9: Excitation temperature created on different thoria samples placed in the simulated remote sensing analysis condition

Sample	Excitation temperature (K)
$\text{ThO}_2\text{-B}$	5890
$\text{ThO}_2\text{-S}$	5785
$\text{ThO}_2\text{-D}$	5860
$\text{ThO}_2\text{-MOS}$	5620

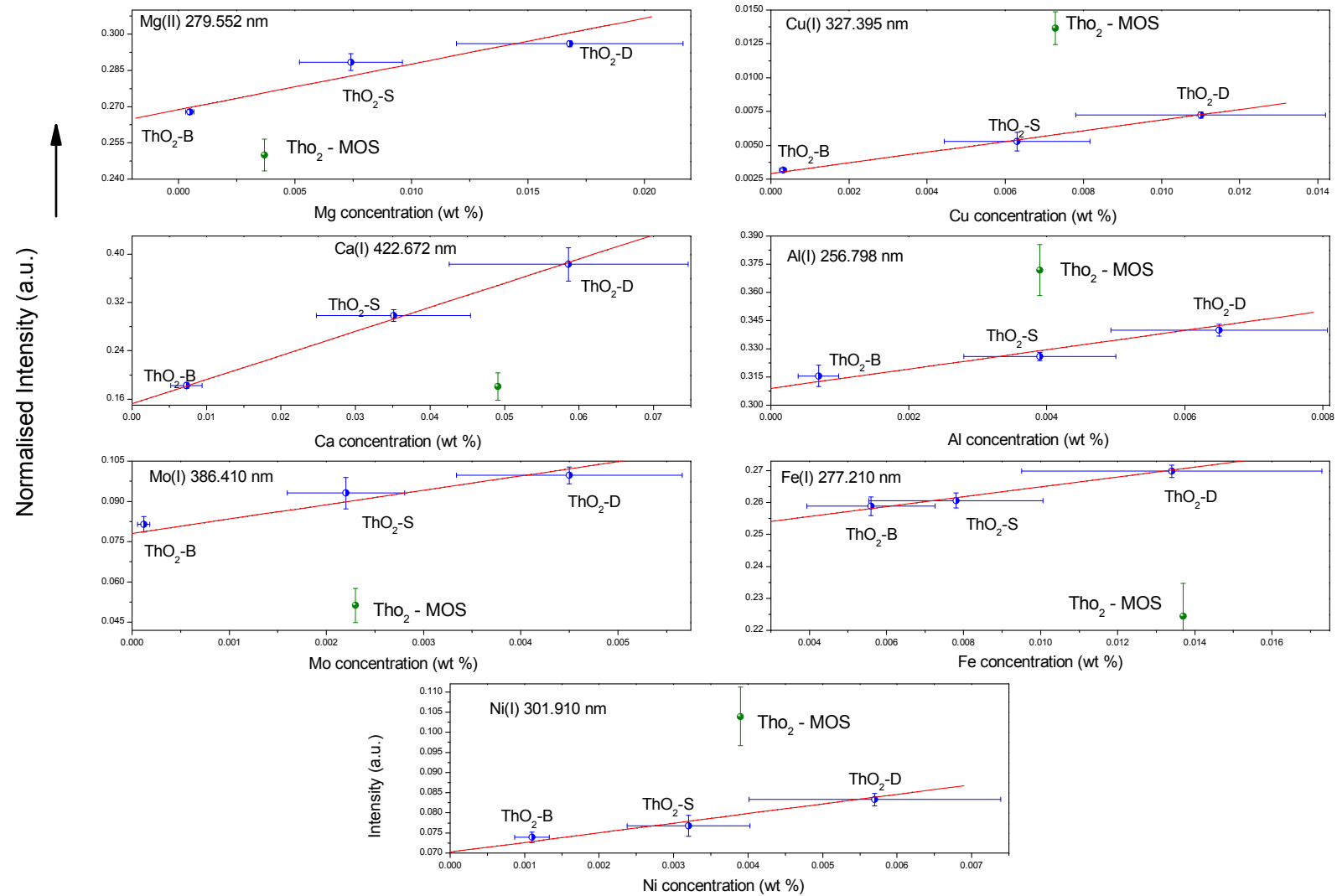


Figure 3.8: Calibration curves obtained for different impurities in thoria by LIBS including out of line signal from ThO₂ – MOS sample.

3.3.4. Conclusions

It is known that analysis of ThO_2 for impurities determination by emission spectroscopy is a challenging task. But any analytical method which does not employ the sample dissolution is to be preferred. Owing to the increased thrust for the deployment of Th in nuclear fuel cycle, the investigation reported would be useful for quick characterization of the ThO_2 fuel materials. Moreover, due to the remote analysis capability of LIBS, it can be applied for the direct monitoring during fuel pellet fabrication. Here studies for quantitative determination of elements in Thoria by LIBS was reported. 14 elements were detected and calibration curves were obtained for 7 elements using indigenously developed standards. The detection limits obtained by LIBS for these elements are lower than their specification limits in ThO_2 nuclear fuel. There is a need to develop calibration standards of mixed oxides to facilitate ThO_2 – MOS quantification.

Elemental Characterization in Liquid Matrix by LIBS



Chapter IV

4.1. INTRODUCTION

Applications of LIBS to aqueous samples have not been as plentiful as solid applications, primarily due to poor analytical performance compared to other techniques such as the ICP or flame. Nonetheless, applications of LIBS in liquids have been reported over the last 20 years with remarkable interest observed in the past 5 - 6 years. There are a few problems associated with LIBS of liquid samples such as splashing, surface ripples, quenching of emitted intensity, a shorter plasma life-time etc. [12, 97, 98]. Frequent cleaning of exposed optical components (focusing lens or window) is necessary to remove the accumulated matter ejected and splashed from the liquid sample by incident laser pulses. The miniature shock waves associated with the vaporization of liquid samples create aerosols above the liquid surface and disrupt both incident laser beam and the emitted light returning to the spectrometer. Shock waves also tend to induce waves on the liquid surface, which increase shot-to-shot signal variation and degrade the precision of the spectral measurements. The laser pulses also generate bubbles inside liquids which are transparent at the laser wavelength. These bubbles may reach the liquid surface and change the characteristic of laser induced plasma, thereby affecting the reproducibility of the measurement. The angle of incidence of laser beam at liquid surface changes when bubbles created inside the liquid by laser pulse burst at the surface, or the waves induced on the surface by the laser pulse are not dissipated. This, in turn, can change the fluence of the laser, and hence the emission intensity. The aerosols created by laser-liquid interaction also absorb the laser beam, and partially obstruct it from reaching to the sample surface. This absorption can change the reproducibility of the measurements by affecting the energy delivered to the sample. For many aqueous applications, these problems can be avoided by producing the plasma inside the liquid, if liquid is transparent at laser wavelength. However, the major drawback of this configuration is that it displays reduced line intensity and plasma emission

lifetime due to quenching. This plasma emission lifetime is of the order of $1\mu\text{s}$ or less in liquid, which is significantly lower than air-liquid interface where time interval average is $5\mu\text{s}$ to $20\mu\text{s}$. In spite of these problems associated with LIBS of liquid samples, increased number of publications in this area indicates its importance. Particularly, requirement of online monitoring of pollution as well as some long lived radioactive materials in nuclear waste has made these applications very interesting. To overcome the problems associated with liquid samples, a variety of configurations have been employed for recording the LIBS spectra of liquid samples. Sampling approaches used in LIBS of liquids can be divided into 5 main categories; bulk, droplets, wet aerosols, surface, and jets [12, 97, 99-108].

LIBS has been used for the determination of several elements such as Mg, Ca, Cr, Ni [97] and some chlorinated hydrocarbons (CHCs) in aqueous solutions [101]. LIBS has also been applied for the bulk analysis of aqueous solutions containing alkali metals [12, 109], alkaline earth metals [12, 109, 110], and other metals [12]. Experiments on droplets have been reported for the determination of Li, Na, Mg, Ca, Mn, Al [111, 112] as well as for K [106, 112], Ba [106], Rb, Li, and Cd [75] in a liquid jet. Species in organic solvents have also been determined [12].

A few authors have reported novel approaches that involve changing the original liquid sample into a solid. Schmidt *et al.* [108] demonstrated analysis of divalent and trivalent cations following pre-concentration on a chelating membrane. This approach has also been used to speciate aqueous chromium [114]. Vander Wal *et al.* [115] reported the lowest detection limits to date (10 ppb for many elements) by evaporating solutions onto a graphite surface, then analyzing same way as solids. Sampling frozen solutions was reported by Caceras *et al.* [116] as an alternative to sampling “wet” solutions.

These solid methods appear to be more sensitive than sampling solutions as more energy is available for excitation. In solutions, much of the laser energy incident on a

wet solution is used to vaporize the water. The solid methods are also performed in ambient air and don't suffer from significant plasma quenching. Additional advantages of the present technique are: (a) no splashing occurs on the surface of the liquid and no drastic reduction in plasma emission intensity is observed; (b) no pre-enrichment of the solution is required; (c) it is much easier to handle solid than liquid samples, making quantitative analysis with detection limits of the order of a few ppm possible, sufficient for direct application; and (d) neither optical transparency of the liquid nor a sophisticated fiber-coupling procedure arrangement or alignment are necessary.

This Chapter discusses the development of analytical methodologies using LIBS for the quantification of elements in liquids. This Chapter has been sub-divided according to the region of Periodic Table from where the elements are selected – (i) high atomic number (Z) elements (U and Th) (ii) middle Z elements (Ru, Rh and Pd) (iii) low Z elements (B and Li).

4.2. METHODOLOGY FOR LIQUID ANALYSIS

In this Chapter, a different approach based on the Vander Wal's [115] developed method i.e., solid surface analysis technique without modifying the present equipment setup was tried. The instrumental set-up described in Chapter II shows the sample chamber of the present system which is vertical. Hence this approach was considered for the present study. In the solid surface analysis technique, the liquid was added drop wise by a volumetric pipette (Eppendorf, Germany) to a solid support and then it was dried with the help of a hot air blower. Subsequently, the material was allowed to cool to room temperature and was then mounted in the sample holder for analysis (Figure 4.1). The solid surface analysis technique exploits the strengths of LIBS without the problems inherent to liquid analysis while maintaining the main advantages of the LIBS. In the present thesis, Whatman-42 membrane filter paper and Graphite planchet were used as solid sample supports depending on the sample nature.

4.3. DETERMINATION OF HIGH ATOMIC NUMBER ELEMENT (U & Th) IN SOLUTION BY LIBS

4.3.1. Background

LIBS is a promising and attractive technique for application to nuclear materials as the technique is non-destructive and involves minimum sample preparation steps. The latter feature helps in reducing the radiation exposure of the analysts involved in the analysis of nuclear materials. Also since the technique can be directly applied for analyzing solid samples, it eliminates the problems associated with recovery of actinide elements from solutions.

There are very few publications for LIBS quantification of high atomic number (Z) elements like actinides in liquid matrix. Wachter *et al.* [100] showed the determination of U in solution by bulk analysis method with detection limit of 0.1g/L. Samek *et al.* [36] also analyzed U by laminar liquid jet method. Otulu [117] quantified U in dry aerosol by LIBS.

In this section, an experimental set-up for analyzing Th and U separately and also in the presence of each other in aqueous solutions is described, while maintaining the main advantages of the LIBS i.e. less sample preparation steps and in situ measurement.

4.3.2. Samples preparation & analysis

Stock solutions of Th and U were prepared by dissolving known amounts of U_3O_8 and $Th(NO_3)_4 \cdot 5H_2O$ in suprapure nitric acid (M/s. Merck). Concentration of U in the stock solution was determined using biamperometry, employing Ti(III) as reductant. For Th stock solution, complexometric titration with EDTA using xylenol orange as indicator was used. Suitable dilutions were made from the stock solutions to prepare standard solution with Th and U concentrations in the range of 0 to 5000 ppmw shown in Table 4.1 to established calibration plots.

Synthetic mixtures of Th & U were prepared by mixing the individual solutions of U and Th on weight basis. All the mixtures were made by keeping U amount nearly same ($\pm 2\%$), and Th amount was varied so that Th/U amount ratio ranged from 0.005 to 0.5 (Table 4.2).

Volumetric pipette (Eppendorf, Germany) was used to transfer 40 μL of solution drop wise to the Whatman-42 membrane filter paper. The solution spread circularly over the filter paper with a radius of approximately 1 cm. The solution was evaporated to dryness with the help of a hot air blower. Subsequently, the paper was allowed to cool to room temperature and was then mounted in the sample holder. The spatial extent of the sample was marked on the filter paper so that the analysis could be performed over a region of 1 cm diameter where both U & Th are expected to be uniformly distributed.

All experiments were carried out under identical conditions of laser fluence, repetition frequency and acquisition delay. Triplicate analyses were performed on all samples including the calibration samples as well as the unknowns. The emission lines for Th & U determination were selected from the regions where minimal spectral interferences were observed and their intensities were ratioed w.r.t. C(I) 193.029 nm. Among the two most intense C(I) lines 193.029 nm and 247.856 nm, the latter is relatively intense but the emission peak profile was much cleaner for the former and was, therefore, used. Fe(I) at 249.064 nm present in the filter paper contributes to the back-ground at the C(I) 247.856 nm line as shown in Figure 4.2.

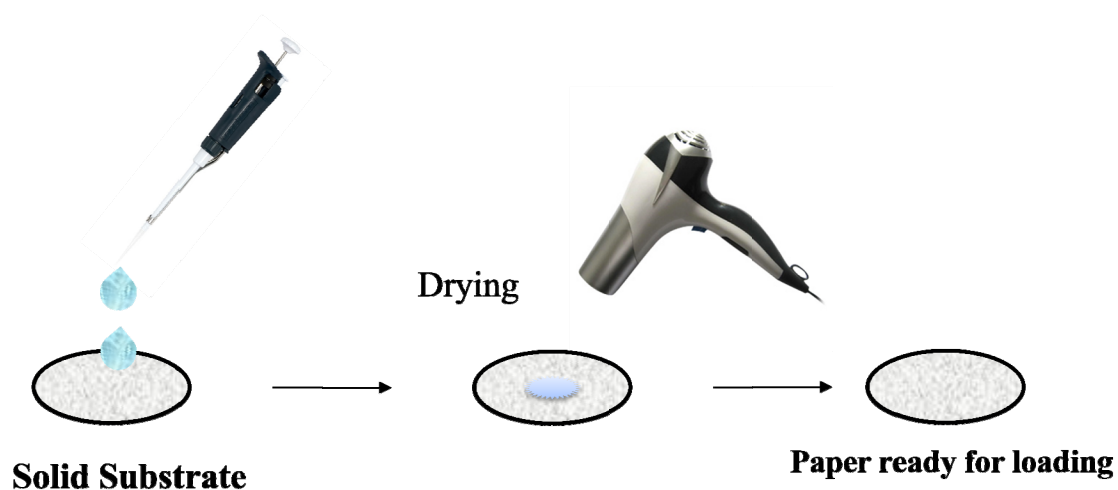


Figure 4.1: Sample loading procedure for solid surface analysis technique.

Table 4.1: Concentrations of pure U and Th solutions prepared for analysis

Solution ID	U conc. (ppmw)	Solution ID	Th conc. (ppmw)
U1	4997	Th1	4500
U2	3205	Th2	2500
U3	1846	Th3	1500
U4	801	Th4	919
U5	619	Th5	672
U6	388	Th6	468
U7	234	Th7	179
U8	100	Th8	109
U9	50	Th9	66
U10	20	Th10	46
U11	10	Th11	24

Table 4.2: Concentrations of the pure U and Th solutions used to prepare mixtures for analysis

Solution ID	U conc. (ppmw)	Th conc. (ppmw)	Th:U
FSM1	6678	3160	0.473
FSM2	6690	2177	0.325
FSM3	6712	1226	0.183
FSM4	6547	553	0.085
FSM5	6531	216	0.033
FSM6	6765	122	0.018
FSM7	6719	75	0.011
FSM8	6728	54	0.008
FSM9	6585	34	0.005

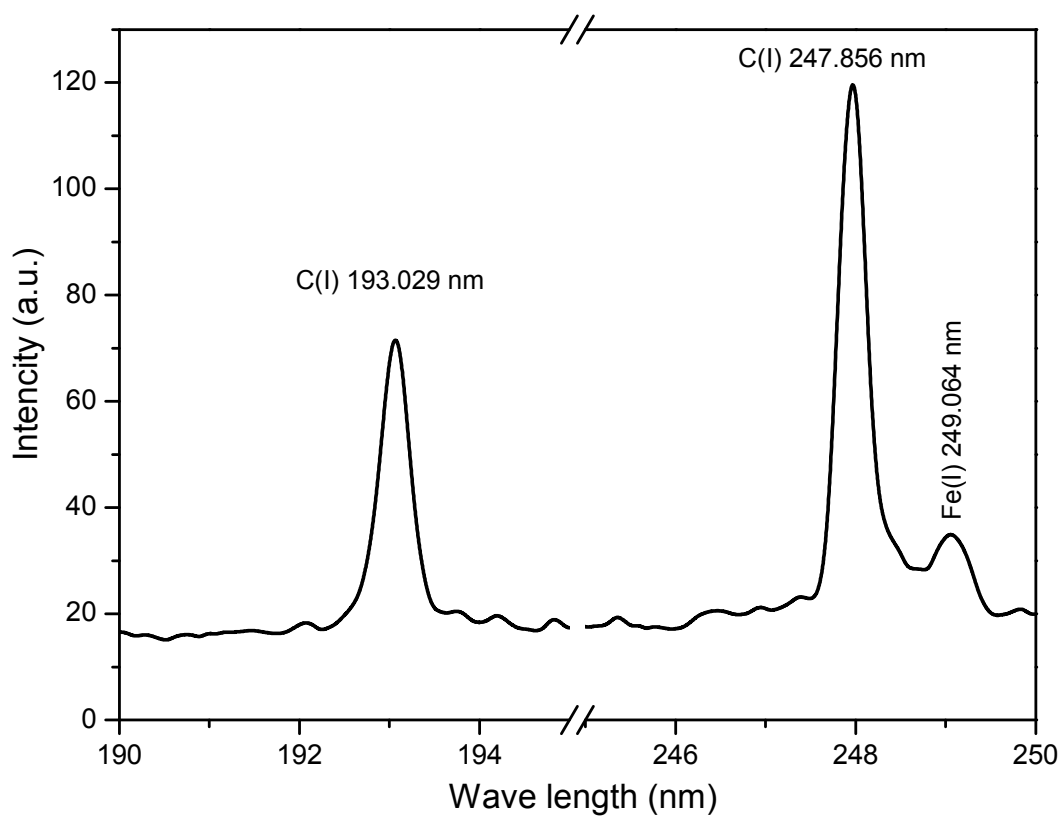


Figure 4.2: Carbon emission lines from Whatman – 42 membrane based filter paper.

4.3.3. Results & discussions

4.3.3.1. Selection of emission line

The spectral region (180–850 nm) used for recording the emission lines contained most of the strong emission lines of both U and Th. The spectra obtained using pure Th and pure U solutions under the identical conditions of analyses (laser fluence and acquisition delay) are shown in Figure 4.3. It was observed that there are a number of emission lines which can be employed for determination. The selection of emission lines for the qualitative and quantitative determination of U and Th was based on the following criteria:

- (a) The spectral lines that are usually employed in other emission spectroscopic experiment like ICP-AES etc.
- (b) No strong spectrally interfering emission from the other actinide element within ± 0.3 nm, so as to allow determination of U & Th in a mixture.
- (c) Emission line with $E_{\text{lower}} = 0$ or as low as possible were preferred. Though the emission line with ground state near to or equal to zero has the possibility of self-absorption, but they have the highest sensitivity and this property is very useful especially when the concentration of the species of interest is very low.
- (d) The emission line should have a high transition coefficient (A).
- (e) High signal to noise ratio (SNR) should exist under the conditions of analysis by LIBS.

By careful comparison of the emission spectra, two lines for U and three lines for Th were selected. The spectral lines considered for LIBS analysis and their available spectroscopic data are listed in Table 4.3.

4.3.3.2. Effect of substrate

Our approach consisted of evaporation of the analyte solution on a commercially available filter paper (Whatman-42) substrate followed by LIBS analysis of the substrate surface. The data reported on the concentrations of different trace elements in the Whatman–42 membrane filter paper are given in Table 4.4. Since both Th and U were not present in the

filter paper and no observable spectral lines for these two elements were seen during the LIBS analysis of blank filter paper, this was selected as substrate to minimize the blank contribution. It may also be mentioned that care has to be taken to completely dry the liquid on the filter paper for obtaining reliable results. A small amount of moisture, if present, drastically reduces the emission intensity of the lines of interest and leads to erratic results. At fluence corresponding to laser energies of higher than 100 mJ, slight charring of the filter paper was observed and hence the laser energy was fixed at around 100 mJ for the present work.

4.3.3.3. Time resolution

As reported in the application of LIBS on solids, time-resolved spectroscopy is essential for improving the sensitivity in any LIBS experiment. An adequate selection of acquisition delay time involves a compromise between signal-to-background ratio and line intensities. In the present work, an acquisition delay of 600 ns was selected for recording spectral lines corresponding to 100 mJ of laser energy to obtain the optimum SNR.

4.3.3.4. Reproducibility

The reproducibility was evaluated by observing the intensity of the Th(II) 401.913 nm line emission by carrying out replicate analyses from the same filter paper as well as by using a number of filter papers. Replicate analyses by using the same filter paper yielded a relative standard deviation (RSD) of about 20%. The signal intensity was also found to decrease with successive analyses. This was attributed to loss of significant amount of absorbed analyte or could be due to damage of the filter paper. An RSD of about 2% was obtained for the line intensity for ten analyses using 10 independent filter papers, which indicated very good reliability of the LIBS analysis. Reproducibility for U(II) 367.007 nm was also determined and was found to be nearly the same as that for Th(II) 401.913 nm line. Figure 4.4 shows the results of these measurements.

Table 4.3: *Characteristics of Spectral lines employed for LIBS analysis of U and Th*

Element	λ_{ij} (nm)	A_{ij} ($10^8 s^{-1}$)	E_j (cm^{-1})	E_i (cm^{-1})
U(II)	367.007	0.26	914.765	28154.45
U(II)	409.013	0.19	1749.123	26191.309
Th(II)	283.729	-	6213.490	41447.959
Th(II)	318.019	0.88	1521.896	32957.429
Th(II)	401.913	0.41	0	24873.983
λ_{ij} is the transition wavelength, A_{ij} is the transition probability, E_i and E_j are the energies of the upper and lower level, respectively.				

Table 4.4: *Trace elements in the Whatman – 42 membrane filter paper [118]*

Element	ppmw	Element	ppmw	Element	ppmw
Al	2	Cr	0.3	N	12
Sb	<0.02	Cu	0.3	K	1.6
As	<0.02	F	0.2	Si	< 2
Ba	<1	Fe	6	Na	33
B	1	Pb	0.2	S	< 5
Br	1	Mg	1.8	Zn	0.6
Ca	13	Mn	0.05		
Cl	80	Hg	<0.005		

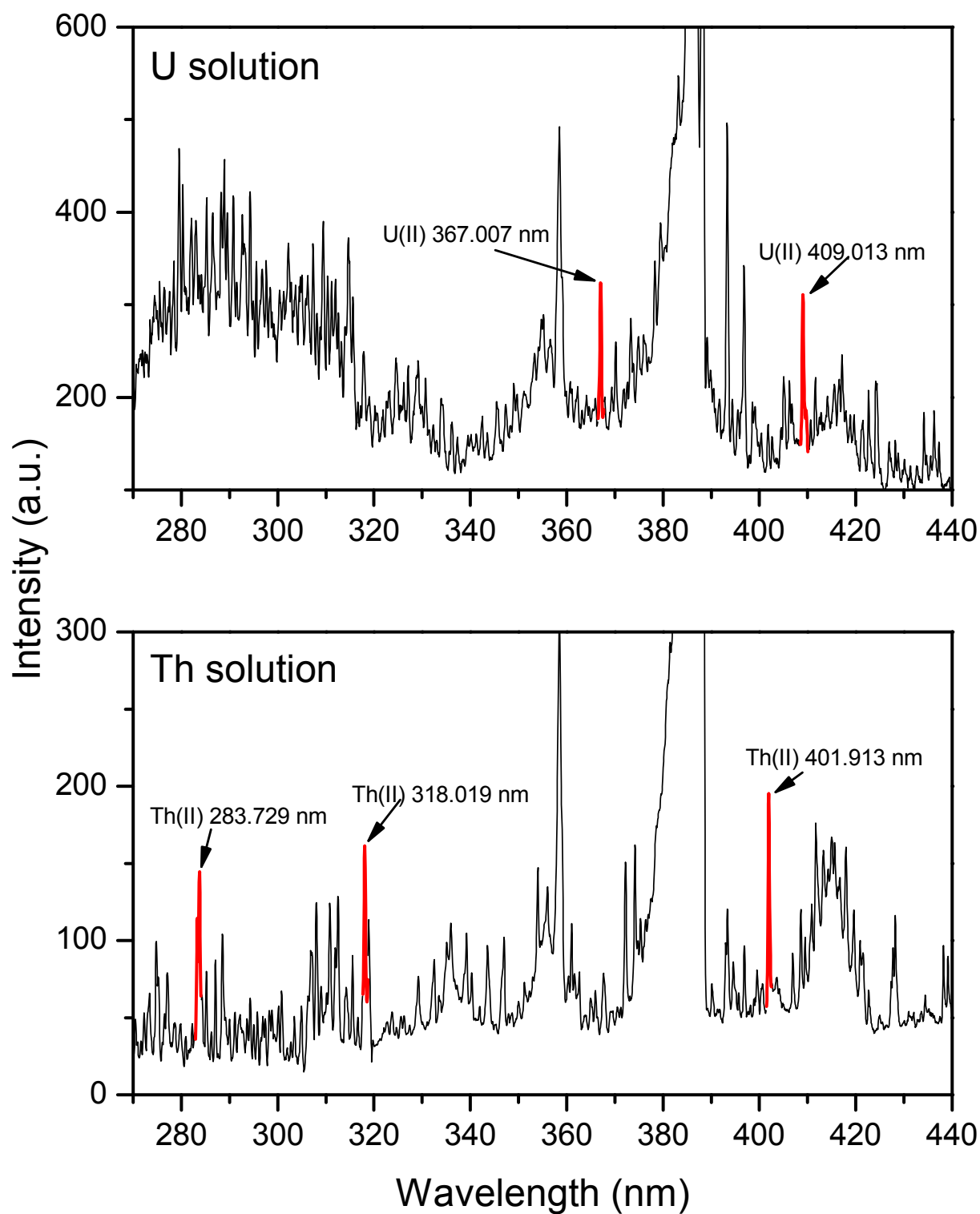


Figure 4.3: Emission spectra of U and Th obtained by LIBS under identical conditions of analysis.

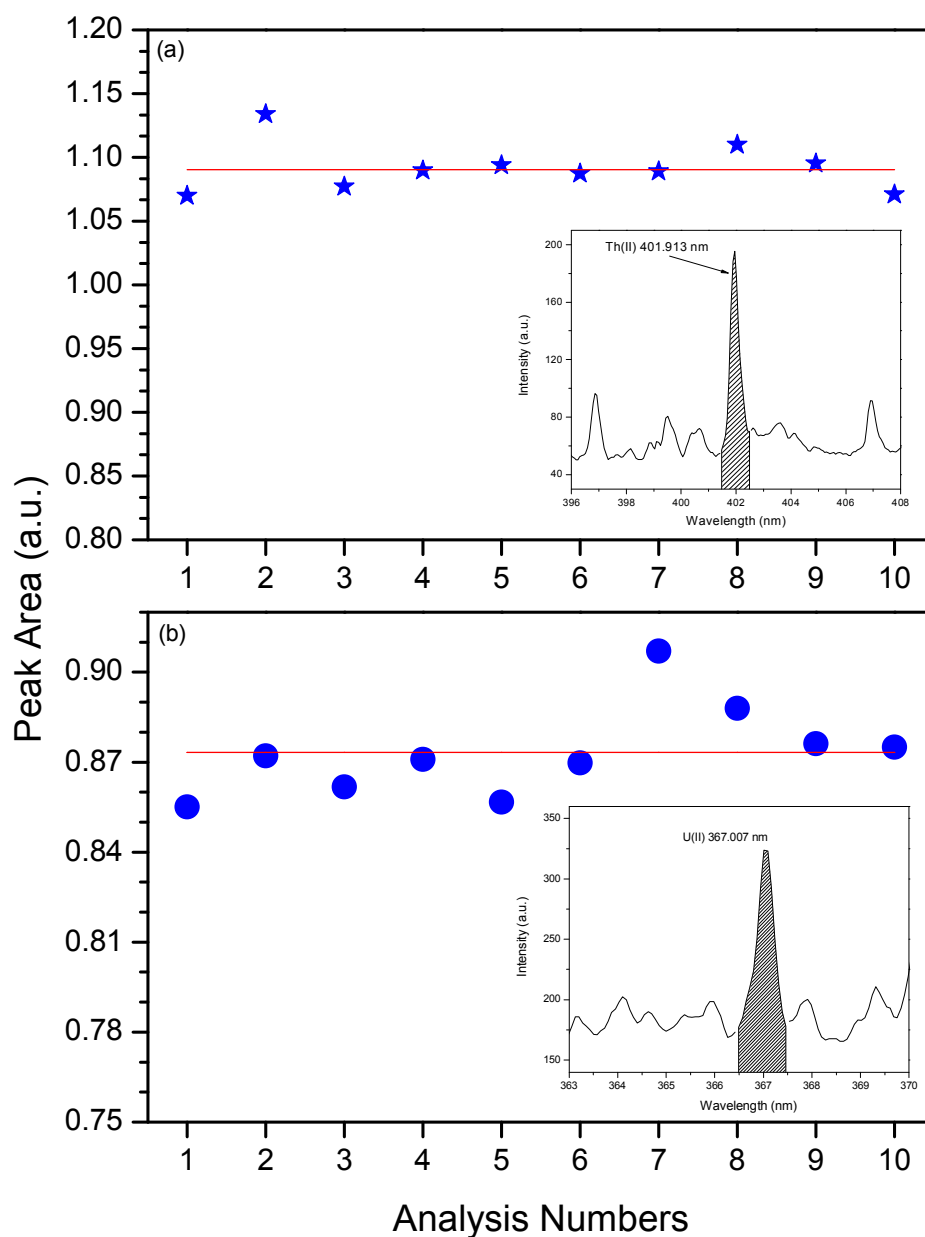


Figure 4.4: Reproducibility of (a) Th(II) 401.913 nm (b) U(II) 367.007 nm line emission from ten measurements carried out using independent filter papers under the identical experimental conditions. The horizontal straight line represents mean value and the inset shows peak region used for integration.

4.3.4. Calibration curves

4.3.4.1. Individual elemental calibration & LOD

For obtaining the calibration curves for Th and U, standard solutions were used. The experimental data for the concentrations of Th or U and the normalized intensities of the spectral lines were fitted to polynomial equations of degree one and two, and the results are listed in Table 4.5. Figure 4.5 shows the calibration curves for Th and U. Saturation effects were observed for Th and U above 1000 ppmw and 800 ppmw, respectively. The calibration curves deviated from linearity due to self-absorption. This effect was much more pronounced for Th and hence the data corresponding to the higher concentration of Th are not shown in the Figure 4.5. For the higher concentrations of U, a polynomial equation of degree two was used to fit the data. In the case of Th, interestingly even in the low concentration range of 0 to 1000 ppmw, the two distinct concentration regions namely 0 to 180 ppmw and 180 to 1000 ppmw with different calibration curves were obtained.

The limit of detection (LOD) for both Th and U was determined according to the definition $3\sigma_B/s$, (discussed in previous Chapter III). In this work, σ_B was determined from 10 measurements of blank signals under the same experimental conditions, where the sample was a filter paper with only deionized water. Table 4.6 gives the LODs determined from different spectral lines of Th and U. Th quantification in a solution by LIBS is reported in this study for the first time. To verify the calibration of our investigations, two standard solutions of U and Th were prepared and analyzed. In the case of U, the 367.007 nm and 409.013 nm lines yielded accuracy values of 2.2% and 4.8%, respectively. Relative precision in both the cases was less than 5%. Among the three spectral lines of Th, 283.729 nm and 318.019 nm lines gave an accuracy of about 10% with precision more than 10%. The calibration curve corresponding to 401.913 nm emission line gave an accuracy of 4% with 7% precision.

Table 4.5: *Fitted parameters obtained from calibration curves for U and Th using polynomial equation $y = a + bx + cx^2$*

Element	Analytical line (nm)	Concentration range (ppmw)	a	b	c	R*
U	367.007	0 - 5000	0.0078	5.59×10^{-5}	-4.71×10^{-9}	0.999
	367.007	0 - 800	0.0081	5.30×10^{-5}	0	0.999
	409.013	0 - 5000	0.0097	4.56×10^{-5}	-3.56×10^{-9}	0.999
	409.013	0 - 800	0.0106	4.12×10^{-5}	0	0.997
Th	283.729	0 - 180	0.0124	4.56×10^{-4}	0	0.995
	283.729	180 - 1000	0.0673	1.59×10^{-4}	0	0.998
	318.019	0 - 180	0.0166	4.03×10^{-4}	0	0.931
	318.019	180 - 1000	0.0700	1.92×10^{-4}	0	0.999
	401.913	0 - 180	0.0315	1.32×10^{-3}	0	0.997
	401.913	180 - 1000	0.1840	4.92×10^{-4}	0	0.998
Th (In the case of mixture calibration)	401.913	0 – 0.0035 (Th/U)	0.6475	15.122	0	0.999
	401.913	0 – 0.5 (Th/U)	0.6901	11.281	-5.426	0.999
*R denotes regression coefficient						

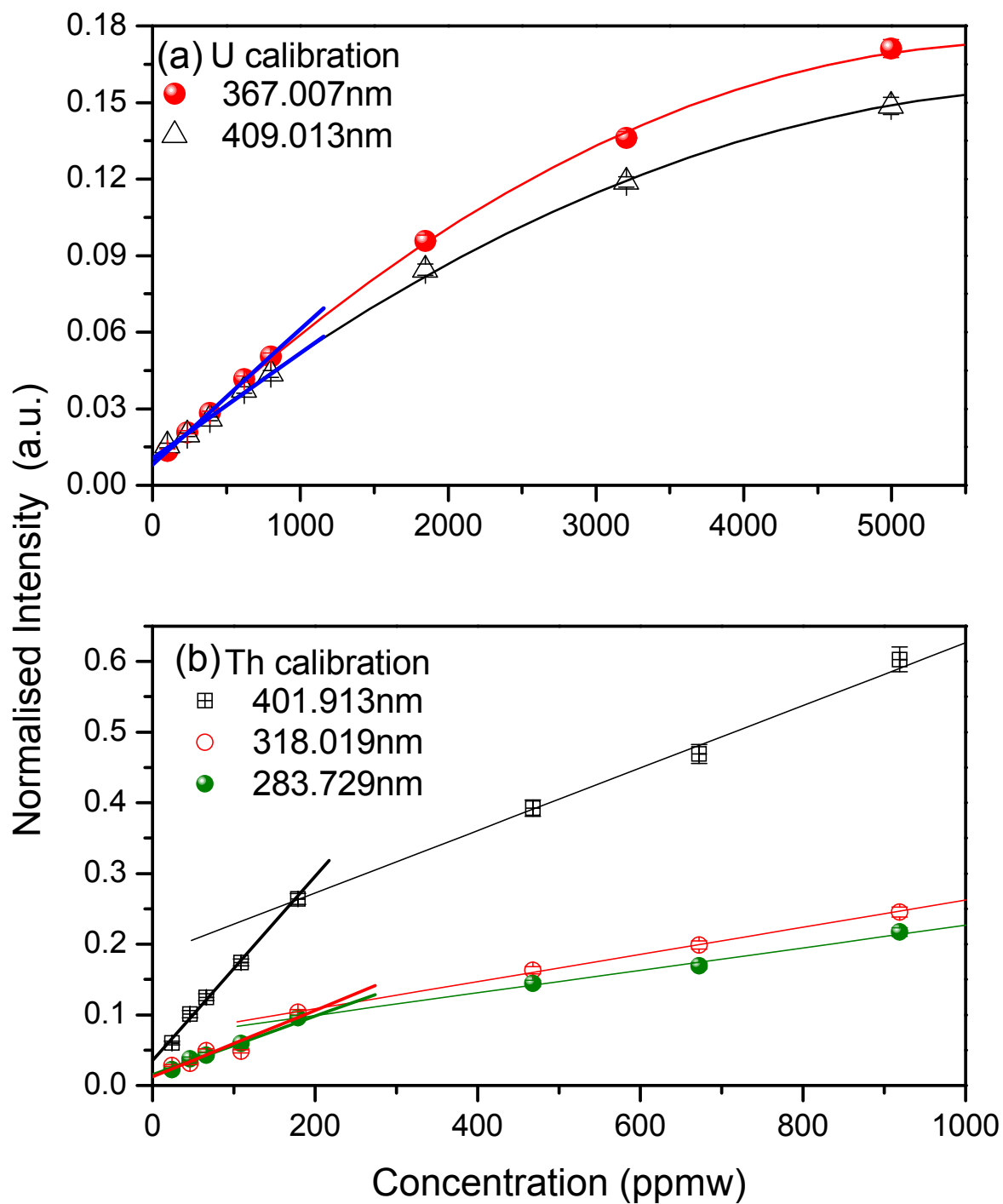


Figure 4.5: Calibration curves of (a) U and (b) Th in aqueous solution fitted with polynomial equation. Error bars show standard deviation from multiple measurements at each concentration value.

Table 4.6: *Limits of detection for U and Th*

Element	Analytical line (nm)	LOD (ppmw)
U(pure)	367.007	18.5
	409.013	24.6
Th(pure)	283.729	1.6
	318.019	2.25
	401.913	0.72
Th (<i>in presence of bulk of U</i>)	401.913	0.0007 [#]
[#] denotes Th/U amount ratio		

Table 4.7: *Comparison of analytical results of LIBS with expected values.*

Sample No.	Th/U amount ratio		(X/Y)
	Expected value (X)	LIBS value (Y)	
1	0.2373 ± 0.0003	0.2371	1.001
		0.2399	0.989
		0.2406	0.986
2	0.0859 ± 0.0006	0.0813	1.057
		0.0845	1.017
		0.0862	0.997

4.3.4.2. Th – U mixture calibration & LOD

LIBS is always associated and affected by matrix effects.. Therefore, the calibration curves obtained using pure elements cannot be used for a solution containing a mixture of two or more elements. In the present case of U and Th, this problem is further aggravated due to the complex emission spectra of both the elements. It can be noticed from pure Th spectrum (Figure 4.3), that there is a band of spectral lines in the 405 nm to 425 nm region, making U(II) 409.013 nm line unsuitable for any analytical purpose. The U(II) 367.007 nm emission line also had significant spectral interference from Th(I) 366.998 nm line. This makes it difficult to quantify trace amount of U in bulk of Th. However, determination of trace amount of Th in presence of bulk of U was possible, since Th(II) 401.913 nm emission line is free from any spectral interference from U emission lines. The other two lines of thorium viz. Th(II) 283.729 nm and Th(II) 318.019 nm are affected either completely or partially by spectral interference from U emission lines. Calibration curve obtained by plotting intensity ratio of Th(II) 401.913 nm with respect to U(II) 367.007 nm vs. Th/U amount ratio is shown in Figure 4.6. The response of the Th/U signal was found to be linear up to Th/U amount ratio of 0.035, beyond which the saturation effect was observed.

To verify the calibration, two fuel pellets of Th and U were used as unknowns. The Th/U amount ratio in these pellets was determined by electrochemical (for U) and complexometric titration (for Th) methods after quantitative dissolution of the pellets. The results obtained from triplicate analyses by LIBS from the solutions agreed within 3 % with the expected Th/U amount ratios with a relative standard deviation of about 3 % (Table 4.7). The LOD was determined to be 0.0007 for Th/U amount ratio.

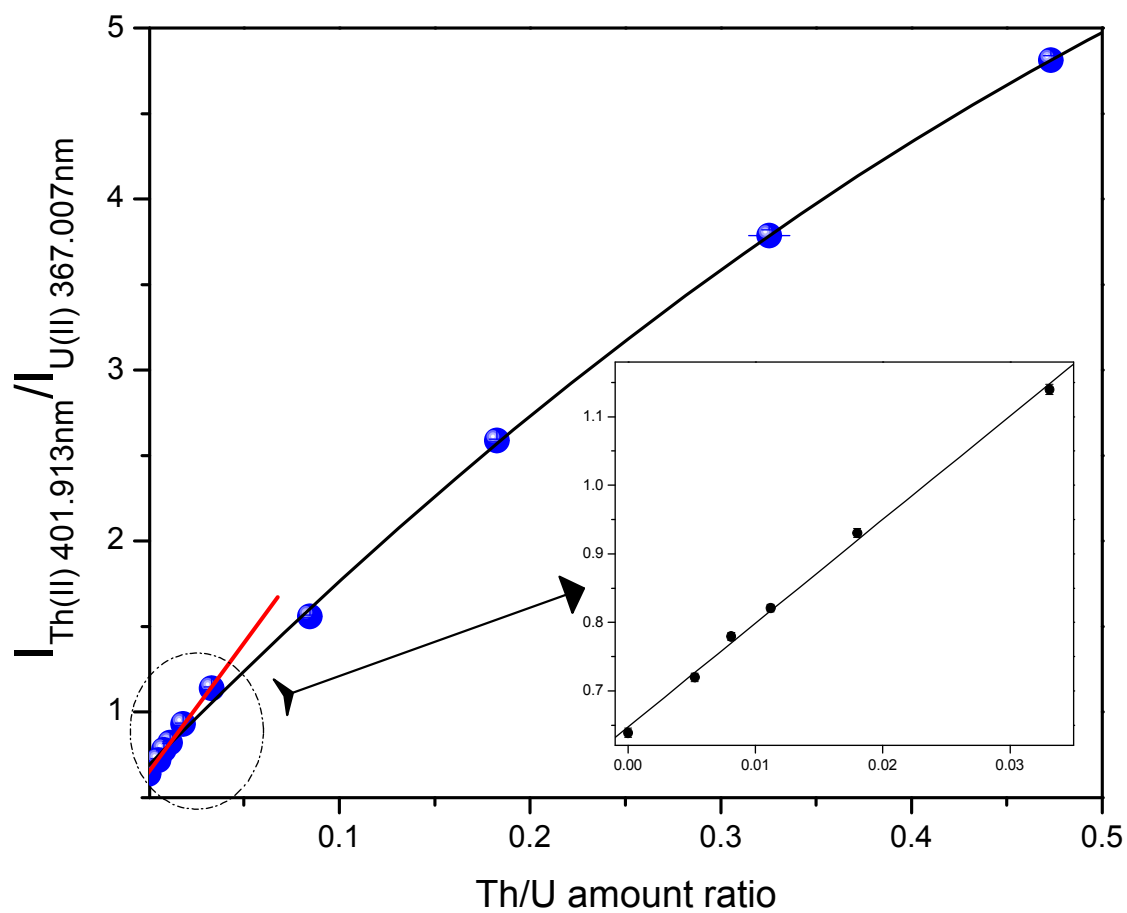


Figure 4.6: Calibration curve of U-Th mixture in aqueous solution. Error bars show standard deviation from multiple measurements at each value.

4.3.5. Conclusions

LIBS has been developed for the determination of Th and U in aqueous solutions. From the above observations, it can be concluded that LIBS is useful for the determination of trace amounts of Th in presence of bulk of uranium, while the same is not possible for trace determination of U in presence bulk of Th due to significant interference from Th emission lines. The developed LIBS methodology will be highly useful since the radioactive analytical waste generated by other analytical methods can be reduced significantly. LIBS can also be employed for the determination of Th & U in mixed oxide pellets of Th & U but it might be necessary to quantitatively dissolve the pellets before analysis.

4.4. DETERMINATION OF MIDDLE ATOMIC NUMBER ELEMENTS (PLATINUM GROUP METALS) IN SOLUTION BY LIBS

4.4.1. Background

Uranium based nuclear fuels are employed worldwide for the production of electricity. The process of thermal neutron induced fission of ^{235}U leads to the production of a wide range of fission products with mass numbers ranging from 70 to 170 in varying quantities. The radioactive fission products (short-lived as well as long-lived) form a major component of nuclear waste generated during reprocessing of irradiated fuel in the nuclear fuel cycle. Some stable fission products are also formed during the fission process.

The platinum group of metals (PGMs) is an important group of elements which have a wide range of applications, but their natural resources are limited. The abundances of Pd, Rh and Ru in earth crust are 0.6 ppt, 0.2 ppt and 1 ppt, respectively [119]. These metals are used for catalytic processes in the production of hydrogen, in the electronic and electrochemical industries, anti-corrosion alloys, dental applications, catalytic converters in automotive industry etc. Among the platinum group metals (PGM) only three, namely palladium (Pd), rhodium (Rh) and ruthenium (Ru) are formed to significant extent during the fission process with their actual amounts depending on the type of reactor system as well as on the burn-up of the fuel [120]. It is estimated that in a commercial light water reactor, about 4 kg and in a fast breeder reactor, 19 kg of PGMs are produced per tonne of heavy metal undergoing fission in the fuel [121]. Nearly 1000 tonnes of PGMs are estimated to be present in high level liquid waste (HLLW) all over the world [122]. The demand for these noble metals continues to grow steadily. As the number of nuclear power plants increases, the availability of these metals is likely to increase and thus can serve as an important alternative resource to meet the increasing needs of noble metals [123].

During the reprocessing of the irradiated nuclear fuel by PUREX process, PGMs get distributed between high level solid waste and high level liquid waste. A significant amount of PGMs can be recovered from HLLW with complex processing techniques [122, 124, 125]. One of the most important requirements of a recycling process is a fast and reliable analytical procedure for quantification of the PGMs during the various stages of processing. It is necessary due to the high radioactivity associated with the samples. The composition of nuclear HLLW solution is very complex, with as many as 30 elements present in it with varying concentrations. Therefore, the quantification of Pd, Rh and Ru without matrix separation becomes extremely difficult. The voltametric [125] and spectrophotometric methods [122] are applied for the determination of Pd^{2+} in HLLW. Cavalli et al. described the inductively coupled plasma optical emission spectrometric method (ICP-OES) [126] for the determination of Pd in synthetic nuclear waste. Most of these techniques cannot be applied for on-line analysis or in the presence of other matrix elements.

Laser induced breakdown spectroscopy (LIBS) is an attractive analytical technique for the rapid determination of concentrations of the PGMs with the capability of providing real-time analytical data in HLLW in a single run. Previous sections have showed the applicability of solid sample support (namely Whatman – 42 membrane based filter paper) for liquid samples analyses by LIBS. In this section, the work carried out for quantifying PGMs namely Pd, Rh and Ru separately and in simulated high level liquid waste (SHLLW) using graphite planchet as a solid support is described. The effect of presence of uranium (U) in SHLLW on the quantification of PGM is also discussed.

A number of LIBS studies for the determination of Pd and Rh have been reported. Martin *et al.* [127] employed LIBS for determining of total Pd that was dispersed in specially synthesized bacterial cellulose membrane. Lucena *et al.* used LIBS for mapping the spatial distribution [128] as well as for quantification [129, 130] of Pt, Rh, and Pd in car catalytic

converters. These authors also studied the distribution of Pt in catalytic converters with increasing time of use of the catalyst [131]. Palacios *et al.* used LIBS for mapping Pt, Pd and Rh in auto catalyst [132]. Asimellis *et al.* [133] presented an application of LIBS for fast and accurate analysis of Pt, Pd and Rh concentrations in actual slurry pellet samples from auto catalyst scrap.

This section presents the studies performed on the application of LIBS for the determination of PGMs namely Pd, Ru and Rh in nuclear waste. To the best of our knowledge, detection and quantification of Ru by LIBS is reported for first time in this study.

4.4.2. Preparation of samples

Since the commercial liquid standards were not available in our laboratory, stock solutions of Pd, Rh and Ru were prepared from master solutions of Pd, Rh and Ru in HCl already available with us. These master solution were prepared by dissolving known amounts of anhydrous PdCl₂, RhCl₃ and RuCl₃ (Alfa Aesar, India), in concentrated HCl. The solutions were evaporated to dryness and quantitative amount of HNO₃ was added to prepare 3M HNO₃ solution of Pd, Rh and Ru. The solutions were converted to nitric acid medium to emulate the HLLW condition. The stock solution of U was prepared by dissolving known amount of U₃O₈ in supra-pure nitric acid (M/s. Merck). Concentration of U in the stock solution was determined using biamperometry employing Ti(III) as reductant. Concentrations of the Pd, Rh and Ru were determined by quadrupole based inductively coupled plasma mass spectrometry (ICP-MS). Suitable dilutions were made from these stock solutions to prepare individual standards with concentrations in the range of 0 to 800 ppmw to establish calibration plots. A SHLLW was supplied by Waste Management Division (WMD), BARC, Mumbai, India (SHLLW - 1). The composition of SHLLW - 1 shown in Table 4.8 was equivalent to high-level radioactive waste generated during reprocessing of irradiated fuel from PHWR (Pressurized Heavy Water Reactor) with burn-up of ~7 GWd/tHM (gigawatt

day per ton of heavy metals) and 3 years of cooling [134]. From this standard, two more synthetic waste solutions (SHLLW - 2 to SHLLW - 3) were prepared as shown in Table 4.9 by quantitative addition of U and PGMs, respectively. Mixtures of PGMs with U were also prepared (PGM – 1 to PGM – 4) by mixing the individual solutions of Pd, Rh, Ru and U on weight basis in such a manner that the PGMs amount remained nearly same ($\pm 5\%$) in all the solutions but U amount varied from 0 to 2500 ppmw as shown in Table 4.10. Spectroscopically pure graphite planchets (Ted Pella, Inc.) of 32 mm diameter and 1.6 mm width were used as solid sample support. The sample loading procedure was the same as described in the section 4.3.2.

4.4.3. Results & discussion

4.4.3.1. Selection of emission lines for analysis

4.4.3.1.1. Pure solution

LIBS spectrum in the 180–850 nm wavelength region was recorded, which contained almost all the strong emission lines of Pd, Rh and Ru. Among the several emission lines available from the emission spectra of individual PGMs, only those emission lines were chosen which provided a reasonably linear and good intensity variation over the concentration range of this study. Table 4.11 gives the list of emission lines which were selected based on the criteria described above for this work along with their calibration parameters.

4.4.3.1.2. Simulated high level liquid waste

Though a number of emission lines can be used for quantification of individual PGMs, all of them are not useful for the analysis of SHLLW, since many of these emission lines are spectrally interfered by the emission of other elements present in SHLLW. To select the most appropriate emission lines for the determination of Pd, Rh and Ru, the spectra of pure Pd, pure Rh, and pure Ru were compared with that of the SHLLW - 2. Figure 4.7 shows

a comparison of the four spectra under identical conditions of analysis. Among the emission lines selected for construction of individual calibration curves (Table 4.11), five emission lines were identified which were spectrally pure, Pd(I) 276.309 nm, Pd(I) 340.457 nm, Rh(II) 233.477, Ru(II) 245.657 nm and Ru(I) 372.802 nm. Pd(I) 340.457 nm has been used in a number of previous studies for Pd quantification [128 - 133], but to the best of our knowledge, Pd(I) 276.309 nm and Rh(II) 233.477 have not been used for quantification in LIBS, but Rh(II) 233.477 nm has been used in ICP-AES [135]. The analytical use of Pd(I) 324.270 nm, Pd(I) 360.954 nm and Pd(I) 363.469 nm in SHLLW was interfered by strong contribution from Y(II) 324.227 nm, Sm(II) 360.949 nm and Sm(II) 363.429 nm lines present in the SHLLW. The Rh determination was a bit more challenging, because the Rh lines had larger interference with the present sample matrix. Examination of the comparative spectral profile (Figure 4.7) indicates that the Rh(II) 233.477 nm line was the best choice to develop the application in SHLLW matrix. The two most commonly used Rh emission lines Rh(I) 339.681 nm and Rh(I) 343.488 nm were spectrally interfered by intense Pd(I) 340.457 nm and Pd(I) 344.139 nm emission lines, respectively. Rh(II) 242.709 nm, Rh(I) 270.373 nm and Rh(I) 369.235 nm were spectrally interfered by combination of several emission lines from Pd, Mn, Cr and Mo. Among the Ru emission lines in Table 4, Ru(II) 245.657 nm, Ru(II) 240.272 nm and Ru(II) 349.894 nm have been used in ICP- AES work [136, 137]. Except for Ru(II) 245.657 nm and Ru(I) 372.802 nm, other Ru emission lines were found to be spectrally interfered by matrix.

Table 4.8: *Composition of SHLLW-1 used in present study (acidity 3M HNO₃)*

Constituent	Concentration (ppmw)	Constituent	Concentration (ppmw)
Ba	60	Na	5500
Ce	60	Nd	120
Cr	120	Ni	110
Cs	320	Pr	90
Fe	720	Sm	86
K	220	Sr	30
La	180	Y	60
Mn	430	Zr	4
Mo†	140		

†Mo was added for Tc

Table 4.9: *Concentrations of added elements in other SHLLW used in the present study*

Constituent	Concentration (ppmw)	
	SHLLW-2	SHLLW-3
U	0	6340
Pd	526	421
Rh	250	210
Ru	32	40

Table 4.10: *Composition of PGM mixtures with varying U concentrations*

Constituent	Concentration (ppmw)			
	PGM-1	PGM-2	PGM-3	PGM-4
U	0	501	1226	2503
Pd	318	309	316	310
Rh	327	318	336	317
Ru	46	41	44	42

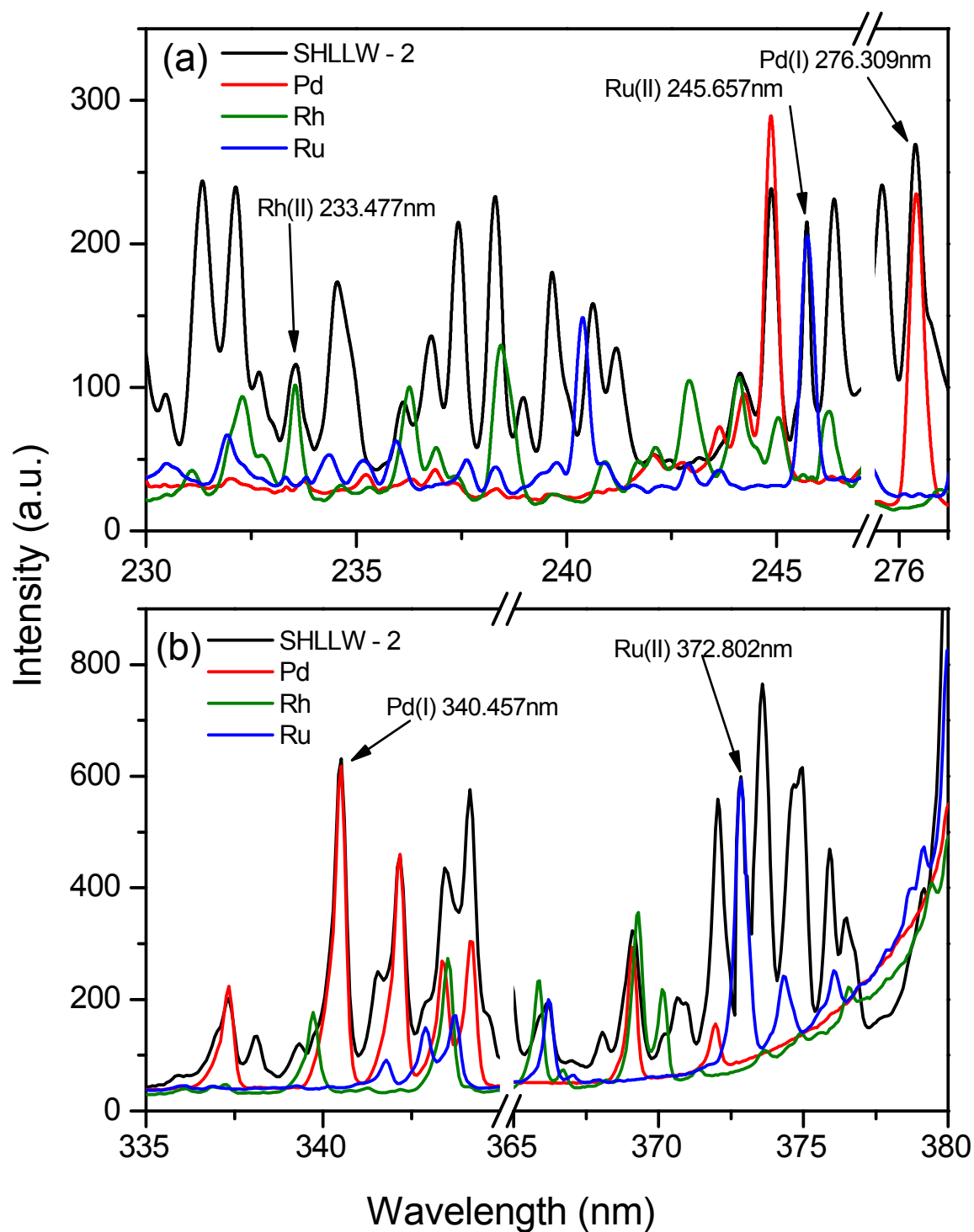


Figure 4.7: Comparison of the spectra of the individual PGMs with the SHLLW - 2 under identical conditions of analysis in the emission range (a) 230 – 277 nm (b) 335 – 380 nm.

Table 4.11: Calibration parameters for spectral lines employed for LIBS analysis of Pd, Rh and Ru

Element	Wavelength (nm)	y_0	A	t	m	c	R^2
Pd	Pd(I) 276.309	0.754	-0.760	0.142	-	-	0.991
	Pd(I) 324.270	0.306	-0.304	0.049	-	-	0.990
	Pd(I) 340.457	1.444	-1.405	0.053	-	-	0.995
	Pd(I) 360.954	1.389	-1.388	0.055	-	-	0.994
	Pd(I) 363.469	2.246	-2.196	0.099	-	-	0.991
Rh	Rh(II) 233.477	-	-	-	1.112	0.002	0.996
	Rh(II) 242.709	-	-	-	1.177	0.003	0.992
	Rh(I) 270.373	-	-	-	2.325	0.008	0.988
	Rh(I) 339.681	-	-	-	7.353	0.004	0.985
	Rh(I) 343.488	-	-	-	10.314	0.035	0.982
	Rh(I) 369.235	-	-	-	12.332	0.010	0.981
Ru	Ru(II) 240.272	0.127	-0.124	0.035	-	-	0.996
	Ru(II) 245.657	0.278	-0.274	0.050	-	-	0.996
	Ru(II) 267.877	0.304	-0.295	0.048	-	-	0.993
	Ru(I) 349.894	0.306	-0.298	0.018	-	-	0.996
	Ru(I) 366.337	0.217	-0.212	0.032	-	-	0.993
	Ru(I) 372.802	1.025	-0.996	0.029	-	-	0.996

4.4.3.2. Optimization of experimental conditions

Signal to noise ratio (SNR) was chosen as a figure of merit for optimizing the analysis conditions. In this work, for individual PGMs, the variation of the SNR with laser energy (E_L) and acquisition delay time (t_d) was studied for one emission line, which was chosen based on its spectral purity. To study the effect of both these two independent experimental parameters, the SNR was measured by varying t_d at particular E_L value. Among the selected emission lines chosen previously (Table 4.11), the most intense emission line for each element, i.e., Pd(I) 324.270 nm, Rh(I) 369.235 nm and Ru(I) 372.802 nm, were selected for optimization study.

Figure 4.8 shows a 3-Dimensional plot of E_L vs. t_d vs. SNR for the Pd(I) 324.270 nm. It is seen that at $t_d < 2.5 \mu\text{s}$ and $t_d > 4.5 \mu\text{s}$, LIBS signal increases monotonically with laser energy until the plasma density becomes too high at E_L of 85 mJ. At still higher laser energy, due to the shielding of laser light, analyte signal starts decreasing. In the range $4.5 \mu\text{s} > t_d > 2.5 \mu\text{s}$, the analyte signal was found to increase till E_L of 100 mJ and SNR was found to be the highest at t_d of 3.5 μs . Hence laser energy of 100 mJ and acquisition delay of 3.5 μs were chosen as optimum analysis conditions for Pd. Similar experiments with Rh(I) 369.235 nm and Ru(I) 372.802 nm showed that the optimum E_L was 100 mJ and t_d was 2.5 μs and 3.5 μs , respectively (Figure 4.9). Since the final objective is to analyze all the PGMs simultaneously, optimum conditions of analysis of 100 mJ and 3.5 μs were fixed, which yielded the best SNR for all the three elements simultaneously.

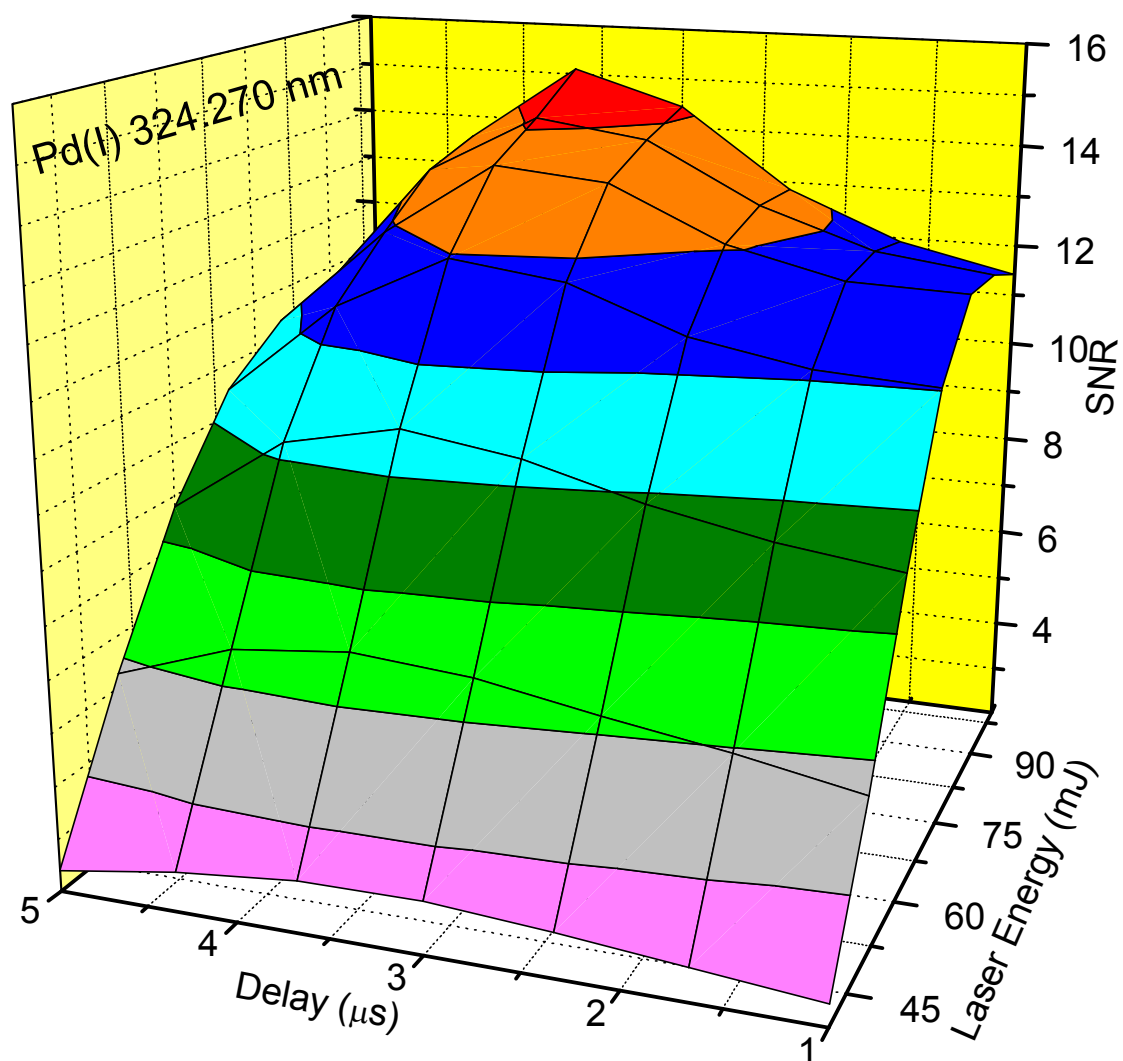


Figure 4.8: Variation of SNR of Pd(I) 324.270 nm with laser energy and acquisition time delay.

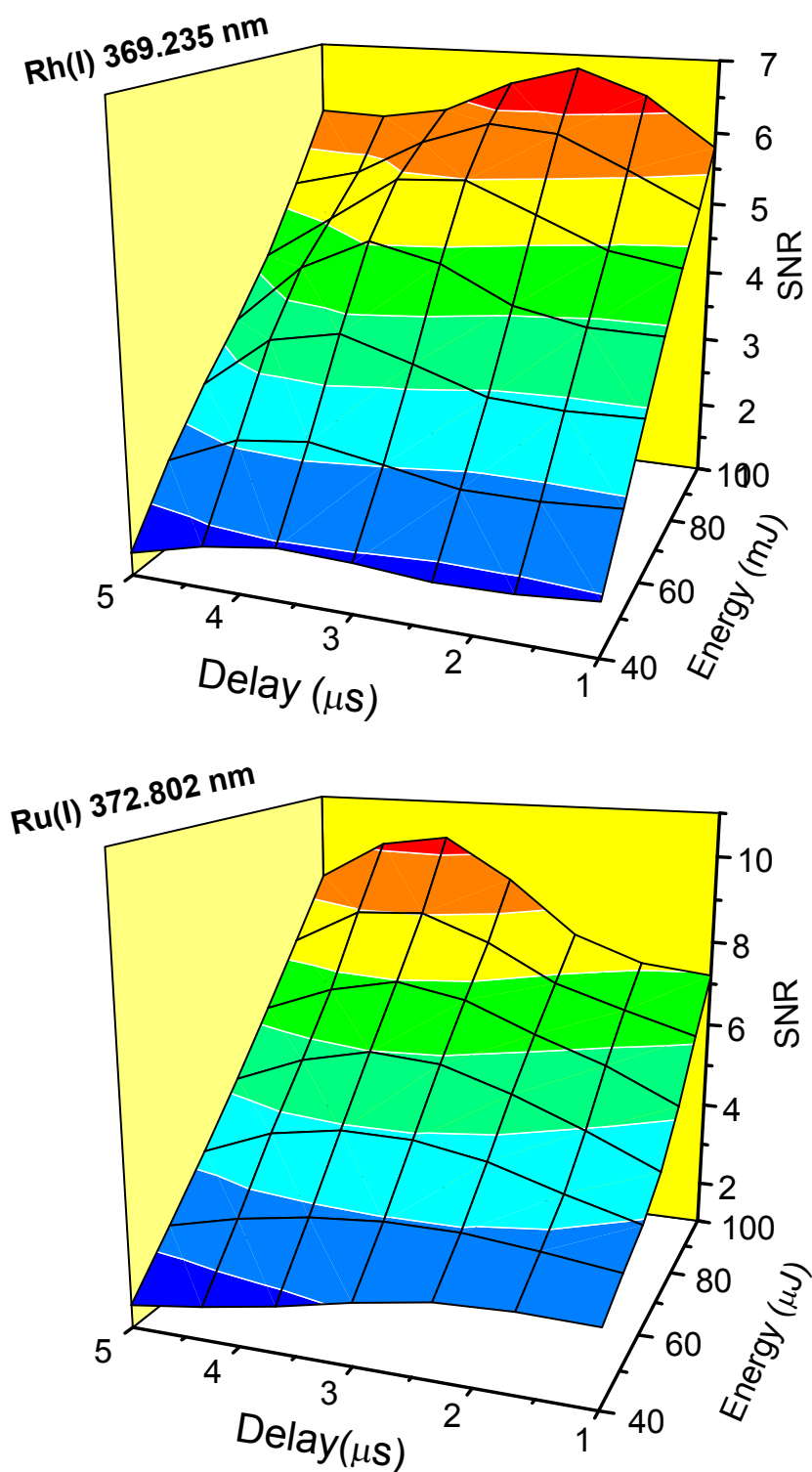


Figure 4.9: Variation of SNR of (a) Rh(I) 369.235 nm and (b) Ru(I) 372.802 nm with laser energy and acquisition time delay.

4.4.3.3. Calibration curves

Standard solutions of the individual PGMs were used to obtain the calibration curves of all the selected spectral lines of the different PGMs. The calibration plots were obtained by plotting the concentration of the individual PGM as a function of the ratio of the individual PGM emission line intensity with respect to C(I) 193.091 nm. This normalization procedure was followed to reduce the effect of shot to shot variations in the laser energy during the analysis. Among the two most intense C(I) lines 193.091 nm and 247.856 nm, the latter is relatively more intense but is spectrally interfered by Fe, which can be present in significant amounts in SHLLW and hence was not used for normalization. Figures 4.10 to 4.12 show the calibration curves obtained for the three PGMs in this study.

Self-absorption can be observed in laser induced plasma depending upon the analytical line used. The non-linear equation (Eq. 3.1), used in our previous study [Section 3.2.3.4], which can account for self-absorption, was used to fit the calibration data. For Rh, self-absorption was not observed, and the normalized intensity data were found to increase linearly with concentration and hence a linear equation (Eq. 4.1) was used for obtaining the calibration curve.

$$y = mx + c \quad \text{.....(4.1)}$$

where x denotes concentration of individual PGM and y stands for normalized emission line intensity. Table 4.11 gives the details of the calibration obtained for different emission lines of the PGMs. All the emission lines tabulated can be used for analytical purpose, depending on their spectral purity. In the present scenario of SHLLW matrix and instrumental resolution capability, five of these lines were selected for analytical purpose as discussed in Section 4.4.3.1.2.

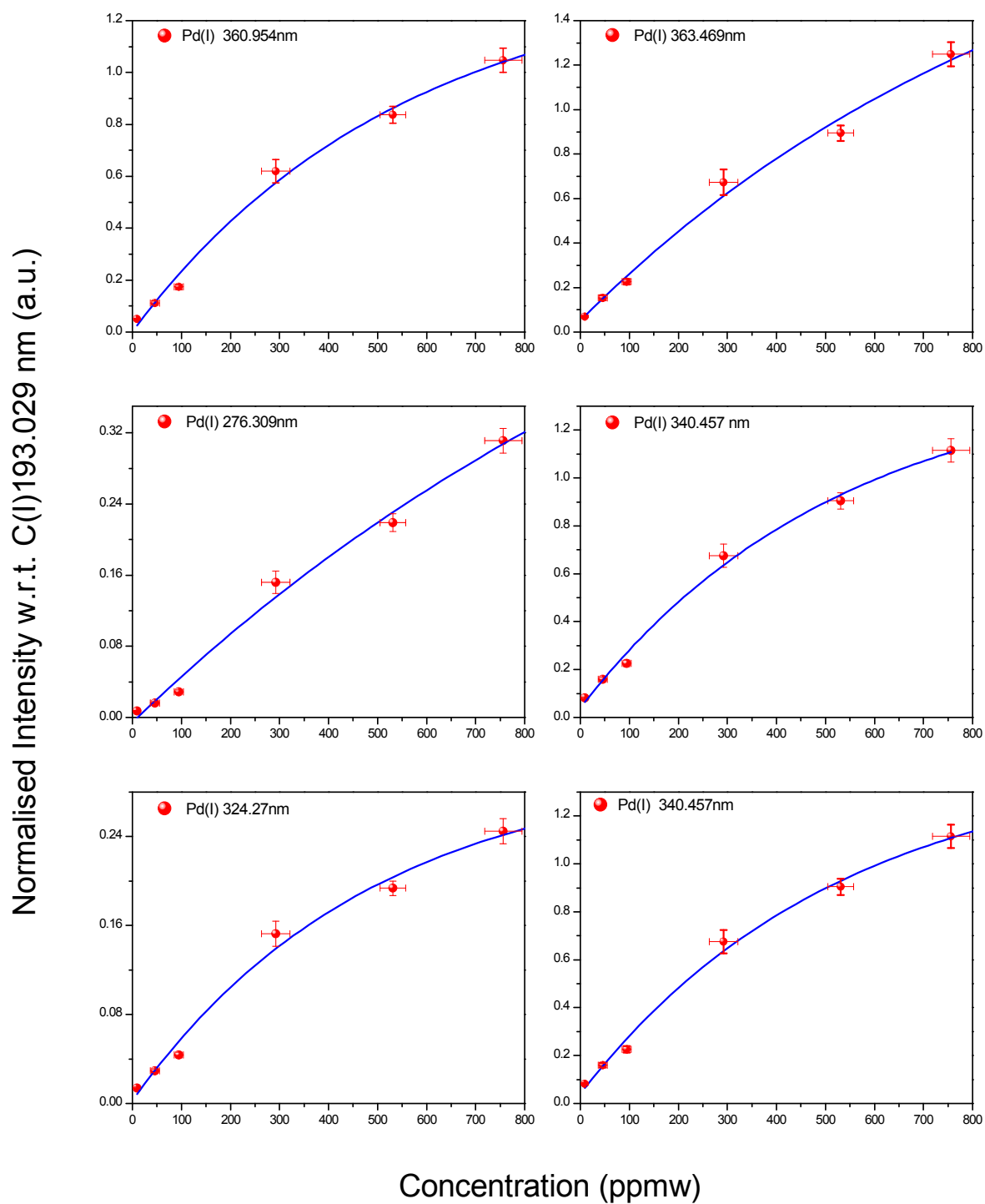


Figure 4.10: Normalized elemental emissions from LIBS as a function of concentration of Pd.

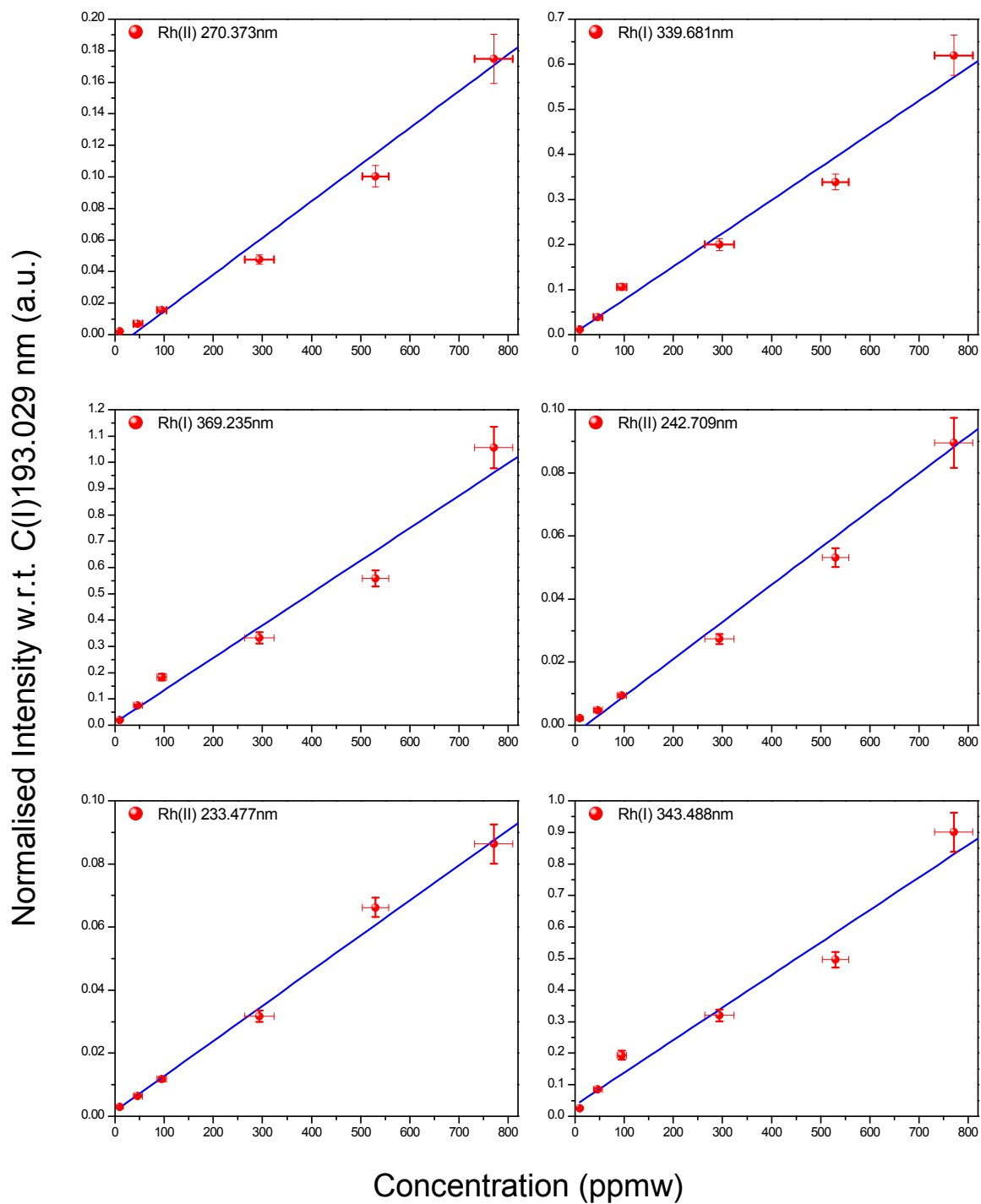


Figure 4.11: Normalized elemental emissions from LIBS as a function of concentration of Rh.

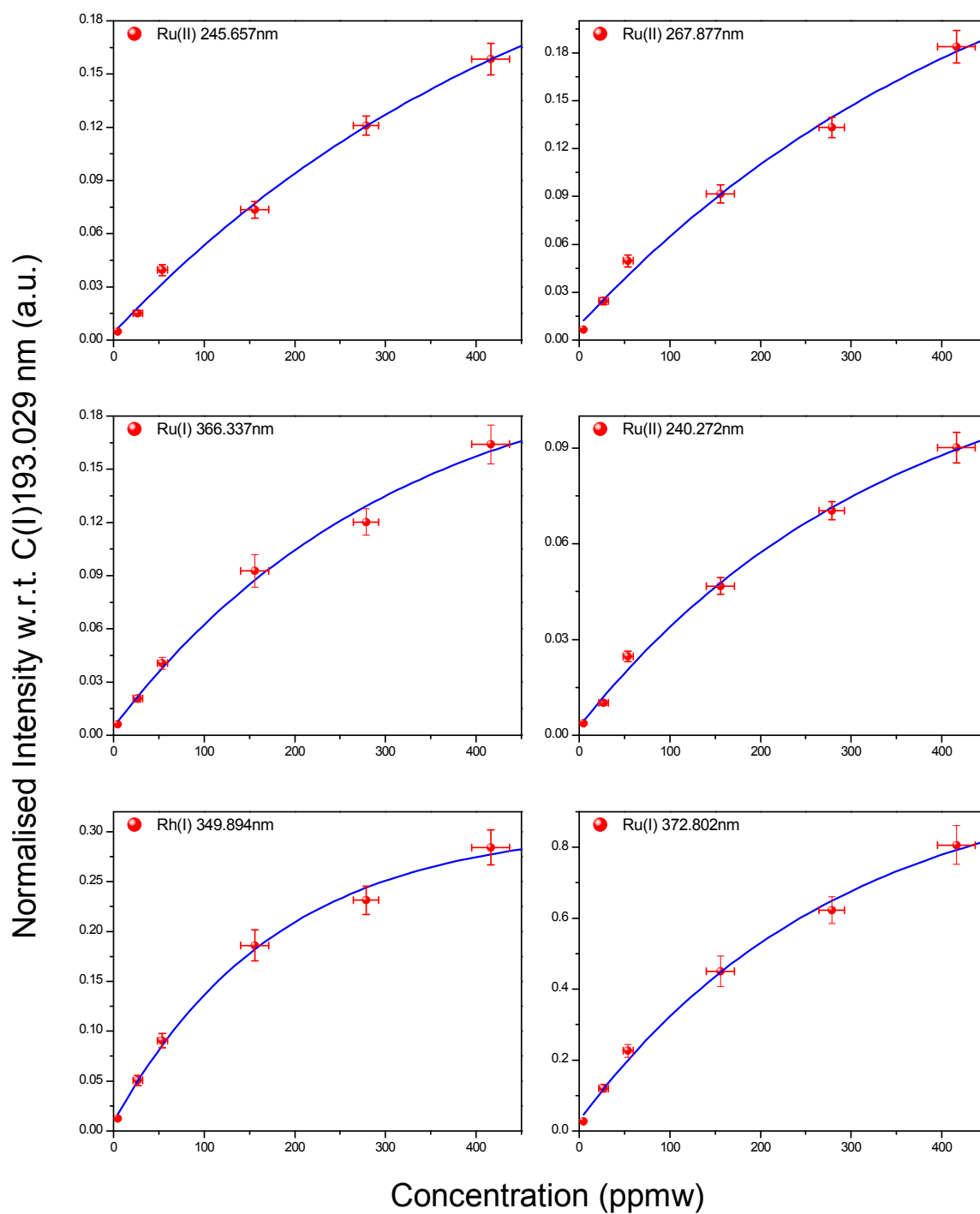


Figure 4.12: Normalized elemental emissions from LIBS as a function of concentrations of *Ru*.

4.4.4. Analytical results

Individual calibration curves of Pd, Rh and Ru were first validated by analyzing a mixture of three PGMs (PGM – 1). The results obtained are shown in Table 4.12. The values agreed well with the expected results within the analytical uncertainty of the method, which indicated that the calibration curves are suitable for analyses of these metals in their mixtures, which would be encountered in the process streams.

Table 4.13 gives the results of the analyses of the two synthetic waste samples SHLLW – 2 and SHLLW – 3. Only difference between these two solutions was the amount U present in the sample, (no U in the SHLLW – 2 mixture). From the results shown in Table 4.13, it can be observed that the concentration values for Pd, Rh and Ru obtained by the LIBS methodology are higher than the expected values in SHLLW – 3, while satisfactory agreement was obtained in case of SHLLW – 2. This clearly indicates the effect of U on the LIBS analysis, possibly the spectral interferences due to the complex emission spectrum of U. The effect of spectral interference is not avoidable due to the limitation of the spectral resolution in the present instrument (0.6 nm at 300nm). U emits huge number of emission lines, and in the present instrumental resolution, it is almost impossible to resolve all these lines, causing formation of a band of spectral emission. When U is present in the mixture with other elements, the emissions of other elements seem to ride over this band of U emission and hence the intensity of a particular emission line becomes higher than the true intensity resulting in positively biased results. The studies in this work have shown that there is limitation in the determination of PGMs in SHLLW solutions containing U in the range of 6000 ppmw. However, it may be noted that the concentration of U expected in HLLW solution under normal reprocessing conditions is in the range of 500 - 1000 ppmw [124].

Table 4.12: Comparison of analytical results for PGMs determination in a mixture of only three PGMs (PGM – 1) sample with expected values

Element	Emission wavelength (nm)	Concentration in PGM - 1 (ppmw)		
		LIBS (A)	Expected (B)	A/B
Pd	Pd(I) 276.309	338 ($\pm 11\%$) [§]	318	1.06
	Pd(I) 340.457	305 ($\pm 12\%$)		0.96
Rh	Rh(II) 233.477	346 ($\pm 8\%$)	327	1.06
Ru	Ru(II) 245.657	41 ($\pm 9\%$)	46	0.89
	Ru(I) 372.802	48 ($\pm 8\%$)		1.04

[§] represent one standard deviation calculated from three independent analysis

Table 4.13: Comparison of analytical results for PGMs determination in two different SHLLW samples with expected values

Element	Emission wavelength (nm)	Concentration in SHLLW – 2 (ppmw)			Concentration in SHLLW – 3 (ppmw)		
		LIBS (A)	Expected (B)	A/B	LIBS (A)	Expected (B)	A/B
Pd	Pd(I) 276.309	531 ($\pm 13\%$) [§]	526	1.01	600 ($\pm 12\%$)	421	1.42
	Pd(I) 340.457	499 ($\pm 12\%$)		0.95	-		-
Rh	Rh(II) 233.477	278 ($\pm 9\%$)	250	1.11	287 ($\pm 9\%$)	210	1.37
Ru	Ru(II) 245.657	30 ($\pm 15\%$)	32	0.95	54 ($\pm 13\%$)	40	1.36
	Ru(I) 372.802	36 ($\pm 9\%$)		1.13	73 ($\pm 8\%$)		1.82

[§] same as Table 4.12

Table 4.14: *Comparison of analytical results for PGMs determination in SHLLW – 3, after TBP washing of sample, with expected values*

Element	Emission wavelength (nm)	Concentration in SHLLW – 3 (ppmw)		
		LIBS (A)	Expected (B)	A/B
Pd	Pd(I) 276.309	467 ($\pm 11\%$) [§]	421	1.11
	Pd(I) 340.457	407 ($\pm 11\%$)		0.97
Rh	Rh(II) 233.477	218 ($\pm 11\%$)	210	1.04
Ru	Ru(II) 245.657	42 ($\pm 12\%$)	40	1.05
	Ru(I) 372.802	36 ($\pm 14\%$)		0.90

[§] the uncertainties represent one standard deviation calculated from data obtained by three independent LIBS analysis

To evaluate the effect of U concentration on the determination of PGMs in SHLLW, different solutions having nearly identical concentration of PGMs but different amount of U (PGM – 2 to PGM - 4) were analyzed. Figure 4.14 shows the variation of both normalized intensity as well as the absolute intensity of Pd (I) 276.309 nm and Ru (I) 372.802 nm with concentration of U. It can be seen that upto U concentration of 700 ppmw, the normalized as well as absolute intensities for the both are almost the same as those of the solution without any U (i.e. PGM-1). This can be presumed as the tolerance limit for the content of U in SHLLW without significantly affecting data for the determination of PGMs. Similar results were also obtained for Pd(I) 340.457 nm, Rh(II) 233.477 and Ru(II) 245.657 nm emission lines. To ascertain this observation, U was extracted from SHLLW – 3 by 30% tributylphosphate (TBP) with dodacane as a diluent. For extraction, 5 mL of SHLLW – 3 and 5 mL of 30% TBP were taken in a separating funnel and the solution was mechanically shaken for 5 minutes. After allowing the mixture to settle for 5 minutes for complete separation of aqueous and organic phases, the organic phase was removed. The extraction process was repeated thrice. To remove any dissolved TBP in aqueous phase, aqueous phase was shaken with 5 mL of dodacane and was then drained out. The purified SHLLW – 3, which is expected not to contain significant amounts of U was then analyzed by LIBS and Pd, Rh and Ru concentrations were determined. The results are shown in Table 4.14. It can be seen that there is good agreement among the experimental and the expected values. As mentioned earlier, since the concentration of U is expected to be in the range of 500 - 1000 ppmw in the actual waste solutions, the studies reported clearly show the applicability of the methodology for quantification of Pd, Rh and Ru in SHLLW. It is also to be noted that prior determination of U in such solutions is anyway necessary before any recovery process and can be taken as a guideline for employing the TBP extraction, if necessary.

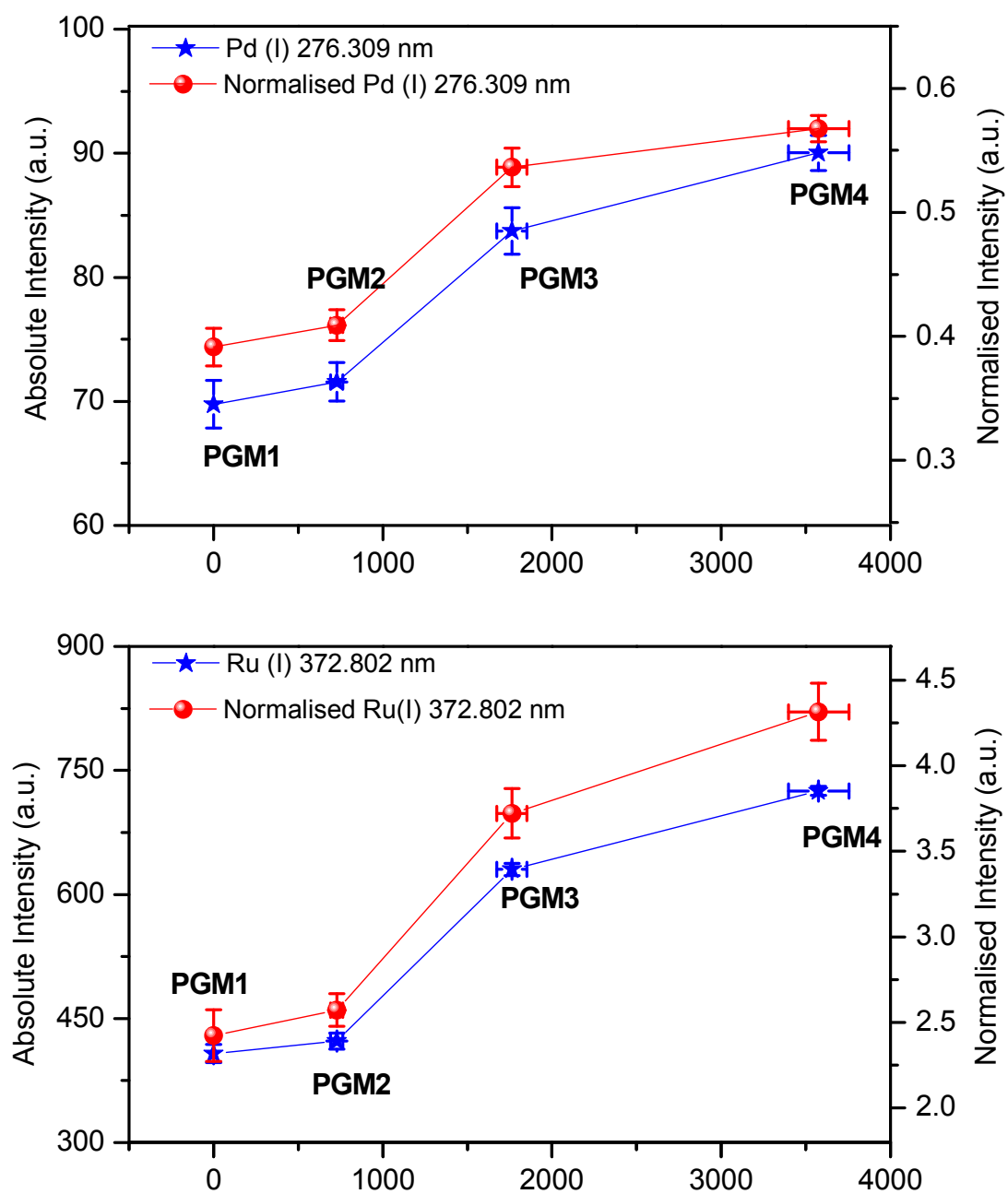


Figure 4.14: Effect of varying U concentration of the absolute and normalized intensities of $Pd(I)276.309\text{ nm}$ and $Ru(I) 372.802\text{ nm}$ emission lines.

4.4.5. Conclusions

The LIBS methodology reported in this Section for the determination of PGMs in SHLLW will be useful for the rapid characterization of PGMs in high level nuclear waste samples. Since LIBS provides an independent approach based on different physico-chemical principle for the determination of PGMs, it can also be employed for evaluating the other analytical methodologies. The method is applicable over a wide range of concentrations, and hence the problems usually associated with dilution, pH maintenance, etc. in other methodologies are not encountered in this method. Also since LIBS is a non-contact method, and has remote analysis capabilities, it is attractive in HLLW solutions due to the high radioactivity associated with such samples. The tolerance limit for U concentration in SHLLW was found to be 700 ppmw for LIBS analysis. This limitation can also be circumvented by extraction of U with TBP. With the availability of a LIBS spectrometer with better resolution than that used in the present case, the limitation due to the presence of U in the samples can be addressed suitably.

4.5. DETERMINATION OF LOW ATOMIC NUMBER ELEMENTS (B & Li) IN SOLUTION BY LIBS

4.5.1. Determination of B in ground water samples

4.5.1.1. Background

Boron (B) is an essential element for plants and its deficiency affects plant growth and yield. At the same time, an excessive amount of B is toxic to plants and limits the crop productivity in many environments [138]. B is often found in rocks and soil and is slowly leached into the ground water. B can also be released into the environment during manufacturing of commercial products such as pesticides. Because boron is widespread in our environment and in the food chain, we all have some amount of this element in our bodies. It is estimated that daily intake of B, on an average, is 10 to 25 mg through the food consumed. In animal studies, ingestion of high levels of B affected the testes and sperm of males, and caused birth defects in the offspring of exposed pregnant females. These reproductive and developmental effects occurred at much higher levels of B than are commonly found in drinking water. There is still some uncertainty about the health effects of low levels of B in human beings and, therefore, limits of B concentration in drinking water have been fixed in a conservative way to protect human health. The safe concentrations of B in drinking water and irrigation water are indicated to be below $\text{mg}\cdot\text{dm}^{-3}$ (i.e. less than $\mu\text{g}\cdot\text{g}^{-1}$ of B) in the guidelines on water quality [139]. It has also been reported that B/Cl amount ratio in ground water samples is an important factor for identification of the contamination source of salinity in ground water [140, 141]. Thus determination of B in ground water samples is of great interest.

For the determination of elements of low atomic numbers, only a few analytical methods are available. Further, for elements like B where adventitious contamination of sample is quite possible during any sample pretreatment, there is a need to develop and

validate methods which do not involve elaborate sample preparation steps. Inductively coupled plasma mass spectrometry (ICP-MS), inductively coupled plasma atomic emission spectrometry (ICP-AES), thermal ionization mass spectrometry and high performance liquid chromatography (HPLC) have been reported for the determination of B in ultra-pure water at ng.L^{-1} levels [142-158]. But these methods are not suitable for on-site analyses. In addition, due to the non-availability of certified reference materials for B in ground water sample, there is a need to develop different methodologies based on independent physico-chemical principles to enhance confidence in the data. It was, therefore, considered worthwhile to develop LIBS for monitoring of B in ground water.

In the previous Sections, applicability of using solid sample support method was shown. However, for B, Whatman-42 filter paper could not be used as it contains around $1 \mu\text{g.g}^{-1}$ B [118]. Since B concentration in ground water is expected to be a few hundred ng.g^{-1} , spectroscopically pure graphite planchets free of B were used in the present work.

There have been a few reports of B determination in solid by LIBS. Kurniawan et al. quantified B in glass by LIBS using direct irradiation of glass [145]. Uhl et al. applied LIBS for quantification of B in treated wood [146]. Fichet et al showed the application of standard addition methodology in UO_2 and PuO_2 samples for B analysis, but due to high background, the detection limits quoted were very poor [71]. B also can be determined directly in liquids; however, only one example (on Ni support) has been described in the literature by Pardede *et al* in liquid matrix by LIBS [147]. The LOD reported in this method is comparable to that achieved in the present work, but the methodology employed is very complicated, has high sample requirement and is difficult to apply for in-field purpose. In this method, using 250 mL sample solution, element of interest was deposited on a supra-pure Ni plate which was then irradiated with laser in a vacuum chamber (1-10 torr).

This Section describes LIBS methodology developed for the determination of B in ground water samples, using spectroscopically pure graphite planchets as a solid support. The results are compared with those obtained by commonly used ICP-AES method.

4.5.1.2. Sample preparation & analysis

Standard stock of $20 \mu\text{g.g}^{-1}$ aqueous solution of B was prepared by dissolving known amount of boric acid (M/s Merck) in de-ionized Milli-Q water having resistivity of greater than $18.2 \text{ M}\Omega\text{-cm}$ at 25°C . The solution was subsequently diluted to obtain B concentrations up to $0.1 \mu\text{g.g}^{-1}$. Ground water samples collected from the states of Tamilnadu (TN1 and TN2) and Gujarat (GU1 to GU3), India were analyzed for determining the concentration of B. Graphite planchets (Ted Pella Inc.) of 32 mm diameter and 1.6 mm width were used as a solid sample support. Sample loading procedure is same as described in Section 4.3.2. Spotting the ground water samples onto the planchet results in always almost the same surface area of deposit after drying the droplet, but this may not be true with high level of surfactant. Since a very small amount of sample was loaded on the planchet, the surfactant effect will be very small and was not considered in the present study. Triplicate analyses were done for each of the calibration standards as well as the ground water samples. Standard solutions of Fe, Cr, Al and Mo were also prepared by dissolving the $\text{Fe}(\text{NO}_3)_3$, $\text{K}_2\text{Cr}_2\text{O}_7$, $\text{Al}(\text{NO}_3)_3$ and $(\text{NH}_4)_6\text{Mo}_7\text{O}_{24}$, respectively, in nitric acid to study their interferences and then diluting with Milli-Q water to obtain a concentration of $100 \mu\text{g}$ of each metal per gram of solution.

4.5.1.3. Results & discussion

4.5.1.3.1. Selection of substrate

Many factors that favored the choice of graphite planchet as the substrate material were:

- i. Inexpensive and easy to handle.

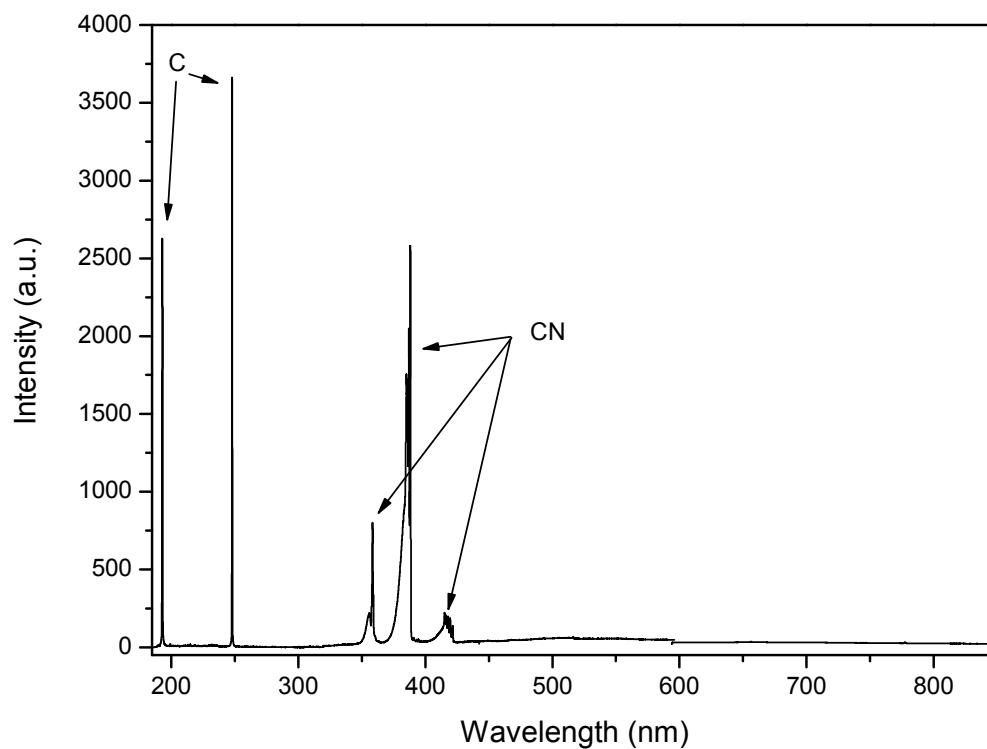


Figure 4.15: LIBS spectrum of boric acid solution on a graphite planchet (laser fluence 50 $J.cm^{-2}$ and acquisition delay 1.5 μs).

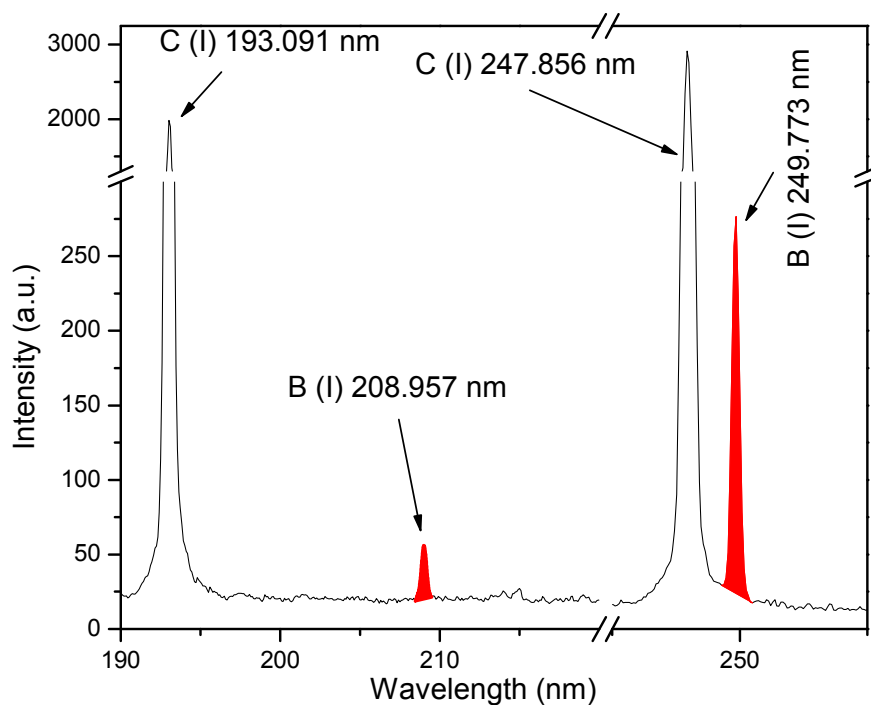


Figure 4.16: LIBS spectrum of graphite disk at a laser fluence of 50 $J.cm^{-2}$ and acquisition delay of 1.5 μs .

- ii. A simple chemical composition with only a few emission lines, resulting in reduced spectral interferences, as shown in the Figure 4.15. It can be seen that apart from the two C(I) emission lines, three regions in the spectrum cannot be used for analytical purpose, i.e. CN radical emission bands in the spectral region of 347-363 nm, 370-389 nm and 410-423 nm [148]. However, these regions are not important in present case.
- iii. Graphite does not react chemically with B. The solution on drying gets adsorbed on the planchet.

4.5.1.3.2. Selection of emission lines

The spectral region used for recording the emission lines of B was from 185–850 nm, which contains almost all the emission lines of B. A typical spectrum of B, obtained by LIBS, in 190-270 nm emission range, using laser fluence of 50 J.cm^{-2} and acquisition delay of 1.5 μs , is shown in Figure 4.16. The two most intense emission lines of boron, B(I) 208.957 nm and B(I) 249.773 nm, were identified and selected for use. The lines selected were not completely resolved with the existing instrumental resolution. The B(I) 208.957 nm line is composed of the B(I) 208.891 nm and B(I) 208.957 nm, where as the B(I) 249.773 nm line is composed of B(I) 249.677 nm and B(I) 249.773 nm. At the present instrumental resolution (0.6 nm at 300 nm), it is not possible to resolve these doublets. Hence the gross intensity under the peak area was considered for construction of calibration curves. Spectroscopic data of these emission lines are listed in Table 4.15.

Normalization of the intensities of B(I) 208.957 nm and B(I) 249.773 nm emission lines was done with respect to C(I) 193.091 nm and C(I) 247.856 nm emission lines, respectively. Carbon emission line was chosen as internal normalization line since graphite was the sample support and after adsorption of liquid sample over its surface, it can be considered as a graphite sample containing a few ppm of B. So the C emission lines can be considered as matrix emission lines. Normalization is usually carried out to minimize the effect of variation of laser fluence from shot-to-shot data.

4.5.1.3.3. Optimization procedure

The signal to noise ratio (SNR) was chosen as the figure of merit for the optimization procedure. The emission spectra were recorded at different laser fluences (15, 20, 35, 40 and 50 J.cm⁻²) to study the effect of laser fluence on signal to noise ratio (SNR) of B(I) 249.773 nm. Figure 4.17 shows the dependence of SNR on incident laser fluence for B present in a test sample having concentration of 1 µg/g. The SNR was found to increase with increase in incident laser fluence from 15 to 50 J.cm⁻². At laser fluence higher than 50 J.cm⁻², the carbon emission line C(I) 247.856 nm, which will be used for normalization showed pixel saturation. Hence laser fluence was not increased further and was restricted to 50 J.cm⁻² for all analyses.

Figure 4.17 also shows the effect of variation of acquisition delay on SNR at a fixed laser fluence of 50 J.cm⁻². An acquisition delay time of 1.5 µs was found to give the best SNR for the B(I) 249.773 nm emission line and was selected as optimum.. The signal acquisition gate window was at 10 µs which is fixed in the present instrument.

4.5.1.3.4. Effect of interfering elements

The possible spectral interferences expected for the emission lines of B at B(I) 208.957 nm are due to Al(I) 208.915 nm and Mo(II) 208.952 nm; and for B(I) 249.773 nm line are due to Fe(I) 249.653 nm and Cr(I) 249.630 nm. 100 µg.g⁻¹ of Al, Mo and Cr solution on analyzing by LIBS, under the experimental conditions optimized for B, did not show any significant interference in the two emission lines of B viz. B(I) 208.957 nm and B(I) 249.773 nm. 100 µg.g⁻¹ of Fe solution was found to contribute to the B(I) 249.773 nm emission line equivalent to a B concentration of 200 ng.g⁻¹. The concentrations of Al, Mo, Cr and Fe in the ground water samples determined by ICP-AES are shown in Table 4.16. Since these concentrations are less than µg.g⁻¹, no pretreatment for their removal was necessary in the present work.

Table 4.15: *Characteristics of spectral lines employed for B determination by LIBS*

λ_{ij} (nm)	A_{ij} ($10^8 s^{-1}$)	E_j (cm^{-1})	E_i (cm^{-1})	g_j	g_i
B(I) 208.891	1.8	0	47856.93	2	4
B(I) 208.957	0.36	15.254	47856.93	4	4
B(I) 249.677	1.2	0	40039.65	2	2
B(I) 249.773	2.4	15.254	40039.650	4	2

Table 4.16: *Concentrations of elements in ground water samples (giving spectral interference at boron emission lines in LIBS) determined by ICP-AES*

Element	Concentration ($\mu g/g$) of the element in ground water sample				
	TN1	TN2	GU1	GU2	GU3
Fe	<0.01	<0.01	<0.01	<0.01	<0.01
Cr	<0.01	<0.01	<0.01	<0.01	<0.01
Mo	0.21	<0.02	0.12	<0.02	0.06
Al	<0.07	0.09	<0.05	<0.05	<0.05

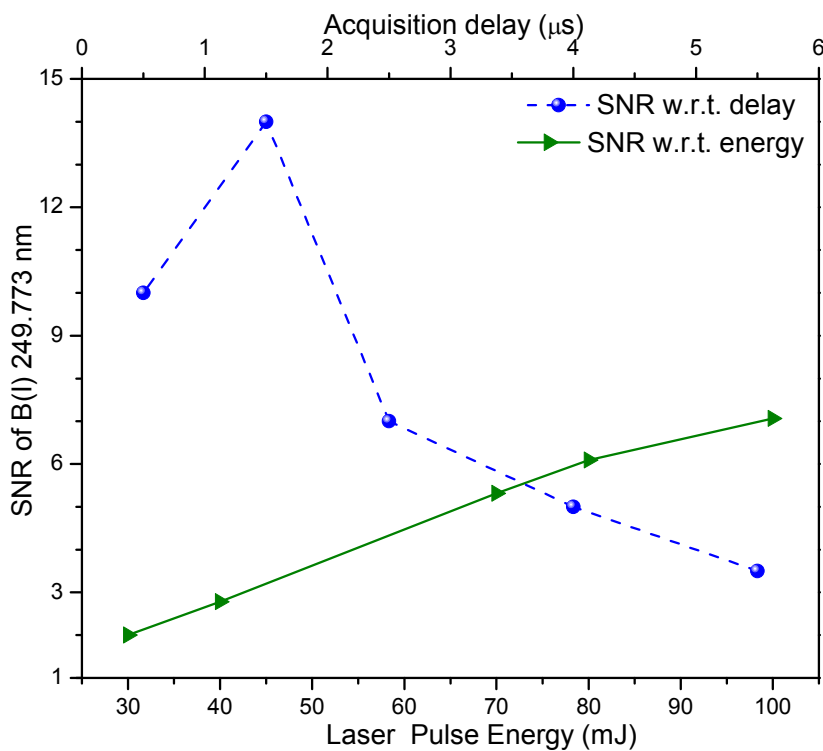


Figure 4.17: The dependence of the SNR of the B(I) 249.773 nm emission line on laser fluence and acquisition delay.

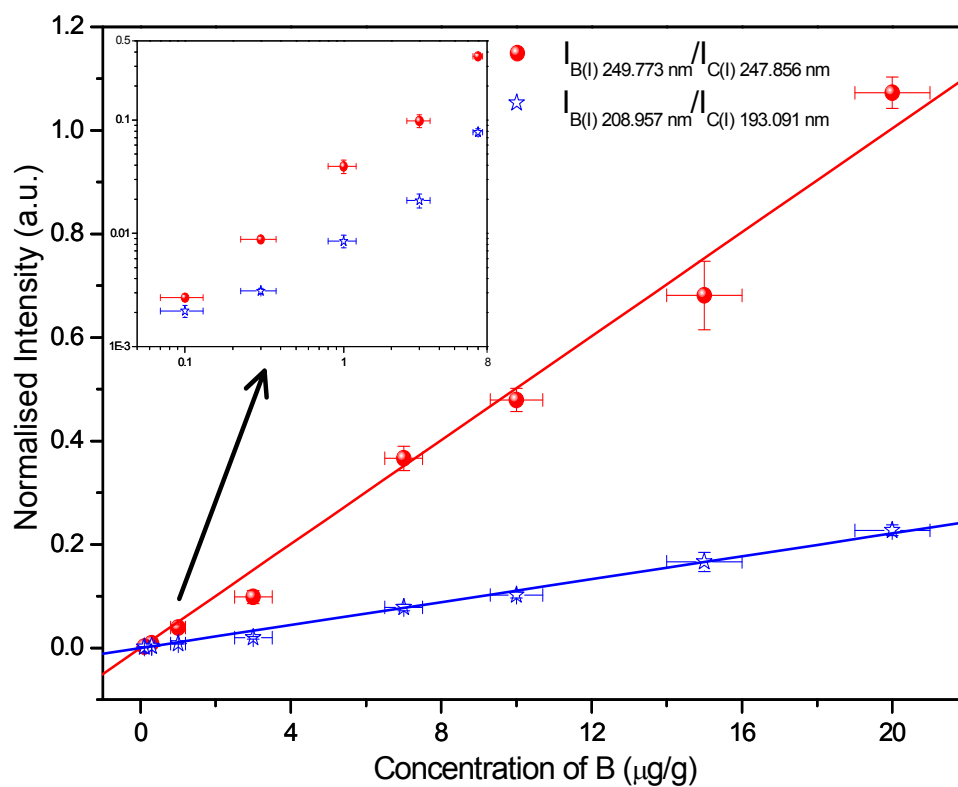


Figure 4.18: Normalized boron emission intensity as a function of concentration of boron.

4.5.1.3.5. Calibration curves

The calibration curves obtained by plotting the normalized intensities of the two selected emission lines of B versus the corresponding concentrations of B are shown in Fig. 4.18. Each point, in these figures, corresponds to an average of triplicate measurements and the error bars are the standard deviations ($\pm 1\sigma$). Both the emission lines B(I) 208.957 nm and B(I) 249.773 nm showed good linearity up to B concentration of $20 \mu\text{g.g}^{-1}$. The linearity of the calibration points in the sup-ppm range is also shown in the inset of Fig. 4.18 in logarithmic scale. The slope of the calibration curve for B(I) 249.773 nm emission line was approximately 5 times higher than that for B(I) 208.957 nm (Table 4.17).

4.5.1.3.6. B in ground water samples

Ground water samples were analyzed under the identical conditions of analyses as those used for the calibration samples. Table 4.18 gives the results obtained for B concentration in the ground water samples by LIBS. The results obtained by ICP-AES are also included in the Table 4.18 for comparison. As is seen, there is good agreement in the results obtained by the two methods which clearly shows the applicability of LIBS for this work. The detection limit for the LIBS methodology used for B quantification in ground water is given in Table 4.19 and this is compared with LODs of other two methods. It can be seen that these limits are comparable to those reported in the literature and well below the acceptable limits of B concentration in ground water. Table 4.20 compares the LODs reported in literature with that obtained in the present work. LOD obtained in the present work is an order of magnitude better than most of the previously reported values.

Table 4.17: *Fitted parameters obtained from calibration curves for B*

Emission Line (nm) (y = mx)		Slope (m)	R ²
Analytical (for boron)	Normalizing element (carbon)		
B(I) 208.957	C (I) 193.091	0.011	0.998
B(I) 249.773	C(I) 247.856	0.050	0.994

Table 4.18: *Comparison of boron concentration values determined by LIBS, in ground water samples with ICP-AES*

Sample	LIBS		ICP-AES (µg/g)
	Emission line (nm)	B concentration (µg/g)	
TN1	249.773	0.25 ± 0.01	0.19 ± 0.01
	208.957	0.21 ± 0.01	
TN2	249.773	2.05 ± 0.03	1.70 ± 0.05
	208.957	1.80 ± 0.11	
GU1	249.773	0.17 ± 0.01	0.12 ± 0.01
	208.957	-	
GU2	249.773	0.28 ± 0.01	0.29 ± 0.01
	208.957	0.32 ± 0.02	
GU3	249.773	0.25 ± 0.02	0.19 ± 0.01
	208.957	0.20 ± 0.01	

Table 4.19: Limits of detection (LODs) of LIBS and those reported by other methods

Method	LOD ($\mu\text{g/g}$)	Comments	Reference
LIBS	0.01	50 μL of sample, only drying of the sample	Present work
FIA	0.1	Preferred in absence of complex matrix	[150]
PGNAA	0.2	15 g of sample size with 9 hrs counting	[151]

PGNAA : prompt gamma neutron activation analysis

FIA: flow-injection analysis

Table 4.20: Comparison of detection limits for boron determination by LIBS

Physical form of material	LOD ($\mu\text{g/g}$)	Matrix	Comments	Reference	Boron line / matrix line
Liquid	0.01	Carbon planchet	Atmosphere pressure	This work	249.773 / C (193.091)
Solid	1.5, 0.3	Wood	Single-shot and 20-shot measurements	[146]	249.773 / C (247.857)
Solid	65	UO ₂	Nuclear fuel pellets at 532 nm laser	[71]	249.773
Solid	30, 40	Glass	Air atmosphere at 1 and 5 torr	[145]	345.1
Liquid	0.054	Electro-deposition on nickel electrode	Vacuum sample chamber	[147]	249.773

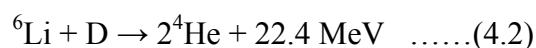
4.5.1.4. Conclusion

The solid sample support (graphite planchet) based LIBS method for the determination of sub-ppm amounts of B in ground water samples is simple and rapid and has several advantages over other existing methods. The method does not require any pre-concentration or pre-treatment which eliminates the chances of B contamination. In addition to the simplicity and rapidity, it can be used as an on-field real time analytical method for analysis of ground water. The graphite planchet used in the developed methodology is highly pure and shows no significant contribution to B signal at both the wavelengths, thereby improving the LOD.

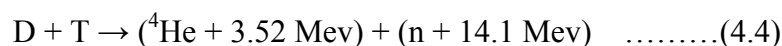
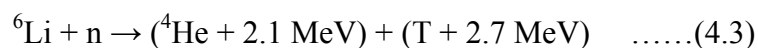
4.5.2. Determination of Li in organic solution

4.5.2.1. Background

The world wide actual projects of the future Fusion Reactor (FR) power plants are based on the overall nuclear fusion reaction



The role of the lithium-6 fuel is to generate tritium by the ${}^6\text{Li}(n, \alpha)\text{T}$ nuclear reaction (Eq. 4.3) inside the blanket of a thermonuclear reactor by exploiting the fast neutrons (n) generated from the D-T fusion (Eq. 4.4)



Since the products of reaction given in Eq. 4.3 will release total energy of 4.8 MeV inside the blanket, the engineering of the second step (Eq. 4.3) must provide removal and recovery of tritium needed for (Eq. 4.4) and of the heat which is an important fraction (21.4%) of the overall process. One of the research lines to make this process (Eq. 4.3) feasible for the FR is based on blanket engineering concepts using Li-ceramics in a way

similar to that developed for the fission reactor power plants using U-Pu oxide ceramics as fuels [152].

Lithium based oxide ceramics such as Li_2TiO_3 , Li_2ZrO_3 and Li_4SiO_4 have been proposed as tritium breeding materials for fusion reactor blankets [153-156]. Among them, lithium titanate (Li_2TiO_3) shows the best chemical stability in air and the most excellent tritium release characteristics at lower temperature. Moreover, it displays acceptable mechanical strength and low activation [157-159]. For the preparation of lithium-containing ceramic powders, several synthetic techniques including solid state reaction, co-precipitation, solution combustion process and sol-gel process are available [160-162]. In Bhabha Atomic Research Centre (BARC), Sol-Gel is one of the well studied processes for the preparation of gel microspheres of UO_2 , ThO_2 , $(\text{U}, \text{Pu})\text{O}_2$, $(\text{Th}, \text{U})\text{O}_2$ etc. [163]. Sol-Gel process was hence developed for the preparation of Li containing ceramic materials of required size and characteristics [164].

In the Sol-Gel process, the Gel particle is actually made of Ti – hydroxide network in which Li ion is trapped. The concentration of Li ion needs to be optimum (1.65 M) in the Gel so that the ultimate product is stoichiometric Li_2TiO_3 . The Gel particle once produced is washed with ^6Li containing organic solution to remove unreacted and unused materials, while maintaining Li/Ti stoichiometry in Gel. The number of washings required need be standardized so that the Li concentration in Gel does not deviate from the expected value. The washed solutions which contain enriched ^6Li also needed be analyzed for Li content prior to the recovery process.

The process required a simple and robust technique, which is capable of Li determination to standardize the various steps of the sol-gel process. Determination of inorganic constituents in an organic matrix (HMTA, urea, etc.) by the conventionally used techniques such as ICPMS, ICP-OES, TXRF etc. requires removal of organics. Whenever the

organic components are difficult to remove by conventional methods such as evaporation, combustion methods are employed which can lead to loss of volatile inorganic components like Li, which is unacceptable in the sol-gel process. Moreover, the mixture containing HMTA and NH_4NO_3 becomes explosive upon heating [165]. Among the other methods, acid – base titration or flame photometer [166] method can be used, but is not suitable as a fast approach and solution also needs be diluted to ppm level. It was, therefore, considered worthwhile to investigate the possibility of employing LIBS for the determination of Li.

4.5.2.2. Sample preparation & analysis

The Li_2TiO_3 microspheres were obtained by the internal gelation process as described by Vittal Rao *et al* [167]. LiNO_3 and TiCl_3 solutions were mixed with 3M solution of HMTA ((hexamethylenetetramine) and urea mixture at 0°C to obtain feed solution. This feed solution was then dispersed as droplets through a stainless steel capillary having internal diameter of 0.8 to 1.0 mm into hot silicone oil (silicone oil $\sim 90^\circ\text{C}$) kept in a glass column. These droplets on contact with hot oil make gel microspheres and become hard as they travel down the column. After separating the gel microspheres from the oil, they are washed initially with CCl_4 (3/4 times) to remove the adhering silicone oil and then they are dried. After the particles are dried, they are digested in 1.55M LiOH at 333 K in an air oven for 18 hours. Finally these particles are washed to remove the unreacted materials and unused chemicals from the microspheres to prevent their cracking during sintering of the microspheres. Since the microspheres are made of ^6Li , washing is also done with ^6Li containing solution so that leaching of Li from the sol-gel particles during washing can be minimized. A ^6Li containing organic mixture (0.54 M NH_4NO_3 + 0.24 M NH_4Cl + 0.075 M HMTA + 0.075 M Urea + LiOH) was used for washing. In order to study the pickup/leaching of Li from the microspheres during the washing, 16 wash samples from different stages were collected and analyzed.

11 synthetic samples of Li in the concentration range of 33 mM to 2M were prepared by dissolving analytical grade LiNO_3 in the same organic composition as stated earlier. Membrane based Whatman – 42 filter paper was used as the sample substrate in this work. The data reported on the concentrations of different trace elements in Whatman–42 membrane filter paper shows no Li is present in the filter paper. Also no observable spectral lines for Li were seen during the LIBS analysis of blank filter paper which was selected as substrate with negligibly small blank contribution [118]. 20 μL of solution was used for analysis. Sample loading procedure was the same as described in Section 4.3.2.

4.5.2.3. Results & discussion

The methodology applied is very much similar to the other methodology discussed earlier in this chapter. Initially, by carefully studying the spectra, 5 lithium emission lines were selected for this work. These are Li(I) 670.79 nm, Li(I) 610.364 nm, Li(I) 812.644 nm, Li(I) 497.174 nm, Li(I) 460.288 nm. Spectroscopic data of these emission lines are listed in Table 4.21. All these emission lines selected are doublet and were not completely resolved with the existing instrument (resolution 0.6 nm at 300 nm) available in our laboratory. Hence the gross intensity under the peak area was used for construction of calibration curves. One of the samples was used to study the effect of laser fluence and acquisition delay, in order to obtain the optimum analysis conditions for Li determination. Figure 4.19 shows the dependence of signal to noise ratio (SNR) on incident laser fluence as well as on acquisition time delay for Li present in a test sample. 100 mJ laser energy and 2.5 μs acquisition time delay were found to be the best conditions. .

Maintaining the above optimized conditions, calibration curve was constructed as shown in Figure 4.20. Li(I) spectral line 670.79 nm was found to be very sensitive and provided a linear calibration up to 0.54M Li concentration. But in view of the detector

saturation above this concentration level, it cannot be used for sample having concentration more than 0.54M at the present instrumental conditions applied.

The other emission lines namely, Li(I) 812.644 nm, Li(I) 497.174 nm, Li(I) 460.288 nm were observed only above the concentration of 0.5M of Li. But these three lines showed a linear dependency on concentration with much lesser sensitivity compared to Li(I) 670.79 nm line as shown in Table 4.21. The Li(I) 610.364 nm emission line was found to be an inappropriate analytical emission line, as its dynamic range was very narrow, only from 0.35M to 0.7M of Li. Hence, depending on the probable range of the solution, appropriate calibration line needs be chosen. Alternatively, solution can be diluted to a concentration below 0.54M so that the most sensitive calibration line, i.e., Li(I) 670.79 nm can be used. Since the principle advantage of LIBS is no or minimal sample preparation, hence the second approach which involves dilution was not adopted in this work. More-over, since the expected concentration of the solution was above 0.5M, the calibration curves based on Li(I) 812.644 nm, Li(I) 497.174 nm, Li(I) 460.288 nm were used.

Two different sets of samples PI and PII, each consisting of 8 washing solutions of replicate stages were taken and analysed. Figure 4.21 gives the result obtained. The variation of Li concentration in the washing clearly indicates that in both the cases, at least 3 - 4 washings are needed. Li pickup from wash solution is significant during initial washings. Thereafter, Li concentration remains constant. The data from Li(I) 812.644 nm calibration line were not considered as the results were inconsistent with the other two duplicate samples. This is probably due to the very low sensitivity of the line as shown earlier and may also be due to the fact that this is close to IR region, where sensitivity of the instrument is not good.

Table 4.21: *Characteristics of Spectral lines employed for LIBS analysis of Li along with their fitted parameters obtained from calibration curves.*

Species	Wavelength λ_{ij} (nm)	A_{ij} (10^8s^{-1})	E_j (cm^{-1})	E_i (cm^{-1})	Slope	Intercept
Li(I)	460.288	0.223	14903.957	36623.312	1483	-682
Li(I)	497.174	0.673	14903.957	35012.06	352	-168
Li(I)	610.364	0.686	14903.957	31283.053	-	-
Li(I)	670.790	0.369	0	14903.622	10241	18
Li(I)	812.644	0.349	14903.957	27206.066	651	-3.9

λ_{ij} is the transition wavelength, A_{ij} is the transition probability, E_i and E_j are the energies of the upper and lower level, respectively

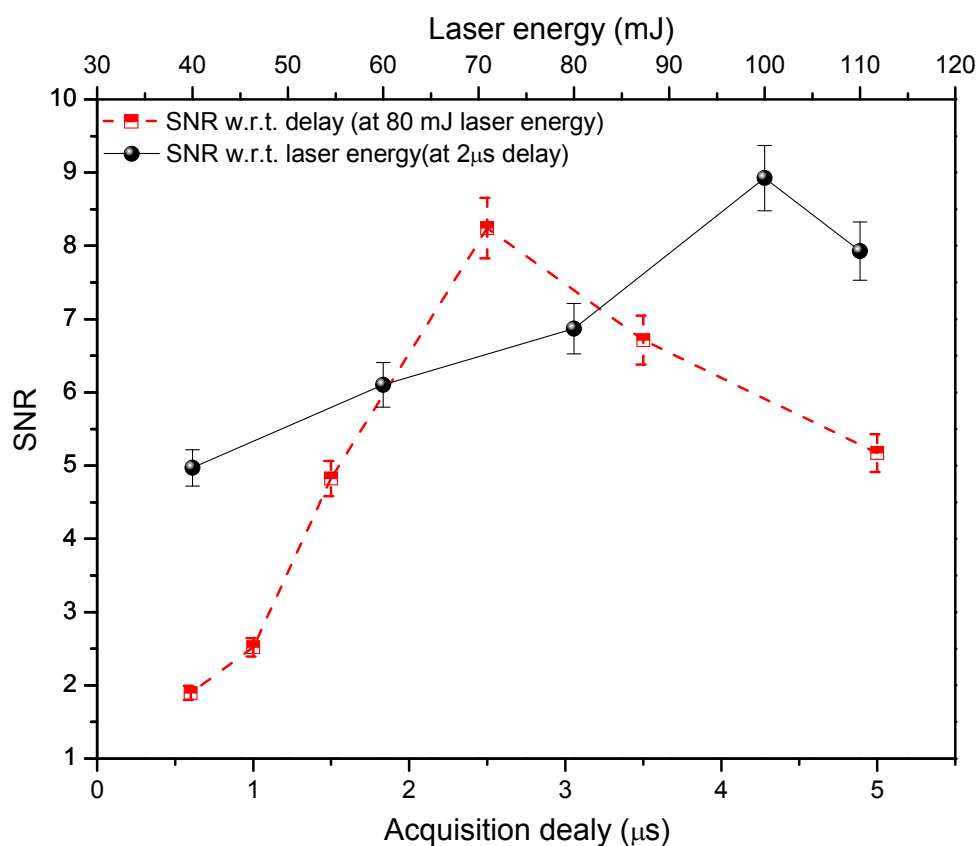


Figure 4.19: *The dependence of the SNR of the Li(I) 670.79 nm emission line on laser fluence and acquisition delay.*

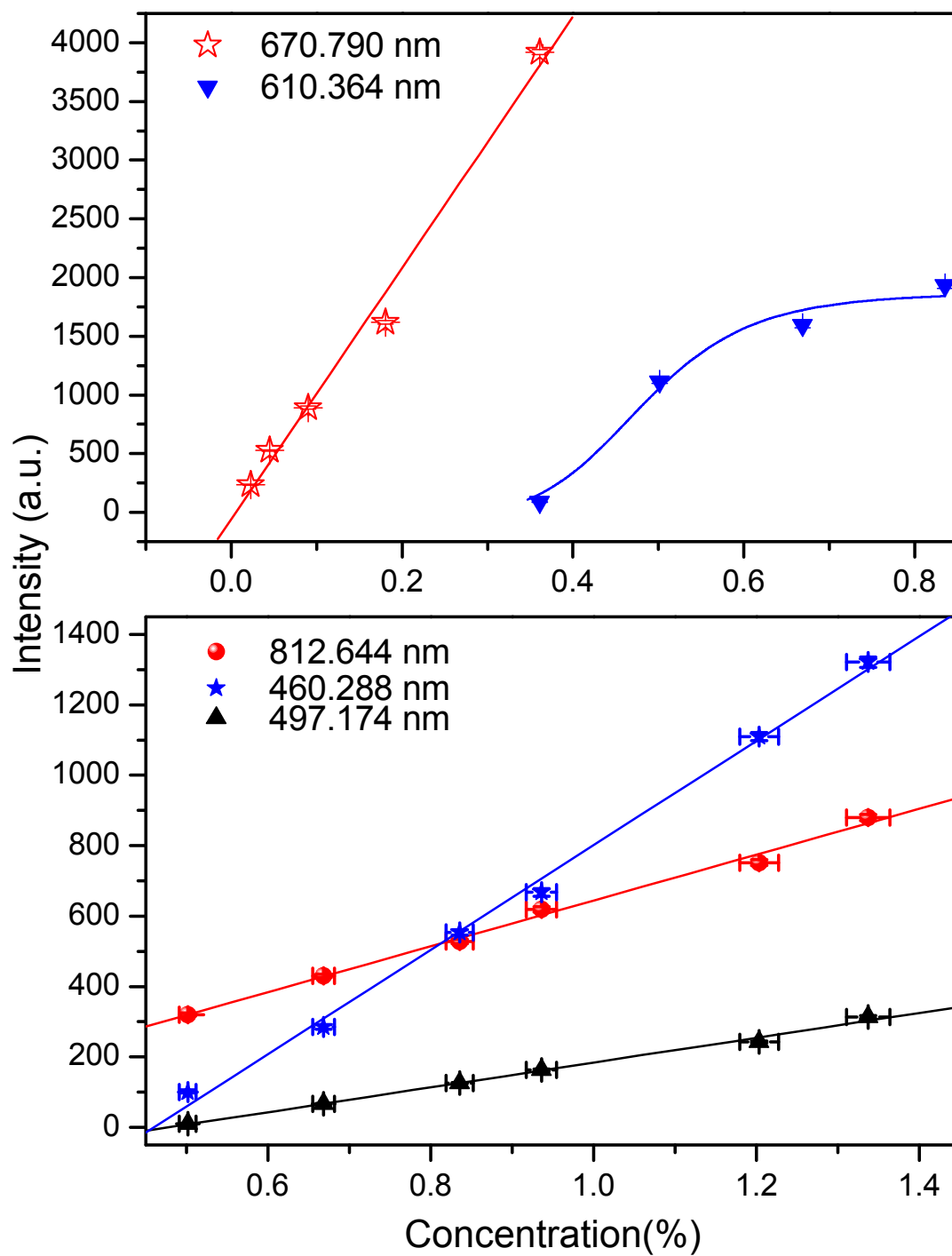


Figure 4.20: Calibration curve of Li in organic mixture solution. Error bars show standard deviation from multiple measurements at each value.

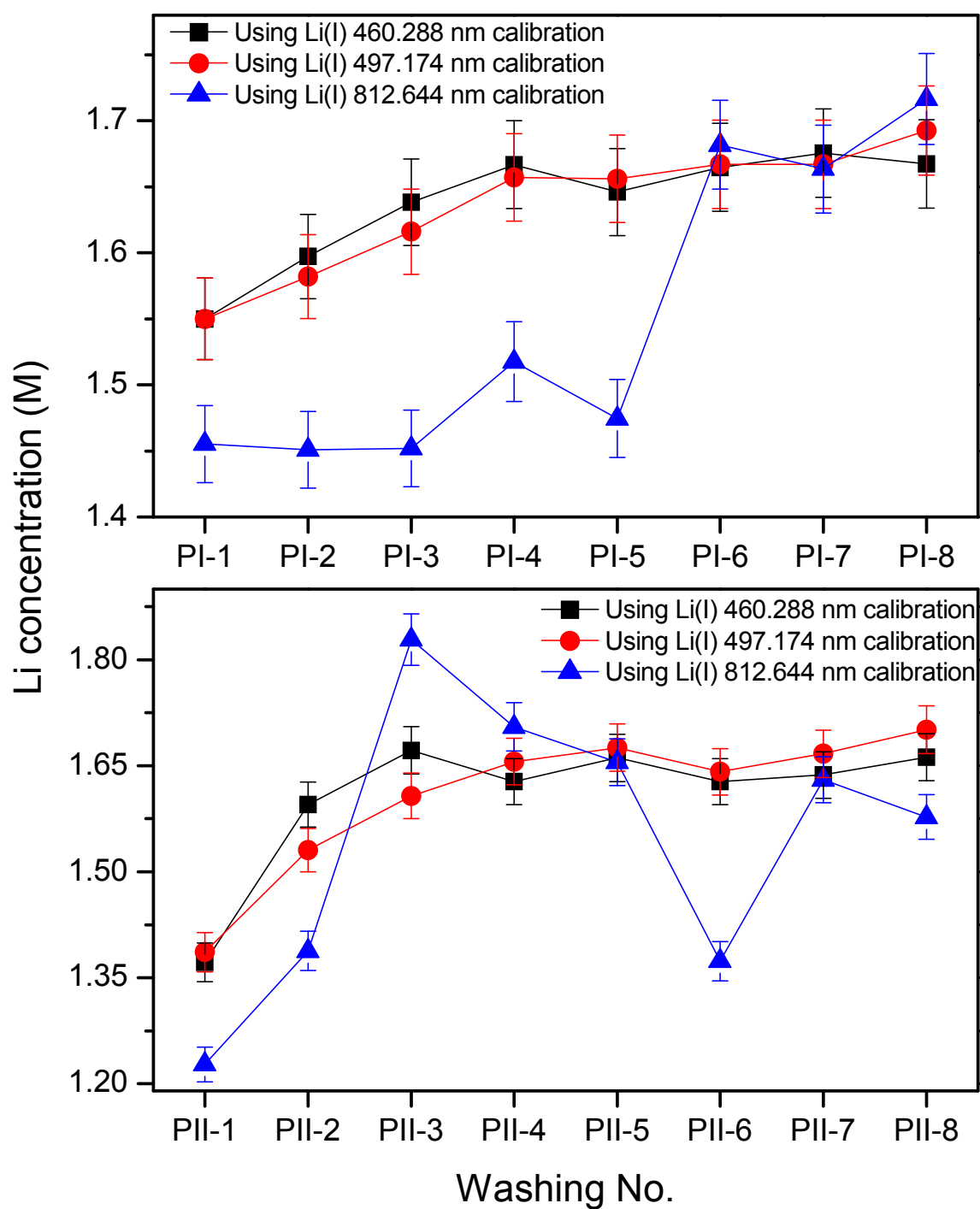


Figure 4.21: Comparison of the Li concentrations determined for two sets of wash solution by different calibration lines.

4.5.2.4. Conclusion

The results from these experiments demonstrate the usefulness of the present method for the determination of Li in complex chemical matrix containing various organic materials and solvent. These studies were found to be highly useful in the optimization of the washing conditions in sol-gel process for obtaining phase pure lithium titanate sol-gel particle. Among the emission lines selected, the one near IR was found to be unsuitable for quantitative results. The precision of the method is 5-8%. The LIBS methodology developed in this work is fast and precise and can be employed on a routine basis for lithium determination in solutions containing organic constituents.

Identification of Material by Spectral Correlation Study



Chapter V

5.1. INTRODUCTION

Identification of documents of various qualities, forms and sizes (e.g. will paper, badges, passports, credit cards etc.) is required for various applications. Examples of documents forged include driver permits, cheques, health care cards for accessing expensive medical services from hospitals and physicians, passports for illegal entry into countries and partial tampering of will paper or “last-wish” paper. Recent advances in desk-top publishing equipment and color copiers pose an increasing threat to the security of these documents.

In governmental confidential documents, replacing one of the pages of the document is the easiest forgery case. Currently, important government documents rely on special paper, ink and water marking to prevent forgery. Elemental profile of paper of same quality varies from company to company and even with the time of production. This is because of variation in the soil quality as well as environment in the forests from where trees are used by the paper producing company. During a confidential document printing, all the pages will generally belong to paper from a single company and same production time. Hence, if a few particular pages are replaced by the forger at a later stage, it should be possible to identify the forgery by elemental profiling. Neutron activation analysis (NAA) has been used to obtain elemental profiling [168]. Laser induced breakdown spectroscopy (LIBS) is a promising alternative technique for rapid identification of forged document instead of NAA which is time consuming and depends upon the availability of a nuclear reactor or a neutron source.

Gornushkin *et al* have shown that simple statistical correlation methods, such as linear and rank correlations, can be successfully applied for the identification of solid and particulate materials without trace or bulk quantifications [169, 170]. A nearly 100% reliable identification was achieved based on the use of thousands of data points (pixels) representing the sample spectrum in a relatively large spectral window. Anzano *et al.* [171] employed this methodology for characterization of post-consumer commercial plastic waste widely used for

household and industrial purpose. Jurado-López et al. [172] used rank correlation method for rapid identification of alloys used in the manufacture of jewellery. Mateo et al. [173] showed the capability of linear correlation method for depth profiling by LIBS. Rodriguez-Celis et al. [174] compared glass spectra from car windows using linear and rank correlation methods and showed effective discrimination at 95% confidence level.

In this Chapter, the application of parametric (linear) and non-parametric (rank) correlations for identification of several confidential papers using LIBS is discussed.

5.2. EXPERIMENTAL

5.2.1. Materials

The paper samples used in the present work were those used for Yearly Confidential Report (YCR) writing in the Department of Atomic Energy (DAE), India. YCR paper pages were collected for the last 10 years (1999 – 2008) for analysis. The pages were initially classified according to the year of YCR writing. Among the YCR writing pages of a particular year, some contained watermarks, which were different for different years. Those pages which contained watermark were used as library samples for the particular year printed on it and the rest of the pages of that particular year without watermark were used as unknown. Tables 5.1 and 5.2 give details of the paper used for generating library and used as unknown samples, respectively.

5.2.2. Sample preparation

No major sample preparation step was necessary; the results are increased throughput and greater convenience. The papers were cut into small circles (diameter ~3 cm) which were placed on a double-sided tape stuck to a glass slide which was placed in the sample holder. Care was taken so that the piece of paper was firmly stuck to the slide in order to avoid any air gap between them.

Table 5.1: *Printed information on YCR papers used for generating of LIBS library*

Sample No.	Year of use	Water mark
L1	1999	<i>RAJAMANI</i>
L2	2000	<i>CARD</i>
L3	2001	<i>SYMBOLIC</i>
L4	2002	<i>ASHOK</i>
L5	2003	BALLARPURI
L6	2004	<i>CENPULP</i>
L7	2005	<i>ANDHRA</i>
L8	2006	<i>SIRPUR</i>
L9	2007	<i>SIMPLEX LEDGER</i>
L10	2008	<i>SUDARSHAN CHKRA</i>

Table 5.2: *Printed information on YCR papers used as unknown*

Sample No.	Year of use	Sample No.	Year of use
X1	1999	X6	2004
X2	2000	X7	2005
X3	2001	X8	2006
X4	2002	X9	2007
X5	2003	X10	2008

5.2.3. LIBS spectral library for papers

Library of LIBS spectra from 10 different papers was generated for identification of different YCR papers having no water mark. The library spectrum of YCR paper was obtained by performing LIBS on ten different pieces of paper, obtained by cutting the particular paper at random positions. The spectra were obtained by averaging 10 laser shots spectra with laser energy of 50 mJ (i.e. irradiance of 3.6 GW/cm^2), acquisition delay of $2 \mu\text{s}$ and a repetition rate of 1 Hz. These 10 spectra were averaged to construct the library spectrum for that particular YCR paper. All spectra were stored in a computer and used on a day-to-day basis without renewing. It was found that the last two channels of CCDs (460 – 620 nm and 620 – 850 nm) do not provide much of the elemental information except for C_2 swan-bands and Na doublet at 588 nm. Hence these were not included in generation of library. Gornushkin *et al* [175] have shown that masking of spectrum in correlation analysis improves the analytical result, but in the present study, it was not considered as it makes the method time consuming, and our aim was to develop a rapid method for identification.

For each of the unknown paper samples, similar to the library samples, LIBS spectra were recorded on ten different pieces of paper, obtained by cutting each unknown YCR paper at random positions.

An inbuilt program for correlation analysis in Microsoft Excel 2003 was used for computation of correlation coefficients among the LIBS spectrum of unknown and library spectra.

5.3. RESULTS & DISCUSSION

Paper when exposed to intense laser radiation which is sufficient for breakdown produced atomization of all the elements present. From the produced plasma, emission lines were recorded. A part of the spectra obtained by LIBS for library papers (L1, L2, L3 and L4) are shown in Figure 5.1. The spectra are almost identical, since main matrix composition is

same for papers, suggesting the need to use powerful statistical methods for detection of the very small differences present in the paper materials. It is a Departmental policy of DAE to purchase fresh YCR paper in bulk every year preferably from a different supplier to minimize the possibility of forging. It is known that the geographical origin of raw material for paper production has sufficient effect on trace profiling of paper materials, thereby generating different spectral patterns in LIBS. The YCR papers are stored in both pre- and post- used stages in ambient conditions to avoid any unnecessary contamination.

Each channel consisted of 2048 pixels. Hence from two channels, 4096 data points were available, which are enough to permit statistical analysis like linear correlation and non-parametric rank correlation. Linear correlation measures the similarity in trend and the correlation coefficient “r” is expressed as,

$$r_{(\text{linear})} = \frac{\sum_i (x_i - \bar{x})(y_i - \bar{y})}{\sqrt{\sum_i (x_i - \bar{x})^2} \sqrt{\sum_i (y_i - \bar{y})^2}} \quad \dots (5.1)$$

where x_i and y_i are the intensity values of library spectrum and unknown LIBS spectrum, respectively, at pixel i . In our case, i varied from 1 to 4096. \bar{x} is the mean of x_i 's, and \bar{y} is the mean of y_i 's. The value of “r” lies between -1 and 1; $r = 1$ corresponds to complete positive correlation. Non-parametric rank correlation coefficient is another statistical approach which shows the similarity of the measurements. The equation for nonparametric rank correlation is the same as equation 1 with x and y replacing their corresponding ranks R 's and S 's, respectively:

$$r_{(\text{rank})} = \frac{\sum_i (R_i - \bar{R})(S_i - \bar{S})}{\sqrt{\sum_i (R_i - \bar{R})^2} \sqrt{\sum_i (S_i - \bar{S})^2}} \quad \dots (5.2)$$

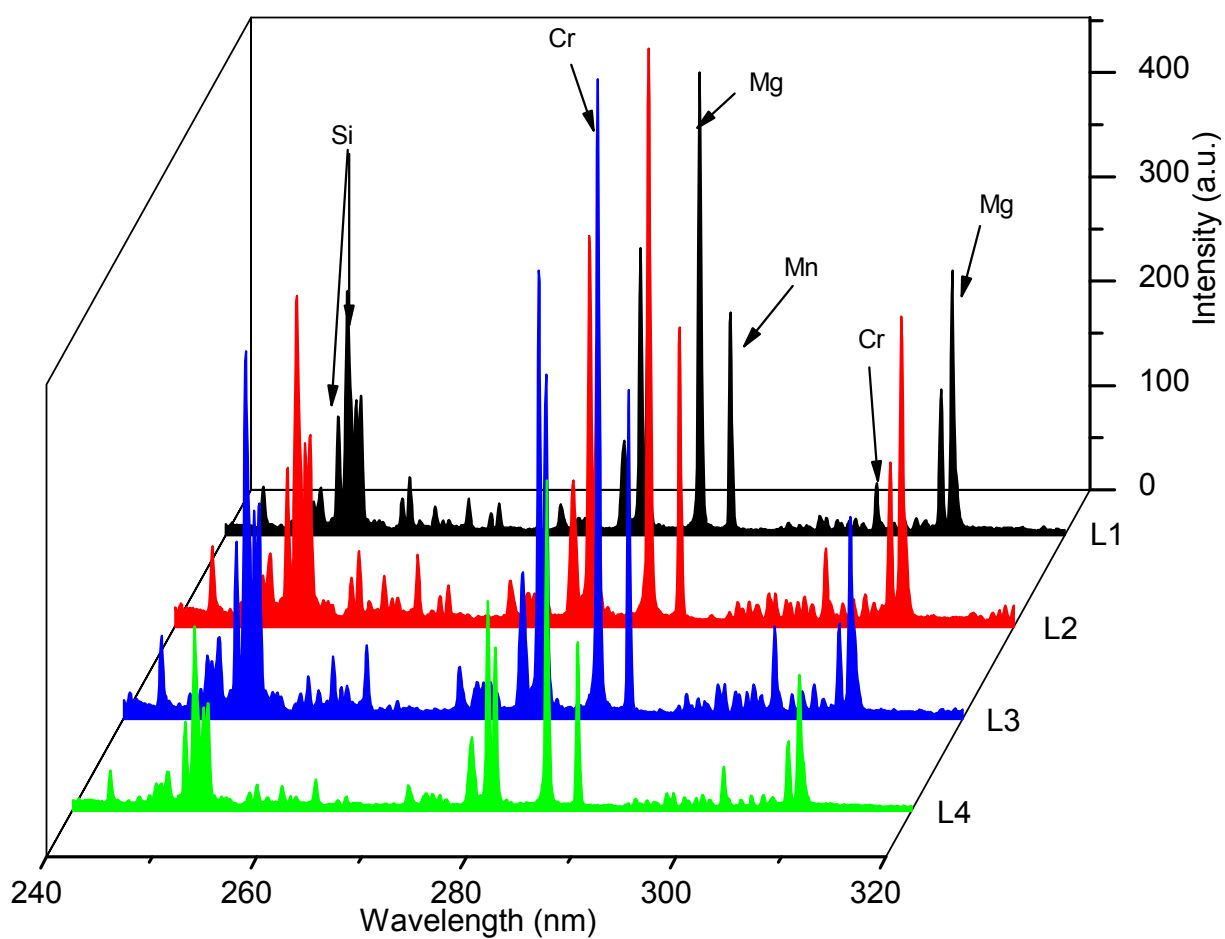


Figure 5.1: Part of the LIBS spectra of four YCR papers used to develop library.

The ranks are numbers 1, 2, 3, ..., N, where N is the total number of data points (or pixels in the present case, 4096), which replaces the true values of x and y in accordance with their magnitudes. For example, the most intense pixel in the spectrum obtained in the present study was assigned the number 4096 with number 1 assigned to the least intense pixel, i.e., the rank increases with increase in intensity. It is important to emphasize that if a correlation is proven non-parametrically, then it really exists [176].

Both the correlation methods were applied for the identification of the unknown YCR papers. Typical correlation plots for the above mentioned two correlation methods are shown in Figure 5.2 for L1 – X1. Table 5.3 shows results obtained when library paper L4 was linearly correlated with spectra of unknown YCR papers X1 to X10. All the 10 LIBS spectra of each of the ten unknown YCR papers were correlated with 10 library spectra and the average correlation coefficient values are shown in Figure 5.3a for linear correlation and in Figure 5.3b for rank correlation.

From Figures 5.3a and b, it is clear that the identical pair of samples are (L1 – X1), (L2 – X2), (L3 – X3), (L4 – X4), (L5 – X5), (L6 – X6), (L7 – X7), (L8 – X8), (L9 – X9) and (L10 – X10). From Tables 5.1 and 5.2, it is evident that the observed identical pair of paper actually belongs to the same year YCR paper branch, i.e., 100% identification is achieved.

Apart from the difference in the average values of correlation coefficients, other statistical tests were also performed. Initially F- test was done between the distributions of correlation coefficient values and significance of F test was calculated. When the calculated significance of F was less than 0.1, the difference in variances was considered as significant and the Student t-test was applied assuming unequal variance from which the probability that two distributions of correlation coefficients had different means was calculated. For the other scenario, the Student's t –test was performed assuming equal variance performed. Annexure I contains the detailed discussion and example of the calculations.

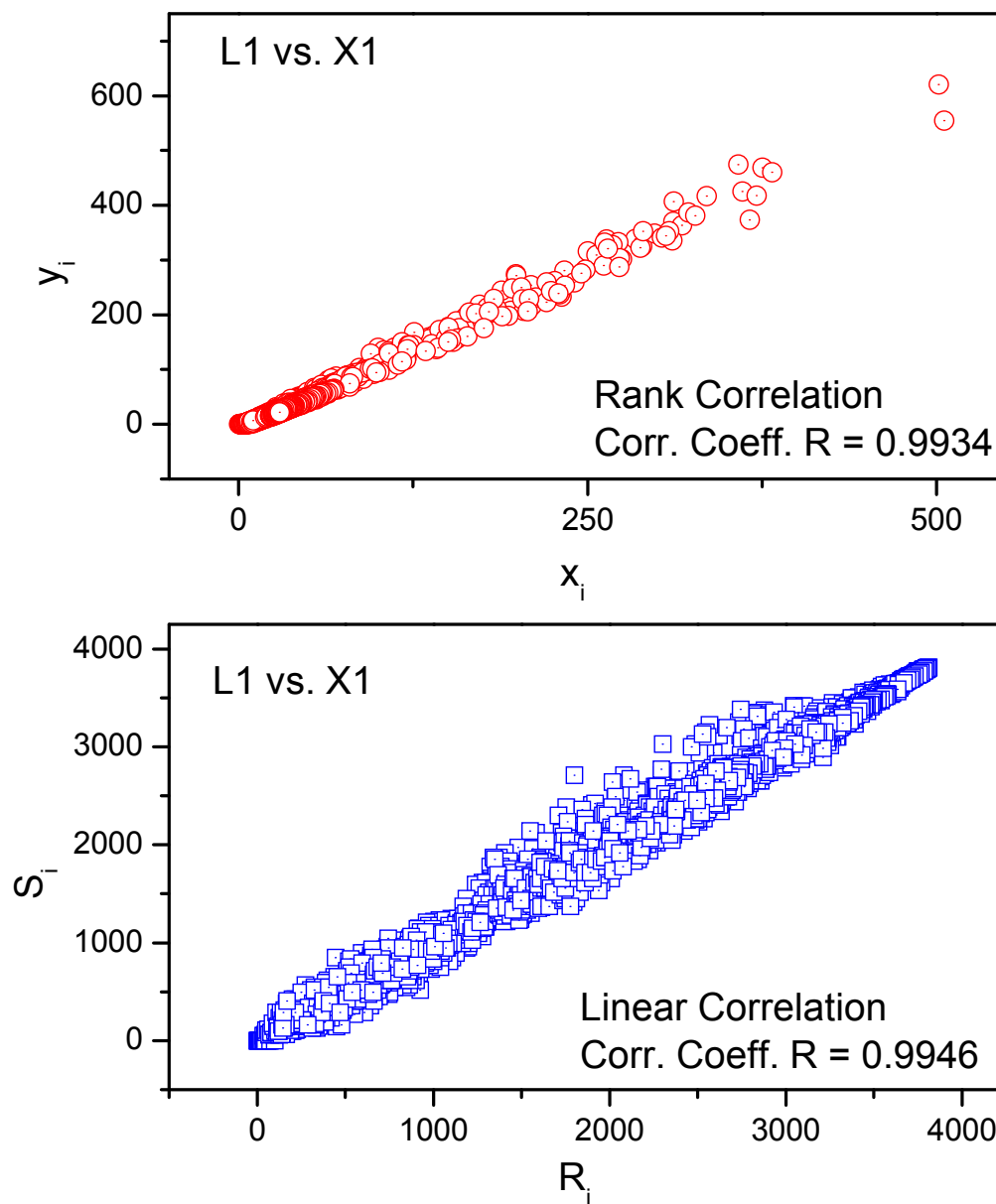


Figure 5.2: Linear and rank correlation plots for the sample L1 (library) vs. unknown X1.

Table 5.3: *Linear correlation coefficient values when L4 was linearly correlated with spectra of X1 to X10 samples*

Sample No.	Linear correlation coefficient (r)									
	L4 vs. X1	L4 vs. X2	L4 vs. X3	L4 vs. X4	L4 vs. X5	L4 vs. X6	L4 vs. X7	L4 vs. X8	L4 vs. X9	L4 vs. X10
1	0.9642	0.9683	0.9629	0.9901	0.8518	0.9342	0.9342	0.93632	0.91632	0.9632
2	0.9517	0.9696	0.9497	0.9956	0.8985	0.9717	0.9417	0.91632	0.89632	0.9502
3	0.9388	0.9693	0.9515	0.9934	0.9023	0.9388	0.952	0.9465	0.9265	0.9665
4	0.9396	0.9617	0.9473	0.9938	0.8941	0.9396	0.9396	0.90632	0.88632	0.9599
5	0.9441	0.9682	0.9277	0.9962	0.898	0.9341	0.9375	0.98632	0.92632	0.9632
6	0.9550	0.9658	0.9248	0.9941	0.9114	0.9412	0.9412	0.9073	0.8873	0.9673
7	0.9414	0.9539	0.8997	0.9948	0.9204	0.9414	0.9514	0.9452	0.9252	0.9652
8	0.9381	0.9781	0.9318	0.9836	0.8728	0.9381	0.9481	0.9248	0.9048	0.9548
9	0.9488	0.9732	0.9185	0.9959	0.8985	0.9488	0.9499	0.8997	0.9097	0.9597
10	0.9539	0.9592	0.9230	0.9944	0.9223	0.8939	0.9439	0.9318	0.9118	0.9518
Mean	0.9476	0.9667	0.9337	0.9932	0.8970	0.9382	0.9440	0.9301	0.9091	0.9602
Standard deviation	0.0086	0.0070	0.0189	0.0038	0.0213	0.0190	0.0062	0.0257	0.0153	0.0061

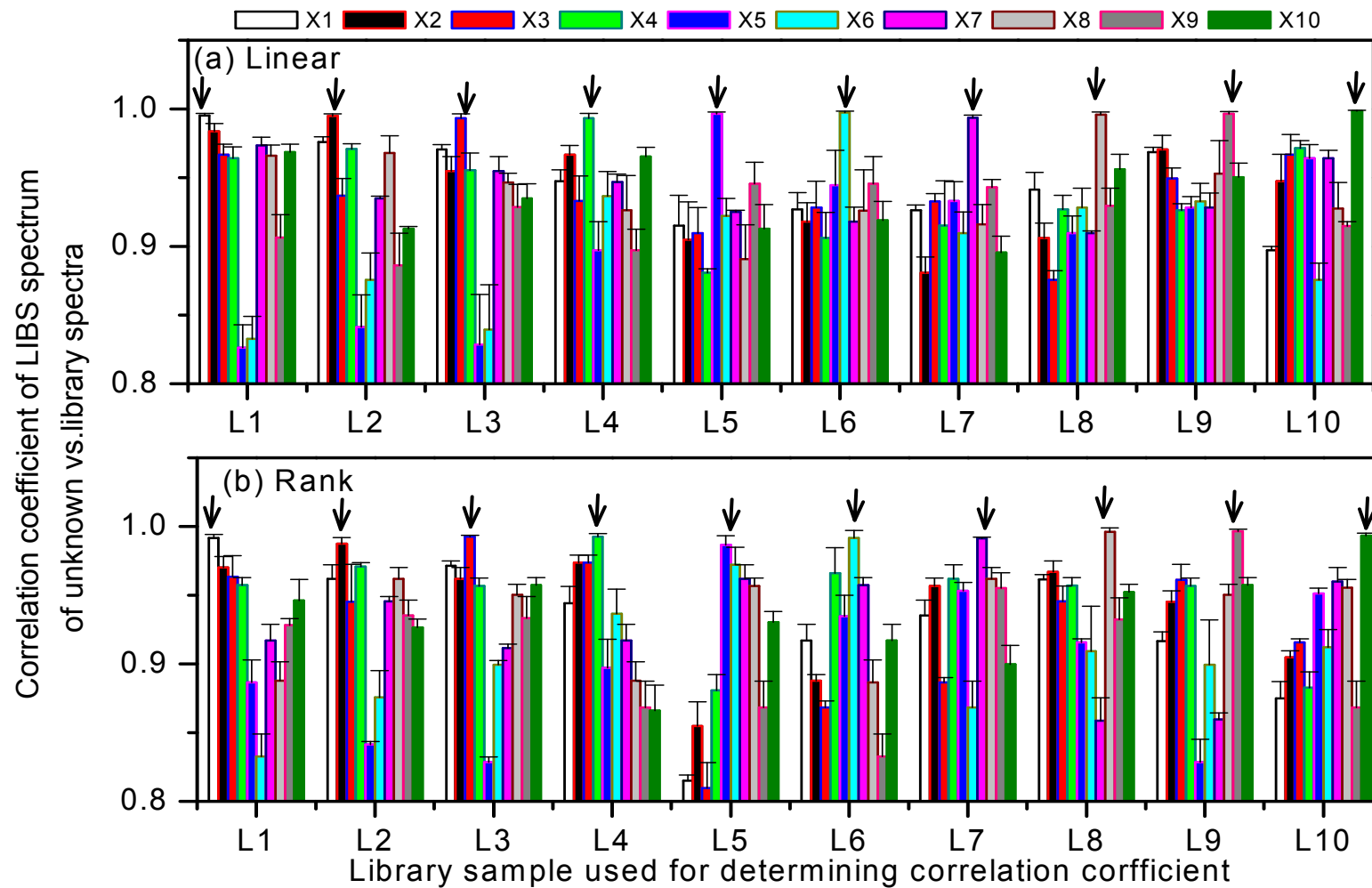


Figure 5.3: Linear (a) and rank (b) correlation coefficients for the YCR papers. Arrows indicate samples showing the best correlation coefficients. If identification is correct, the indicated sample is the same as the library sample given on the x-axis.

Table 5.4a: *Calculated probabilities that differences in YCR papers were detected using 50 shot-averaged library spectra using linear correlation*

Unknown paper samples↓	Library paper sample →									
	L1	L2	L3	L4	L5	L6	L7	L8	L9	L10
X1	0	0.9998	1	1	1	1	0.9997	1	1	1
X2	1	0	1	1	1	1	1	1	1	1
X3	1	1	0	1	0.9999	1	1	1	0.9999	1
X4	1	1	1	0	1	1	1	0.9998	1	1
X5	1	1	1	1	0	1	1	1	1	1
X6	1	1	0.9997	1	1	0	1	1	1	0.9998
X7	1	1	1	1	1	1	0	1	1	1
X8	1	1	1	0.9998	1	1	1	0	1	1
X9	1	1	1	1	1	1	1	1	0	1
X10	0.9997	1	1	1	1	0.9996	1	1	1	0

Table 5.4b: *Calculated probabilities that differences in YCR papers were detected using 50 shot-averaged library spectra using rank correlation.*

Unknown paper samples ↓	Library paper sample →									
	L1	L2	L3	L4	L5	L6	L7	L8	L9	L10
X1	0	1	0.9999	1	0.9999	1	0.9999	1	0.9999	0.9999
X2	1	0	0.9963	1	0.9963	0.9963	0.9963	0.9963	1	1
X3	1	0.9998	0	0.9995	1	1	1	1	1	1
X4	0.9999	1	1	0	0.9999	0.9999	1	1	0.9999	1
X5	1	1	1	1	0	0.9963	0.9963	0.9963	0.9963	0.9963
X6	1	0.9999	1	0.9999	1	0	1	1	1	1
X7	0.9963	1	0.9963	1	0.9999	1	0	0.9999	1	0.9979
X8	1	1	1	1	1	1	1	0	0.9963	0.9963
X9	1	0.9999	0.9999	0.9999	1	0.9963	0.9999	1	0	1
X10	0.9963	0.9963	0.9963	1	0.9999	1	0.9963	0.9999	1	0

Tables 5.4a and 5.4b show that the probability of the two distributions of correlation coefficients had different means. The diagonal elements in Table 5.4a correspond to the correlation (using linear correlation coefficient) of the sample with itself, all exhibiting a zero probability of difference. The same is also given in Table 5.4b using rank correlation coefficient. All the probabilities given in the Tables 5.4a and 5.4b as 1.0, differ from 1.0 by negligibly small value, less than 10^{-8} . As can be seen from Table 5.4, almost 100% matching is achieved using both the linear and rank correlations. It is well known that if a correlation is proven non-parametrically, i.e., by rank correlation, then it really exists. For the application and methodology discussed in this work, there was no significant difference between the two approaches i.e. linear and rank correlation.

5.4. CONCLUSION

Laser-induced breakdown spectroscopy methodology has been developed for instant reliable classification of different types of papers materials by using statistical correlation analysis. Linear and non-parametric (rank) correlations were used for classification of spectral data with approximately the same results. The robustness of the technique was demonstrated by the nearly 99% reliable identification of almost all the analyzed papers. The most attractive features of the technique are its simplicity, non-destructiveness, low cost and a good potential for identification of various kinds of paper, provided that the spectral library is available for the same variety of papers. The analysis time is minimal (about a few minutes) and the technique has excellent potential for on-line, real-time forensic analysis.

Annexure I

In Chapter V, Table 5.3 shows the linear correlation coefficient of L4 with spectra of unknown YCR papers, X1 to X10. It is clear from the table that the column L4 vs. X4 shows the best correlation and hence X4 must belong to L4 origin. But L4 vs. X2 and L4 vs. X10 also show high correlation coefficient values. Hence to examine whether the r-values of L4 vs. X4 column and that of L4 vs. X2 and L4 vs. X10 belong to same or different distribution of values, statistical calculation was carried out.

F-test (Fisher's test):

An F-test [177] is used to find out if the standard deviations of two populations are equal i.e. if the precisions are similar or dissimilar. This test can be a two-tailed test or a one-tailed test. The two-tailed version tests against the alternative that the standard deviations are not equal. The one-tailed version only tests in one direction that is the standard deviation from the first population is either greater than or less than the second population standard deviation. The F hypothesis test is defined as,

$$H_0 \text{ (null hypothesis): } s_1^2 = s_2^2 \text{ (two populations have the same variance)}$$

$$H_a \text{ (alternate hypothesis): } s_1^2 \neq s_2^2$$

The formula for F is simply

$$F = \frac{s_1^2}{s_2^2} \dots\dots\dots(\text{A.1})$$

where s_1 and s_2 are the sample variances. The variance are arranged so that $F > 1$. If the performances are not very different, then the estimates s_1 , and s_2 do not differ much and their ratio (and that of their squares) should not deviate much from unity. The calculated F value

Annexure I

(F_{cal}) is then compared with the applicable F value in the F-table critical value (F_{cri}) [11]. To read the table, it is necessary to know the applicable number of degrees of freedom for s_1 , and s_2 . These are calculated by:

$$df_1 = n_1 - 1 \quad \text{and} \quad df_2 = n_2 - 1 \quad \dots (A.2)$$

where n is the number of samples. In case, $F_{calc} > F_{cri}$, we reject the null hypothesis that the two standard deviations are equal.

For the Table 5.3, first F-test was performed between the r-values of L4 vs. X4 against the other r-values of different columns. Table 6.1 shows the F-test results for significance level of 0.1. The F_{cri} for $df_1 = df_2 = 9$ is 2.4403. All the F_{cal} are higher than F_{cri} . Hence it can be stated with 90% certainty that there is a difference between the standard deviations of the two populations.

The p-value, probability, or significance of F-test associated with the test for equality of variance is also shown in Table 6.1. The p-value or significance of F-test is the probability, if the test statistic in reality were distributed as it would be under the null hypothesis, of observing a test statistic (as extreme as, or more extreme than) the one actually observed. These p-values are obtained by comparing F-tables of different significance level. It can be seen that in all the cases the significance is less than 0.1, and so the difference in variances was considered as significant and t-test was applied assuming unequal variance. If it would have been more than 0.1, t-test would have been applied assuming equal variance.

Student's t-test:

The t-statistic was introduced in 1908 by William Sealy Gosset, ("Student" was his pen name). t-test is used to find whether the means are statistically different or not. Here the H_0 (null hypothesis) is the means do not significantly differ or are same.

A single analysis of a test sample can be regarded as literally sampling the imaginary set of a multitude of results obtained for that test sample. The uncertainty of such sub-sampling is expressed by

$$\mu = \bar{x} \pm t \frac{s}{\sqrt{n}} \quad \dots(\text{A.3})$$

Where, μ = "true" value (mean of large set of replicates), \bar{x} = mean of subsamples, t = a statistical value which depends on the number of data and the required confidence, s = standard deviation of mean of subsamples, n = number of subsamples (The term $\frac{s}{\sqrt{n}}$ is also known as the standard error of the mean.)

The equation (A.3) can be written in a different way:

$$t = \frac{|\bar{x} - \mu|}{s/\sqrt{n}} \quad \dots(\text{A.4})$$

When using the t-test for two small sets of data (n_1 and/or $n_2 < 30$), a choice of the type of test must be made depending on the similarity (or non-similarity) of the standard deviations of the two sets. If the standard deviations are sufficiently similar, Student t-test with equal variances is used. When the standard deviations are not sufficiently similar, an alternative procedure for the t-test with unequal variance is used. The criterion for the choice is the passing or non-passing of the F-test, that is, if the variances do or do not significantly differ. Therefore, for small data sets ($n < 30$) like in the present case, the F-test precedes the t-test.

➤ When comparing two sets of data, where s_1 , and s_2 are similar according to F-test, Equation (A.2) is rewritten as:

$$t_{cal} = \frac{|\bar{x}_1 - \bar{x}_2|}{\sqrt{\frac{(n_1 - 1)s_1^2 + (n_2 - 1)s_2^2}{n_1 + n_2 - 2}}} \bigg/ \sqrt{\frac{n_1 + n_2}{n_1 n_2}} \quad \dots(\text{A.5})$$

Annexure I

Where, \bar{x}_1 = mean of data set 1, \bar{x}_2 = mean of data set 2, n_1 = number of data in set 1, n_2 = number of data in set 2, s_1 = standard deviation of data set 1, s_2 = standard deviation of data set 2. The applicable number of degrees of freedom df is here calculated by

$$df = n_1 + n_2 - 2 \quad \dots(A.6)$$

➤ When comparing two sets of data, where s_1 and s_2 , are dissimilar according to F-test calculation:

$$t_{cal} = \frac{|\bar{x}_1 - \bar{x}_2|}{\sqrt{\frac{s_1^2}{n_1} + \frac{s_2^2}{n_2}}} \quad \dots(A.7)$$

Then an "alternative" critical t-value is determined by the following equation:

$$t_{alt} = \frac{t_1 \frac{s_1^2}{n_1} - t_2 \frac{s_2^2}{n_2}}{\frac{s_1^2}{n_1} + \frac{s_2^2}{n_2}} \quad \dots(A.8)$$

where, $t_1 = t_{tab}$ at (n_1-1) degrees of freedom, $t_2 = t_{tab}$ at (n_2-1) degrees of freedom. Now the t-test can be performed as usual.

If $t_{cal} < t_{alt}$ then the null hypothesis applies which shows that the means do not significantly differ is accepted and if $t_{cal} > t_{alt}$, then null hypothesis is rejected.

As stated earlier, the t-test was performed assuming unequal variance.. Table 6.2 shows the Student t-test results for the L4 vs X4 against other sets. In all cases except with itself, $t_{cal} > t_{alt}$, hence the means do significantly differ. The p-values are obtained by comparing t-tables of different significance level. The p-values indicate the probability of the null hypothesis being right, i.e., both the set of r-values belong to same distribution. Hence the value (1-P) gives the probability of the r-values for L4 vs. X4 belonging to different distribution than the other r-values set. Similarly other set were also statistically analyzed.

Table 6.1: *F-test results between the set of r-values of L4 vs. X4 against the other r-values of different columns*

	L4 vs. X1	L4 vs. X2	L4 vs. X3	L4 vs. X4	L4 vs. X5	L4 vs. X6	L4 vs. X7	L4 vs. X8	L4 vs. X9	L4 vs. X10
Mean	0.9476	0.9667	0.9337	0.9932	0.897	0.9382	0.944	0.9301	0.9163	0.9602
St. Dev.	0.0086	0.007	0.019	0.0038	0.0213	0.019	0.0062	0.0261	0.8963	0.0061
Variance	7.40E-05	4.90E-05	3.57E-04	1.44E-05	4.54E-04	3.61E-04	3.84E-05	6.60E-04	2.34E-04	3.72E-05
Observations	10	10	10	10	10	10	10	10	10	10
df	9	9	9	9	9	9	9	9	9	9
F value against (L4 vs. X4)*	5.197	3.395	25.039	---	31.510	25.200	2.644	45.933	16.231	2.582
p-value	0.011025	0.041493	0.000025	---	0.000010	0.000025	0.081846	0.000002	0.000153	0.086920

*F_{cri} (9,9) = 2.4403

Table 6.2: *Student t-test results between the set of r-values of L4 vs. X4 against the other r-values of different columns*

	L4 vs. X1	L4 vs. X2	L4 vs. X3	L4 vs. X4	L4 vs. X5	L4 vs. X6	L4 vs. X7	L4 vs. X8	L4 vs. X9	L4 vs. X10
t _{cal}	15.31	10.54	9.74	0.00	14.09	8.98	21.54	7.70	16.93	14.57
t _{alt}	2.18	2.14	2.23	2.1	2.23	2.23	2.13	2.26	2.44	2.13
p - value	3.08E-09	4.85E-08	2.03E-06	1.00E+00	6.38E-08	4.24E-06	1.07E-12	3.01E-05	1.09E-08	2.93E-10
1- P	1	1	1	0	1	1	1	1	1	1



References

- [1] P.D. Maker, R.W. Terhune and C.M. Savage, Quantum Electronics, Eds. P. Grivet and N. Bloembergen, Columbia Univ. Press, New York, 1964.
- [2] L.J. Radziemski and D.A. Cremers. Eds., Laser-Induced Plasma and Applications, Marcel Dekker, New York, 1989.
- [3] A. Einstein, Phys. Z. 18 (1917) 121; English translation on the Quantum Theory of Radiation, by D. ter Haar, The Old Quantum Theory (Pergamon Press, New York, 1967).
- [4] T.H. Maiman, Stimulated optical emission in ruby, Nature 187 (1960) 493-494.
- [5] F. Brech and L. Cross, Optical microemission stimulated by ruby laser, Appl. Spectrosc. 16 (1962) 59.
- [6] D.A. Cremers and L.J. Radziemski, Handbook of laser-induced breakdown spectroscopy, Wiley, New York, 2006.
- [7] E.R. Runge, R.W. Minck and F.R. Bryan, Spectrochemical analysis using pulsed laser source, Spectrochim. Acta Part B 20 (1964) 733-735.
- [8] Y.B. Zeldovich and Y.P. Raizer, Cascade ionization by light pulse, Sov. Phys. JETP 20 (1965) 772-789.
- [9] J. Debras-Guédon and N. Liodec , De l'utilisation du faisceau d'un amplificateur a ondes lumineuses par émission induite de rayonnement (laser á rubis), comme source énergétique pour l'excitation des spectres d'émission des éléments. C.R. Acad. Sci. 257 (1963) 3336-3339.
- [10] L.J. Radziemski, T.R Loree, D.A. Cremers and N.M. Hoffman, Time-resolved laser-induced breakdown spectrometry of aerosols, Anal. Chem. 55 (1983) 1246-1252.
- [11] D.A. Cremers and L.J. Radziemski, Detection of chlorine and fluorine in air by laser-induced breakdown spectrometry, Anal. Chem. 55 (1983) 1252-1256.

- [12] D.A. Cremers, L.J. Radziemski, and T.R Loree, Spectrochemical analysis of liquids using the laser spark, *Appl. Spectrosc.* 38 (1984) 721-729.
- [13] L.J. Radziemski, Review of selected analytical applications of laser plasmas and laser ablation: 1987–1994, *Microchem. J.* 50 (1994) 218-234.
- [14] K. Song, Y.I. Lee and J. Sneddon, Applications of laser-induced breakdown spectrometry (LIBS), *Appl. Spectrosc. Rev.* 32 (1997) 183-235.
- [15] D.A. Rusak, B.C. Castle, B.W. Smith and J.D. Winefordner, Recent trends and the future of laser-induced breakdown spectroscopy, *Trends Anal. Chem.* 17(1998) 453-461.
- [16] X.D. Hou, and B.T. Jones. Field instrumentation in atomic spectroscopy, *Microchem. J.* 66 (2000) 115-145.
- [17] R. Noll, Terms and notations for laser-induced breakdown spectroscopy, *Anal. Bioanal. Chem.* 385 (2006) 214-218.
- [18] R.E. Russo, X.L. Mao, H. Liu, J. Gonzalez, S.S. Mao, Laser ablation in analytical chemistry—a review, *Talanta* 57 (2002) 425-451.
- [19] R.E. Russo, X.L. Mao, C. Liu, J. Gonzalez, Laser assisted plasma spectrochemistry: laser ablation, *J. Anal. At. Spectrom.* 19 (2004) 1084-1089.
- [20] D. Bleiner, Z. Chen, D. Autrique and A. Bogaerts, Role of laser-assisted melting and vaporization of metals during ICP-MS and LIBS analysis, investigated with computer simulations and experiments, *J. Anal. At. Spectrom.* 21 (2006) 910-921.
- [21] C. Liu, X.L. Mao, S.S. Mao, X. Zeng, R. Greif and R.E. Russo, Nanosecond and femtosecond laser ablation of brass: particulate and ICPMS measurements, *Anal. Chem.* 76 (2004) 379-383.
- [22] J.F. Ready, Effects of high power laser radiation, New York: Academic Press, 1971.

- [23] Y.V. Afanasyev, O.N. Krokhin and G.V. Sklizkov, IEEE J. Quantum. Electron. QE-2 (1966) 483-486.
- [24] O.N. Krokhin in Laser Handbook vol. 2 ed. F.T. Arecchi and E.O. Schulz-duBois, Amsterdam, North Holland, 1972, pp 1371.
- [25] A.M. Prokhorov, IEEE J. Quantum. Electron. QE-9 (1973) 503-510.
- [26] R.S. Adrain and J. Watson, Laser microspectral analysis: a review of principles and applications, J. Phys. D: Appl. Phys., 17 (1984) 1915-1940.
- [27] J.D. Winefordner, I.B. Gornushkin, T. Correll, E. Gibb, B.W. Smith, and N. Omenetto, Comparing several atomic spectrometric methods to the super stars: special emphasis on laser induced breakdown spectrometry, LIBS, a future super star, J. Anal. At. Spectrom. 19 (2004)1061-1083.
- [28] G.M. Weyl, In Laser-induced plasmas and applications, L.J. Radziemski and D.A. Cremers, Eds., Marcel Dekker, New York 1989.
- [29] C.A. Sacchi, Laser-induced electric breakdown in water, J. Opt. Soc. Am. B 8 (1991) 337-345.
- [30] Y. Lee, K. Song, and J. Sneddon, Laser induced breakdown spectrometry, Nova Science Publishers, New York, 2000.
- [31] R.G. Root, Laser induced plasmas and applications, Marcel Dekker, New York, 1989.
- [32] X.L. Mao, W.T. Chan, M.A. Shanon, and R.E. Russo, Plasma shielding during picosecond laser sampling of solid materials by ablation in He versus Ar atmosphere, J. Appl. Phys. 74 (1993) 4915-4922.
- [33] H.R. Griem, Plasma spectroscopy, New York: McGraw-Hill, 1964.
- [34] R.W.P. McWhirter, 1965, Spectral intensities, in: R.H. Huddleston, S.L. Leonard (Eds.), Plasma Diagnostic Techniques, Academic Press.

- [35] V. Lazic, R. Barbini, F. Colao, R. Fantoni, and A. Palucci, Self-absorption model in quantitative laser induced breakdown spectroscopy measurements on soils and sediments, *Spectrochim. Acta Part B* 56 (2001) 807-820.
- [36] O. Samek, D.C. Beddows, J. Kaiser, S.V. Kukhlevsky, M. Liska, H.H Telle and J. Young, Application of laser induced breakdown spectroscopy to in-situ analysis of liquid samples, *Opt. Eng.* 39 (2000) 2248-2262.
- [37] W. Lochte-Holtgreven (Ed.), *Plasma Diagnostics*, North Holland Publishing Company, 1968.
- [38] Y. Lee and J. Sneddon, Recent developments in laser-induced breakdown spectrometry, *ISIJ International*, 42 (2002) 129-136.
- [39] A. Miziolek, V. Palleschi and I. Schechter, *Laser Induced Breakdown Spectroscopy*, Cambridge University Press, 2006.
- [40] U. Panne, C. Haisch, M. Clara and R. Niessner, Analysis of glass melts during the verification process of fly and bottom ashes by laser-induced plasma spectroscopy Part I: normalization and plasma diagnostics, *Spectrochim. Acta Part B* 53 (1998) 1957-1968.
- [41] G. Bekefi, *Principles of laser plasmas*, Wiley, New York, 1976.
- [42] E. Tognoni, V. Palleschi, M. Corsi and G. Cristoforetti, Quantitative micro-analysis by laser- induced breakdown spectroscopy: a review of the experimental approaches, *Spectrochim. Acta Part B* 57(2002) 1115-1130.
- [43] M. Capitelli, A. Casavola, G. Colonna and A. De Giacomo, Laser-induced plasma expansion: theoretical and experimental aspects, *Spectrochim Acta Part B* 59 (2004) 271-289.

- [44] IUPAC. Compendium of Chemical Terminology, 2nd ed. (the "Gold Book"). Compiled by A. D. McNaught and A. Wilkinson. Blackwell Scientific Publications, Oxford, 1997, <http://goldbook.iupac.org/L03540.html> .
- [45] L.M. Cabalim, D. Romero, J.M. Baena, J.J. Laserna, Effect of surface topography in the characterization of stainless steel using laser induced breakdown spectroscopy, *Surf. Interface. Anal.* 27 (1999) 805-810.
- [46] Jack Edward Pender, Ph. D. thesis, Laser-induced breakdown spectroscopy of aqueous solutions, Applications and matrix interference, University of South Carolina, 2004.
- [47] R. Iffländer and S. Weber, *Solid-state lasers for materials processing*, Springer, Berlin, 2001.
- [48] S. Kück, L. Fornasiero, E. Mix and G. Huber, Excited state absorption and stimulated emission of Nd^{3+} in crystals. Part 1: $\text{Y}_3\text{Al}_5\text{O}_{12}$, YAlO_3 , and Y_2O_3 , *Appl. Phys. B* 67 (1998) 151-156.
- [49] W.T. Silfvast, *Laser Fundamentals*, Cambridge University Press, 2008.
- [50] J.M. Harnly and R.E. Fields, Solid-state array detectors for analytical spectrometry, *Appl. Spectrosc.* 51 (1997) 334A-351A.
- [51] S.B. Howell (eds. 2), *Handbook of CCD Astronomy* Cambridge University Press, Cambridge UK, 2006.
- [52] G.C. Holst (eds. 2), *CCD Arrays Cameras and Displays*, JCD Publishing and SPIE, Winter Park and Bellingham, 1998.
- [53] L. Canevea, F. Colaoa, F. Fabbria, R. Fantonia, V. Spizzichinoa and J. Striberb, Laser-induced breakdown spectroscopy analysis of asbestos, *Spectrochim. Acta Part B* 60 (2005) 1115-1120.

- [54] H. Hakkanen, J. Houni, S. Kaski and J.E.I. Korppi-Tommola, Analysis of paper by laser-induced plasma spectroscopy, *Spectrochim. Acta Part B* 56 (2001) 737-742.
- [55] N. Carmona, M. Oujja, E. Rebollar, H. Romich and M. Castillejo, Analysis of corroded glasses by Laser Induced Breakdown Spectroscopy, *Spectrochim. Acta Part B* 60 (2005) 1155-1162.
- [56] J. Anzano, B. Bonilla, B. Montull-Ibor, and J. Casas, Aromatic Herbal Products Analysis by Laser-Induced Breakdown Spectroscopy, *Scholarly Research Exchange* (2008) 152607.
- [57] S. Gaspard, M. Oujja, E. Rebollar, C. Abrusci, F. Catalina and M. Castillejo, Characterization of cinematographic films by laser induced breakdown spectroscopy, *Spectrochim. Acta Part B* 62 (2007) 1612-1617.
- [58] J. Anzano, R. Lasheras, B. Bonilla and J. Casas, Classification of polymers by determining of C1:C2:CN:H:N:O ratios by laser-induced plasma spectroscopy (LIPS), *Polymer Testing* 27 (2008) 705–710.
- [59] R. Sattmann, I. Monch, H. Krause, R. Noll, S. Couris, A. Hatzia Apostolou, A. Mavromanolakis, C. Fotakis, E. Larrauri and R. Miguel, Laser-Induced breakdown spectroscopy for polymer identification, *Applied Spectroscopy* 52 (1998) 323-476.
- [60] S. Kaski, H. Haˆkkaˆnen and J. Korppi-Tommola, Determination of Cl/C and Br/C ratios in pure organic solids using laser-induced plasma spectroscopy in near vacuum ultraviolet, *J. Anal. At. Specm.* 19 (2004) 474 – 478.
- [61] A.A.I. Khalil, M. Richardson, C. Barnett and L. Johnson, Double pulse UV laser induced breakdown spectroscopy of stainless steel, *J. Appl. Spectrosc.* 73 (2006) 735-742.

- [62] M.E. Essington, G.V. Melnichenko, M.A. Stewart, and R.A. Hull, Soil metals analysis using laser-induced breakdown spectroscopy, *Soil Sci. Soc. Am. J.* 73 (2009) 1469-1478.
- [63] A.S. Eppler, D.A. Cremers, D.D. Hickmott, M.J. Ferris and A.C. Koskelo, Matrix effects in the detection of Pb and Ba in soils using laser-induced breakdown spectroscopy. *Appl. Spectrosc.* 50 (1996) 1175–1181.
- [64] J. L. Gottfried, F. C. De Lucia Jr., C. A. Munson, and A. W. Miziolek, Strategies for residue explosives detection using laser-induced breakdown spectroscopy, *J. Anal. At. Spectrom.* 23 (2008) 205-216.
- [65] J. L. Gottfried, Frank C. De Lucia Jr, C.A. Munson and A.W. Miziolek, Laser-induced breakdown spectroscopy for detection of explosives residues: a review of recent advances, challenges, and future prospects, *Anal. Bioanal. Chem.*, 395 (2009) 283-300.
- [66] M. Kuzuya, M. Murakami and N. Maruyama, Quantitative analysis of ceramics by laser-induced breakdown spectroscopy, *Spectrochim. Acta Part B* 58 (2003) 957-965.
- [67] S. Mahmooda, S.A. Abbasi, S. Jabeen and M.A. Baig, Laser-induced breakdown spectroscopic studies of marbles, *J. Quantitative Spectrosc. Radiative Transfer.* 111 (2010) 689-695.
- [68] L. Fornarini, F. Colao, R. Fantoni, V. Lazic and V. Spizzicchino, Calibration analysis of bronze samples by nanosecond laser induced breakdown spectroscopy: A theoretical and experimental approach, *Spectrochim. Acta Part B* 60 (2005) 1186-1201.
- [69] Q. Sun, M. Tran, B.W. Smith and J.D. Winefordner, Zinc analysis in human skin by laser induced-breakdown spectroscopy, *Talanta* 52 (2000) 293–300.

- [70] C.M. Davies, H.H. Telle, A.W. Williams, Remote in situ analytical spectroscopy and its applications in the nuclear industry, *Fresenius J. Anal. Chem.* 355 (1996) 895-899.
- [71] P. Fichet, P. Mauchien, and C. Moulin, Determination of impurities in uranium and plutonium dioxides by laser-induced breakdown spectroscopy, *Appl. Spectrosc.* 53 (1999) 1111–1117.
- [72] X.K. Shen and Y.F. Lu, Detection of uranium in solids by using laser-induced breakdown spectroscopy combined with laser-induced fluorescence, *App. Optics* 47 (2008) 1810-1815.
- [73] H. Liu, Z. Zhang, A. Quentmeier and K. Niemax, Measurement of uranium isotope ratio in solid sample by laser ablation and double-beam diode laser atomic absorption, *Spectroscopy and Spectral Analysis* 24 (2004) 1244-1247.
- [74] B.W. Smith, A. Quentmeier, M. Bolshov and K. Niemax, Measurement of uranium isotopes in solid samples using laser ablation and diode laser-excited atomic fluorescence spectrometry, *Spectrochim. Acta Part B* 54 (1999) 943.
- [75] C.A. Smith, M. A. Martinez, D. K. Veirs and D.A. Cremers, Pu-239/Pu-240 isotope ratios determined using high resolution emission spectroscopy in a laser-induced plasma, *Spectrochim. Acta Part B* 57 (2002) 929-958.
- [76] A.I. Whitehouse, J. Young, I.M. Botheroyd, S. Lawson, C.P. Evans and J. Wright, Remote material analysis of nuclear power station steam generator tubes by laser-induced breakdown spectroscopy, *Spectrochim. Acta Part B* 56 (2001) 821-830.
- [77] M.M. Tripathi, K.E. Eseller, Fang-Yu Yueh and J.P. Singh, Multivariate calibration of spectra obtained by Laser Induced Breakdown Spectroscopy of plutonium oxide surrogate residues, *Spectrochim. Acta Part B* 64 (2009) 1212–1218.
- [78] http://www.appliedphotonics.co.uk/Libs/libs_nuclear.htm

- [79] J. B. Hedrick, U.S. Geological Survey, Mineral Commodity Summaries, January 1998, p.177.
- [80] <http://www.uic.com.au/nip67.htm>
- [81] R.K. Sinha and A. Kakodkar, Design and development of the AHWR-the Indian thorium fuelled innovative nuclear reactor, Nuclear Engineering and Design 236 (2006) 683-700.
- [82] <http://physics.nist.gov/PhysRefData/Handbook/index.html>
- [83] R.K. Winge, V.J. Peterson and V.A. Fassel, Inductively Coupled Plasma-Atomic Emission Spectroscopy: Prominent Lines, Appl. Spectrosc. 33(1979) 206-219.
- [84] B. Castle, K. Talabardon, B.W. Smith, J.D. Winefordner, Variables Influencing the Precision of Laser-Induced Breakdown Spectroscopy Measurements, Appl. Spectrosc. 52 (1998) 649-657.
- [85] B. Sall'e, D.A. Cremers, S.M. Roger, C. Wiens, Laser-induced breakdown spectroscopy for space exploration applications: Influence of the ambient pressure on the calibration curves prepared from soil and clay samples, Spectrochim. Acta Part B 60 (2005) 479-490.
- [86] D. Alamelu, A. Sarkar and S.K. Aggarwal, Laser-induced breakdown spectroscopy for simultaneous determination of Sm, Eu and Gd in aqueous solution, Talanta 77 (2008) 256-261.
- [87] C. Aragon, J. Bengoechea, J.A. Aguilera, Influence of the optical depth on spectral line emission from laser-induced plasmas, Spectrochim. Acta Part B 56 (2001) 619-628.
- [88] C. Aragon, J.A. Aguilera, F. Penalba, Improvements in quantitative analysis of steel composition by laser-induced breakdown spectroscopy at atmospheric pressure using an infrared Nd:YAG laser, Appl. Spectrosc. 53 (1999) 1259-1267.

- [89] V.D. Allred, S.R. Buxtona and J.P. McBride, Characteristic Properties of Thorium. Oxide Particles, J. Phys. Chem. 61 (1957) 117-120.
- [90] K.J. Grant, G.L. Paul and J.A. O'Neill, Time-Resolved Laser-Induced Breakdown Spectroscopy of Iron Ore, Appl. Spectrosc. 44 (1990) 1711-1714.
- [91] M. Doubek, G. Baglino and S. Deron, Report on intercomparison exercise SR-64. Determination of impurities in U₃O₈, Seibersdorf Laboratories, IAEA/RL/116, (1985)
- [92] D.A. Cremers, The Analysis of Metals at a Distance Using Laser-Induced Breakdown Spectroscopy, Appl. Spectrosc. 41 (1987) 572-579.
- [93] L. M. Cabalin and J. J. Laserna, Experimental determination of laser induced breakdown thresholds of metals under nanosecond Q-switched laser operation, Spectrochim. Acta Part B, 53 (1998) 723-730.
- [94] http://www.appliedphotonics.co.uk/Libs/capabilities_libs.htm
- [95] V. Palleschi, A. Ciucci, S. Rastelli, E. Tognoni, Method for quantitative analysis of atomic components of materials by LIBS spectroscopy measurements, Patent no. WO99/49301 (1999).
- [96] Handbook of Chemistry and Physics, 62nd edition, CRC Press, 1981–1982, pp. E349–E351.
- [97] G. Arca, A. Ciucci, V. Palleschi, S. Rastelli, E. Tognoni, Trace element analysis in water by laser-induced breakdown spectroscopy technique, Appl. Spectrosc. 51 (1997) 1102-1105.
- [98] L. St-Onge, E. Kwong, M. Sabsabi, E.B. Vadas, Rapid analysis of liquid formulations containing sodium chloride using laser-induced breakdown spectroscopy, J. Pharm. Biomed. Anal. 36 (2004) 277–284.

- [99] J.E. Pender, Laser-induced breakdown spectroscopy of aqueous solutions, Applications and matrix interference, Master thesis, University of South Carolina, 2004.
- [100] J.R. Watcher and D.A. Cremers, Determination of uranium in solution using laser induced breakdown spectroscopy, *Appl. Spectrosc.* 41 (1987) 1042-1048.
- [101] L. M. Berman and P. J. Wolf, Laser induced breakdown spectroscopy of liquids: aqueous solution of nickel and chlorinated hydrocarbon, *Appl. Spectrosc.* 52 (1998) 438-443.
- [102] C. Haisch, J. Liermann, U. Panne, and R. Niessner, Characterization of colloidal particle by laser induced plasma spectroscopy, *Anal. Chim. Acta.* 346 (1997) 23-25.
- [103] Y. Ito, O. Ueki, S. Nakamura, Determination of colloidal iron in water by laser-induced breakdown spectroscopy, *Anal. Chim. Acta.* 299 (1995) 401-405.
- [104] S. Nakamura, Y. Ito, K. Sone, H. Hiraga and K. I. Kaneko, Determination of an iron suspension in water by laser-induced breakdown spectroscopy with two sequential laser pulses, *Anal. Chem.* 68 (1996) 2981-2986.
- [105] C.W. Ng, W.F. Ho, and N.H. Cheung, Spectrochemical analysis of liquids using laser-induced plasma emissions: Effects of laser wavelength on plasma properties, *Appl. Spectrosc.* 51 (1997) 976-983.
- [106] W.F. Ho, C.W. Ng, and N.H. Cheung, spectrochemical analysis of liquids using laser-induced plasma emissions: Effects of laser wavelength, *Appl. Spectrosc.* 51 (1997) 87-91.
- [107] A. Kumar, F.Y. Yueh, T. Miller and J.P. Singh, Detection of trace elements in liquids by laser-induced breakdown spectroscopy with a Meinhard nebulizer, *Appl. Opt.* 42 (2003) 6040-6046.

- [108] N.E. Schmidt and S.R. Goode, Analysis of aqueous solutions by laser-induced breakdown spectroscopy of ion exchange membranes, *Appl. Spectrosc.* 56 (2002) 370–374.
- [109] R. Knopp, F.J. Scherbaum and J.I. Kim, Laser induced breakdown spectroscopy (LIBS) as an analytical tool for the detection of metal ions in aqueous solutions, *Fresenius J. Anal. Chem.* 355 (1996) 16–20.
- [110] T. Kitamori, T. Matsui, M. Sakagami and T. Sawada, Laser breakdown spectrochemical analysis of microparticles in liquids, *Chem. Lett.* 12 (1989) 2205–2208.
- [111] D.E. Poulain and D.R. Alexander, Influences on concentration measurements of liquid aerosols by laser-induced breakdown spectroscopy, *Appl. Spectrosc.* 49 (1995) 569–579.
- [112] H.A. Archontaki and S.R. Crouch, Evaluation of an isolated droplet sample introduction system for laser-induced breakdown spectroscopy, *Appl. Spectrosc.* 42 (1988) 741-746.
- [113] N.H. Cheung and E.S. Yeung, Single-shot element analysis of liquids based on laser vaporization at fluences below breakdown, *Appl. Spectrosc.* 47 (1993) 882–886.
- [114] C.R. Dockery, J.E. Pender and S.R. Goode, Speciation of chromium via laser induced breakdown spectroscopy of ion exchange polymer membranes, *Appl. Spectrosc.* 59 (2005) 252–257.
- [115] R.L. Vander Wal, T.M. Ticich, J.R. West and P.A. Householder, Trace metal detection by laser-induced breakdown spectroscopy, *Appl. Spectrosc.* 53 (1999) 1226–1236.
- [116] J.O. Caceres, L.J. Tornero, H.H. Telle and A.G. Urena, Quantitative analysis of trace metal ions in ice using laser-induced breakdown spectroscopy, *Spectrochim. Acta Part B* 56 (2001) 831–838.

- [117] O. Otulu, Quantitative determination of uranium, strontium, thorium, rubidium, nickel, cobalt, and manganese in dry aerosols by laser-induced breakdown spectroscopy; MS thesis, Mississippi State University, 1996.
- [118] Cellulose Filters, Whatman, www.whatman.com/CelluloseFilters.aspx
- [119] <http://environmentalchemistry.com/yogi/periodic>
- [120] F.P. Roberts, Radiation characterization of reactor produced Rh, Pd, Ru, Tc, Battelle Northwest Laboratory Technical Report No BNWL-1693, 1972.
- [121] R.P. Bush, Recovery of platinum group metals from high level radioactive waste, *Platinum Metals Rev.* 35 (1991) 202-208.
- [122] Y. Kondo and M. Kubota, Precipitation behavior of platinum group metals from simulated high level liquid waste in sequential denitration process, *J. Nucl. Sci. Technol.* 29 (1992) 140-148.
- [123] A. Dakshinamoorthy, P.S. Dharmi, P.W. Naik, N.L. Dudwadkar, S.K. Munshi, P.K. Dey and V. Venugopal, Separation of palladium from high level liquid waste of PUREX origin by solvent extraction and precipitation methods using oximes, *Desalination* 232 (2008) 26-36.
- [124] S.H. Lee, K.R. Kim, J.S. Shon, J.H. Yoo and H. Chung, Precipitation characteristics of palladium from a simulated radioactive liquid waste by ascorbic acid, *Korean J. Chem. Eng.* 16 (1999) 166-169.
- [125] V. T. Aher, M. M. Palrecha, A. V. Kulkarni and G. C. Shah, Determination of palladium in synthetic nuclear wastes by differential pulse voltammetry, *J. Radioanal. Nucl. Chem.* 252 (2002) 573-576.
- [126] P. Cavalli, G. Rossi and N. Omenetto, Determination of palladium in nuclear-waste samples by inductively coupled plasma emission-fluorescence spectrometry, *Analyst* 108 (1983) 297 - 304.

- [127] M. Martin, B. Evans, H. O'Neill and J. Woodward, Laser-induced breakdown spectroscopy used to detect palladium and silver metal dispersed in bacterial cellulose membranes, *Appl. Opt.* 42 (2003) 6174-6178.
- [128] P. Lucena, J.M. Vadillo and J.J. Laserna, mapping of platinum group metals in automotive exhaust three-way catalysts using laser-induced breakdown spectrometry, *Anal. Chem.* 71 (1999) 4385-4391.
- [129] P. Lucena and J.J. Laserna, Three-dimensional distribution analysis of platinum, palladium and rhodium in auto catalytic converters using imaging-mode laser-induced breakdown spectrometry, *Spectrochim. Acta Part B* 56 (2001) 177-185.
- [130] P. Lucena, J.M. Vadillo and J.J. Laserna, Compositional mapping of poisoning elements in automobile three-way catalytic converters by using laser-induced breakdown spectrometry, *Appl. Spectrosc.* 55 (2001) 267-272.
- [131] P. Lucena, J.M. Vadillo and J.J. Laserna, Spatial distribution of catalytically active elements and deactivants in diesel-engine automobile converters by laser-induced plasma spectrometry, *J. Anal. At. Spectrom.* 17 (2002) 548-551.
- [132] M.A. Palacios, M.M. Gomez, M. Moldovan, G. Morrison, S. Rauch, C. McLeod, R. Ma, J. Laserna, P. Lucena, S. Caroli, A. Alimonti, F. Petrucci, B. Bocca, P. Schramel, S. Lustig, M. Zischka, U. Wass, B. Stenbom, M. Luna, J.C. Saenz, J. Santamarva and J.M. Torrens, Platinum-group elements: quantification in collected exhaust fumes and studies of catalyst surfaces, *Sci. Total Environ.* 257 (2000) 1-15.
- [133] G. Asimellis, N. Michos, I. Fasaki and M. Kompitsas, Platinum group metals bulk analysis in automobile catalyst recycling material by laser-induced breakdown spectroscopy, *Spectrochim. Acta Part B* 63 (2008) 1338-1343.
- [134] S.A. Ansari, P.K. Mohapatra, D.R. Raut, V.C. Adya, S.K. Thulasidas and V.K. Manchanda, Separation of Am(III) and trivalent lanthanides from simulated high-

- level waste using a hollow fiber-supported liquid membrane, *Sep. Purif. Technol.* 63 (2008) 239-242.
- [135] R. Kovacevic, M. Todorovic, D. Manojlovic, and J. Mutic, Development of inductively coupled plasma atomic emission spectrometry for palladium and rhodium determination in platinum-based alloy, *J. Iran. Chem. Soc.* 5 (2008) 336-341.
- [136] P. Pohl, B. Prusisz and W. Zyrnicki, Application of metalfix chelamine prior to the determination of noble metals by the inductively coupled plasma atomic emission spectrometry, *Talanta* 67 (2005) 155-161.
- [137] F. Maillard, A. Bonnefont, M. Chatenet, L. Guetaz, B.D. Cottignies, H. Rouse and U. Stimming, Effect of the structure of Pt-Ru/C particles on CO_{ad} monolayer vibrational properties and electrooxidation kinetics, *Electrochim. Acta* 53 (2007) 811-822.
- [138] R.N. Sah, P.H. Brown, Techniques for boron determination and their application to the analysis of plant and soil samples, *Plant and Soil* 193 (1997) 15-33.
- [139] G.W. vanLoon, S.J. Duffy, A global perspective, *Environmental Chemistry*, 2nd edition, Oxford, UK: Oxford University Press, 2005.
- [140] A. Vengosh, K.G. Heumann, S. Juraske, R. Kasher, Boron isotope application for tracing sources of contamination in groundwater, *Environ. Sci. Technol.* 28 (1994) 1968-1974.
- [141] A. Vengosh, J. Spivack, Y. Artzi, A. Ayalon, Boron, strontium and oxygen isotopic and geochemical constraints for the origin of the salinity in ground water from the Mediterranean Coast of Israel, *Water Resour. Res.* 35 (1999) 1877-1894.
- [142] R. Wickham, R. Godec, Proceedings of Semiconductor Pure Water and Chemicals Conference, Hillsboro, 2001, USA, p. 15-33.
- [143] D. Darbouret, I. Kano, Ultrapure water blank for boron trace analysis, *J. Anal. Atom. Spectrom.* 15 (2000) 1395-1399.

- [144] B. Gorenc, J. Marsel, G. Tramw, Application of ion-exchange to mass spectrometric determination of boron in mineral waters, *Microchim. Acta.* 58 (1970) 24-28.
- [145] H. Kurniawan, S. Nakajima, J.E. Batubara, M. Marpaung, M. Okamoto, K. Kagawa, Laser-induced shock wave plasma in glass and its application to elemental analysis, *Appl. Spectrosc.* 49 (1995) 1067-1072.
- [146] A. Uhl, K. Loebe and L. Kreuchwig, Fast analysis of wood preservers using laser induced breakdown spectroscopy, *Spectrochim. Acta Part B* 56 (2001) 795-806.
- [147] M. Pardede, H. Kurniawan, M.O. Tjja, K. Ikezawa, T. Maruyama, K. Kagawa, Spectrochemical analysis of metal elements electrodeposited from water samples by laser-induced shock wave plasma spectroscopy, *Appl. Spectrosc.* 55 (2001) 1229-1236.
- [148] M. Baudelet, L. Guyon, J. Yu, J.P. Wolf, T. Amodeo, E. Fréjafon and P. Laloi, Spectral signature of native CN bonds for bacterium detection and identification using femto second laser-induced breakdown spectroscopy, *Appl. Phys. Lett.* 88 (2006) 63901.
- [149] H.J. vandeWiel Determination of elements by ICP-AES and ICP-MS. Horizontal – 19: National Institute of Public Health and the Environment, 2003.
- [150] S.D. Kumar, B. Maiti, P.K. Mathur, Determination of boron by flow injection analysis using a conductivity detector, *Anal. Chem.* 71 (1999) 2551-2553.
- [151] P.S. Ramanjaneyulu, Y.S. Sayi, T.N. Nathaniel, A.V.R. Reddy, K.L. Ramakumar Determination of boron in water samples by chemical prompt gamma neutron activation analysis. *J. Radioanal. Nucl. Chem.* 273 (2007) 411-414.
- [152] C.E. Johnson, Tritium behavior in lithium ceramics, *J. Nuclear Mat.* 270 (1999) 212-220.

- [153] C.E. Johnson, G.W. Hollenberg, N. Roux and H. Watanabe, Current experimental activities for solid breeder development, *Fusion Eng. Des.* 8 (1989) 145-153.
- [154] P.A. Finn, K. Kurasawa, S. Nasu, K. Noda, T. Takahashi, H. Takeshita, T. Tanifuji and H. Watanabe, Proceedings of the 9th IEEE Symposium on Engineering Problems of Fusion Research Vol. II, 1981, p. 1200.
- [155] N. Roux, G. Hollenberg, C. Johnson, K. Noda and R. Verrall, Summary of experimental results for ceramic breeder materials, *Fusion Eng. Des.* 27 (1995) 154-166.
- [156] J.D. Lulewicz and N. Roux, First results of the investigation of Li_2ZrO_3 and Li_2TiO_3 pebbles, *Fusion Eng. Des.* 39–40 (1998) 745-750.
- [157] C. Alvani, S. Casadio, V. Contini, A. Di Bartolomeo, J.D. Lulewicz and N. Roux, Li_2TiO_3 pebbles reprocessing, recovery of ^6Li as Li_2CO_3 , *J. Nucl. Mater.* 307–311 (2002) 837-841.
- [158] J.P. Kopasz, J.M. Miller and C.E. Johnson, Tritium release from lithium titanate, a low-activation tritium breeding material, *J. Nucl. Mater.* 212–215 (1994) 927-931.
- [159] N. Roux, J. Avon, A. Floreancing, J. Mougin, B. Rasneur and S. Ravel, Low-temperature tritium releasing ceramics as potential materials for the ITER breeding blanket, *J. Nucl. Mater.* 233–237 (1996) 1431-1435.
- [160] C.H. Jung, J.Y. Park, S.J. Oh, H.K. Park, Y.S. Kim, D.K. Kim and J.H. Kim, Synthesis of Li_2TiO_3 ceramic breeder powders by the combustion process, *J. Nucl. Mater.* 253 (1998) 203-212.
- [161] O. Renoult, J.P. Boilot, J.P. Korb and M. Boncoeur, Lithium sol-gel ceramics for tritium breeding applications, *J. Nucl. Mater.* 223 (1995) 126-134.
- [162] O. Renoult, J.P. Boilot and M.J. Boncoeur, Alkoxide–Hydroxide route for the preparation of $\gamma\text{-LiAlO}_2$ -based ceramics, *J. Am. Ceram. Soc.* 77 (1994) 249-253.

- [163] V.N. Vaidya, S.K. Mukerjee, J.K. Joshi, R.V. Kamat, D.D. Sood, A study of chemical parameters of the internal gelation based sol-gel process for uranium dioxide, *J. Nucl. Mater.* 148 (1987) 324 - 331.
- [164] S. Suryanarayana, N. Kumar, Y.R. Bamankar, V.N. Vaidya, D.D. Sood, Fabrication of UO_2 pellets by gel pelletization technique without addition of carbon as pore former, *J. Nucl. Mater.* 230 (1996) 140 - 147.
- [165] Ashok Kumar, T.V. Vittal Rao, S.K. Mukerjee, V.N. Vaidya, Recycling of chemicals from alkaline waste generated during preparation of UO_3 microspheres by sol-gel process, *J. Nucl. Mater.* 350 (2006) 254 - 263.
- [166] M.S.Y. Haddadin, S. Khattari Daniela Caretto, and R.K. Robinson, Potential intake of lithium by the inhabitants of different regions in Jordan, *Pak. J. Nutrition* 1 (2002) 39-40.
- [167] T.V. Vittal Rao, Y.R. Bamankar, S.K. Mukerjee, Proceedings of the XIV International Sol-Gel Conference (ISGC) held at Montpellier, France during September 2 – 7, 2007, 210.
- [168] N.D. Chattopadhyay, A.K. Basu, A.B.R. Tripathi, C.A. Bhadkambekar and S.K. Shukla, Proceedings of DAE –BRNS discussion meet on current trends and future perspective of neutron activation analysis (CFNAA), BARC, India, 2006, pp. 137.
- [169] I.B. Gornushkin, A. Ruoz-Medina, J.M. Anzano, B.W. Smith and J.D. Winefordner, Identification of particulate materials by correlation analysis using a microscopic laser induced breakdown spectrometer, *J. Anal. At. Spectrom.* 15 (2000) 581-586.
- [170] I.B. Gornushkin, B.W. Smith, H. Nasajpour and J.D. Winefordner, Identification of solid materials by correlation analysis using a microscopic laser-induced plasma spectrometer, *Anal. Chem.* 71 (1999) 5157-5164.

- [171] J. Anzano, M.E. Casanova, M.S. Bermúdez and R.J. Lasheras, Rapid characterization of plastics using laser-induced plasma spectroscopy (LIPS), *Poly. Test.* 25 (2006) 623–627.
- [172] A. Jurado-López and M.D. Luque de Castro, Rank correlation of laser-induced breakdown spectroscopic data for the identification of alloys used in jewelry manufacture, *Spectrochim. Acta Part B* 58 (2003) 1291-1299.
- [173] M.P. Mateo, G. Nicolas, V. Pinon, A. Yanez, Improvements in depth-profiling of thick samples by laser-induced breakdown spectroscopy using linear correlation, *Surf. Interface Anal.* 38 (2006) 941-948.
- [174] E.M. Rodriguez-Celis, I.B. Gornushkin, U.M. Heitmann, J.R. Almirall, B.W. Smith, J.D. Winefordner and N. Omenetto, Laser induced breakdown spectroscopy as a tool for discrimination of glass for forensic applications, *Anal. Bioanal. Chem.* 391 (2008) 1961-1968.
- [175] I.B. Gornushkin, U. Panne, J.D. Winefordner, Linear correlation for identification of materials by laser induced breakdown spectroscopy: Improvement via spectral filtering and masking, *Spectrochim. Acta Part B* 64 (2009) 1040–1047.
- [176] W. H. Press, B. P. Flannery, S. A. Teukolsky and W. T. Vetterling, *Numerical recipes: the art of scientific computing*, Cambridge University Press, New York, 1986.
- [177] G.W. Snedecor and W.G. Cochran, *Statistical Methods*, Eighth Edition, Iowa State University Press, 1989.
- [178] <http://www.statsoft.com/textbook/distribution-tables>



List of publications

Refereed Journals

1. Determination of thorium and uranium in solution by laser-induced breakdown spectrometry
Arnab Sarkar, D. Alamelu & S.K. Aggarwal
Applied Optics 47 (2008) G58 - G64.
2. Laser induced breakdown spectroscopy for determination of uranium in thorium - uranium mixed oxide fuel materials
Arnab Sarkar, D. Alamelu & S.K. Aggarwal
Talanta 78 (2009) 800-804.
3. Laser induced breakdown spectroscopic quantification of platinum group metals in simulated high level nuclear waste
Arnab Sarkar, V.M. Telmore, D. Alamelu & S.K. Aggarwal
Journal of Analytical Atomic Spectrometry 24 (2009) 1545-1550.
4. Determination of trace constituents in thoria by laser induced breakdown spectrometry
Arnab Sarkar, D. Alamelu & S.K. Aggarwal
Journal of Nuclear Materials 384 (2009) 158-162.
5. Laser induced breakdown spectroscopy for rapid identification of different types of paper for forensic application
Arnab Sarkar, S.K. Aggarwal & D. Alamelu
Analytical Methods 2 (2010) 32-36.
6. Determination of sub-ppm levels of boron in ground water samples by laser induced breakdown spectroscopy
Arnab Sarkar, S.K. Aggarwal, K. Sashibhusan & D. Alamelu
Microchimica Acta 168 (2010) 65-69.

7. LIBS for determination of Li in organic wash solution during preparation of lithium based oxide ceramics by Sol-Gel

Arnab Sarkar, D. Alamelu, T.V.V. Vittal Rao, Y.R. Bamankar, S.K. Mukherjee & S.K. Aggarwal

Optics & Laser Technology 43 (2011) 736-739.

International Conferences

1. Determination of thorium and uranium in solution using laser induced breakdown spectroscopy (LIBS)

Arnab Sarkar, D. Alamelu & S.K. Aggarwal

North American Symposium of Laser Induced Breakdown Spectroscopy (**NASLIBS 07**), New Orleans, LA, USA, 8 - 10 October 2007.

Paper No. P_23, Page 65.

2. Laser induced breakdown spectrometry of lithium determination during preparation of Li_2TiO_3 microspheres by Sol-Gel process

Arnab Sarkar, D. Alamelu, T. V. Vittal Rao, Y. R. Bamankar, S. K. Mukerjee and S. K. Aggarwal

5th International Conference on Laser Induced Breakdown Spectroscopy (**LIBS 2008**). Adlershof, Berlin, Germany, 22-26 September 2008.

Paper No. CP3, Page No. 142.

3. Quantitative determination of various elements in simulated high level waste (SHLW) by laser induced breakdown spectroscopy

Arnab Sarkar, D. Alamelu & S.K. Aggarwal

Ibid, Paper No. CP4, Page No. 52.

4. LIBS for characterization of thoria based fuels
S. K. Aggarwal, D. Alamelu and Arnab Sarkar
2nd North American Symposium on Laser-Induced Breakdown Spectroscopy
(**NASLIBS 2009**). New Orleans, LA, USA, 13-15 July, 2009.
Paper No. P-69, Page 117.

National Conferences

1. Laser induced breakdown spectrometry (LIBS) for the determination of trace impurities in thoria
Arnab Sarkar, D. Alamelu & S.K. Aggarwal
National Laser Symposium (**NLS – 6**), 5th – 8th December, 2006, Indore, Madhya Pradesh.
Paper No. 11.21, Page No. 90.
2. Laser induced breakdown spectroscopy for determination of uranium in thorium - uranium mixed oxide fuel
Arnab Sarkar, D. Alamelu & S.K. Aggarwal
National Laser Symposium (**NLS - 8**), 7-10 January, 2009, LASTEC, Delhi 2009.
Paper No. SA11-020, Page No. 94.
3. LIBS for analysis of liquids using solid substrate
D. Alamelu, Arnab Sarkar & S.K. Aggarwal
Meghnad Saha Memorial Symposium on Emerging Trends in Laser Spectroscopy & Application (**MMSETLSA - 2009**), 23 – 25 March 2009, Allahabad, Uttar Pradesh.
Paper No. IT-12, Page No. 27.